



---

**Universidad de Valladolid**

ESCUELA DE INGENIERÍAS INDUSTRIALES

DEPARTAMENTO DE INGENIERÍA QUÍMICA Y TECNOLOGÍA DEL MEDIO  
AMBIENTE

TESIS DOCTORAL:

**INNOVATIVE STRATEGIES TO ENHANCE PROPERTIES OF  
SOLID HYDROGEN STORAGE MATERIALS BASED ON  
HYDRIDES**

Presentada por Miriam Rueda Noriega para optar al grado de  
doctor por la Universidad de Valladolid

Dirigida por:

Dr.- Ing. Ángel Martín Martínez





---

**Universidad de Valladolid**

ESCUELA DE INGENIERÍAS INDUSTRIALES

DEPARTAMENTO DE INGENIERÍA QUÍMICA Y TECNOLOGÍA DEL MEDIO  
AMBIENTE

TESIS DOCTORAL:

**ESTRATEGIAS INNOVADORAS PARA MEJORAR PROPIEDADES  
DE MATERIALES DE ALMACENAMIENTO DE HIDRÓGENO EN  
ESTADO SÓLIDO BASADO EN HIDRUROS**

Presentada por Miriam Rueda Noriega para optar al grado de  
doctor por la Universidad de Valladolid

Dirigida por:

Dr.- Ing. Ángel Martín Martínez



Memoria para optar al grado de Doctor,  
con **Mención Doctor Internacional**,  
presentada por la Ingeniera Química:  
Miriam Rueda Noriega

Siendo el tutor en la **Universidad de Valladolid**:

Dr. D. Ángel Martín Martínez

Y en **Pavia Hydrogen Lab, University of Pavia** (Italia):

Prof. Amedeo Marini

Valladolid, Septiembre de 2016



**UNIVERSIDAD DE VALLADOLID**  
**ESCUELA DE INGENIERÍAS INDUSTRIALES**

**Secretaría**

La presente tesis doctoral queda registrada en el folio  
número \_\_\_\_\_ del correspondiente libro de registro  
número \_\_\_\_\_

Valladolid, a \_\_\_\_\_ de \_\_\_\_\_ de 2016

Fdo. El encargado del registro



**Ángel Martín Martínez**

Profesor Contratado Doctor

Departamento de Ingeniería Química y Tecnología del Medio Ambiente  
Universidad de Valladolid

Certifica que:

MIRIAM RUEDA NORIEGA ha realizado bajo su dirección el trabajo *“Innovative strategies to enhance properties of solid hydrogen storage materials based on hydrides”*, en el Departamento de Ingeniería Química y Tecnología del Medio Ambiente de la Escuela de Ingenierías Industriales de la Universidad de Valladolid. Considerando que dicho trabajo reúne los requisitos para ser presentado como Tesis Doctoral expresan su conformidad con dicha presentación.



Reunido el tribunal que ha juzgado la Tesis Doctoral titulada *“Innovative strategies to enhance properties of solid hydrogen storage materials based on hydrides”* presentada por el Ingeniero Químico Miriam Rueda Noriega y en cumplimiento con lo establecido por el Real Decreto 99/2011 de 28 de enero de 2011 acuerda conceder por \_\_\_\_\_ la calificación de \_\_\_\_\_.

Valladolid, a \_\_\_\_\_ de \_\_\_\_\_ de 2016

PRESIDENTE

SECRETARIO

1er Vocal

2º Vocal

3er Vocal



## INDEX

<b>ABSTRACT</b> .....	7
<b>STATE OF ART</b> .....	13
<b>OBJECTIVES</b> .....	73
<b>CHAPTER 1.</b> Micronization of Magnesium Acetate by Supercritical Antisolvent (SAS) process as precursor for the production of Magnesium Oxide and Magnesium Hydride.....	77
<b>CHAPTER 2.</b> Enhancement of hydrogen release kinetics from ethane 1,2 diamineborane (EDAB) by micronization using Supercritical Antisolvent (SAS) Precipitation .....	101
<b>CHAPTER 3.</b> Production of silica aerogel microparticles loaded with Ammonia Borane by batch and semicontinuous supercritical drying technique .....	123
<b>CHAPTER 4.</b> Improvement of the kinetics of hydrogen release from Ammonia Borane confined in silica aerogel .....	151
<b>CHAPTER 5.</b> Reversible hydrogen sorption in the composite made of Magnesium Borohydride and silica aerogel.....	179
<b>CONCLUSIONS</b> .....	201
<b>RESUMEN</b> .....	207
<b>ACKNOWLEDGEMENTS</b> .....	229
<b>ABOUT THE AUTHOR</b> .....	231



# ÍNDICE DE CONTENIDOS

<b>RESUMEN (INGLÉS)</b> .....	7
<b>ESTADO DEL ARTE</b> .....	13
<b>OBJETIVOS</b> .....	73
<b>CAPÍTULO 1.</b> Micronización de Acetato de Magnesio mediante Proceso SAS de Acetato de Magnesio como precursor de Óxido de Magnesio e Hidruro de Magnesio.....	77
<b>CAPÍTULO 2.</b> Mejora de las cinéticas de liberación de hidrógeno de etano 1, 2 diaminoborano (EDAB) micronizado utilizando precipitación por SAS .....	101
<b>CAPÍTULO 3.</b> Producción de micropartículas de aerogel de sílice cargadas con Borano de Amonio mediante secado supercrítico en batch y proceso semicontinuo .....	123
<b>CAPÍTULO 4.</b> Mejora de las cinéticas de liberación de hidrógeno de Borano de Amonio confinado en aerogel de sílice .....	151
<b>CAPÍTULO 5.</b> Sorción de hidrógeno reversible en el composite formado por Borohidruro de Magnesio y aerogel de sílice .....	179
<b>CONCLUSIONES</b> .....	201
<b>RESUMEN (CASTELLANO)</b> .....	207
<b>AGRADECIMIENTOS</b> .....	229
<b>SOBRE LA AUTORA</b> .....	231



# **ABSTRACT**

**Innovative strategies to enhance properties  
of solid hydrogen storage materials based  
on hydrides**



Nowadays, the development of renewable energy resources is attracting much more attention in order to reduce economic and environmental problems associated to the use of fossil fuels. However, their production is variable during time and they cannot provide a constant supply of energy. The use of '*hydrogen*' as a vector of energy could be a solution to this important limitation.

In the case of onboard applications, the simplest idea would be to use hydrogen as liquid or gas, but these methods have important disadvantages. In the former case, 30% of the energy would be used in order to maintain the cryogenic state of hydrogen. In the latter case, storage of pressurized hydrogen would require huge tanks at high conditions of pressure. For these reasons, the application of fuel cell using hydrogen as their energy source requires the development of new solid state hydrogen storage materials. Hydrides, which are some of the most promising solid compounds, are limited by thermodynamic and kinetic properties that must be overcome before they are used in a real application.

In ***state of the art***, a literature review of different techniques that have been used to improve kinetics and thermodynamic limitations of bulk hydrides is done, mainly focused in nanoconfinement of different (complex) hydrides in a host, technique which preserve the enhanced properties during cycling.

It could be concluded that till now there is not any work in which all the targets for onboard hydrogen storage systems set by the US Department of Energy (DoE) are accomplished. Thus, more investigation is needed and this PhD was defined in this context with the objective of developing a new solid state hydrogen storage material based on hydrides which, by the reduction of particle size (chapters 1 and 2), and by the incorporation and stabilization in a support material (chapters 3-5) can improve the kinetics and reversibility of the hydrogen storage and release processes.

In ***chapter 1***, micronized Magnesium Acetate was used as a precursor of magnesium hydride ( $\text{MgH}_2$ ) and magnesium oxide ( $\text{MgO}$ ). This hydride has been widely studied due to its high hydrogen storage capacity (7.8 wt%) and its low cost. However, high temperatures are required to decompose it (higher than 300 °C), and hydrogen release is slow which make it difficult to use. Thus, nanoengineering was proposed in order to overcome these limitations. In this work, the precursor of  $\text{MgH}_2$  was micronized by Supercritical Anti Solvent (SAS) process comparing to conventional milling. The influence of concentration of precursor in the initial solution, the temperature of SAS process and  $\text{CO}_2$  fraction was studied on the particle size of

the precursor. Unprocessed magnesium acetate particles of 200  $\mu\text{m}$  were converted into sub-micrometric particles with particle sizes ranging from 300 nm to 700 nm after SAS processing with regular spherical morphology and amorphous crystalline structure. In contrast to this homogeneous product, mechanically milled particles showed similar mean particle sizes, but with irregular morphology, crystalline structure and bimodal particle distribution. After hydrogenation or calcination process, the acetate was converted into  $\text{MgH}_2$  and  $\text{MgO}$ , respectively. As consequence of decrease of particle size, hydrogen release kinetics was enhanced due to the reduction of diffusion distances with a direct relationship between the particle size of the precursor and the kinetics of the hydride.

In **chapter 2**, Ethane 1,2 diamineborane (EDAB), a carbon derivative of Ammonia Borane (used in chapters 3 and 4) was used as hydride. EDAB has a high content in hydrogen (10 wt%), which is released below 200  $^{\circ}\text{C}$  in a two-step reaction. Moreover, it is very stable under ambient conditions, which makes it easier and safer to manipulate it in air atmosphere than other candidate hydrides. EDAB was micronized from THF solutions using the same Supercritical Antisolvent (SAS) process. After micronization, prismatic bulk EDAB of about 400  $\mu\text{m}$  with a crystallite size of 100 nm was converted into microspheres of less than 2  $\mu\text{m}$  with a crystal size of 50 nm. In this case, the concentration of the inlet solution, the temperature of SAS process and the fraction of carbon dioxide did not cause an important change on the final properties of EDAB. As result of reduction of particle size, the kinetic of release of hydrogen by thermolysis at 100  $^{\circ}\text{C}$  was significantly enhanced due to the reduction in the diffusion length, reducing the time needed to release hydrogen by a factor of six. Moreover, a suppression of induction time was obtained due to destabilization of the hydride after treatment.

In **chapter 3**, Ammonia Borane (AB) was used as a promising chemical hydride due to its high content in hydrogen (19.6 wt%), low molecular weight (30.7 g/mol), moderate decomposition temperature and stability and safety in handling. However, it has kinetic limitations due to long induction times to disrupt dihydrogen bond and slow release of hydrogen. Moreover, during the decomposition process, the emission of some volatile byproducts such as borazine, diborane or ammonia can be released which could be poisonous for hydrogen fuel cells. In this work, nanoconfinement of AB in a support was proposed as solution to enhance these limitations.

Silica aerogel microparticles were used as support to stabilize and encapsulate the hydride. The formation of aerogel microparticles was done combining sol-gel process and supercritical drying using batch and semicontinuous drying apparatus. Silica aerogel microparticles

produced by the two drying techniques had a surface area ranging from 400 to 800 m<sup>2</sup>/g with more than 1 cm<sup>3</sup>/g of volume of pores and a mean particle diameter ranging from 12 to 30 μm. The influence of shear rate, the amount of catalyst during sol-gel process, the amount of dispersant solvent and hydrophobic surface modification on particle size distribution (PSD) were studied. As result, irregular aerogel particles were obtained for hydrophilic gels, while regular, spherical particles with smooth surfaces were obtained for hydrophobic gels. AB was loaded into silica aerogel microparticles in low concentrations ranging from 1 wt% till 5% wt depending on the surface modification of the aerogel. Impregnation method followed by precipitation of AB using dicloromethane (DCM) was used and then, supercritical batch drying was used in order to obtain dried particles. This low encapsulation efficiency could be explained by the possibility of lost AB during washing with DCM and/or the decomposition of AB during supercritical drying process in presence of silica. By stabilization of AB into silica aerogel microparticles resulted in faster hydrogen release kinetics than unprocessed AB or using conventional mechanical milling.

In **chapter 4**, the concentration of AB homogeneously loaded in the pores of hydrophilic silica aerogel was increased up to 60 wt% due to the innovative process used to produce it and the favorable textural properties of silica aerogels (up to 2 cm<sup>3</sup>/g). It is the first time that more than 50 wt% of AB has been successfully stabilized in a support. It was done by a novel process, based on a simultaneous aerogel drying and ammonia borane gas antisolvent precipitation using pressurized carbon dioxide at subcritical conditions in order to avoid decomposition process from the previous chapter. The influence of the amount of Ammonia Borane loaded on the aerogel on the thermal and structural properties of the material was analyzed. The resulting material showed faster hydrogen release kinetics without induction time by thermolysis at 80 °C and suppression of volatile subproducts in contrast to bulk AB. This fact was due to a significant reduction in the mean size of the hydride after confinement and the presence of SiOH and SiOSi groups of silica aerogel. Furthermore, by nanoconfinement of AB, the morphological properties of the material were preserved after isothermal release of hydrogen avoiding foaming process, which could be favorable properties for a subsequent material regeneration process.

In **chapter 5**, Magnesium Borohydride Mg(BH<sub>4</sub>)<sub>2</sub> was used as a promising hydrogen storage material because of its high hydrogen storage capacity (14,8 wt% H<sub>2</sub>, 0.112 Kg/L). However, it is still limited by slow hydrogen release kinetics and by the harsh conditions required for reversible hydrogen sorption due to the formation of stable intermediates. Composites made

of commercial  $\text{Mg}(\text{BH}_4)_2$  and synthesized silica aerogel microparticles were prepared by thermal treatment in hydrogen. As a result, the sorption properties of the prepared composite were improved due to the destabilization of the hydride by silica; not only reducing the decomposition temperature by 60 °C but also enhancing the kinetics of dehydrogenation at 300 °C, that was two times faster in silica composites than in bulk  $\text{Mg}(\text{BH}_4)_2$ . Additionally, rehydrogenation of the prepared composite at comparatively mild conditions of 390 °C and 110 bar  $\text{H}_2$  was done for the first time, achieving a hydrogen storage material with a reversible release of hydrogen up to 6 wt%  $\text{H}_2$ . Results indicate that silica aerogel chemically interacted with  $\text{Mg}(\text{BH}_4)_2$ , acting as an additive, which could result in different routes with different amounts and types of intermediates, influencing on the kinetics and cyclability of the hydrogen storage material. This research was done at Hydrogen Lab at Pavia (Italy).

# **STATE OF ART**

**Innovative strategies to enhance properties  
of solid hydrogen storage materials based  
on hydrides**



Nowadays, economy and society depend on the use of fossil fuels. It is clear that fossil fuels cannot continue being a primary resource due to their depletion and the economic and environmental problems concerning their use.

As figure 1 shows, more than 70 % of the world greenhouse emissions come from energy sources like electricity production, heating and transportation. For these reasons, the development of alternative and more sustainable energy sources is a priority in order to mitigate these problems. This concern was addressed in Paris at COP21 with the adoption of the first international climate agreement applicable to 195 countries, which has limited the temperature rise to less than 2 °C.

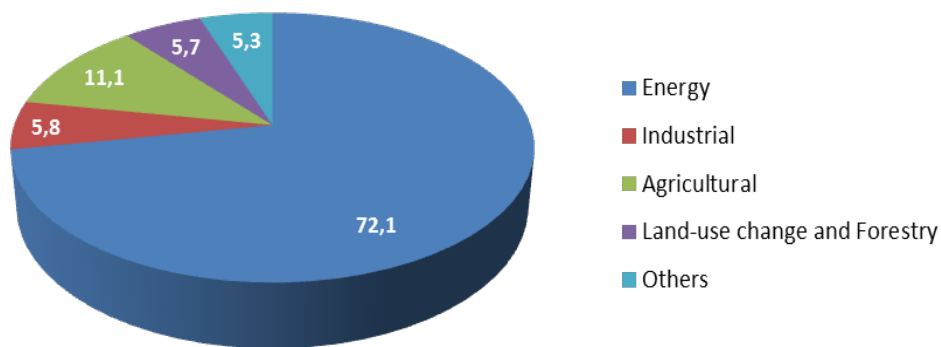


**Figure 1.** Greenhouse Gas Emissions (GHG) by Sector. (Source: World Resource Institute, 2015)

The International Energy Agency (IEA) indicated in its last study that electricity generation and emission of CO<sub>2</sub> have different ratios of growth. It is predicted that emission of CO<sub>2</sub> will remain flat whereas electricity demand will grow by more than 40 %, indicating that low-carbon power will grow to almost 45 % in 2030 (figure 2). According to this trend, in the last years the use of renewable energies has significantly increased, which is estimated to generate nowadays more than 22% of global electricity.

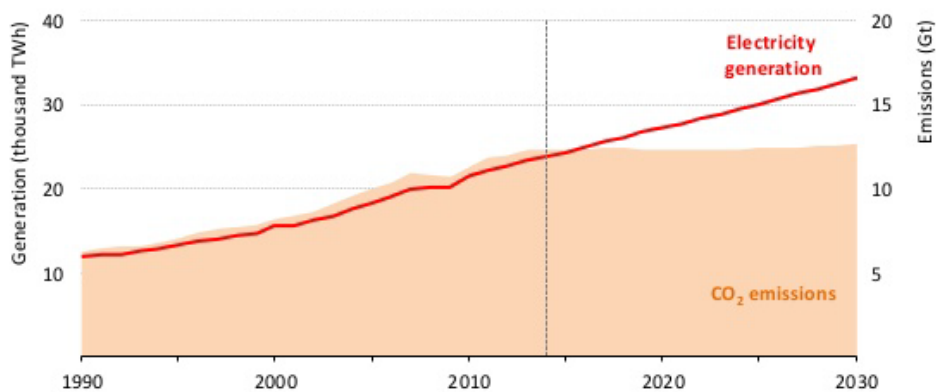


**Figure 2.** Global electricity generation vs. CO<sub>2</sub> emissions (Source: World Energy Outlook, 2015)

Nevertheless, the generalized application of these cleaner energy sources still faces important limitations, such as fluctuations in the production of energy due to weather changes or other random events, and difficulties in storing the excess energy produced in periods of low demand. The use of the energy generated from renewable sources in mobile applications such as vehicles or small electronic equipment is also hindered by the difficulties associated with the storage and transportation of this energy.

Some of these drawbacks can be solved using hydrogen as an energy vector which is known as 'hydrogen economy' or 'hydrogen society' (figure 3). Hydrogen is an excellent fuel because of its high specific heat of combustion (three times more of energy per unit of mass than gasoline) and its clean combustion in a fuel cell which only generates water (with zero CO<sub>2</sub> emissions). Hydrogen can be produced from water (by electrolysis, thermal decomposition, thermochemical processes, photolysis etc.) using renewable energy sources whose process needs to be optimized in order to reach higher efficiencies. After combustion in a fuel cell, it can be used in a wide range of applications; from portable systems which needs low power to automotive or aerospace field including stationary and onboard power. In this way, the use of hydrogen as fuel contributes to mitigate air pollution in cities and economical and environmental sustainability.

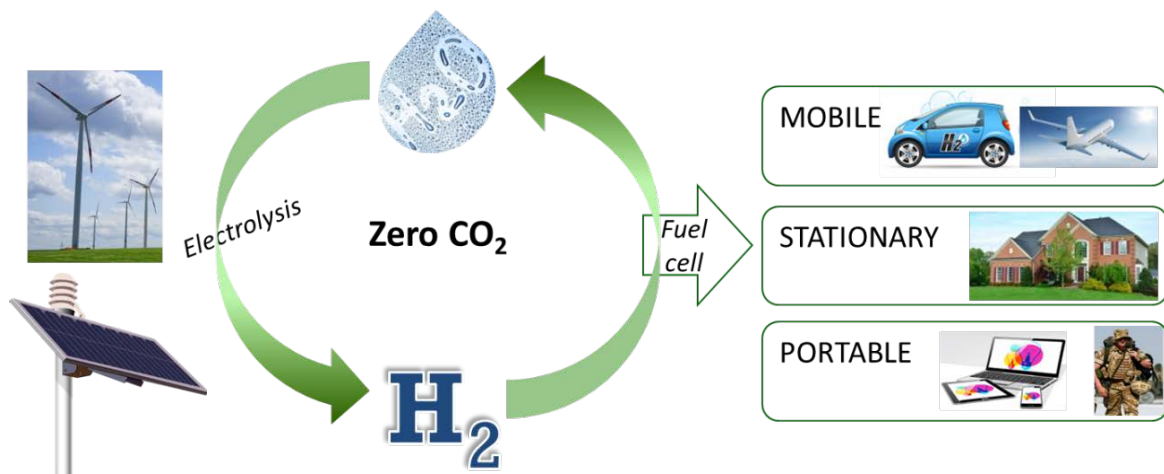


**Figure 3.** Hydrogen economy

However, storing hydrogen in small mobile applications or in vehicles presents new challenges. In these applications, it is especially important to reduce the weight and space required by the hydrogen storage system as much as possible. The simplest and most obvious solutions could be to use hydrogen in the liquid or gas state. However, these methods have some disadvantages: with cryogenic liquid systems, 30 % of the energy would be wasted just in

condensing the hydrogen and maintaining it in the liquid state ( $T_b = -252.8$  °C at 1 bar), and compressed deposits are huge at very high conditions of pressure (350-700 bar) (Züttel 2004). Therefore, a compact, safe, reliable, inexpensive and energy efficient method of storing hydrogen is needed which accomplish the targets set by the US Department of Energy for 2020 for automotive hydrogen systems: a hydrogen storage gravimetric capacity of 5.5 wt%  $H_2$  (1.8 kWh/kg) and a volumetric capacity of 0.040 kg/L (1.3 kWh/L), with a maximum cost of 333 \$/kg  $H_2$  stored.

For these reasons, developing a new solid state hydrogen storage system is a challenge. Among the different hydrogen storage alternatives, chemical and complex hydrides, which are solid compounds that liberate  $H_2$  during their thermal decomposition, are some of the most promising alternatives (Marrero-Alfonso et al. 2009). However, these compounds still present thermodynamic and kinetic limitations.

- *Thermodynamic limitations*, because, in general, the proposed hydrides for hydrogen storage are very stable. They need high temperatures in order to be decomposed and release hydrogen. This limitation can be improved by the addition of compounds which destabilize the hydrides
- *Kinetic limitations* because high times are required to release and uptake hydrogen. This time can be reduced shortening diffusion distances with a reduction of particle size of the hydride.

Different techniques have been tested in order to address these limitations and enable the use of these hydrides in a real application (Liu & Zhang 2012).

### 1. Addition new chemical species

This approach is based on introducing new chemical species that reacts with the metal, forms an intermediate compound which reduce the heat of formation of the hydride and therefore destabilize it releasing hydrogen at lower temperature (Vajo & Olson 2007). However, the storage capacity usually decreases slightly (Bérubé et al 2007). The pioneer of this strategy was Reilly and Wiswall on hydrogen storage in  $Mg_2Cu$ . This specie was reversibly hydrogenated into  $0.75MgH_2 + 0.5MgCu_2$  with a temperature of equilibrium at 1 bar 40 °C lower than that of pure  $MgH_2$  (J. J. Reilly 1967). Similar results have been demonstrated in other systems such as  $LiBH_4/MgX$  for  $X=H_2, F, Cl, OH, O, S, Se, Ni,$  and  $Si$  among others;  $LiBH_4$  or  $LiH$  with hydrocarbons (Vajo & Olson 2007).

## 2. Doping hydrides

It is another strategy in order to weaken metal-H and H-H bonds and thus reduce transition state barriers of hydrogen reactions (Bald et al. 2007)(Liu et al. 2009).

Several works have been done using this technique. In the case of complex metal hydrides such as  $\text{NaAlH}_4$ , doping them with a few mol% of Ti lowered the decomposition temperature, improved kinetics, and most importantly, allowed rehydrogenation of the decomposition products (Bogdanović et al. 2000) and reduced the heat of formation. Also in the hydride  $\text{LiAlH}_4$ , thermodynamic and kinetic properties were improved after the addition of  $\text{TiCl}_3$  which reduced the temperature of dehydrogenation (Langmi et al. 2010).

Doping Mg with carbon nanotubes or graphite also enhanced kinetics without losing storage capacity (Bérubé V; Radkéd G; Dresselhaus M; Chen G 2007). In the case that Sc, Ti, Cu and Zn were added, thermodynamic properties were improved (Andrievski 2011).

## 3. Cation substitution

Cation substitution to form dual-cation hydride is generally used as a technique to modify thermodynamic properties. Although this modification is effective to destabilize the reactant, the modified crystal structure is usually not maintained during repeated hydrogenation-dehydrogenation cycles.

## 4. Nanoengineering

Nanoengineering is a promising solution to reduce the crystallite size and increase the surface area of the hydride. These changes are associated to an increase of surface energy of the metal and hydride phases and reduction of diffusion lengths, properties which improve the decomposition rate [7]. Moreover, nanoscale synthesis reduce the heat of formation of metal hydrides, resulting in faster kinetics and better storage efficiencies (Bérubé et al 2007). More importantly, thermodynamics of hydrogen desorption/adsorption of complex metal hydrides usually can be adjusted by controlling particle size.

A summary of the benefits and drawbacks of nanoengineering on metal hydride properties are shown in table 1.

	<b>Storage capacity</b>	<b>Kinetics</b>	<b>Enthalpy of formation</b>	<b>Heat transfer</b>	<b>Cyclability</b>	<b>Release T</b>
<b>Increased surface area</b>	Increased physisorption	Increased surface dissociation	Decreased	Decreased	Potentially decreased	Potentially decreased
<b>Increased grain boundaries</b>	Decreased	Increased diffusion	Potentially decreased	Decreased	Potentially decreased	Potentially decreased
<b>Increased porosity</b>	Potentially increased physisorption	Faster gas diffusion	No effect	Decreased	No effect	No effect
<b>Formation of nanocomposites</b>	Mean of the components	Potentially decreased	Potentially decreased	Decreased	Potentially increased or decreased	Decreased
<b>Doping/alloying</b>	Potentially increased or decreased	Decreased	Decreased	Potentially increased or decreased	Potentially increased or decreased	Decreased

*Table 1. Summary of the benefits and drawbacks of nanoengineering on selected metal hydride properties. Source: (Bérubé et al 2007)*

Different methods can be used in order to reduce the size of the metal hydride particles such as laser ablation, vapour condensation (Hearley A; Redmont S. 2004), sputtering or ball milling of the metal hydride (Bérubé et al 2007) among others. Ball milling is the most frequently used method due to its scalability and ease of use. It can be classified into three different types according to the function: mechanical grinding (without compositional change during milling), mechanical alloying (ball milling to synthesize alloys from metal elements) and reactive ball milling (milled under gas atmosphere) (Shao et al. 2012).

With this method, hydrogen release kinetics is enhanced due to the reduction of the diffusion lengths without any cost of a catalyst or a reduction of storage capacity. Milling can also induce other material changes, such as an increase in the number of defects, create more disorder and strain into the material and therefore improve surface properties (Andrievski 2011). A positive effect of high energy milling and decrease of nanoparticles size on absorption and desorption processes has been confirmed in many studies, mainly with  $MgH_2$  (Andrievski 2011). (Shao et al. 2012) reviewed different nanoprocessing methods for Mg hydrides concluding that thermodynamics did not change with nanosize above 5nm. The effect of ball time on the structural phase transformations and dehydrogenation behaviour of  $NaAlH_4$ - $MgH_2$  was also studied by (Bendyna et al. 2015), obtaining the best results for the mixture milled for 120 min since longer milling times were not advantageous for the rates and consumed more

electricity. Also the kinetics and microstructure properties were studied in the system  $Mg_{1-x}Ti_x$  obtained by reactive ball milling using three different routes. Milling conditions (time, ball to powder ratios, rotation velocities and degrees of filling) were tested in the system  $LiH-MgB_2$  doped with  $TiCl_3$  by (Busch et al. 2015) reaching a crystal size of 5 nm, a surface area of  $15 \text{ m}^2/\text{g}$  for an optimum energy transfer of 20 kJ/g.

The most effective method for simultaneously synthesize nanostructures of hydrides is mechanical milling/alloying (Varin et al. 2005). Another method to synthesize nanostructure hydrides is mechano-chemical activation synthesis (MCAS) which works with high energy ball milling of a (complex) hydride mixed with a metal (Varin et al. 2008).

Despite these advantages, the control and reproducibility of results obtained with milling is poor, because the product often shows severe agglomeration problems and the microcrystals are trapped in thick films over mill walls and balls that make it difficult to recover the product from inside the mill.

Apart from the inhomogeneity of the product after milling, the particle size of the milled hydride increases after hydrogen cycling due to sintering during hydrogen exchange, having a non desired effect on cycling capacity and reversibility (Vajo & Olson 2007). As shown in the following section, this limitation can be overcome using porous scaffold structures which avoid particle growth during cycling.

## 5. Confinement in a support

Encapsulation and confinement leads to high dispersion of the material within the support with the following three effects (Schuth 2006):

1. Kinetics are improved, since mass transfer distances are minimized (kinetics are enhanced for nanoparticles up to 30-50 nm (Nielsen et al. 2009)). Moreover, stabilizing the hydride in a support preserves the size of the hydride during hydrogen release and uptake cycles.
2. Thermodynamics are altered, since large surface effects of nanosized powders can lead to additional energetic contribution, which in favorable cases leads to destabilization. (Thermodynamic improvements occur for small nanoparticles 2-5nm (Nielsen et al. 2009))
3. The incorporation leads to hindered access of air and moisture and thus to improve safety.

Moreover, theoretically, a complex hydride embedded in the nanoscale void can display completely reversible decomposition because of enhanced diffusion in the void (Fichtner 2009).

Confinement of different hydrides has been studied:

## Mg(BH<sub>4</sub>)<sub>2</sub>

Mg(BH<sub>4</sub>)<sub>2</sub> is a promising complex hydride due to its high gravimetric capacity of 14.8 wt% and 146.5 Kg/m<sup>3</sup>, exceeding the ultimate targets from DoE. The limitations of the borohydrides are the slow kinetics and the high H<sub>2</sub> desorption temperatures. However, Mg(BH<sub>4</sub>)<sub>2</sub> has the lowest desorption temperature (starts at 270 °C) compared to other borohydrides.

Some of the drawbacks of this complex hydride are the low reversibility due to the formation of stable intermediates during decomposition and the different routes proposed during its decomposition. (Soloveichik et al. 2009) reviewed different pathways proposed from different authors.

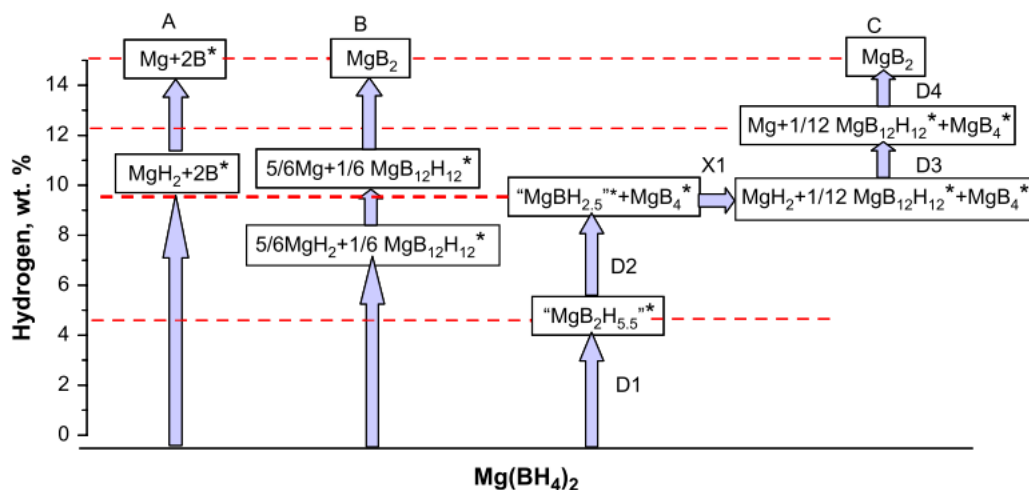


**Figure 4.** Pathways of decomposition proposed for Mg(BH<sub>4</sub>)<sub>2</sub>. Source: (Soloveichik et al. 2009)

Confinement is proposed in order to overcome the limitations (kinetics and thermodynamics) of this hydride and preserve the properties during cycling, recently reviewed in (Saldan 2016)(Zavorotynska et al. 2015). Table 2 shows the different works published till now which study the confinement of this hydride in a host.

Ref.	Host	Surface properties ( $m^2/g$ - $cm^3/g$ )	MBH wt%	Method of infiltration <sup>(1)</sup>	$E_a$ system 1 <sup>st</sup> step <sup>(2)</sup> (KJ/mol)	$E_a$ system 2 <sup>nd</sup> step <sup>(2)</sup> (KJ/mol)
(Fichtner et al. 2009)  (Wahab et al. 2013)  (Yan et al. 2013)	Bulk hydride				311±20  45.9  40±11	161
(Fichtner et al. 2009)	Carbon aerogel	860/0.61	44.3 (63% in pores)	WI with diethyl ether	176	189
(Wahab et al. 2013)	CMK-3	1559/1.67	50	WI	-	-
(Wahab et al. 2013)	CMK-3+5%Ni	1499/1.63	50	WI	16.18	-
(Au et al. 2014)	Carbon	-/0.52	30% in pores	MI Mg+treatment $B_2H_6$	-	-
(Yan et al. 2013)	Carbon aerogel	605/0.52	18	MI $MgH_2$ + treatment $B_2H_2$ by milling	102±6	-
(Ampoumogli et al. 2011)	CMK-3	1500/1.5	40	WI with $NH_3$	-	-

<sup>(1)</sup>WI: wet impregnation MI: melt infiltration

<sup>(2)</sup>In the first step,  $Mg(BH_4)_2$  is converted into  $MgH_2$ , and in the second into  $Mg$ .  $H_2$  is released in both steps.

Table 2. Review of  $Mg(BH_4)_2$  confined in a support

As decomposition of  $Mg(BH_4)_2$  occurs before melting, wet impregnation seems to be the most promising infiltration method. In (Fichtner et al. 2009) and (Wahab et al. 2013), the presence of the hydride was checked by the reduction of surface properties. In (Fichtner et al. 2009), surface area and volume of the pores decreased to 159  $m^2/g$  and 0.03  $cm^3/g$  respectively, whereas in (Wahab et al. 2013) decreased to 127  $m^2/g$  and 0.22  $cm^3/g$ . After confinement, DSC analyses showed a change during the thermodecomposition, which was more significant in the second decomposition peak (Fichtner et al. 2009). Authors presumed that infiltration led to spatial restrictions which impeded material transformation and imposed additional activation

barriers which could be thermally activated. Moreover, in (Wahab et al. 2013) a reduction of 155 °C was observed with respect to the decomposition temperature of bulk hydride, a reduction which was improved to almost 200 °C after the addition of Ni as catalyst, similar to (Ampoumogli et al. 2011) whose peak temperature was decreased to 200 °C. As result of the synergic effect of the catalyst and nanoconfinement, not only thermodynamic was improved but also the kinetic rates were enhanced more than 10 times. In all the works, confinement caused a broadening in the peaks of calorimetric analyses due to the higher degree of disorder created by the intimate contact with the scaffold and a loss of crystallinity due to the formation of amorphous or nanocrystalline compounds.

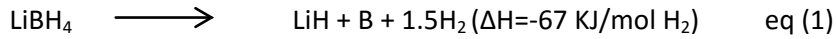
As decomposition tends to occur before melting, in (Yan et al. 2013) and (Au et al. 2014) Mg/MgH<sub>2</sub> was melted in the carbon host and then treated with B<sub>2</sub>H<sub>6</sub>. In both cases, a reduction of surface properties was also observed after infiltration, and the pore structure in carbon aerogel in (Yan et al. 2013) was damaged due to ball milling. After this process, NMR indicated the presence of a peak related to MgB<sub>12</sub>H<sub>12</sub> and a small amount of Mg(BH<sub>4</sub>)<sub>2</sub> (Au et al. 2014) improving the reactivity to B<sub>2</sub>H<sub>6</sub> in the sample with Ni addition.

In (Yan et al. 2013), nanostructured samples started to release H<sub>2</sub> 150 °C before than bulk Mg(BH<sub>4</sub>)<sub>2</sub>, but B<sub>2</sub>H<sub>6</sub> (possibly adsorbed from the treatment) was released apart from H<sub>2</sub>. Also around 30% reversibility was successfully obtained by rehydrogenation at 150 bar H<sub>2</sub> and 200 – 270 °C for 20 hours, whereas harsher conditions were necessary to rehydrogenate the bulk hydride. In this case, due to the destruction of the pores, nanoconfinement effect could not be related to this improvement, and the reduction of the H<sub>2</sub> release temperature and the possibility to rehydrogenate the compound at milder conditions were attributed to the formation of nanostructures reducing the particle size of the hydride to nanoscale, reducing also the diffusion distances and therefore the activation energy (see table 2).

## **LiBH<sub>4</sub>**

This complex hydride has a high gravimetric (13.8 wt%) and volumetric (0.092 Kg/L) hydrogen storage capacity. However, it is necessary to overcome some thermodynamic and kinetic limitations to have a promising reversible hydrogen storage system.

LiBH<sub>4</sub> is decomposed in a two steps-reaction, as indicates equations 1 and 2. Overall, this compound releases 18.5 wt% H<sub>2</sub>, but LiH needs high temperature (above 600 °C) to release its content in hydrogen. Therefore, this last step is usually not considered in most applications, thus obtaining LiH as final decomposition product.



Regarding reversibility, bulk LiH and boron can be rehydrogenated above 600 °C and 350 bar H<sub>2</sub>. To sum up, the high desorption temperature (~500 °C) and the evolution of toxic diborane (B<sub>2</sub>H<sub>6</sub>) on decomposition appear to limit its practical application as a hydrogen storage medium. In this case, the micronization would not solve the problem because the surface energy of the hydride (0.12 J/m<sup>2</sup>) is lower than that of the subproducts (LiH=0.44 J/m<sup>2</sup>) and therefore, nanosizing would imply more stabilization compared to the macrocrystal (Ngene et al. 2016). Therefore, the proposed alternative is to confine this hydride within a support. The most investigated, till now, is carbon, but also silica, TiO<sub>2</sub>, metal organic frameworks (MOF) or polymers have been studied.

In the case that carbon was used as host, the method that has been more investigated is melt infiltration (Gross et al. 2008)(Vajo & Olson 2007)(Shane et al. 2010)(Liu et al. 2011)(Gao et al. 2014)(Gao et al. 2012)(Ngene et al. 2016)(Ngene, Verkuijlen, et al. 2011)(Ngene, van Zwiene, et al. 2010)(Liu et al. 2010), as decomposition occurs at higher temperature than melting of the hydride which avoid the decomposition of the hydride during infiltration.

For example, (Gross et al. 2008)(Vajo & Olson 2007) infiltrated this hydride into the pores of a carbon aerogel by capillary action using melt infiltration at 280-300 °C. Different carbon aerogels with different surface properties were studied, filling up to 90% of the pores. As a result, the rate of dehydrogenation was significantly enhanced, being 50 times faster compared to LiBH<sub>4</sub> milled with nonporous graphite. The decomposition temperature was lower (by 100 °C) and activation energy decreased with decreasing pore size, indicating that the dehydrogenation energy was lower after infiltration. Regarding reversibility, it was also enhanced after nanoconfinement because the pore size limited the size of the agglomerates and reduced diffusion distances, increasing the contact between LiH and B. Rehydrogenation at 100 bar H<sub>2</sub> and 400 °C for 2 h resulted in the formation of LiBH<sub>4</sub>, but also some residual LiH was observed, obtaining better cyclability with carbon hosts with smaller pores. Therefore, the solution could be to use a carbon scaffold with the smallest pores and highest volume of pores, which might be obtained using supercritical drying conditions.

(Shane et al. 2010) applied Raman spectroscopy to study the influence of pore size in the defects of LiBH<sub>4</sub>-carbon system. (Liu et al. 2011) studied the thermodecomposition of this complex hydride after nanoconfinement in three carbon supports with different pore size (2,4

and 9 nm). Dehydrogenation temperature decreased, with a larger reduction when the pore size of the scaffold was lower, as it is shown in the figure 5. Also the cyclability, in terms of the amount of  $H_2$  reversibly stored, was improved in the carbon scaffold with higher microporosity.

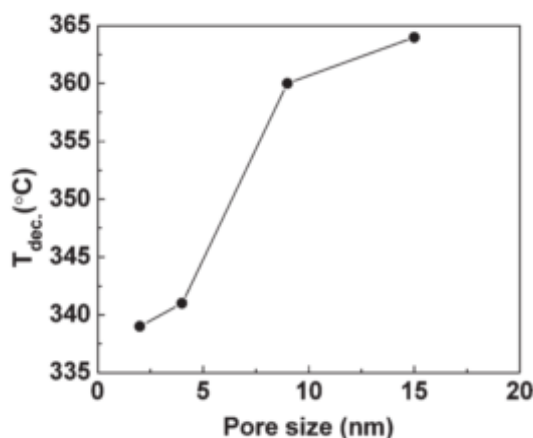
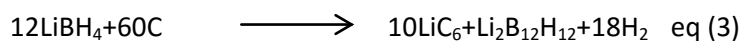


**Figure 5.** Pore-size dependence of dehydrogenation temperature of nanoconfined  $LiBH_4$  in different carbon templates with a loading of 10 wt%. Source: (Liu et al. 2011)

The influence of surface groups in carbon obtained with different treatments (in Argon, with nitric acid or in hydrogen flux) was also studied by (Gao et al. 2014). This aspect had not an important influence on the decomposition of the hydride but played an important role on the rehydrogenation at 55 bar and 330 °C for 12 h, as a lower reversible  $H_2$  capacity was obtained using carbon with higher density of polar surface groups in contrast to carbon with almost no functional groups. Therefore, apart from surface properties (surface area, volume and size of pores), the surface groups in the support played an important role on the cyclability of nanoconfined samples.

Moreover, the reversibility could be improved adding Li species to  $LiBH_4$  infiltrated in carbon. In this way, 72% of reversibility has been demonstrated (Gao et al. 2012) after addition of 8 wt% Li/LiH.

It has been shown that  $LiBH_4$  nanoconfined in carbon supports by melt infiltration presents improved thermodynamic and kinetic properties with respect to the hydride. (Ngene et al. 2016), demonstrated that the graphitic scaffold not only destabilized the hydride (accomplishing decomposition at a temperature more than 150 °C lower than with bulk hydride), but also changed the pathway of decomposition to a single step (equation 3). In contrast, (Gross et al. 2008) used the same support and proposed the same mechanism of decomposition as with bulk  $LiBH_4$  (equation 1 and 2) .



In this way, 18.1 wt% H<sub>2</sub> was released at 400 °C, being the first time that complete decomposition was attained at this temperature, as with bulk hydride generally complete decomposition is only achieved above 600 °C, even in presence of non-porous graphite. Rehydrogenation was also feasible by treatment at 50 bar H<sub>2</sub> and 325 °C for 3 hours, in contrast to the negligible reversibility of bulk LiBH<sub>4</sub>. The concentration of hydride nanoconfined in HSAG-500 was also studied within the range 15-30 wt%, obtaining the best results with 15 wt% samples, as at higher concentration some hydride was deposited out of the pores. Moreover at the concentration of 15 wt%, LiC<sub>x</sub> was formed, whereas at higher concentration it was decomposed into LiH (as bulk hydride) and LiC. In this work, it was demonstrated that nanoconfinement in a support resulted in better kinetics, increased the reversibility and the capacity of hydrogen (for the first time) which is usually reduced by the penalty of weight scaffold by reversible interactions between Li and graphitic carbon.

These properties can even be improved by addition of 3.75 wt% Ni as catalyst (Ngene, Verkuijlen, et al. 2011). As result of the synergic effect of nanoconfinement and addition of catalyst, hydrogen release started at lower temperature (below 200 °C). Also rehydrogenation at 320 °C, 40 bar H<sub>2</sub> for 2 hours was improved, as it was faster and more amount of H<sub>2</sub> was regenerated, 9.2 wt% H<sub>2</sub>/g LiBH<sub>4</sub> in the system with addition of Ni in contrast to 6 wt% H<sub>2</sub>/g LiBH<sub>4</sub> in C/LiBH<sub>4</sub> system. This was explained by the formation of Ni<sub>x</sub>B (detected by Extended X-ray Absorption Fine Structure spectroscopy, EXAFS) which acted as catalyst during hydrogenation and enhanced the stability of the microstructure in carbon support upon cycling, avoiding phase separation or acting as a center for nucleation of LiBH<sub>4</sub>. The formation of this compound could also promote a change in the decomposition pathway (Ngene, van Zwiene, et al. 2010). Increasing Ni concentration from 3.75 to 7.5 wt% did not have a significant effect on the hydrogen release.

The same procedure was followed with LiAlH<sub>4</sub> (Ngene et al. 2016), using wet impregnation as infiltration method and THF as solvent. After nanoconfinement, the decomposition pathway was changed. Also, it facilitated the full decomposition into LiC<sub>x</sub> (instead of LiH), Al, and H<sub>2</sub> at a relatively low temperature (300 °C) due to Li intercalation into graphite, while the macrocrystalline LiAlH<sub>4</sub> supported on non-porous graphite decomposed into Al, LiH and traces of undecomposed Li<sub>3</sub>AlH<sub>6</sub>.

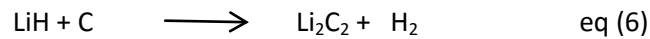
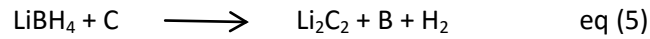
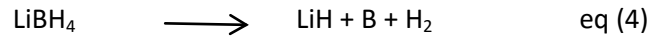
In bulk  $\text{LiBH}_4$  or even in  $\text{LiBH}_4$  physically mixed with carbon, the release of  $\text{H}_2$  is accompanied by formation of contaminants such as diborane,  $\text{B}_2\text{H}_6$ . The formation of this gas could be suppressed by nanoconfinement in nanoporous carbon (Liu et al. 2010)(Liu et al. 2011). Authors indicated that the carbon framework may prevent the formation of diborane and the decomposition pathway could be altered by the presence of the framework through size confinement and/or surface interaction effects, as evidenced by the wetting behavior. Alternatively, this result may suggest that  $\text{LiBH}_4$  decomposing from a noncrystalline state (as the compound is in amorphous state due to the nanoconfinement) cannot produce  $\text{B}_2\text{H}_6$ , as in (Liu et al. 2011) it was demonstrated that the release of this gas decreased with pore size.

Similar results were obtained when wet impregnation was used as infiltration method, using MTBE (Cahen et al. 2009)(Brun et al. 2010) or THF (Fang et al. 2008)(Christian & Aguey-Zinsou 2010) as solvent. Lower decomposition temperature with only one decomposition step was obtained in confined samples (with a maximum load of 36 wt%  $\text{LiBH}_4$  in the pores of this scaffold), avoiding formation of intermediate compounds (Cahen et al. 2009). However, in this work, reversibility was not accomplished (Cahen et al. 2009)(Brun et al. 2010) as the chemical inertness of boron could not be overcome and the pathway followed during decomposition was the same as that of bulk hydride, with some extra irreversible exothermic reaction with surface groups ( $-\text{COOH}$ ,  $-\text{OH}$ ) of the carbon support, confirmed by NMR analyses (Brun et al. 2010).

Nanoconfinement in the pores of carbon supports improved the decomposition of this hydride reducing the dimensions, which means reduction of diffusion length and therefore corresponding improvement of hydrogen exchange kinetics, accompanied by inhibition of agglomeration, which allowed maintaining the kinetic properties during cycling (Fang et al. 2008). (Christian & Aguey-Zinsou 2010) confined less than 2 wt%  $\text{LiBH}_4$  in carbon nanotubes attributing the size as responsible of the destabilization, changing the mechanism of decomposition (three steps were converted into one) and lowering the activation energy ( $88 \pm 5$  KJ/mol). It was the first time that  $\text{LiBH}_4$  was released at such low temperature ( $T_{\text{peak}}=140$  °C) due to the synergistic effects of size, reduction in diffusion paths and confinement effects.

(Y.Zhang, et al 2007) proposed milling as method of nanoconfinement, although some authors do not accept this method as infiltration technique because this method generally only allows to reduce the size of the hydride or to form a mixture of elements (hydride and support) reducing the distances between them but not to infiltrate a hydride in the pores of a support. Moreover, milling could destroy the pore structure of the scaffold. In this case, a mesoporous

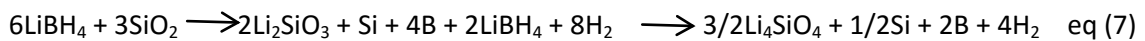
carbon material (CMK-3) was milled at 450 rpm for 5 h with LiBH<sub>4</sub> in a weight ratio 1:1 obtaining nanodispersed particles of LiBH<sub>4</sub> of about 5 nm which 'seemed to be' embedded in the scaffold. As result, the nanocomposite was less stable with lower heat of dehydrogenation and lower decomposition temperature (see table 3). Rehydrogenation was feasible under 30 bar H<sub>2</sub> for 100h, with 6 wt% H<sub>2</sub> of reversible capacity. Also, they proposed a mechanism after identification of the different phases.



The decomposition reflected two mechanisms: first, nanodispersion of LiBH<sub>4</sub> in CMK-3 improved the thermal stability and the diffusion and recombination of the elements to rehydrogenate the borohydride. On the other hand, it served as reactive exerting synergic effects on the dehydrogenation in both cases.

Apart from carbon supports, other hosts have been explored. In (Ngene, Adelhalm, et al. 2010), 10-65 wt% LiBH<sub>4</sub> was confined in silica support (SBA-15) by melt infiltration, successfully obtaining nanoconfined hydride in the pores of the silica till a hydride concentration of 25 wt%. After nanoconfinement, the onset decomposition temperature was reduced by more than 100 °C due to the following factors:

- 1) Nanoscale reduced the dehydrogenation properties obtaining the best results for the silica with highest surface area and volume of pores.
- 2) Catalytic effect of SiO<sub>2</sub>, enhanced due to the reduction of diffusion distances which also increased the reaction rate.
- 3) Reaction with SiO<sub>2</sub> during heating forming silicates, as it is shown in equation (7).



Moreover, rehydrogenation was possible at 450 °C, 100 bar H<sub>2</sub> for 2 h and milder conditions at 300 °C, 170 bar for 3 h; although capacity decreased due to the amount boron lost through reactions with the silica scaffold.

Another possibility is to use TiO<sub>2</sub> scaffolds and nanoconfine LiBH<sub>4</sub> by wet impregnation using THF as solvent (Guo et al. 2013). Excellent kinetics were measured in confined samples as porous TiO<sub>2</sub> acted as a catalyst or destabilizing agent for hydrogen release and at the same

time as support, whose amount played an important role. An excess of catalyst increased the total mass of the composite which goes against the demand of high gravimetric capacity of hydrogen storage; nevertheless too low level of  $\text{TiO}_2$  could not provide enough amount of scaffolds to confine the hydride. Moreover, the composite was 5.5 wt%  $\text{LiBH}_4$  reversible at 400 °C, 46 bar in less than 2 hours, although the regeneration mechanism was still not clear.

Superior dehydrogenation properties could be obtained using Metal-Organic Frameworks, Cu-MOF (Sun et al. 2011). Decomposition in this confined system started at 60 °C in contrast to 380 °C in bulk hydride. On the other hand,  $\text{LiBH}_4$  could be destabilized by nanoconfinement in poly (methyl methacrylate)-co-butyl methacrylate (PMMA-co-BM) using a solution of THF (Gosalawit-Utke et al. 2014). In this case, the decomposition temperature was also reduced ( $T_{\text{onset}}=80$  °C vs 420 °C in milled  $\text{LiBH}_4$ ). Partial dehydrogenation and reversibility by rehydrogenation at 140 °C, 50 bar  $\text{H}_2$  for 12 h was observed due to the interaction between the hydride and PMMA (B and  $\text{OCH}_3$ , and Li with CO). The mechanism during rehydrogenation was also studied and the phases which were rehydrogenated were associated to  $\text{LiBH}_4$  and  $\text{H}_{(4-x)}\text{B}(\text{OCH}_3)_x$ .

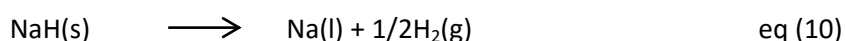
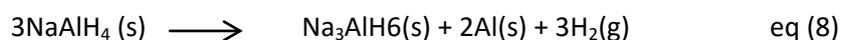
Ref.	Host	Surface properties ( $m^2/g\text{-}cm^3/g\text{-}nm$ )	Method of infiltration	LiBH <sub>4</sub> wt%	T <sub>p</sub> (°C)	Enthalpies (KJ/mol H <sub>2</sub> )	-E <sub>a</sub> (KJ/mol H <sub>2</sub> )
(Gross et al. 2008) (Y.Zhang, et al 2007) (Cahen et al. 2009) (Gosalawit-Utke et al. 2014) (Liu et al. 2010)(Liu et al. 2011) (Guo et al. 2013)	Bulk	-		100	415 400 445/470 495 473	-67	146
(Gross et al. 2008) (Vajo & Olson 2007)	CA1 CA2 AC graphite	770/0.80/13 810/1.38/25 1200/0.58/2 Non-porous	MI (280-300 °C)		381 390 375 453		103±4 111±2 - 146±3
(Liu et al. 2011)	Carbon templates	240-730/0.13-2.3/2-15	MI (300 °C, 60 bar, 30 min)	10/20	338-363		
(Gao et al. 2014)	Carbon	500/0.56	MI	20	340		
(Gao et al. 2012)	Carbon	500/0.65/2-3	MI (300 °C, 10 bar, 30 min)	20			
(Ngene et al. 2016)	Graphite HSAG-500	500/0.66/2-3	MI (295 °C, 100 bar, 30 min)	15-30	330		
(Ngene, et al. 2011)	Carbon HSAG-500+3-10%Ni	500/0.66/2-20	MI (295 °C, 100 bar, 30 min)	5-25	350	Out of scope	

<b>(Ngene, et al. 2010)</b>	Carbon HSAG-500+3.75%Ni vs graphite	500/0.66/2-20	MI (295 °C, 150 bar,30 min)	25-31	350		
<b>(Liu et al. 2010)</b>	Nanoporous carbon (NPC)	598/0.35/2	MI (300 °C, 60 bar, 30 min)	10	339		
<b>(Cahen et al. 2009)</b>	Carbon	1060/1.1/4	WI with MTBE as solvent	33-50	280	Not change	
<b>(Brun et al. 2010)</b>	Carbon_HIPE monolith	459-802/0.18-0.34/0.5	WI with MTBE 0.1M	30	270 -370 (MS analyses)	Largely modified	
<b>(Christian &amp; Aguey-Zinsou 2010)</b>	Carbon nanotubes (CNT)	Diameter=2nm	WI with THF	1.5±0.2	140		88±5
<b>(Y.Zhang, et al 2007)</b>	CMK-3		Milling (450 rpm, 5 h)	50	332	-40	
<b>(Ngene, et al. 2010)</b>	SBA-15	370/0.35/4.7 492/0.51/5 667/0.83/6.5	MI (295°C)	10-65	290 (10 wt%)- 390 (65 wt%)		
<b>(Guo et al. 2013)</b>	TiO <sub>2</sub> scaffolds	184/0.48/12	WI with THF	50	330-413		
<b>(Sun et al. 2011)</b>	Cu-MOF (HKUST-1)	738/2.38/0.9	WI with ether (good solubility LiBH in ether)	50	110 (MS) and Tonset=60 °C		
<b>(Gosalawit-Utke et al. 2014)</b>	PMMA		WI with THF vs milling	8.1	158		

Table 3. Review of LiBH<sub>4</sub> confined in a support

## NaAlH<sub>4</sub>

NaAlH<sub>4</sub> is one of the most investigated hydrides due to its high gravimetric content in hydrogen, which is released in 3 different steps. In the first two steps, the amount released is 3.7+1.8 wt% H<sub>2</sub>, which is released at 180 and 240 °C respectively. Step 3 (with an additional H<sub>2</sub> release of 1.8 wt%) occurs at temperatures higher than 425 °C, and for this reason this last step is usually not considered for hydrogen storage applications. The enthalpies for hydrogen release are 37, 47 and 56 KJ/mol H<sub>2</sub> respectively. This compound releases hydrogen above its melting point. Therefore melt infiltration is one of the most suitable methods to nanoconfine the hydride in the support.



However, high conditions of pressure and temperature or the use of a catalyst are necessary in order to rehydrogenate this compound. Nanoconfinement was also proposed with this complex hydride in order to enhance thermodynamics, kinetics and rehydrogenation conditions.

In general, nanoconfinement of NaAlH<sub>4</sub> in a support, which in most of the works reported is a carbon material, provided several advantages:

1) In most of the cases, the segregation of the phases was avoided in confinement and therefore the process was more reversible (Stephens et al. 2009)(Adelhelm et al. 2010)(Adelhelm et al. 2009)(Li et al. 2011). However, in (Paskevicius et al. 2016), nanoconfined samples had poor cyclability due to phase segregation or reaction between the hydride and the scaffold.

2) Reduction of the diffusion length and improvement of the contact between decomposed products made the rehydrogenation easier (Li et al. 2011). Stephens et al. successfully rehydrogenated the compound at 100 bar H<sub>2</sub> and 160 °C and in (Gao et al. 2010)(Adelhelm et al. 2010) at 155 °C and 55 bar H<sub>2</sub> for at least 4 cycles avoiding the formation of the stable intermediate Na<sub>3</sub>AlH<sub>6</sub>. Also the study of the influence of pressure and time during rehydrogenation was performed. (Li et al. 2011), rehydrogenated successfully at 70 bar H<sub>2</sub> and 150 °C for 2 h during 15 cycles (see figure 6). In (Paskevicius et al. 2016), the absorption of

hydrogen was performed at 100 bar H<sub>2</sub> and 160 °C for 10 h and for 2 cycles, observing the presence of the intermediate NaAlH<sub>6</sub> during rehydrogenation using in-situ powder X-ray diffraction (PXRD) technique. Also, this intermediate was observed by (Nielsen et al. 2012), who rehydrogenated the compound for 4 cycles at 89-92 bar and 160 °C for 10 h. The presence or absence of this intermediate indicated that the pathway followed in every case was different. Also, (Gao et al. 2014) studied the influence of different treatments in carbon scaffolds (thermal treatment under Ar (C\_Ar), or H<sub>2</sub> flow (C\_H), or after surface oxidation by HNO<sub>3</sub> (C\_O)) on reversibility at 55 bar H<sub>2</sub> and 155 °C for 12 h due to the reaction of the hydride with the different surface groups created (95% was reversible in C\_H, 89% in C\_Ar and only 66% in C\_O). In (Verkuijlen et al. 2010) the partial reversibility was studied by NMR due to large metallic Al and a possible oxidation of Na after the dehydrogenation was observed in melt-infiltrated samples. The shift and broadening profiles of confined samples were associated to a close contact of Na and Al atoms with the support material promoting a higher disorder in the material and a possible charge transfer to carbon. Also partial reversibility was found in confined systems at 55 bar H<sub>2</sub> and 150 °C for 10 h in contrast to the negligible reversibility of bulk NaAlH<sub>4</sub> (Gao et al. 2012). Increasing the pressure during rehydrogenation till 170 bar H<sub>2</sub> did not varied the amount of H<sub>2</sub> rehydrogenated, but the temperature played an important role. However, in (Pinkerton 2011) better kinetics of hydrogenation were obtained at higher pressure in the range 19.8-96 bar H<sub>2</sub> at 140 °C for 12 h. The biggest capacity loss occurred in the first cycle, and it was associated to the reaction of NaH and impurities of carbon on the surface. Reversibility was improved (93% reversible) in the case that Na was added with a ratio Na/Al=1.3; it seemed that the addition of Na was an efficient strategy to maintain the full H<sub>2</sub> cycling capacity (Gao et al. 2012). In (Pinkerton 2011) the weight loss after cycling was attributed to gradual oxidation by impurities in the gas flow due to long hydrogenation times. The lowest conditions reported to rehydrogenate NaAlH<sub>4</sub> was observed in (Xiong et al. 2012) confining the hydride in Ti\_OMC (ordered mesoporous carbons) and obtaining partial reversibility at 23 bar and room temperature due to the combined effects of nanoconfinement and a catalyst (TiO<sub>2</sub>). Different conditions of rehydrogenation were tested obtaining the highest hydrogenation capacity at 104 bar H<sub>2</sub>, 160 °C for 18 h. The capacity decreased due to agglomeration of Al and/or NaAlH<sub>4</sub> during cycling, but the compound exhibited an acceptable cycling stability (80% initial H<sub>2</sub> was released in the 11<sup>th</sup> cycle). However, the capacity was 2.31 wt%, much lower than the theoretical capacity (5.6 wt%), a result which could be due to the decomposition during infiltration (more pressure would be necessary to avoid this

phenomena) or incomplete reversibility due to the decomposition during melt infiltration (crystals of Al were observed).

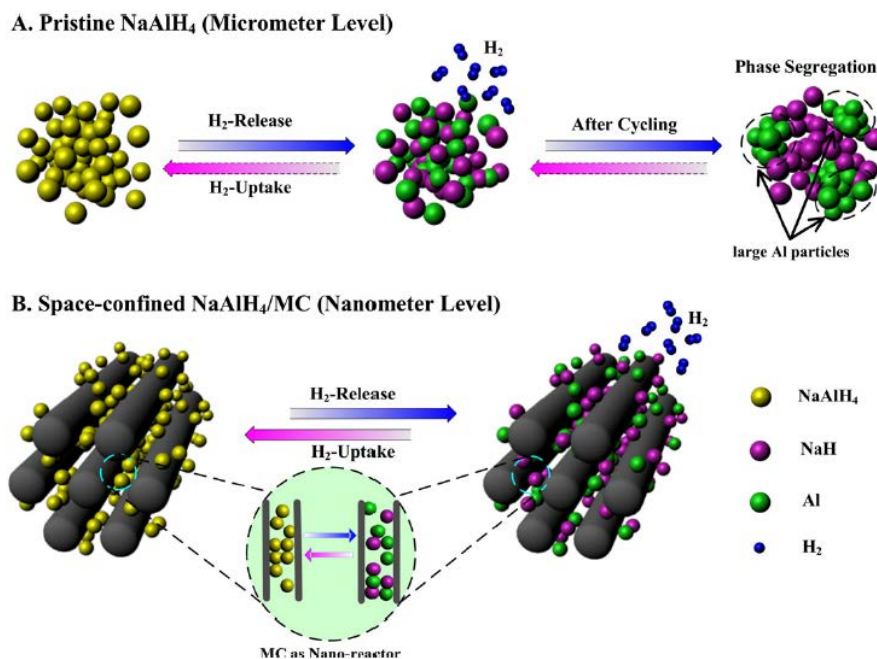


**Figure 6.** Phase distribution in pristine NaAlH<sub>4</sub> and the space-confined NaAlH<sub>4</sub>/MC upon multiple cycling.

Source: (Li et al. 2011)

3) If kinetic is enhanced without any catalyst, this improvement is related to the reduction in particle size. In (Stephens et al. 2009) kinetics and reversibility was improved in NaAlH<sub>4</sub>. In (Li et al. 2011), kinetic was also enhanced (induction time was suppressed) due to a synergetic effect of mesoporous carbon which acted not only as scaffold but also as catalyst, although the nanoconfinement effect was more pronounced than the effect of the catalyst. In this work, kinetic modeling studies suggested that one-dimensional nucleation and growth was the rate controlling step in the early stage, and the diffusion of the substance and the phase boundary migration were the rate-controlling steps in the late stage.

In (Paskevicius et al. 2016) rapid desorption kinetics were obtained in the first cycle but a slight degradation in further cycles was associated to reaction between scaffold and NaAlH<sub>4</sub> or nanoconfinement degradation. In (Pinkerton 2011) much better kinetics and higher desorbed H<sub>2</sub> for infiltrated and milled samples was observed. Activated carbon gave very similar results as ball milling with carbon aerogels, whereas in graphene and graphite samples only a small improvement in the dehydrogenation rate was obtained. Even a low concentration of activated carbon of 9.1 wt% resulted in an improvement on kinetics that could not be ascribed solely to nanoscale effect; also a catalyst effect should be taken into account. These authors

also performed some experiments with addition of 3 %mol  $\text{TiCl}_3$  improving the kinetics in contrast to bulk hydride. In the case of (Xiong et al. 2012),  $\text{TiO}_2$  showed a good catalytic effect, improving the kinetic in this way:  $\text{Ti-OMC} (T_{\text{onset}} < 60 \text{ }^\circ\text{C}) < \text{addition 3 \%mol TiO}_2 (T_{\text{onset}} = 100 \text{ }^\circ\text{C}) < \text{OMC}$ .

4) Decrease of decomposition temperature due to the reduction also of the particle size (Stephens et al. 2009)(Adelhelm et al. 2009)(Adelhelm et al. 2010), studying the influence of the concentration of the hydride in the surface on temperature decomposition (Adelhelm et al. 2009) and the influence of pore size, from 4 to 200 nm (Fan et al. 2013) (Nielsen et al. 2012). Differential Scanning Calorimetric (DSC) analyses showed a reduction in onset temperature as pore size decreased, more significantly when pore sizes were within 4 – 30 nm (Fan et al. 2013). The reduction in decomposition temperature in macropores was associated to a catalytic property of the carbon support (Fan et al. 2013). Also the influence of  $\text{CO}_2$  activation was studied in (Nielsen et al. 2014) with the same support and melt infiltration conditions than in (Fan et al. 2013). The activation resulted in higher surface area and higher volume of pores which meant higher amount of hydride confined. Moreover, increasing  $\text{CO}_2$  activation time promoted the decrease of reaction rate with higher stability during 4 cycles.

5) Pores smaller than 1-2 nm can change the thermodynamics of the process (Gao et al. 2010) (Lohstroh et al. 2010). The broad distribution of the thermodynamic properties (Lohstroh et al. 2010) may be due to the destabilization of the hydride by reduction of particle size since the free energy is influenced by size effects or due to the reaction in the voids of scaffolds forming new phases.

6) The presence of carbon changed the hydrogen release profile obtaining only one step of decomposition, independently of the size of the pores (Adelhelm et al. 2010), although obtaining better cyclic stability at lower pore size (Fan et al. 2013). In (Gao et al. 2010) the influence of surface properties was studied in the pathway of dehydrogenation of  $\text{NaAlH}_4$  obtaining only one step for nanoporous composite whereas in nonporous graphite two decomposition steps were observed as in the case of bulk  $\text{NaAlH}_4$ , due to the difference in the decomposition mechanism of NaH.

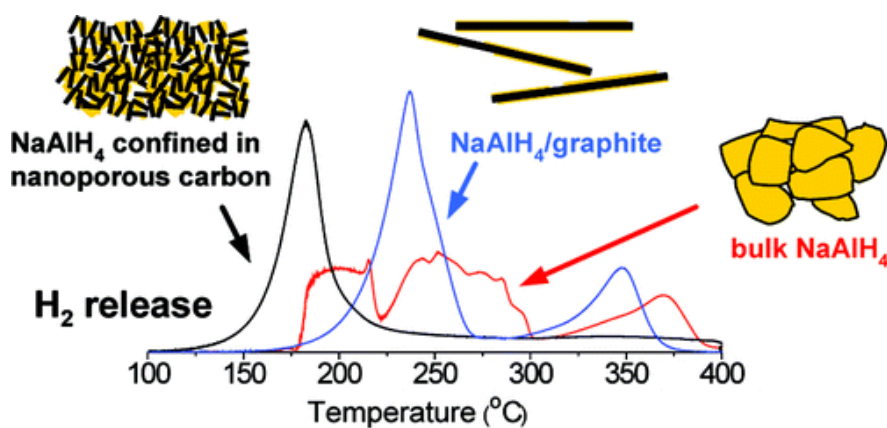


**Figure 7.** Influence of confinement of  $\text{NaAlH}_4$  in carbon on hydrogen release. Source: (Gao et al. 2010)

In (Adelhelm et al. 2010) the influence of the concentration of hydride was studied using the same support and conditions than (Gao et al. 2010). Till 20 wt%  $\text{NaAlH}_4$  could be infiltrated by melting in the pores whereas at higher concentrations, the hydride started to crystallize outside of the carbon. TPD analyses showed the improvement in the dehydrogenation after nanoconfinement, starting the release of  $\text{H}_2$  at 110 °C and releasing  $\text{H}_2$  in only 1 step.

In (Nielsen et al. 2011) the favorable synergic effect between nanoconfinement and catalytic Ti effect on dehydrogenation temperature was showed, which was drastically reduced. Rehydrogenation was also successful at 100 bar  $\text{H}_2$ , 160 °C for 10 h in contrast to bulk hydride. Authors considered this a promising technique which improved the amount loaded and avoided aggregates of Al in the surface. They suggested to apply melt infiltration in several steps and higher pressure to avoid decomposition of the hydride and formation of Al aggregates (also obtained in (Li et al. 2011)), and aerogels as supports in order to optimize volume of the pores. Another approach to obtain better surface properties was the activation of carbon aerogel with  $\text{CO}_2$  (Paskevicius et al. 2016) resulting in higher surface area and volume of pores.

In most of this works nanoconfinement was performed by melt infiltration, but also wet impregnation using THF as suitable solvent was proposed (Chumphongphan et al. 2014)(Balde et al. 2006)(Balde et al. 2008)(Schuth 2006).

In (Chumphongphan et al. 2014) the effect of the infiltration technique was studied, comparing wet and melt infiltration. In the case of melt infiltration, some crystals of Al and  $\text{NaAlH}_4$  were present due to partial decomposition (Al) or high loading ratio of hydride per scaffold which left the hydride excess outside of the pores. However, using wet impregnation, an amorphous spectra was obtained, and therefore more amount of  $\text{NaAlH}_4$  could be infiltrated in the pores

avoiding the decomposition of the hydride. In both cases, confined samples decomposed at lower temperature than bulk hydride.

A small amount of hydride (2-9 wt% NaAlH<sub>4</sub>) was impregnated in carbon nanofibers (Baldø et al. 2006)(Balde et al. 2008)(Christian & Aguey-Zinsou 2010) improving kinetics due to the nanosize effect and reabsorbing 26% (115 °C, 90 bar H<sub>2</sub>) due to the limited phase segregation (Baldø et al. 2006). Also, in (Balde et al. 2008) the influence of particle size of hydride varied (2-10 nm/19-30 nm/1-10 μm) by changing drying conditions was studied. As result, lower H<sub>2</sub> desorption temperature and lower E<sub>a</sub> was obtained for smallest particles due to the synergistic effects of size, reduction in diffusion paths and possible confinement effects. Even, in the case of the particles with size in the range 2-10 nm, the E<sub>a</sub> was lower than that of the system NaAlH<sub>4</sub> catalyzed with Ti. However, the limitation in this case was the slow concentration of hydride (only 2 wt%) which could be increased by encapsulating in nanocavities.

Other supports were tested to confine this complex hydride such as silica (Zheng et al. 2008) or MOFs (Bhakta et al. 2009)(Stavila et al. 2012)(Bhakta et al. 2012) using wet or melt infiltration as techniques to confine the hydride into the support. After confinement, similar results were observed. In (Zheng et al. 2008), 20 wt% of hydride was loaded via incipient impregnation in OMS (ordered mesoporous silica), as figure shows. The hydride was present in the scaffold as amorphous in contrast to crystalline peaks in milled samples. The decomposition of the impregnated sample occurred at a temperature 15 °C lower than that of the bulk hydride due to the destabilization when the size was reduced to nanoscale and the reduction of interdiffusion length. Kinetics at 150 °C and 180 °C were also improved, as it was the reversibility due to phase segregation was suppressed.

In (Bhakta et al. 2009) the hydride was confined in the MOF KHUST-1 by wet impregnation using THF as solvent, resulting in an improved dehydrogenation. The nanoscale hydride (<1.5 nm) decomposed at 100 °C less than the bulk compound. The decomposition started at 70 °C and was followed by different steps at higher temperatures. The same support and method of infiltration was used in (Bhakta et al. 2012), obtaining small particles (<2 nm) uniformly dispersed throughout the Cu-BTC support. Kinetics of decomposition was much faster than bulk hydride with dehydrogenation at lower temperature. Also the thermodynamic was different (13 °C lower in the melting temperature) which could be tuned by particle size. Regarding the pathway of decomposition was changed, 2 steps from bulk were converted into one producing nanoclusters of NaH+Al or NaAl, without the formation of the intermediate Na<sub>3</sub>AlH<sub>6</sub>.

In another work (Stavila et al. 2012),  $\text{NaAlH}_4$  was infiltrated in MOF(Mg) by melt infiltration which previously was impregnated with  $\text{TiCl}_4$ . The MOF destabilized the hydride, starting hydrogen release at 50 °C in contrast the temperature of 150 °C required with bulk hydride. At 200 °C, the bulk hydride released 2.5 wt%  $\text{H}_2$ , while confined samples released 4.5 wt%  $\text{H}_2$  which corresponded to almost full dehydrogenation to NaH. Similar results were obtained using Ti as catalyst in the first dehydrogenation. MOF doped without Ti had a limited reversibility (rehydrogenated at 105 bar  $\text{H}_2$  and 100 °C for 2h), whereas with Ti the compound was stable for 4 cycles desorbing 4.1, 3.9, 3.7 and 3.6 wt%  $\text{H}_2$  respectively. Also the pathway was changed: in confined samples dehydrogenation took place in only one step without the formation of intermediate phases and most of the Al and NaH was converted into  $\text{NaAlH}_4$ .

Ref.	Host	Surface properties (m <sup>2</sup> /g-cm <sup>3</sup> /g-nm)	Method of infiltration	NaAlH <sub>4</sub> wt%	T <sub>p</sub> (°C)	Enthalpies (KJ/mol H <sub>2</sub> )	-E <sub>a</sub> (KJ/mol H <sub>2</sub> )
(Grochala et al 2004) (Zheng et al. 2008) (Adelhelm et al. 2009) (Nielsen et al. 2011) (Li et al. 2011) (Fan et al. 2013) (Stavila et al. 2012) (Bhakta et al. 2012)	Bulk			100	247 240/275	-60 -56 -37/-47/-56	118-132 115-130/155 79.5
(Adelhelm et al. 2010)	HSAG-500 KS-6	500/0.65/2-3 20/0.07/-	MI (200 °C, 200 bar, 15min)	5-40	180		
(Adelhelm et al. 2009)	HSAG-500	500/0.66/-	MI (not reveled conditions) vs milling	10-40	<200		
(Li et al. 2011)	Mesoporous carbon (MC)	801/1/4	MI (178 °C, 30 bar,10 min)	26			46±5
(Paskevicius et al. 2016)	CO <sub>2</sub> activated carbon aerogels (3) with Ti (7.5-8 wt%)	900-1800/1.2-2/-	MI( 189 °C, 200 bar, 15 min) vs ball milling	40-50			

<b>(Gao et al. 2010)</b>	HSAG-500 KS-6	500/0.65/2-3 20/0.07	MI(180 °C,180-190 bar)	5-80	<200 (till 20wt%)		
<b>(Nielsen et al. 2012)</b>	Carbon aerogel	584-718/0.26- 1.39/10	MI (189 °C, 210-230 bar,15 min)	13-42	146-162 (f pore size)		
<b>(Gao et al. 2014)</b>	Carbon with different surface modifications	450-500/0.5-0.6/-	MI	20	~180	-9-(-80)	
<b>(Gao et al. 2012)</b>	Carbon	500/0.65/2-3	MI(180 °C, 170 bar, 15 min)	20			
<b>(Pinkerton 2011)</b>	Carbon aerogel vs AC vs graphene	746/0.84/13 942/0.71	MI (204 °C, 278 bar, 4 h) vs ball milling 1 h	53			
<b>(Xiong et al. 2012)</b>	Ti_OMC	427/0.34/4-5	MI(185 °C,142 bar,1 h)				
<b>(Stephens et al. 2009)</b>	Carbon aerogel	-/0.8/13	MI (189 °C, 183 bar,8-10 h) vs milling	48.6			
<b>(Fan et al. 2013)</b>	Carbon	-/-/4-200	MI (184 °C, 140-150 bar, 15 min)	70-85	150-200 (depending on pore size)		69.7 (4 nm)/84.9 (30 nm)
<b>(Nielsen et al. 2014)</b>	Activated carbon aerogel	700-2040/0.9- 2.2/8-10	MI (189 °C, 210- 230bar,15min)	34-57	147-184 (depending on time CO <sub>2</sub> activation)		
<b>(Lohstroh et al. 2010)</b>	Activated carbon nanofiber (ACF)	1815/0.66/<4	MI (190 °C, 160 bar, 1 h)	30-50			

<b>(Nielsen et al. 2011)</b>	Carbon aerogel+3 wt% Ti	735/1.26/17	MI (189 °C, 199 bar)	33.3	125-180		
<b>(Chumphongphan et al. 2014)</b>	CMK-1	-	WI with THF vs MI (185 °C, 125 bar, 15 min)	20-50	<200		
<b>(Baldø et al. 2006)</b>	Carbon nanofibers	-	WI using THF	9			116
<b>(Balde et al. 2008)</b> <b>(Christian &amp; Aguey-Zinsou 2010)</b>	Carbon nanofibers(CNF)	130/-/1-30	WI with THF	2-9			58-118 (depending on pore size)
<b>(Zheng et al. 2008)</b>	Ordered Mesoporous Silica (OMS)	-/-/10nm	WI with THF	20	225/265		
<b>(Bhakta et al. 2009)</b>	MOF KHUST-1	-	WI with THF	4	<200		53
<b>(Stavila et al. 2012)</b>	MOF(Mg)+3%mol Ti	1530/0.6/-	MI(195 °C, 250 bar, 2 h)	21			57.4
<b>(Bhakta et al. 2012)</b>	MOF(Cu_BTC = HKUST-1)	1460/-/-	WI with THF	4.1	130-155	-47.3 (7 units higher than bulk)	53.3

*Table 4. Review of NaAlH<sub>4</sub> confined in a support*

## MgH<sub>2</sub>

Magnesium (Mg) is a cheap and abundant material, with high theoretical gravimetric (7.6 wt%) and volumetric (110 g/L) density of hydrogen, and good reversibility (Mg /MgH<sub>2</sub>) (Konarova et al. 2011), making it suitable for large-scale hydrogen storage application.

However, its use is hampered by slow kinetics and unfavorable thermodynamics. Some other problems are related to the possible passivation by formation of an oxide layer surrounding the metal, which slows down the kinetics. Also, the diffusion constant of hydrogen atoms is much smaller in MgH<sub>2</sub> than in Mg. Thus, by hydrogenation, the initial formation of MgH<sub>2</sub> occurs as a fast process, but during it a shell near the surface hydride encloses the metal and decreases the hydrogen kinetics and reduces the reversible hydrogen storage upon cycling (Nielsen et al. 2009).

Moreover, direct incorporation of Mg (or MgH<sub>2</sub>) into an aerogel scaffold is difficult due to the lack of wetting of Mg on carbon surfaces and solution infiltration is also infeasible due to the low solubility of Mg and MgH<sub>2</sub> in conventional solvents (Zhang et al. 2009). Because of this, it is necessary to find other methods in order to infiltrate this hydride. One of the alternatives that have been explored is the impregnation of a precursor of Mg in the scaffold which is then converted into MgH<sub>2</sub> (Nielsen et al. 2009) (Paskevicius et al. 2011) (Liu et al. 2013) (Zhang et al. 2009) (Konarova et al. 2011) (Konarova et al. 2012) (Konarova et al. 2013) (Zhao-Karger et al. 2010) (Jeon et al. 2011).

One of the most investigated hosts with this hydride was carbon aerogels (CA) (Nielsen et al. 2009) (Gross et al. 2009) (Paskevicius et al. 2011) (Liu et al. 2013), getting loadings lower than 20 wt% MgH<sub>2</sub> in all the studies. The carbon aerogel served for two purposes: first, it provided an array of discrete sites where the MgH<sub>2</sub> particles could form, and second, these sites were separated by a carbon framework that restricted the growth of the MgH<sub>2</sub> particles (Paskevicius et al. 2011). In this work, confined samples had slower kinetics than ball milled, possibly due to the high content of carbon.

In (Nielsen et al. 2009) the influence of surface properties on the final thermodynamic and kinetic properties of the hydride after nanoconfinement was studied. Faster kinetics and lower desorption temperature were obtained with the CA with lower pore size and therefore lower average size of MgH<sub>2</sub>. However, no thermodynamic changes were observed because pore sizes were higher than 2 nm in both supports. On the other hand, 81% MgH<sub>2</sub> was reversibly released after confinement.

The influence of decorated CA with Ni or Cu (1-6 wt%) was studied (Gross et al. 2009). Thermodynamic properties did not change because Mg nanoparticles were bigger than 1.3 nm (this is the maximum calculated diameter size to have improvement effects on the thermodynamic properties). The best results were obtained in nanoconfined samples with Ni\_CA, followed by Cu\_CA and CA. Also MgH<sub>2</sub> milled with carbon was compared with confined samples, obtaining 20-fold faster dehydrogenations in the latter samples.

Results showed that thermodynamic properties of confined Mg nanoparticles were promoted and the 'nanosize effect' played a key role in reducing the thermodynamic stability of MgH<sub>2</sub>. The other main reason was that the larger ratio of surface atoms in confined samples enhanced the diffusion of hydrogen into the grains of Mg. Additionally, the absorption kinetics of Mg was significantly improved by the reduction in particle size (Liu et al. 2013).

Granular carbon was used in (Zhang et al. 2009), improving the dehydrogenation rate by 5 times after confinement in contrast to ball milled samples. A similar enhancement by a factor of 4 was observed in (Zhao-Karger et al. 2010). Moreover, it was checked that nanoconfinement avoided aggregation for 10 cycles, during which 12 wt% MgH<sub>2</sub> was reversible without variation in kinetics.

The influence of the conditions to convert the precursor of Mg into MgH<sub>2</sub> was also investigated (Konarova et al. 2011)(Konarova et al. 2012). In (Konarova et al. 2011), the influence of time during decomposition of precursor was analyzed, obtaining the lowest decomposition temperature for 4 h. Moreover, the influence of pressure of hydrogen in the range 20-60 bar and temperature (200-250 °C) was studied in (Konarova et al. 2012). In this case, the best kinetics and decomposition temperature were obtained at 220 °C.

The confinement in silica supports (SBA-15) in contrast to carbon host (CMK-3) was studied in (Konarova et al. 2013). MgO species were detected in SBA samples revealing the formation of Mg-O-Si bonds through the interaction of Mg with SiOSi or SiOH, which indicated the non compatibility of this host with Mg. Also, the study of the effect of loading of Mg (20-80 wt%) in CMK-3 was analyzed. Lower decomposition temperatures with lower enthalpy and entropy were obtained for samples with lower loadings, suggesting that excess MgH<sub>2</sub> particles with high particle size may be deposited on the surface at loadings higher than 20%. The kinetics was faster than in (Zhang et al. 2009) which could be due to the loading of MgH<sub>2</sub> in the carbon template which played an important role.

Another method to confine MgH<sub>2</sub> in the support was melt infiltration of Mg followed by the hydrogenation of the metal, modifying the surface of the carbon with N or O in order to improve the wetting, as in (De Jongh et al. 2007). This was the first report of nonoxidized particles of Mg successfully confined. Moreover, authors could investigate the 'critical loading' below which no bulk Mg was detected, which was 5-10 wt% for mesoporous carbon and 15-20 wt% in microporous activated carbon, obtaining higher pore filling in the host with smaller pores sizes.

In (Paskevicius et al. 2010) MgH<sub>2</sub> was synthesized according to the equation (11) using LiCl as reaction buffer that restricted the particle growth and promoted nanoparticle formation.



Decomposition temperature and enthalpy was slightly reduced, while kinetics were slower. Therefore, although the mechanochemical synthesis of MgH<sub>2</sub> was a suitable method for producing nanosized, the minor thermodynamic improvements did not justify the added level of synthesis complexity or the hydrogen density penalties for its use as a hydrogen storage solution.

Also a polymer (PMMA) was used as host (Jeon et al. 2011), which could be loaded with 61 wt% Mg. This polymer avoided the formation of a layer of MgO: only a small amount of MgO and Mg(OH)<sub>2</sub> was detected by XRD after 2 weeks. Therefore it was demonstrated that this was a good possibility to achieve stability against air oxidation, preserving the properties for at least 3 cycles. Moreover, authors developed a theoretical model of hydrogenation in which atoms of hydrogen nucleated and accumulated along the material defects and formed a metal hydride (MgH<sub>2</sub>) layer in one dimension, followed by growth and thickening from the metallic core.

Ref.	Host	Surface properties ( $\text{m}^2/\text{g}\text{-cm}^3/\text{g}\text{-nm}$ )	Method of infiltration	MgH <sub>2</sub> wt%	T <sub>p</sub> (°C)	Enthalpies (KJ/mol H <sub>2</sub> )	-E <sub>a</sub> (KJ/mol H <sub>2</sub> )
(Paskevicius et al. 2010) (Liu et al. 2013) (Jeon et al. 2011) (Klimkowicz et al. 2015)	Bulk			100	390/440	-74.06±0.42 -74.7 -75.7±1.1	100 (Mg) 195.3±10 (MgH <sub>2</sub> )
(Nielsen et al. 2009)	CA monolith	723/1.27/22 686/0.65/7	WI with MgBu <sub>2</sub> in heptane+hydrogenation 157 °C/50 bar vs BM	18.2 10	385 368 515(BM)		
(Gross et al. 2009)	CA and Ni_CA/C u_CA	-/0.8/2-30	MI Mg at 700 °C/24 h vs BM	15.6			
(Paskevicius et al. 2011)	CA	-/1.3/1-6	WI with MgBu <sub>2</sub> in heptane vs BM				
(Liu et al. 2013)	CA	1267/1.3/19	WI with MgBu <sub>2</sub>	22.5		-65.1±1.56	29.4 (Mg/CA)
(Zhang et al. 2009)	Granular carbon	-/0.8/13	WI with MgBu <sub>2</sub> +hydrogenation 170 °C/50-55 bar/24 h vs BM	14.8			
(Konarova et al. 2011)	C	-	WI with MgBu <sub>2</sub> +hydrogenation 250 °C/20 bar/30 min/4 h vs BM	90	325 378		

<b>(Konarova et al. 2012)</b>	C	-	WI with MgBu <sub>2</sub> +hydrogenation 200-250 °C/20-60 bar/4 h	95-99	318/364		
<b>(Konarova et al. 2013)</b>	SBA-15 CMK-3	1352/1.4/3.5	WI with MgBu <sub>2</sub> +hydrogenation 250 °C/20 bar vs Decomposition MgBu <sub>2</sub> at 60 bar	20-80	367 253-358(f %MgH <sub>2</sub> ) 395	-52.38±2.16	
<b>(De Jongh et al. 2007)</b>	C	Different supports (micro/meso/with or without O)	MI Mg (625 °C/10 min)	33			
<b>(Paskevicius et al. 2010)</b>	LiCl	salt	Milling LiH+MgCl <sub>2</sub> to form MgH <sub>2</sub> in LiCl			-71.22±0.49	
<b>(Zhao-Karger et al. 2010)</b>	Activated Carbon Fiber	1820/0.79/0.5-3	WI with MgBu <sub>2</sub> vs BM with graphite	22	325 418 (BM)	-63.8±0.5	142.8±2 165.3±14(BM)
<b>(Jeon et al. 2011)</b>	PMMA	Polymer	WI with Cp <sub>2</sub> Mg In THF solution	61			24.5 (absorption) 79.5 (desorption)

BM: ball milling, C: carbon host

Table 5. Review of MgH<sub>2</sub> confined in a support

## CaBH<sub>4</sub>

CaBH<sub>4</sub> is one of the most promising hydrides, with 11.6 wt% of hydrogen and low reaction enthalpy (32 KJ/mol H<sub>2</sub>). However, the high decomposition temperature and the slow kinetics are important disadvantages. In this case, just one study has been performed using confinement as suitable technique to overcome these limitations.

In (Ampoumogli et al. 2012), CaBH<sub>4</sub> was infiltrated in CMK-3 (1320 m<sup>2</sup>/g, 1.48 cm<sup>3</sup>/g, 3-5 nm) by wet impregnation using liquid ammonia, filling 70 %vol of the pores. As a result, a reduction of surface area and volume of pores (microporous and mesoporous) by a factor of 4 was observed. Calorimetric analyses showed an improvement during the decomposition after confinement. Bulk CaBH<sub>4</sub> released hydrogen at T<sub>p</sub>= 380 °C and 447 °C whereas after confinement the decomposed material was transformed into a multi-featured pattern pointed out a different pathway. A shift of almost 100 °C was observed, as the material started to release H<sub>2</sub> at 150 °C in contrast to 300 °C in bulk hydride. When TiCl<sub>3</sub> was added as catalyst, the decomposition was shifted to even lower temperatures. This could be associated to the reaction between Ti and B or its derivative which weakend B-H or B-B bonds during the decomposition process, although the exact details are still unclear and should be studied more deeply.

## NaBH<sub>4</sub>

NaBH<sub>4</sub> has a high content in H<sub>2</sub> (10.8 wt%) but high temperatures are necessary to release it (>500 °C). Moreover, it is not reversible at moderate conditions of pressure and temperature, which limits its applications in the bulk form. It has been proved that ball milling is not an appropriate technique for this hydride due to its high stability and the heavy deformation conditions caused by milling (Varin & Chiu 2005).

However, nanoconfinement of this hydride in carbon supports, confirmed by decrease of the surface area of the support, enhanced the decomposition process, lowering the temperature to release hydrogen and improved the reversibility, as presented in the table (Ampoumogli et al. 2011)(Ngene, van den Berg, et al. 2011) (Chong et al. 2015).

In (Ngene, van den Berg, et al. 2011), two different methods of nanoconfinement (wet and melt infiltration) were compared in contrast to a simple physical mixing. The lowest decomposition temperature was obtained in samples prepared by wet impregnation, followed by melt infiltration and physical mixture. This difference suggested the presence of different

sizes due to different interaction of carbon with molten  $\text{NaBH}_4$  and the solution. The small difference in the hydrogen released in the first desorption could be due to a possible oxidation or partial decomposition during synthesis and handling. The most promising result was the successful reversibility (rehydrogenation done at 325 °C, 60 bar  $\text{H}_2$  for 5 h) in nanoconfined samples (43% reversibility) in contrast to bulk  $\text{NaBH}_4$ .

XRD and NMR results confirmed the difference in the decomposition pathway between bulk and nanoconfined samples: in the case of bulk samples, crystalline Na after dehydrogenation and amorphous  $\text{Na}_{12}\text{B}_{12}\text{H}_{12}$  were rehydrogenated into crystalline Na, NaH and amorphous  $\text{Na}_{12}\text{B}_{12}\text{H}_{12}$ , while with nanoconfined samples, only crystalline carbon and  $\text{NaBO}_2$  plus amorphous  $\text{Na}_{12}\text{B}_{12}\text{H}_{12}$  and  $\text{NaBH}_4$  were found after rehydrogenation. Therefore the barrier to reversibility in bulk  $\text{NaBH}_4$  was not due to the stability of  $\text{Na}_{12}\text{B}_{12}\text{H}_{12}$  but rather due to the inability of NaH and  $\text{Na}_{12}\text{B}_{12}\text{H}_{12}$  to react with hydrogen to form  $\text{NaBH}_4$  at moderate conditions because of phase separation and poor kinetics of solid-state diffusion. These problems could be avoided in nanoconfined samples.

In (Chong et al. 2015), nanoparticles of  $\text{NaBH}_4$  with sizes ranging from 2 to 16 nm were 'wrapped' in graphene using wet chemistry. Decomposition temperature was shifted to lower temperatures than in previous works, with faster rehydrogenations (by a factor of 2) at similar conditions and higher cyclability (6 cycles) in nanoconfined samples than in milled samples. After rehydrogenation, nanoparticles of  $\text{NaBH}_4$  were wrapped by thin graphene sheets in a spherical shape of 45.6 nm. In contrast, in ball milled samples after the dehydrogenation–rehydrogenation cycle, nanoparticles showed irregular shapes and were distributed throughout the flake-like thick graphene layers. Due to this, encapsulating the hydride in graphene resulted in shorter hydrogen diffusion path modifying the decomposition into Na, B and  $\text{H}_2$  with only traces of  $\text{Na}_2\text{B}_{12}\text{H}_{12}$ , preventing the agglomeration, separation or seepage during cycling.

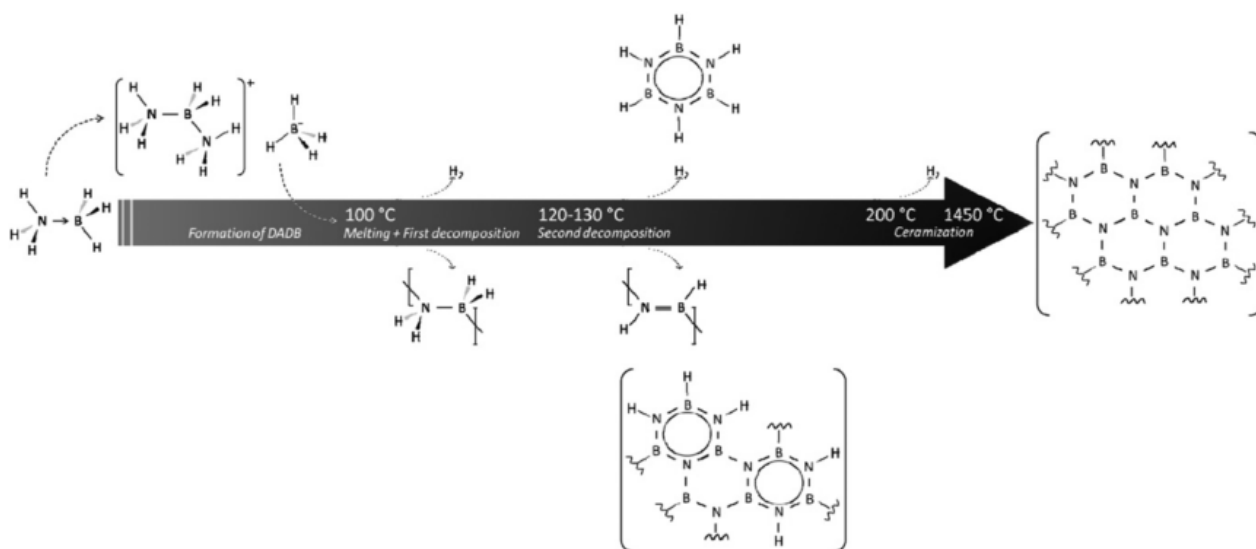
Ref.	Host	Surface properties (m <sup>2</sup> /g-cm <sup>3</sup> /g-nm)	Method of infiltration	NaBH <sub>4</sub> wt%	Ton (°C)	Tmax (°C)	1 <sup>st</sup> des (wt%)	3 <sup>rd</sup> des (wt%)
(Ngene et al. 2011)	Bulk	-	-	100	473	515	8.1 (600 °C)	0.9 (325°C_60bar,5h)
(Ngene et al. 2011)	Carbon	7	Mixing	25	320	500	8.1 (600 °C)	~3(325°C_60bar,5h)
(Ngene et al. 2011)	Carbon	500/0.66/2	MI (520 °C,5 bar,25 min)	25	300	450	7.9 (500 °C)	~3
(Ngene, van den Berg, et al. 2011)	Carbon	500/0.66/2	WI (water pH=13)	25	250	350	6.7 (450 °C)	~3
(Chong et al. 2015)	graphene	-	BM	75	113	412	6.3	6.1(350 °C,40 bar,6 h)
(Chong et al. 2015)	graphene	-	WI (n-propylamine)	75	40	350	7.0	7.1
(Ampoumogli et al. 2011)	CMK-3	1500/15/3.5	WI (NH <sub>3</sub> )	20	235	380		Under investigation

Table 6. Review of NaBH<sub>4</sub> confined in a support

## Ammonia borane (AB)

Ammonia borane (AB) has attracted attention due to its high  $H_2$  content (19.6 wt%), stability at room temperature, release of hydrogen under moderate conditions in 3 steps (6.5 wt% in every step), low molecular mass (30.7 g/mol) and non-toxicity.

The first equivalent of hydrogen desorbs between 100 and 120 °C (depending on heating rate) to yield polyaminoborane  $(BH_2NH_2)_x$ . The reaction is moderately exothermic (-21 kJ/mol). Increasing the temperature till 150 °C releases the second equivalent of hydrogen to yield polyiminoborane  $(BHNH)_x$  and trace quantities of borazine. However, below 100 °C the kinetic is slow and the emission of poisonous byproducts (borazine, ammonia and diborane) during decomposition process could be harmful for the fuel cell. According to (Moussa et al. 2012), the proposed decomposition mechanism is the following:



**Figure 8.** Reaction paths during the thermal decomposition of ammonia borane. Source: (Moussa et al. 2012)

In order to improve kinetics, thermodynamics and reduce the amount of non desired volatile gases, among others, nanoconfinement AB in a support was proposed as a solution by several authors. According to (Jongh & Adelhelm. 2010), the host choice depends on:

**Lightness:** a compromise has to be found to obtain a composite host, having a material-based with enough hydrogen density.

**High porosity/specific surface area:** the more porous the host, the more confined the AB would be; tuning the porosity range (micro to macro) should have an effect on the nanoconfinement.

Inertness (toward AB): it is imperative that the host does not irreversibly react with AB to form materials with no interest in hydrogen storage; nevertheless, if it offers functional groups that may facilitate H<sub>2</sub> release, this criterion may be disregarded.

Low cost: this is for evident reasons of technological applications and commercialization.

Abundance: it is important not to be short of resources.

To these requirements, (Moussa et al. 2012) adds renewability, a green criterion.

Different hosts have been tested, mainly carbon, silica supports (Autrey et al. 2004)(Gutowska et al. 2005)(Lai et al. 2012)(Paolone et al. 2009)(Wang et al. 2009) and also some metal organic frameworks (MOF) (Gadipelli et al. 2011)(Z. Li et al. 2010)(Zhong et al. 2011).

- Regarding **mesoporous silica supports**, 50 wt% AB was confined by wet impregnation using MeOH or THF as solvent (see table). Two different silica supports have been tested, SBA-15 (Autrey et al. 2004)(Gutowska et al. 2005)(Lai et al. 2012) and MCM-41(Lai et al. 2012)(Paolone et al. 2009)(Wang et al. 2009), with surface areas around 1000 m<sup>2</sup>/g and a volume of pores in the range 0.8-1.2 cm<sup>3</sup>/g.

In the case of using SBA-15, the scaffold allowed controlling the dehydropolymerization of AB and as result, the following improvements were observed:

1. Suppression of formation of borazine (Autrey et al. 2004)(Gutowska et al. 2005).
2. Lower decomposition temperature (T<100°C) (Autrey et al. 2004).
3. Lowered activation energy to release H<sub>2</sub>, estimated in (Gutowska et al. 2005).
4. Modification of the enthalpy which could be explained by the different non-volatile products (Gutowska et al. 2005).
5. Faster decomposition kinetic (Gutowska et al. 2005). This could be explained by the defect sites that initiate the dehydropolymerization at lower temperature, and by interfacial catalysis by Si-OH groups which could result in catalysis for the thermolysis of AB and control the product distribution.

When MCM-41 was used as support, anelastic spectroscopy and DCS analyses were done to evaluate the changes in the physical properties of AB embedded in silica (Paolone et al. 2009). Nanoscaffolding was able to prevent the structural phase transition that was observed in bulk AB. In (Wang et al. 2009), hyperpolarized Xe NMR was used to probe the change in the porosity of the mesoporous support adding AB (from 33 to 75 wt%), because BET did not

provide reliable results for all AB-coated MCM samples because a relatively high vapor pressure of AB prevented accurate measurements.

- With 33 wt% AB, all AB was infused into mesopores channels, suggesting that a fraction of the surface area had a coating more than one monolayer thick.
- 50 wt% AB started to be deposited outside channels.
- With 75 wt%AB, more AB was deposited outside, partially blocking mesopores. It was necessary to remark that it was not observed a difference between 50 wt% and 75 wt%AB in BET analyses.

Thus, authors suggested that 22 wt% of AB was the optimum loading to reach an ideal single monolayer coating of AB inside the mesopores channels of this support, MCM-41, assuming uniform coating on all surfaces. These results suggested that the more AB was exposed to the silica surface, the lower was the temperature needed to release hydrogen.

In (Lai et al. 2012), the differences of nanoconfinement using SBA-15 or MCM-41 were studied. In both cases, the temperature of decomposition was lower and the total exothermic enthalpy was higher after nanoconfinement due to the larger degree of intermolecular hydrogen bonding of neat AB. The amount of borazine and diborane was lower after confinement in SBA-15 than in MCM-41, whereas the amount of ammonia was higher in confined samples in SBA-15 than in MCM-41 and bulk AB. This was explained by the different mechanism that was followed to release hydrogen in confined systems in contrast to neat AB. MCM-41 released less borazine and diborane but more ammonia due to lower pore sizes and higher surface area to form smaller particles and therefore higher contact between O (Lewis base) from silica and  $BH_3$  (Lewis acid) from AB.

- Regarding **MOFs**, different supports have been tested. Only 8 wt% was infiltrated in JUC-32 (Z. Li et al. 2010) due to the low volume of pores which were almost blocked after filling with AB, whereas up to 26 wt%AB was nanoconfined in Mg-MOF-74 (Gadipelli et al. 2011). This was the first trial done with MOF (Z. Li et al. 2010), in which improved thermal release of hydrogen was obtained. It was the lowest decomposition temperature observed up to now comparing with the rest of supports. Authors also observed the suppression of formation of volatile gases by the synergistic effect of nanoconfinement and catalyst (metal  $Y^{3+}$ ). On the other hand, the influence of higher amount of AB confined in the proposed MOF was studied in (Gadipelli et al. 2011). Lower loadings of AB resulted in lower decomposition temperatures, faster kinetics without induction time and suppression of volatile byproducts. In

the composite, it could be that N-B and B-H bonds were weakened, which could lead to enhanced desorption kinetics as well as a decrease of dehydrogenation temperature. In (Zhong et al. 2011) the zeolite ZIF-8 was tested due to its stability, robustness and commerciability. In this case, more AB was confined, till 50 wt%. However, no improvement was observed in contrast to a simple mixing of AB and ZIF-8. It is noticeable, than in both cases (mixing and confined samples) better kinetics without induction time, reduction of volatile gases and lower temperature of decomposition were obtained. This was explained because ZIF-8 acted as a catalyst.

- The most studied support was **carbon** host: carbon cryogels (CC), mesoporous carbon supports (CMK-3) or carbon nanotubes (CNT) were some of the materials tested. In general, after confinement, thermodynamics and kinetics of decomposition of AB were enhanced, reducing or even suppressing the amount of borazine released during the decomposition. Different explanations and studies have been performed.

In (Feaver et al. 2007), the improvement in the decomposition after confinement was explained by the smaller size of AB. Nanocrystalline AB had larger surface energy, destabilizing hydrogen bonding network of AB and lowering the barrier to release it (Sepehri et al. 2008). Also, the dangling bonds of the inner surface of the carbon cryogel, having intimate contact with the AB, exerted catalytic influence on the dehydrogenation of AB or at least served as the initial nucleation site for the phase transition of AB leading to hydrogen release (Feaver et al. 2007).

The improvement in the dehydrogenation was explained as follows (Sepehri et al. 2007):

1. Hydroxyl groups on the surface of CC catalyzed the thermolysis of AB.
2. Defect sites in the CC mesoporous scaffold, possibly in combination with the hydroxyl groups, initiated the reaction at lower temperature.
3. Limited diffusion of AB provided by the CC mesoporous structure increased the frequency of interactions, effectively accelerating the dehydrogenation process.
4. Surface interaction destabilized the hydrogen bonding network of neat AB, resulting in a lower barrier to hydrogen release.

In (Sepehri et al. 2009) the modification of CC with B and N was studied. Lower dehydrogenation temperature and faster kinetics were observed in modified carbon because of larger surface energy and further destabilization as a result of surface modification. The lower activation energy and dehydrogenation by the presence of B and the excess of OH

groups on the surface of BN\_CC provided surface interactions that disrupted the dihydrogen bonding in AB, lowering the induction time and the barrier to release hydrogen.

In (Li et al. 2009) the addition of Li to the mesoporous carbon CMK-3 was studied. Without any additive, CMK-3 acidity and the functional groups of OH and COOH played an important role in the dehydrogenation and decomposition pathway, as they interacted easily with B-H bonds of AB. The mechanism proposed in this work (figure 9) can explain the enhancement of dehydrogenation, a large amount of  $\text{NH}_3$  that was released and the suppression of borazine. When Li was added, ammonia and borazine was suppressed completely. Also, the catalytic effect of Li-based catalyst with the confinement resulted in further acceleration of the kinetics, starting to release hydrogen at 55 °C.

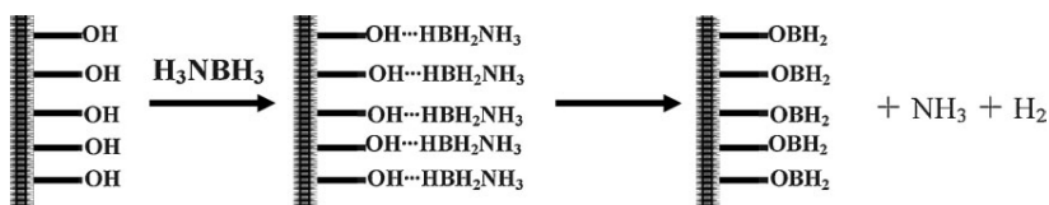


**Figure 9.** The mechanism of hydrogen release of AB/CMK-3 nanocomposite. Source: (Li et al. 2009)

In (Moussa et al. 2012), similar results were obtained. In this case, AB confined in activated carbon (AC) was compared with milling process (see table 7). It was observed that during release of hydrogen, foaming and expansion process was avoided in the composite in contrast to bulk AB. Better thermodecomposition results (no induction time, without formation of borazine) after confinement due to OH and COO groups resulted in release of hydrogen at milder conditions, even at room temperature which could be a problem to store for long time. According to this work, the dehydrogenation of AB in AC was followed by 2 simultaneous pathways, as figure 10 shows:

- 1) Acid base reaction between COOH and  $\text{BH}_3$ , forming an intermediate (see figure 10) , with B-O bond which acted as dehydrocoupling germ and helped to explain the  $\text{H}_2$  evolution at room temperature.
- 2) Typical thermolytic decomposition.

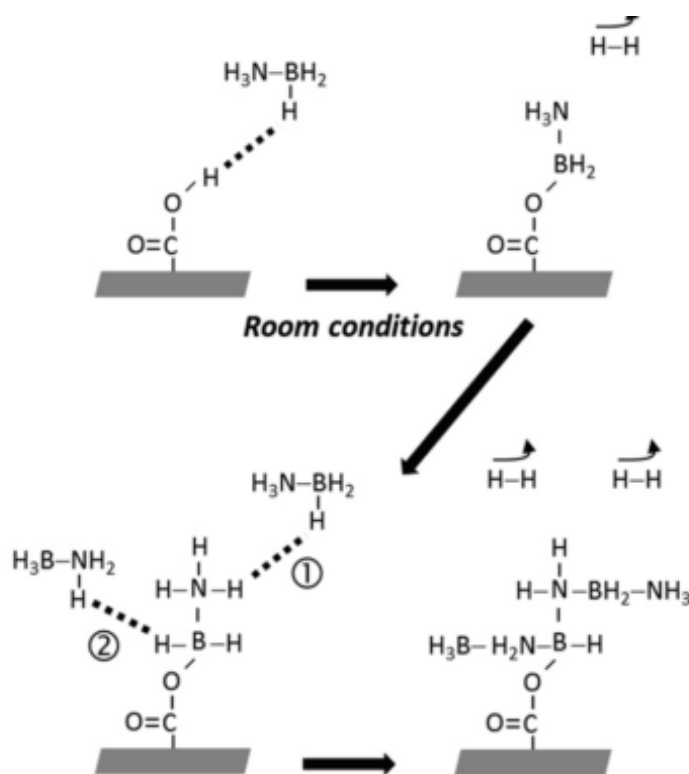


**Figure 10.** Acid catalysis of the carboxyl groups of AC. Source: (Moussa et al. 2012)

In (Sepahri et al. 2008), the influence of the pore size (7,9 and 16 nm) in the carbon support was studied. Dehydrogenation temperature and activation energy was lower in nanoconfined samples than in neat AB, decreasing the values with pore size. The host acted as an agent, reducing hydrogen diffusion distances, increasing the frequency of reaction and accelerating the dehydrogenation.

In (S. F. Li et al. 2010) AB was incorporated into 10 wt%Pt-functionalized carbon nanotubes (Pt\_CNT) milled, then put in an ice water under  $\text{NH}_3$  flow and by ultrasonic treatment AB was impregnated into the channels by capillary forces. With this method, no solvent was used, and the load was controllable and uniform. Analyses showed that the majority of the pores were impregnated with AB but excess AB formed layers outside the scaffold. As result, lower dehydrogenation temperature (see table 7) was tested after milling due to only a catalytic effect. For confined samples, further improvement in the kinetics without induction time and foaming process, decreasing the amount of byproducts during decomposition was observed. These improvement were associated to the synergetic effects of CNT, nanoparticles of Pt as catalyst and nanoconfinement.

- Also the influence of Polymethyl Acrylate (PMMA) was studied in (Alipour et al. 2015), obtaining better results in the sample with 25 wt% PMMA, 20 wt% AB in 10 wt% multiwall

carbon nanotubes (MWCNT). Improvement of the thermodynamic properties due to the reduction of the reaction enthalpy and suppression of byproducts with only 1 step in MWCNT samples was obtained. The interaction between O in the carbonyl group of PMMA and B in the AB molecule during solution preparation and the electrospinning process led to B–O bonds formation which weakened the B–H and B–N bonds.

- In (Zhao et al. 2010), only PMMA was used confining from 20 to 80 wt% AB (PAB samples) and resulting in a water-resistant system. No borazine and diborane was present in PAB samples but ammonia was released at temperatures higher than 90 °C. The formation of B–O bond suggested the interaction between O in CO group of PMA and B in the AB during preparation, and weakened B–H and B–N bonds, similarly to carboxyl groups in carbon hosts. As result, the kinetics were improved, dehydrogenation temperature was lower and boracic byproduct was suppressed.

Ref.	Host	Surface properties ( $m_2/g\text{-cm}^3/g\text{-nm}$ )	Method of infiltration	AB wt%	Melting (°C)	1 <sup>st</sup> T <sub>p</sub> (°C)	2 <sup>nd</sup> T <sub>p</sub> (°C)	Enthalpies (KJ/mol)	Weight loss (%) per unit of sample	-E <sub>a</sub> (KJ/mol)
(S. F. Li et al. 2010) (Sepehri et al. 2009)	Bulk			100	105-110	110-124	150-160	-20-(-29)	~45	(-138) (-184)
(Autrey et al. 2004)	SBA-15	1000/-/3	WI with MeOH	50		96				
(Gutowska et al. 2005)	SBA-15	900/1.2/7.5	WI with MeOH	50				-1 ±1		-67±5
(Lai et al. 2012)	MCM-41	1009/0.85/2.7	WI with MeOH	50	No	100		-39.7	21.74/18.25	
	SBA-15	817/1.13/6.45	WI with MeOH	50		99		-32.7		
(Paolone et al. 2009)	MCM-41		WI with THF	33/50						
(Wang et al. 2009)	MCM-41	900/0.75/-	WI with THF	33-75						
(Gadipelli et al. 2011)	MOF-74	1100/-/-	WI with MeOH	26	No	100		Reduction	16 (till 200)	
(Z. Li et al. 2010)	JUC-32	659/0.27/-	WI with MeOH	8		<b>84</b>				
(Zhong et al. 2011)	ZIF-8	1253/-/0.3-1.2	MeOH vs. mixing	40/50		86	116 and 129			
(Feaver et al. 2007)	CC	300/0.70/2-20	WI with THF	Till 24		90		-120		
(Sepehri et al. 2008)	C	350-500/0.69-0.97/2-50	WI with THF	33/50		98/102/110 (7/9/16nm)*≠values for ≠ΔT	No			120/150 (7/16nm)

<b>(Sepehri et al. 2007)</b>	CC	500/0.7/2-20	WI with THF	40						
<b>(Sepehri et al. 2009)</b>	CC modified with B and N	446/0.96/15.8	WI with THF	50-60		109 (CC)/103(BNCC)				150(CC)/115 (BNCC)
<b>(Li et al. 2009)</b>	CMK-3 and 5% Li-catalyst	1150/1.5/-	WI with MeOH	50		95/90 (with Li)		-2.1		-98±5 (AB-Li-CMK3)
<b>(Moussa et al. 2012)</b>	Activated carbon	716/0.36/-	Capillary impregnation at 0 °C with MeOH or THF vs BM	50	~114	~117		1.6/3.0/5.9 (AC/ABTHF/MeOH/Mill)		64±8
<b>(S. F. Li et al. 2010)</b>	10%Pt-CNT (carbon nanotubes)	168.5/-/-	WI with NH <sub>3</sub> flow at 0 °C by ultrasonic treatment	50	Hardly detected	108	150	-8.1(BM)/-7.5 (BM with Pt)/-2.6	10.8 (225 °C)	106.2
<b>(Alipour et al. 2015)</b>	MWCNT(2-10%)in PMMA(25%)	-	Electrospinning	5-25	106/80 (MWCNT)	112/85	140/ no peak (MWCNT)	-10.66 /-1.83	11.10/2.88 (till 200 °C)	
<b>(Zhao et al. 2010)</b>	PMA (poly methyl acrylate)	-	WI with acetonitrile and MeOH	20/80		95.1/96.1 (20/80 wt% AB)	No	-4.9		

Table 7. Review of Ammonia Borane confined in a support

### **Li<sub>3</sub>BN<sub>2</sub>H<sub>8</sub>**

With nearly 12 wt% H<sub>2</sub>, it is limited by high desorption temperature and poor reversibility. To overcome these limitations, the hydride was confined by melt infiltration in activated carbon (2880 m<sup>2</sup>/g, 1.27 cm<sup>3</sup>/g, ~2.0 nm) and carbon aerogels (770 m<sup>2</sup>/g, 0.8 cm<sup>3</sup>/g, ~13 nm) (Wu et al. 2009). 33 wt% of hydride was successfully infiltrated without H<sub>2</sub> loss during infiltration obtaining better properties in nanoscaffolds with larger surface areas, larger pores volumes and smaller pores sizes. As a result, the desorption temperature was decreased (324 °C for bulk, 320 °C for 13 nm aerogels and 305 °C for activation carbon with pores of 21 nm). The infiltration into smaller pores size resulted in lower energy barrier which meant lower activation energy for H<sub>2</sub> desorption. The pathway of decomposition was changed after confinement, increasing the amount of ammonia released in the scaffold sample. More investigation is necessary to confirm this fact.

Regarding reversibility, 32% was successfully rehydrogenated at 50 bar, 300 °C for 10 h whereas bulk hydrides could not be recycled at the same conditions. At higher conditions (80 bar for more than 20 h), the reversibility increased into 75%.

### **Several complex hydrides in a support**

Several works have demonstrated that confining several complex hydrides in a support resulted in enhanced properties of the hydride during desorption of hydrogen.

In (Zhao-Karger et al. 2012) LiBH<sub>4</sub>/Mg(BH<sub>4</sub>)<sub>2</sub> was infiltrated in carbon IrH<sub>33</sub> with a ratio 0.74:0.27 wt by melt infiltration at 190 °C, 40 bar of H<sub>2</sub> for 1 h. An amorphous structure was obtained whose elements were homogeneously distributed along the carbon scaffold, as evidenced by mapping in TEM. TGA/DSC analyses showed that in nanoconfined samples, the release of H<sub>2</sub> took place in only one step at lower temperature in contrast to the four steps in bulk samples. Also MS analyses showed the elimination of B<sub>2</sub>H<sub>6</sub> gas in infiltrated samples confirming a different reaction pathway. Raman analyses showed that MgB<sub>12</sub>H<sub>12</sub>, which is a stable intermediate formed after decomposition of Mg(BH<sub>4</sub>)<sub>2</sub> was destabilized after carbon nanoconfinement which could explain the enhanced desorption rate.

In (Nielsen et al. 2010) carbon aerogels were infiltrated with MgBu<sub>2</sub> in heptane solution to convert it into MgH<sub>2</sub> (10 vol%) and then LiBH<sub>4</sub> (45 vol%) was melt infiltrated at 50 bar H<sub>2</sub> (molar ratio 2:1). Nanoconfinement improved kinetics and thermodynamics and the mechanism of decomposition was changed. Desorption of hydrogen was decreased during

cycling in bulk and confined samples. However faster kinetics with lower decomposition temperatures was obtained in confined systems, as it is shown in table 8. Confined samples were reversible for 4 cycles, and rehydrogenation was tested at several conditions: at 70 bar H<sub>2</sub>, 370 °C for 35 h; 390 °C, 98 bar H<sub>2</sub> for 68 h and 390 °C, 93 bar H<sub>2</sub> for 88 h. Higher conditions of pressure and temperature were necessary to recycle bulk hydride. Adding MgH<sub>2</sub> to confined system resulted in better reversibility: 92% of initial H<sub>2</sub> was reversible for 3 cycles in contrast to 40% in (Gross et al. 2008).

<b>T<sub>peak</sub></b> <b>(°C)</b>	<b>Nanoconfined</b> <b>(°C)</b>	<b>Bulk</b> <b>(°C)</b>	<b>Process</b>
A	113	117	Orthorrombic to hexagonal
B	267	290	Melting LiBH <sub>4</sub> . ΔT=23 (the same as (Gross et al. 2008))
C	332	364	Dehydrogenation of MgH <sub>2</sub> . No borane gases
D	351	462	Dehydrogenation of LiBH <sub>4</sub> . No borane gases
wt% loss (260-470°C)	4.7	9.2	Not completed (total is 11.5 wt%)

Table 8. Decomposition temperatures in confined system 10MgH<sub>2</sub>-45LiBH<sub>4</sub>-45carbon aerogel (in %vol)

## CONCLUSIONS AND PERSPECTIVES FUTURES

Hydrides are promising hydrogen storage materials, although thermodynamic and kinetics limitations must be overcome and reversibility must be achieved before they are used in a mobile application. Nanoconfinement is one of the most promising alternatives till now. Melt and wet impregnation are the most used infiltration methods to confine hydrides in a support. However, melt infiltration can only be used when decomposition temperature of the hydride occurs after melting point; and in the case of wet impregnation it is necessary to find an adequate solvent which does not react with the hydride.

Carbon is the most studied support because it has relatively low weight, high pore volume, it is chemically inert with most of the hydrides, and it is abundant at low cost. The maximum hydride loading that has been achieved in carbon supports is 50 wt%, an amount that can be improved using scaffolds with more volume of pores. Apart from this, silica, metal organic frameworks (MOF), polymers and TiO<sub>2</sub> supports have been tested, among others.

In general, after confinement, the following properties were observed, which were more visible at lower concentration of hydride (to be sure that all of it was encapsulated in the pores of the support) and lower pore size:

- Surface properties of the support decreased due to infiltration of the hydride in the pores.
- The decomposition of the hydride started before obtaining broader peaks in calorimetric analyses due to the higher degree of disorder created by the intimate contact with the scaffold and a loss of crystallinity due to the formation of amorphous or nanocrystalline compounds.
- Thermodynamics was improved due to the reduction in particle size, which was visible at sizes lower than 5 nm, mainly in the range 1-2 nm.
- Kinetics was also improved due to the reduction of particle size and therefore reduction of diffusion distances and larger ratio of surface. This improvement was larger as pore size was lower. In some cases, support also acted as catalyst, so kinetics were improved by the synergetic effect of reduction particle size and catalytic effect.
- Cyclability was enhanced because the pores limited the agglomeration of the subproducts, **avoiding the segregation of the phases**. After confinement, more hydrogen could be regenerated in some cases. This was frequently related with the

formation of lower amount of stable intermediate species. In several cases, encapsulating the hydride in the support resulted in a change of the decomposition mechanism, altered by the presence of the support through size confinement and/or surface interaction effects. Also, solid-state diffusion during rehydrogenation was enhanced after nanoconfinement.

- In the case that other gases are formed together with hydrogen during the decomposition of the hydride, after nanoconfinement these gases were reduced or even suppressed due to the reduction of the size and/or change of mechanism and/or surface interactions.

In order to improve the results obtained till now, a scaffold with smaller pores and higher volume of pores is needed. Because of this aspect, silica aerogel obtained after supercritical drying was used in this thesis which could be a promising scaffold due to its outstanding properties preserved during drying process.

Regarding the needs for future work in this field, it would be necessary to study more in detail the mechanism of decomposition of bulk hydrides in contrast to confined samples. This aspect is not sufficiently studied, but it is very important in order to understand the behavior of the material and improve its stability when it is used in repeated hydrogen charge/discharge cycles.

## References

- Adelhelm, P. et al., 2010. Comprehensive Study of Melt Infiltration for the Synthesis of NaAlH<sub>4</sub>/C Nanocomposites. *Chemistry of Materials*, 22(9), pp.2233–2238.
- Adelhelm, P., de Jong, K.P. & de Jongh, P.E., 2009. How intimate contact with nanoporous carbon benefits the reversible hydrogen desorption from NaH and NaAlH<sub>4</sub>. *Chemical communications (Cambridge, England)*, (41), pp.6261–3.
- Alipour, J., Shoushtari, A. & Kafrou, A., 2015. Ammonia borane confined by poly ( methyl methacrylate )/ multiwall carbon nanotube nanofiber composite , as a polymeric hydrogen storage material. *Journal of Materials Science*, 50, pp.3110–3117.
- Ampoumogli, A. et al., 2011. Nanostructured composites of mesoporous carbons and boranates as hydrogen storage materials. *Journal of Alloys and Compounds*, 509(SUPPL. 2), pp.S705–S708.
- Ampoumogli, A. et al., 2012. Synthesis and characterisation of a mesoporous carbon/calcium borohydride nanocomposite for hydrogen storage. *International Journal of Hydrogen Energy*, 37(21), pp.16631–16635.
- Andrievski, R. a, 2011. Hydrogen in metallic nanomaterials. *Russian Chemical Reviews*, 80(9), pp.855–868.
- Au, Y.S. et al., 2014. Pore Confined Synthesis of Magnesium Boron Hydride Nanoparticles. *The Journal of Physical Chemistry C*, 118, pp.20832–20839.
- Autrey, T. et al., 2004. Chemical hydrogen storage in nano-structured materials. Control of hydrogen release and reactivity from ammonia borane complexes. *ACS Division of Fuel Chemistry, Preprints*, 49(1), pp.4–5.
- Bald, C.P. et al., 2007. Active Ti species in TiCl<sub>3</sub>-doped NaAlH<sub>4</sub>. Mechanism for catalyst deactivation. *Journal of Physical Chemistry C*, 111(6), pp.2797–2802.
- Balde, C.P. et al., 2008. Sodium Alanate Nanoparticles - Linking Size to Hydrogen Storage Properties. *Journal of the American Chemical Society*, 130(19), pp.6761–6765.
- Baldø, C.P. et al., 2006. Facilitated Hydrogen Storage in NaAlH<sub>4</sub> Supported on Carbon Nanofibers. *Angewandte Chemie - International Edition*, 45, pp.3501–3503.
- Bendyna, J.K., Dyjak, S. & Notten, P.H.L., 2015. The influence of ball-milling time on the dehydrogenation properties of the NaAlH<sub>4</sub>-MgH<sub>2</sub> composite. *International Journal of Hydrogen Energy*, 40(11), pp.4200–4206.

- Bérubé V; Radked G; Dresselhaus M; Chen G, 2007. Size effects on the hydrogen storage properties of nanostructured metal hydrides: A review. *International journal of energy research*, 31(August 2007), pp.637–663.
- Bhakta, R.K. et al., 2009. Metal - Organic Frameworks As Templates for Nanoscale NaAlH<sub>4</sub>. *Journal of the American Chemical Society*, pp.13198–13199.
- Bhakta, R.K. et al., 2012. Thermodynamics and kinetics of NaAlH<sub>4</sub> nanocluster decomposition. *Physical Chemistry Chemical Physics*, 14(22), p.8160.
- Bogdanović, B. et al., 2000. Metal-doped sodium aluminium hydrides as potential new hydrogen storage materials. *Journal of Alloys and Compounds*, 302(1-2), pp.36–58.
- Brun, N. et al., 2010. Preparation of LiBH<sub>4</sub>@carbon micro–macrocellular foams: tuning hydrogen release through varying microporosity. *Energy & Environmental Science*, 3(6), p.824.
- Busch, N. et al., 2015. Influence of milling parameters on the sorption properties of the LiH–MgB<sub>2</sub> system doped with TiCl<sub>3</sub>. *Journal of Alloys and Compounds*, 645, pp.S299–S303.
- Cahen, S. et al., 2009. Improvement of the LiBH<sub>4</sub> hydrogen desorption by inclusion into mesoporous carbons. *Journal of Power Sources*, 189(2), pp.902–908.
- Chong, L. et al., 2015. NaB<sub>4</sub> in “graphene Wrapper:” Significantly Enhanced Hydrogen Storage Capacity and Regenerability through Nanoencapsulation. *Advanced Materials*, 27(34), pp.5070–5074.
- Christian, M. & Aguey-Zinsou, K.-F., 2010. Destabilisation of complex hydrides through size effects. *Nanoscale*, 2(12), pp.2587–90.
- Chumphongphan, S. et al., 2014. Nanoconfinement degradation in NaAlH<sub>4</sub>/CMK-1. *International Journal of Hydrogen Energy*, 39(21), pp.11103–11109.
- Fan, X.L. et al., 2013. Size effect on hydrogen storage properties of NaAlH<sub>4</sub> confined in uniform porous carbons. *Nano Energy*, 2(5), pp.995–1003.
- Fang, Z.Z. et al., 2008. Kinetic- and thermodynamic-based improvements of lithium borohydride incorporated into activated carbon. *Acta Materialia*, 56(20), pp.6257–6263.
- Feaver, A. et al., 2007. Coherent Carbon Cryogel - Ammonia Borane Nanocomposites for H<sub>2</sub> Storage. , (13), pp.7469–7472.
- Fichtner, M., 2009. Properties of nanoscale metal hydrides. *Nanotechnology*, 20(20), p.204009 1–4.

- Fichtner, M. et al., 2009. The kinetic properties of  $\text{Mg}(\text{BH}_4)_2$  infiltrated in activated carbon. *Nanotechnology*, 20(20), p.204029.
- Gadipelli, S. et al., 2011. Nanoconfinement and catalytic dehydrogenation of ammonia borane by magnesium-metal-organic-framework-74. *Chemistry - A European Journal*, 17(22), pp.6043–6047.
- Gao, J. et al., 2010. Confinement of  $\text{NaAlH}_4$  in Nanoporous Carbon : Impact on  $\text{H}_2$  Release , Reversibility , and Thermodynamics. *Journal of Physical Chemistry C*, 114, pp.4675–4682.
- Gao, J. et al., 2012. Enhanced reversibility of  $\text{H}_2$  sorption in nanoconfined complex metal hydrides by alkali metal addition. *Journal of Materials Chemistry*, 22(26), p.13209.
- Gao, J. et al., 2014. Interface effects in  $\text{NaAlH}_4$ -carbon nanocomposites for hydrogen storage. *International Journal of Hydrogen Energy*, 39(19), pp.10175–10183.
- Gosalawit-Utke, R. et al., 2014. Destabilization of  $\text{LiBH}_4$  by nanoconfinement in PMMA-co-BM polymer matrix for reversible hydrogen storage. *International Journal of Hydrogen Energy*, 39(10), pp.5019–5029.
- Grochala, W. & Edwards, P.P., 2004. Thermal decomposition of the non-interstitial hydrides for the storage and production of hydrogen. *Chemical Reviews*, 104(3), pp.1283–1315.
- Gross, A.F. et al., 2008. Enhanced Hydrogen Storage Kinetics of  $\text{LiBH}_4$  in Nanoporous Carbon Scaffolds. *The Journal of Physical Chemistry C*, 112(14), pp.5651–5657. A.
- Gross, A.F. et al., 2009. Fabrication and hydrogen sorption behaviour of nanoparticulate  $\text{MgH}_2$  incorporated in a porous carbon host. *Nanotechnology*, 20(20), p.204005.
- Guo, L. et al., 2013. Enhanced desorption properties of  $\text{LiBH}_4$  incorporated into mesoporous  $\text{TiO}_2$ . *International Journal of Hydrogen Energy*, 38(1), pp.162–168.
- Gutowska, A. et al., 2005. Nanoscaffold mediates hydrogen release and the reactivity of ammonia borane. *Angewandte Chemie - International Edition*, 44(23), pp.3578–3582.
- Hearley A; Redmont S., 2004. US 2004/0065171 A1. , 1(19).
- J. J. Reilly, R.H.W., 1967. Reaction of Hydrogen with Alloys of Magnesium and Copper. *Inorganic Chemistry*, 6(12), pp.0–3.
- Jeon, K.-J. et al., 2011. Air-stable magnesium nanocomposites provide rapid and high-capacity hydrogen storage without using heavy-metal catalysts. *Nature Materials*, 10(4), pp.286–290.

- De Jongh, P.E. et al., 2007. The preparation of carbon-supported magnesium nanoparticles using melt infiltration. *Chemistry of Materials*, 19(24), pp.6052–6057.
- De Jongh, P.E. & Adelhelm, P., 2010. Nanosizing and nanoconfinement: new strategies towards meeting hydrogen storage goals. *ChemSusChem*, 3(12), pp.1332–48.
- Klimkowicz, A. et al., 2015. Hydrogen desorption properties of magnesium hydride catalyzed multiply with carbon and silicon. *Journal of Alloys and Compounds*, 645, pp.S80–S83.
- Konarova, M. et al., 2011. Effect of Synthesis Parameters on the Hydrogen Desorption of MgH<sub>2</sub> / C composite Prepared Using. *internacional journal of energy engineering*, 1(1), pp.26–32.
- Konarova, M. et al., 2013. Effects of nano-confinement on the hydrogen desorption properties of MgH<sub>2</sub>. *Nano Energy*, 2(1), pp.98–104.
- Konarova, M. et al., 2012. Porous MgH<sub>2</sub>/C composite with fast hydrogen storage kinetics. *International Journal of Hydrogen Energy*, 37(10), pp.8370–8378.
- Lai, S.W. et al., 2012. Hydrogen release from ammonia borane embedded in mesoporous silica scaffolds: SBA-15 and MCM-41. *International Journal of Hydrogen Energy*, 37(19), pp.14393–14404.
- Langmi, H.W. et al., 2010. Modification of the H<sub>2</sub> desorption properties of LiAlH<sub>4</sub> through doping with Ti. *Journal of Physical Chemistry C*, 114(23), pp.10666–10669.
- Li, L. et al., 2009. Lithium-catalyzed dehydrogenation of ammonia borane within mesoporous carbon framework for chemical hydrogen storage. *Advanced Functional Materials*, 19(2), pp.265–271.
- Li, S.F. et al., 2010. Platinum nanoparticle functionalized CNTs as nanoscaffolds and catalysts to enhance the dehydrogenation of ammonia-borane. *Journal of Physical Chemistry C*, 114(49), pp.21885–21890.
- Li, Y. et al., 2011. De- / re-hydrogenation features of NaAlH<sub>4</sub> confined exclusively in nanopores. *Acta Materialia*, 59, pp.1829–1838.
- Li, Z. et al., 2010. Ammonia borane confined by a metal-organic framework for chemical hydrogen storage: Enhancing kinetics and eliminating ammonia. *Journal of the American Chemical Society*, 132(5), pp.1490–1491.
- Liu, J., Han, Y. & Ge, Q., 2009. Effect of doped transition metal on reversible hydrogen release/uptake from NaAlH<sub>4</sub>. *Chemistry - A European Journal*, 15(7), pp.1685–1695.

- Liu, J. & Zhang, W., 2012. Improvement on hydrogen storage properties of complex metal hydride. *Hydrogen Storage*. Available at: <http://www.intechopen.com/books/hydrogen-storage>.
- Liu, X. et al., 2010. Controlling the decomposition pathway of LiBH<sub>4</sub> via confinement in highly ordered nanoporous carbon. *Journal of Physical Chemistry C*, 114(33), pp.14036–14041.
- Liu, X. et al., 2011. Systematic pore-size effects of nanoconfinement of LiBH<sub>4</sub>: Elimination of diborane release and tunable behavior for hydrogen storage applications. *Chemistry of Materials*, 23(5), pp.1331–1336.
- Liu, Y. et al., 2013. Study on hydrogen storage properties of Mg nanoparticles confined in carbon aerogels. *International Journal of Hydrogen Energy*, 38(13), pp.5302–5308.
- Lohstroh, W. et al., 2010. Thermodynamic Effects in Nanoscale NaAlH<sub>4</sub>. *Physical Chemistry Chemical Physics*, 11, pp.789–792.
- Marrero-Alfonso, E.Y. et al., 2009. Hydrogen generation from chemical hydrides. *Industrial and Engineering Chemistry Research*, 48(8), pp.3703–3712.
- Moussa, G. et al., 2012. Room-temperature hydrogen release from activated carbon-confined ammonia borane. *International Journal of Hydrogen Energy*, 37(18), pp.13437–13445.
- Ngene, P., Adelhelm, P., et al., 2010. LiBH<sub>4</sub> / SBA-15 Nanocomposites Prepared by Melt Infiltration under Hydrogen Pressure : Synthesis and Hydrogen Sorption Properties. *The Journal of Physical Chemistry C*, 114(13), pp.6163–6168.
- Ngene, P., van den Berg, R., et al., 2011. Reversibility of the hydrogen desorption from NaBH<sub>4</sub> by confinement in nanoporous carbon. *Energy & Environmental Science*, 4(10), p.4108.
- Ngene, P. et al., 2016. Reversible Li-Insertion in Nanoscaffolds: A Promising Strategy to alter the Hydrogen Sorption Properties of Li-based Complex Hydrides. *Nano Energy*, 22, pp.169–178.
- Ngene, P., Verkuijlen, M.H.W., et al., 2011. The role of Ni in increasing the reversibility of the hydrogen release from nanoconfined LiBH<sub>4</sub>. *Faraday Discussions*, 151(0), pp.47–58.
- Ngene, P., van Zwiene, M.R. & de Jongh, P.E., 2010. Reversibility of the hydrogen desorption from LiBH<sub>4</sub>: a synergetic effect of nanoconfinement and Ni addition. *Chemical communications (Cambridge, England)*, 46, pp.8201–8203.
- Nielsen, T.K. et al., 2010. A reversible nanoconfined chemical reaction. *ACS Nano*, 4(7), pp.3903–3908.

- Nielsen, T.K. et al., 2009. Confinement of MgH<sub>2</sub> Nanoclusters within nanoporous aerogel scaffold materials. *ACS Nano*, 3(11), pp.3521–3528.
- Nielsen, T.K. et al., 2011. Improved Hydrogen Storage Kinetics of nanoconfined NaAlH<sub>4</sub> catalyzed with TiCl<sub>3</sub> nanoparticles. *ACS Nano*, 5(5), pp.4056–4064.
- Nielsen, T.K. et al., 2012. Nanoconfined NaAlH<sub>4</sub>: determination of distinct prolific effects from pore size, crystallite size, and surface interactions. *The Journal of Physical Chemistry*, 116(l), pp.21046–21051.
- Nielsen, T.K. et al., 2014. Nanoconfined NaAlH<sub>4</sub>: prolific effects from increased surface area and pore volume. *Nanoscale*, 6(1), pp.599–607.
- Paolone, A. et al., 2009. Absence of the structural phase transition in ammonia borane dispersed in mesoporous silica: Evidence of novel thermodynamic properties. *Journal of Physical Chemistry C*, 113(24), pp.10319–10321.
- Paskevicius, M. et al., 2016. Cyclic stability and structure of nanoconfined Ti-doped NaAlH<sub>4</sub>. *International Journal of Hydrogen Energy*, (February), pp.4–13.
- Paskevicius, M. et al., 2011. Magnesium hydride formation within carbon aerogel. *Journal of Physical Chemistry C*, 115(5), pp.1757–1766.
- Paskevicius, M., Sheppard, D.A. & Buckley, C.E., 2010. Thermodynamic changes in mechanochemically synthesized magnesium hydride nanoparticles. *Journal of the American Chemical Society*, 132(14), pp.5077–5083.
- Pinkerton, F.E., 2011. Comparison of hydrogen cycling kinetics in NaAlH<sub>4</sub>-carbon aerogel composites synthesized by melt infusion or ball milling. *Journal of Alloys and Compounds*, 509(36), pp.8958–8964.
- Saldan, I., 2016. Decomposition and formation of magnesium borohydride. *International Journal of Hydrogen Energy*, 41(26), pp.11201–11224. Available at: <http://linkinghub.elsevier.com/retrieve/pii/S0360319916315026>.
- Schuth, F. et al, 2006. materials encapsulated in porous matrices for the reversible storage of hydrogen Patent.pdf. , pp.1–6.
- Sepehri, S. et al., 2007. Spectroscopic studies of dehydrogenation of ammonia borane in carbon cryogel. *Journal of Physical Chemistry B*, 111(51), pp.14285–14289.
- Sepehri, S., Garcia, B.B. & Cao, G., 2008. Tuning dehydrogenation temperature of carbon–ammonia borane nanocomposites. *Journal of Materials Chemistry*, 18(34), p.4034.

- Sepehri, S., García, B.B. & Cao, G., 2009. Influence of surface chemistry on dehydrogenation in carbon cryogel ammonia borane nanocomposites. *European Journal of Inorganic Chemistry*, (5), pp.599–603.
- Shane, D.T. et al., 2010. LiBH<sub>4</sub> in carbon aerogel nanoscaffolds: An NMR study of atomic motions. *Journal of Physical Chemistry C*, 114(9), pp.4008–4014.
- Shao, H. et al., 2012. Nanotechnology in Mg-based materials for hydrogen storage. *Nano Energy*, 1(4), pp.590–601.
- Soloveichik, G.L. et al., 2009. Magnesium borohydride as a hydrogen storage material: Properties and dehydrogenation pathway of unsolvated Mg(BH<sub>4</sub>)<sub>2</sub>. *International Journal of Hydrogen Energy*, 34(2), pp.916–928.
- Stavila, V. et al., 2012. Reversible Hydrogen Storage by NaAlH<sub>4</sub> Confined within a Titanium-Functionalized MOF-74(Mg) Nanoreactor. *ACS Nano*, 74(11), pp.9807–9817.
- Stephens, R.D. et al., 2009. The kinetic enhancement of hydrogen cycling in NaAlH<sub>4</sub> by melt infusion into nanoporous carbon aerogel. *Nanotechnology*, 204018, pp.1–6.
- Sun, W. et al., 2011. Nanoconfinement of lithium borohydride in Cu-MOFs towards low temperature dehydrogenation. *Dalton transactions (Cambridge, England : 2003)*, 40(21), pp.5673–6.
- Vajo, J.J. & Olson, G.L., 2007. Hydrogen storage in destabilized chemical systems. *Scripta Materialia*, 56(10), pp.829–834.
- Varin, R.A. et al., 2005. Nanocrystalline and non-crystalline hydrides synthesized by controlled reactive mechanical alloying/milling of Mg and Mg–X (X = Fe, Co, Mn, B) systems. *Journal of Alloys and Compounds*, 404–406, pp.494–498.
- Varin, R.A. & Chiu, C., 2005. Structural stability of sodium borohydride (NaBH<sub>4</sub>) during controlled mechanical milling. *Journal of Alloys and Compounds*, 397(1-2), pp.276–281.
- Varin, R.A., Chiu, C. & Wronski, Z.S., 2008. Mechano-chemical activation synthesis (MCAS) of disordered Mg(BH<sub>4</sub>)<sub>2</sub> using NaBH<sub>4</sub>. *Journal of Alloys and Compounds*, 462(1-2), pp.201–208.
- Verkuijlen, M.H.W. et al., 2010. Solid-State NMR Studies of the Local Structure of NaAlH<sub>4</sub>/C Nanocomposites at Different Stages of Hydrogen Desorption and Rehydrogenation. *Journal of Physical Chemistry C*, 114(10), pp.4683–4692.
- Wahab, M.A. et al., 2013. Enhanced hydrogen desorption from Mg(BH<sub>4</sub>)<sub>2</sub> by combining

- nanoconfinement and a Ni catalyst. *Journal of Materials Chemistry A*, 1(10), p.3471.
- Wang, L.-Q. et al., 2009. Hyperpolarized Xe-129 NMR Investigation of Ammonia Borane in Mesoporous Silica. *Journal Of Physical Chemistry C*, 113(16), pp.6485–6490.
- Wu, H. et al., 2009. Size effects on the hydrogen storage properties of nanoscaffolded  $\text{Li}_3\text{BN}_2\text{H}_8$ . *Nanotechnology*, 20(20), p.204002.
- Xiong, R. et al., 2012. Improvement of the hydrogen storage kinetics of  $\text{NaAlH}_4$  with nanocrystalline titanium dioxide loaded carbon spheres (Ti-CSs) by melt infiltration. *International Journal of Hydrogen Energy*, 37(13), pp.10222–10228.
- Y.Zhang, W.Zhang, A.Wang, L.Sun, M.Fan, H.Chu, J.Sun, T.Z., 2007.  $\text{LiBH}_4$  nanoparticles supported by disordered mesoporous carbon : Hydrogen storage performances and destabilization mechanisms  $\text{LiBH}_4$  nanoparticles supported by disordered mesoporous carbon : Hydrogen storage performances and destabilization mechanisms. *International Journal of Hydrogen Energy*, 32(NOVEMBER), pp.3976–3980.
- Yan, Y. et al., 2013. Reversible hydrogen storage in  $\text{Mg}(\text{BH}_4)_2$ /carbon nanocomposites. *Journal of Materials Chemistry A*, 1(37), p.11177.
- Zavorotynska, O. et al., 2015. Recent progress in magnesium borohydride  $\text{Mg}(\text{BH}_4)_2$ : Fundamentals and applications for energy storage. *International Journal of Hydrogen Energy*.
- Zhang, S. et al., 2009. The synthesis and hydrogen storage properties of a  $\text{MgH}_2$  incorporated carbon aerogel scaffold. *Nanotechnology*, 20(20), p.204027.
- Zhao, J. et al., 2010. A soft hydrogen storage material: Poly(methyl acrylate)-confined ammonia borane with controllable dehydrogenation. *Advanced Materials*, 22(3), pp.394–397.
- Zhao-Karger, Z. et al., 2010. Altered thermodynamic and kinetic properties of  $\text{MgH}_2$  infiltrated in microporous scaffold. *Chemical communications (Cambridge, England)*, 46(44), pp.8353–5.
- Zhao-Karger, Z. et al., 2012. Influence of Nanoconfinement on Reaction Pathways of Complex Metal Hydrides. *Energy Procedia*, 29, pp.731–737.
- Zheng, S. et al., 2008. Hydrogen Storage Properties of Space-Confined  $\text{NaAlH}_4$  Nanoparticles in Ordered Mesoporous Silica. *Chemistry of Materials*, 20(9), pp.3954–3958.

Zhong, R. et al., 2011. Improved Hydrogen Release from Ammonia – Borane with ZIF-8. , pp.8–10.

Züttel, A., 2004. Hydrogen storage methods. *Naturwissenschaften*, 91(4), pp.157–172.



# **OBJECTIVES**

**Innovative strategies to enhance properties  
of solid hydrogen storage materials based  
on hydrides**



Bulk hydrides are promising solid hydrogen storage compounds but they are restricted by its thermodynamic and kinetics limitations. The main **aim of this PhD thesis** is to contribute to sustainable hydrogen economy by developing innovative solid hydrogen storage materials based on hydrides with enhanced hydrogen release properties, in terms of: hydrogen release kinetics, decomposition temperature and gaseous byproducts.

Different strategies have been proposed to overcome these limitations. In this thesis, two different strategies are considered: (1) micronization of the hydride in order to reduce particle size and therefore improve kinetics, and (2) confinement in a support to preserve the properties of the material during repeated cycles of use. The specific objectives to do so are the following:

1. Optimization of a supercritical antisolvent process to micronize hydrides by studying of the influence of different process variable of supercritical CO<sub>2</sub> micronization (concentration of solution, temperature of the process, fraction of carbon dioxide) on the particle size of the final micronized hydride and its influence on hydrogen release properties. Comparison with the results of the conventional milling method.
2. Production of an aerogel host with enhanced surface properties for confinement of hydrides, in terms of surface area and pores (volume and size) by batch and semicontinuous process. Study of the influence of aerogel processing conditions (shear rate, amount of catalyst, surface modification and hydrophilic-hydrophobic solvent ration) on the final properties of the scaffold.
3. Development of different processes to confine a (complex) hydride in microparticles of silica aerogel used as support.
4. Study of the influence of surface modification of the support (hydrophilic and hydrophobic silica aerogel) and impregnation process on the final hydrogen release properties of the solid hydrogen storage material. Elucidate the properties that should gather the ideal host and confinement process.

Different hydrides have been tested. They were selected by its promising properties as hydrogen storage materials: Ammonia Borane (AB, 19.6 wt%), 1-2 Ethane Diamineborane (EDAB, 10 wt%), Magnesium Hydride ( $\text{MgH}_2$ , 7.8 wt%) and Magnesium Borohydride ( $\text{Mg}(\text{BH}_4)_2$ , 14.8 wt%). In the first part of the thesis (*chapters 1 and 2*), the effect of micronization using SAS technique was studied out with Magnesium Acetate as precursor of  $\text{MgH}_2$  (*chapter 1*), and EDAB (*chapter 2*). In the second part of the thesis, confinement of the hydride has been proposed as promising alternative. AB has been confined in microparticles of silica aerogel by wet impregnation using MeOH as solvent and DCM as antisolvent followed by supercritical drying (*chapter 3*). Previously, the study of AB and AB in MeOH exposed to different carbon dioxide pressure was performed, in order to evaluate if degradation of the hydride occurred at these conditions. Based on these results, a novel process has been developed in order to increase the concentration of hydride (AB) confined in the support, based on pressurized  $\text{CO}_2$  drying (*chapter 4*). Finally,  $\text{Mg}(\text{BH}_4)_2$  was confined by thermal process in hydrogen atmosphere, studying the cyclability of the hydrogen storage material in contrast to bulk complex hydride (*chapter 5*).

# **CHAPTER 1**

**Micronization of magnesium acetate by  
Supercritical Anti Solvent (SAS) process as  
precursor for the production of magnesium  
oxide and magnesium hydride**



## **Micronization of magnesium acetate by Supercritical Anti Solvent (SAS) process as precursor for the production of magnesium oxide and magnesium hydride<sup>1</sup>**

### **Abstract**

Magnesium acetate was micronized by Supercritical Anti Solvent (SAS) process. By SAS processing, sub-micrometric magnesium acetate particles with particle sizes ranging from 300 nm to 700 nm were obtained, with regular spherical morphology and amorphous crystalline structure. In comparison, mechanically milled particles showed similar mean particle sizes, but with irregular morphology and a bimodal particle size distribution. By calcination, SAS-processed magnesium acetate was converted into magnesium oxide preserving the morphology of particles. By hydrogenation, the acetate was converted into magnesium hydride, a solid-state hydrogen storage metal hydride. The release rate of hydrogen by thermolysis of magnesium hydride was enhanced by the particle size reduction, and there was a direct relationship between the size achieved by SAS micronization of the magnesium acetate precursor and the rate of release of hydrogen from the hydride.

<sup>1</sup>Crystal Growth and Design 14 (2014), 4768-4776

## 1. INTRODUCTION

In the near future, renewable energies will have to be adopted as the main source of energy due to the depletion of fossil fuels. Establishing a new system based on renewable resources is a challenging task for several reasons, including the fluctuating nature of many renewable energy sources. The direct use of renewable energies in mobile applications is also problematic. A possible solution for some of these problems could be to use hydrogen as an energy vector, that is, as an intermediate between energy production facilities and energy consumption sites that can be stored and transported. In order to make this new paradigm a feasible reality, several technical issues must be solved, including the efficient production and storage of hydrogen, and its conversion to electricity<sup>1</sup>.

Storing hydrogen in small mobile applications can be challenging, since the weight and space required by the hydrogen storage system should be reduced as much as possible. As an example, the US Department of Energy has set targets for onboard hydrogen storage systems for vehicles of 5.5 %wt in 2017 and 7.5 %wt as ultimate target<sup>2</sup>. Several prototypes exist based on the most obvious storage concepts: as a compressed gas or as a condensed gas, but these systems are limited by the physical properties of hydrogen. Since hydrogen has a very low density, the volume required to store it as a compressed gas is high, even at high pressures (e.g. 56 L/kg at 200 bar), and due to the low critical temperature of hydrogen, cryogenic temperatures are required to condense it (e.g., -252 °C at 1 bar), resulting in high energy consumptions. For these reasons, a considerable effort has been made in order to develop new solid state hydrogen storage systems, including metallic and chemical hydrides, clathrate hydrates, carbon nanotubes or hybrid metal-organic frameworks<sup>3</sup>.

Among the different solid state hydrogen storage materials, chemical and metallic hydrides are some of the most promising alternatives. These are chemical compounds that release hydrogen by a reversible chemical reaction. For example, upon heating magnesium hydride is decomposed releasing hydrogen according to reaction (1), and it can re-hydrogenated by putting it into contact with gaseous hydrogen at moderate pressures (10 - 50 bar):



Some important advantages of hydrides are their high hydrogen storage capacity (7.8 wt% in the case of magnesium hydride), and their low cost. Furthermore, these compounds are easier to handle than other solid-state hydrogen storage materials, and the development of this technology has enabled to build prototype tanks<sup>4</sup>. Nevertheless, the application of these materials still faces some important limitations, which can be classified into two categories:

Thermodynamic limitations, because most hydrides proposed for hydrogen storage are very stable. High temperatures are required in order to decompose them (e.g., more than 300 °C for equilibrium H<sub>2</sub> pressure of 1 bar in the case of magnesium hydride<sup>5</sup>). And kinetic limitations, since hydrogen uptake and release from hydrides can be very slow.

Kinetic limitations can be largely attributed to the gas-solid nature of hydrogenation and dehydrogenation reactions that can only progress by diffusion of hydrogen through the solid particles<sup>6</sup>. Thus, material processing techniques such as milling are normally used by researchers to solve these limitations, as by particle reduction diffusion lengths are shortened, thus improving kinetics, and a low particle size can contribute to destabilize the hydride and reduce the thermodynamic limitations<sup>7</sup>. However, the preservation of the morphology of particles during hydrogen cycling, with the associated changes in hydride chemical composition, is problematic. Some authors have studied the stabilization of hydrides in mesoporous carbon matrixes in order to preserve their size during hydrogen release and uptake cycles<sup>8</sup>. Other approaches to accelerate hydrogen release include the addition of catalysts, or the chemical modification of the hydride adding destabilizing compounds<sup>9,10,11</sup>. Milling is also useful in these approaches as it facilitates the formation of alloys with these additives and promotes the transformation of crystalline solid materials into less stable amorphous structures. Despite these advantages of top-down milling methods, the control and reproducibility of results obtained with milling is poor, because the product often shows severe agglomeration problems and the produced microcrystals are trapped in thick films over mill walls and balls that make it difficult to recover the product from inside the mill.

Bottom-up crystallization techniques can overcome some of these limitations, enabling a controlled formation of hydride particles with homogeneous properties<sup>12</sup>. In particular, the Supercritical Anti Solvent (SAS) process is a very promising technique that has been largely used to micronize different compounds: polymers, pharmaceuticals, semiconductors, explosives, etc<sup>13</sup>. Advantages of the SAS process include the possibility to selectively control the particle size and the crystallinity of the product by modification of the supersaturation driving force with changes in process conditions<sup>14</sup>, and the operation in an inert CO<sub>2</sub> environment. Furthermore, SAS precipitation of active compounds can be performed inside the pores of porous matrixes such as aerogels or other mesoporous silica matrixes, by coupling the supercritical anti solvent precipitation with the formation of the porous material by supercritical drying<sup>15</sup>.

On the other hand, for application of SAS processing the compound must be soluble in an organic solvent and stable in a CO<sub>2</sub> atmosphere, conditions that are not met by several highly

reactive hydrides, that show very limited compatibility with organic solvents or even react irreversibly with carbon dioxide<sup>16</sup>. This significant limitation of SAS processing for the precipitation of hydrides can be overcome by working with hydride precursors such as organometallic compounds<sup>17</sup> or dehydrogenated species<sup>18</sup> with a suitable compatibility with organic solvents under CO<sub>2</sub> pressure, that after SAS micronization can be converted into hydride microparticles by a hydrogenation reaction.

Following this approach, in this work the micronization of magnesium acetate tetrahydrate from methanol solutions has been performed by Supercritical Antisolvent (SAS) process using supercritical carbon dioxide at different operation conditions. Several process parameters: concentration of the solution, temperature and carbon dioxide molar fraction have been studied analyzing their influence on the properties of particles produced, including its size and morphology, analyzed by laser diffraction and SEM microscopy, and structural parameters, characterized by FT-IR spectroscopy and X-ray diffraction. Particles of magnesium acetate obtained by SAS processing have been used as precursors to obtain magnesium hydride (MgH<sub>2</sub>), a promising hydrogen storage material<sup>3,4,5</sup>, and magnesium oxide (MgO), a catalyst that can enhance the dehydrogenation of magnesium hydride, among other applications<sup>19</sup>. Kinetics of hydrogen release from the resulting hydride have been analyzed employing a volumetric cell at 350 °C.

## 2. EXPERIMENTAL METHODS

### 2.1 Materials

Magnesium acetate tetrahydrate (MgAc, purity: 99.0 wt%) was supplied by Sigma-Aldrich. As shown in the SEM micrograph presented in Figure 1, the material was constituted by prismatic particles of irregular sizes and shapes. In correspondence with this morphology, the particle size distribution of this material was bimodal, with a main peak located around a size of 300 μm, and a secondary peak near 1 μm probably corresponding to fine particles grinded down from the bigger crystals. Methanol (purity: 99.8 wt%) was purchased from Panreac (Spain). Carbon dioxide (purity: 99.95 wt%) was purchased from Carbueros Metálicos S.A. (Spain).

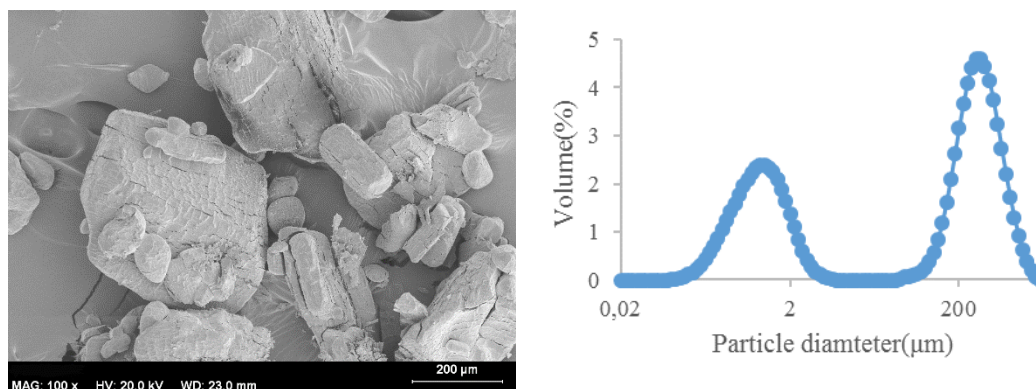


**Figure 1.** SEM image (magnification ratio: 100x, size bar: 200 μm) and particle size distribution of unprocessed Magnesium Acetate

## 2.2 Micronization of magnesium acetate by Supercritical Anti Solvent technique

Supercritical antisolvent precipitation (SAS) was used in order to obtain microparticles of magnesium acetate using methanol as solvent. A schematic diagram of the semi continuous SAS apparatus is shown in Figure 2.

The process takes place in a jacketed vessel of 2.5 L of volume which is heated with a water bath. First, preheated carbon dioxide is pumped with a diaphragm pump (Dosapro Milton Roy, Spain) at 2 Kg/h until stable conditions (pressure and temperature) are reached. In this moment, the organic solvent is pumped to assure stable conditions in the process. Then, 50 mL of the solution is delivered to the precipitator using a chromatographic pump (Gilson mod. 305, maximum flow rate: 25 mL/min, flow rate control with an accuracy of 0.1 mL/min) to be processed. Both solutions are pumped continuously through a coaxial nozzle which is located in the upper zone of the vessel in which the solution flows through the 1/16" inner tube, and CO<sub>2</sub> flows through the 1/4" coaxial annulus. At the outlet of the vessel, the precipitated particles are collected in a metallic frit which consists of a metallic porous disc used to support a polymeric filter with a pore size of 0.1 μm. Another vessel is used to separate the solvent (methanol) and CO<sub>2</sub> after pressure is released in the process. The pressure is controlled with a back pressure valve (model BP66, GO, USA) which is placed after a safety filter to assure that all the particles are collected in the outlet stream. Afterwards, CO<sub>2</sub> flow was maintained for 1 hour in order to assure the total elimination of solvent. After the decompression of the system for 50 minutes, the particles were collected from the filter and stored under dry conditions.

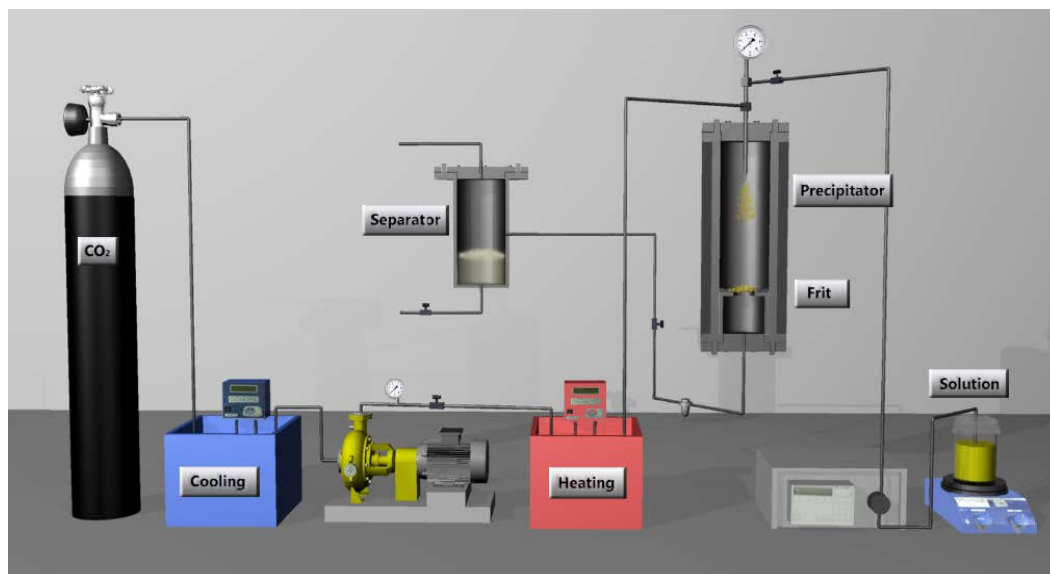


**Figure 2.** Schematic diagram of the Supercritical Anti Solvent apparatus

Several SAS precipitation experiments with different operating conditions were performed to optimize the micronization process, testing the influence of temperature (35-45 °C), concentration of magnesium acetate in the initial methanol solution (10-50 mg/mL), and  $\text{CO}_2$ /methanol proportions ( $\text{CO}_2$  molar fractions: 0.885-0.968). Pressure was maintained at 90 bar assuring the operation in the single phase region of methanol- $\text{CO}_2$  system<sup>20</sup>, which is a favorable condition for a successful micronization by SAS process<sup>13</sup>.

### 2.3 Milling of magnesium acetate

Conventional milling of magnesium acetate took place in a Retsch GmbH PM100 planetary ball mill. It consists of a vessel of 50 mL of zirconium oxide filled with 10 balls of 10 mm of the same material. Samples were milled at 500 rpm for a total time of 1 hour, with periods of 4 minutes of milling in alternate directions separated by turn-off periods of 4 seconds. For safety reasons, charging and discharging of the sample was done in an inert nitrogen atmosphere using a glove box.

### 2.4 Synthesis of magnesium oxide and magnesium hydride from SAS-micronized magnesium acetate

Once the magnesium acetate precursor was micronized using SAS technique, two different products were obtained depending on the treatment of the precursor. Magnesium oxide was obtained after calcination of magnesium acetate at 400 °C for several hours in a furnace. During calcination, dehydration is followed by decomposition of organic part of the molecule, thus forming the oxide<sup>21</sup>. In order to form magnesium hydride, magnesium acetate was

treated with hydrogen at 30 bar H<sub>2</sub> and 350 °C for 8 h. These temperature and hydrogen pressure conditions are well above the equilibrium conditions of formation of magnesium hydride<sup>5</sup>. Thus hydrogenation of magnesium followed the removal of the organic part of the molecule by the thermal treatment. As magnesium hydride is a highly reactive and flammable compound, the hydrogenation reaction (as well as dehydrogenation measurements described in the following section 2.5) were performed in a closed, inerted pressure vessel, without any transfer to different vessels or exposure of the material to open air, and at the end of experiments the hydride was deactivated by calcination with air inside the same vessel before disposal.

### 2.5 Measurement of hydrogen release kinetics

Hydrogen release kinetics from particles of magnesium hydride were measured employing a volumetric cell. Weighed amounts of 0.1 - 0.2 g of micronized magnesium acetate were loaded inside the cell, of 5.4 mL of volume. Air was removed from inside the cell with a vacuum pump, down to an absolute pressure of less than 0.1 bar, and as described in section 2.3, magnesium acetate was hydrogenated by treating it with hydrogen at 30 bar and 350 °C for 8 h. After cooling down the cell, hydrogen was vented from the cell, vacuum was again applied down to a pressure of less than 0.1 bar, and the cell was thermostated at 350 °C. The release rate of hydrogen from the sample by thermal decomposition of magnesium hydride was determined by measuring the increasing gas pressure inside the cell, recorded with a GE Druck DPI-104 pressure transducer with an accuracy of 0.001 MPa.

### 2.6 Product characterization

Particle size distributions were measured from particles in liquid suspension (in acetone in the case of magnesium acetate, and ethanol in the case of magnesium oxide), using a laser diffraction instrument with a diode laser of 4 mW (Autosizer Lo-C, Malvern Instruments). This analytical procedure was performed in triplicate for each sample.

Particle morphology was observed by Scanning Electron Microscopy (SEM) using a Jeol JSM 820 equipment. A gold sputter was used to cover the samples with a thin layer of gold to allow the electron reflection for particle evaluation.

Particle structural properties and crystallinity were examined using an X-ray powder diffractometer (model Bruker Discover D8). The measuring conditions were CuK $\alpha$  radiation,  $\lambda=1.5418$  Å, 2 $\theta$  angle ranging from 5° to 70° with a scan rate of 4 s/step and a step size of 0.020°. Structural properties were also characterized by Fourier Transform Infrared

Spectroscopy (FT-IR), using a BRUKER ALPHA spectrometer with a Platinum-ATR single diffraction sampling module.

### 3. RESULTS AND DISCUSSION

#### 3.1 Micronization of magnesium acetate

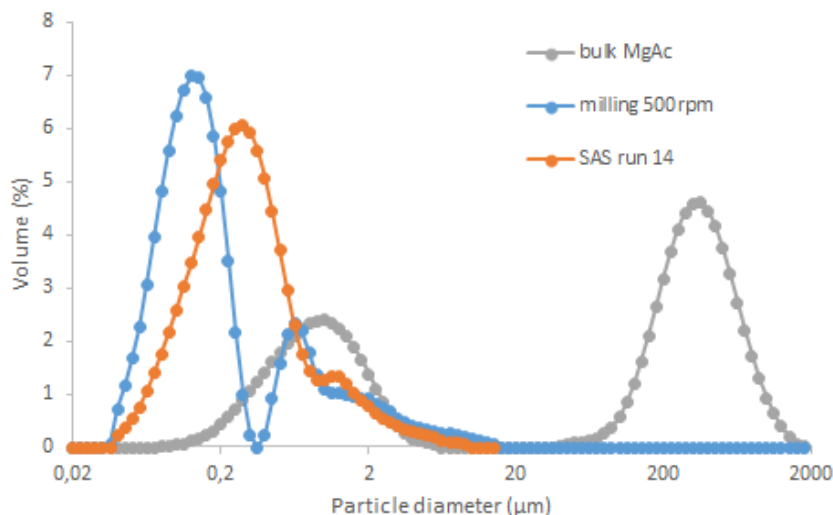
As described in section 2.2, several SAS precipitation experiments were carried out changing process conditions, including: concentration of magnesium acetate in the initial solution, temperature, and CO<sub>2</sub>/methanol proportion. Table 1 summarizes the experimental conditions tested, together with the mean particle size obtained.

Run	T (°C)	c (mg/mL)	xCO <sub>2</sub> (mol frac.)	Mean diameter d <sub>0,5</sub> (µm)	span
0	unprocessed			200±30	3.14
1	40	35.0	0.885	0.69±0.01	3.92
2	40	31.4	0.885	0.61±0.01	3.55
3	40	20.1	0.885	0.48±0.01	3.58
4	40	40.3	0.885	0.74±0.02	3.96
5	40	50.3	0.885	0.66±0.01	3.57
6	45	29.9	0.885	0.69±0.02	3.17
7	35	30.0	0.885	0.52±0.01	3.60
8	40	30.6	0.911	0.51±0.01	3.60
9	40	30.1	0.860	0.58±0.01	3.56
10	40	30.1	0.939	0.57±0.01	3.54
11	40	30.0	0.968	0.51±0.01	4.24
12	35	20.0	0.968	0.34±0.01	3.63
13	35	15.2	0.968	0.29±0.01	3.58
14	35	10.3	0.968	0.30±0.01	3.92

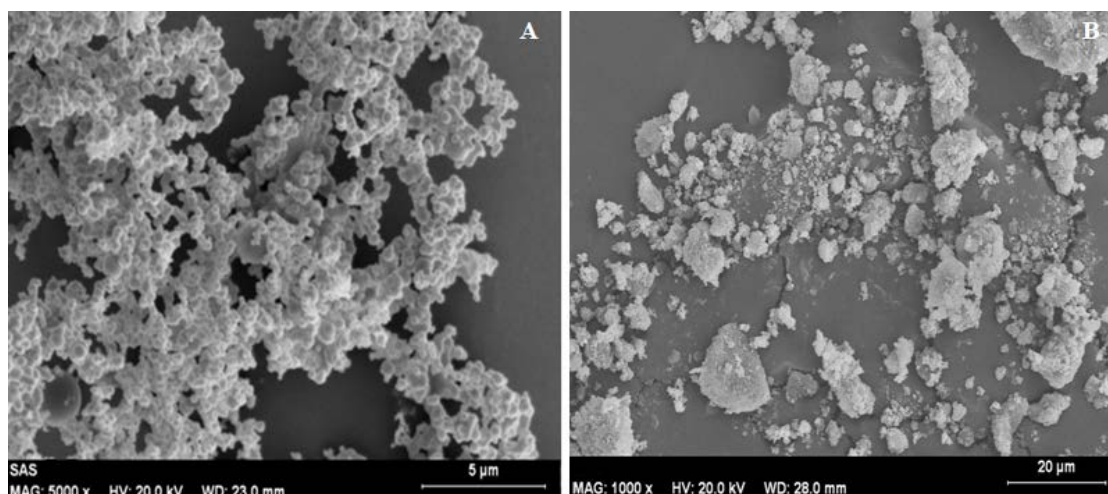
**Table 1.** Micronization of magnesium acetate by SAS technique: experimental conditions and mean particle size

Figure 3 presents a typical particle size distribution obtained by SAS precipitation, in comparison with milled and unprocessed magnesium acetate. It can be seen that both milling and SAS micronization yields a considerable reduction of particle size down to the sub-micrometer range (0.2 µm - 0.5 µm). However, the particle size distribution of the milled product continues being bimodal, while an unimodal distribution is obtained after SAS

processing. Regarding the morphology of the particles, as shown in Figure 4 homogeneous spherical microparticles, but with high agglomeration, are obtained after SAS processing whereas irregular agglomerates are obtained using mechanical milling.



**Figure 3.** Typical particle size distributions of unprocessed, milled and SAS-processed magnesium acetate



**Figure 4.** SEM micrographs of magnesium acetate micronized A) by SAS (magnification ratio 5000 x, size bar 5 μm) and B) by milling (magnification ratio 1000 x, size bar 20 μm)

Regarding the influence of the different SAS process conditions, previous experience on the application of SAS processing indicates that the concentration of the initial organic solution is one of the mean parameters influencing particle size<sup>14</sup>. In this work, two sets of experiments were carried out in order to study this parameter: experiments 1-5, at a fixed temperature of 40 °C and CO<sub>2</sub> molar fraction of 0.885, and experiments 11-14, at a temperature of 35 °C and CO<sub>2</sub> molar fraction of 0.968. The obtained particle size distributions are shown in Figure 5. As shown in this figure, when the concentration of MgAc in the solution was increased, the mean

particle size also increased and the distribution enlarged in both series of experiments. This tendency was more pronounced in the range of concentration 10-20 mg/mL at 35 °C than between 30-40 mg/mL at 40 °C. Comparing the morphology of particles obtained, as presented in Figure 6 it can be observed that the same morphology, consisting of highly agglomerated spherical particles, were obtained in the different experiments, but with slightly larger spherical particles in experiments with higher MgAc concentrations. Samples with higher initial concentrations also showed a higher agglomeration in bigger flocks.

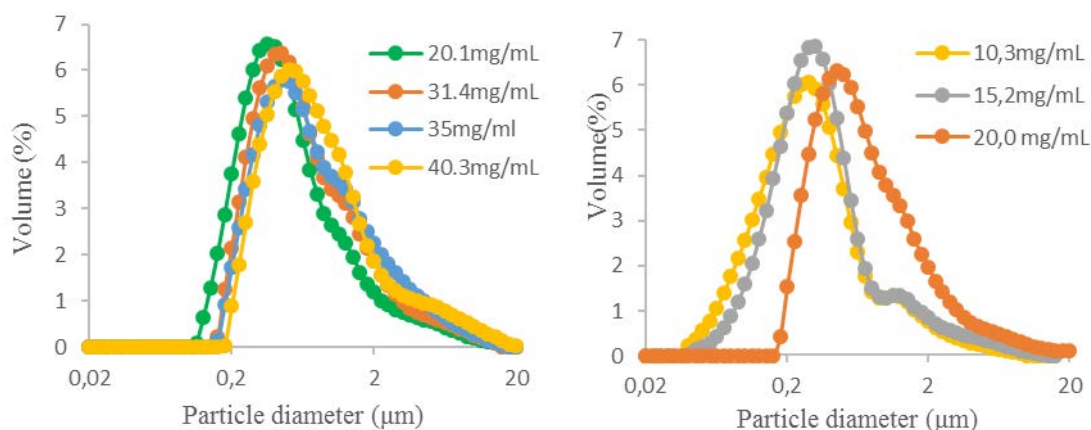


**Figure 5.** Influence of concentration of magnesium acetate on the Particle Size Distribution at 40 °C, 90 bar and  $xCO_2=0.886$  on the left, and at 35 °C, 90 bar and  $xCO_2=0.968$  on the right

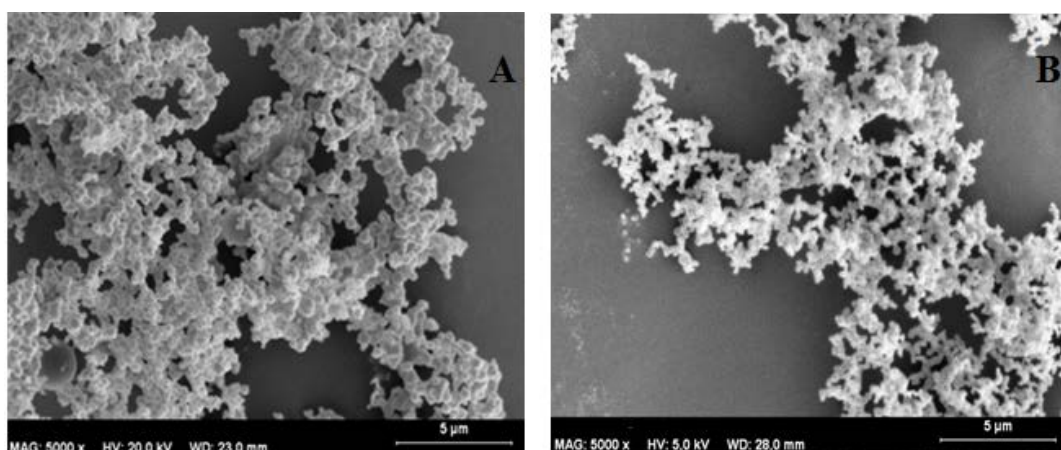


**Figure 6.** SEM images of SAS-processed magnesium acetate, A ) produced at 31.4 mg/mL, 40 °C (experiment 2 of Table 1); B) produced at 15.2 mg/mL, 35 °C (experiment 13 of Table 1). Both micrographs obtained with a magnification ratio of 5000 x, and reported with a size bar of 5  $\mu m$

In most cases, smaller particle sizes are expected at higher initial solute concentrations in processes with very fast particle formation kinetics such as the SAS technique. This is due to the higher supersaturations that can be achieved with higher solute concentrations in these processes, which exponentially increases the rate of formation of new particles by

nucleation<sup>13,22</sup>. However, a trend of increasing particle size at higher concentrations is sometimes observed in SAS experiments. Reverchon et al. proposed that this trend could be due to the formation and growth of particles inside solution droplets, stabilized by a vanishing transient interfacial tension between solution and supercritical CO<sub>2</sub><sup>23</sup>. When the initial concentration of solute is increased, the resulting transient interfacial tension is also increased, enabling to stabilize the droplets during a longer time, and therefore allowing for a higher growth of particles inside these droplets. Another possible explanation is an increase of the growth rate of particles by coagulation and condensation mechanisms<sup>22</sup>.

Another parameter with a strong influence on particle size is the operating temperature. This parameter was analyzed with experiments 2, 6 and 7 of Table 1. As presented in Figure 7, an increase in the operating temperature led to an enlargement of the particle size distribution, associated with an obvious increase in the diameter of the particles as shown in SEM micrographs. This result can be due to the operation at conditions that are closer to the two-phase region of the methanol-carbon dioxide phase diagram when temperature is increased<sup>20</sup>. This proximity can slow down the mixing between organic solvent and supercritical fluid, thus allowing for a longer growth of particles inside a solvent-rich phase.

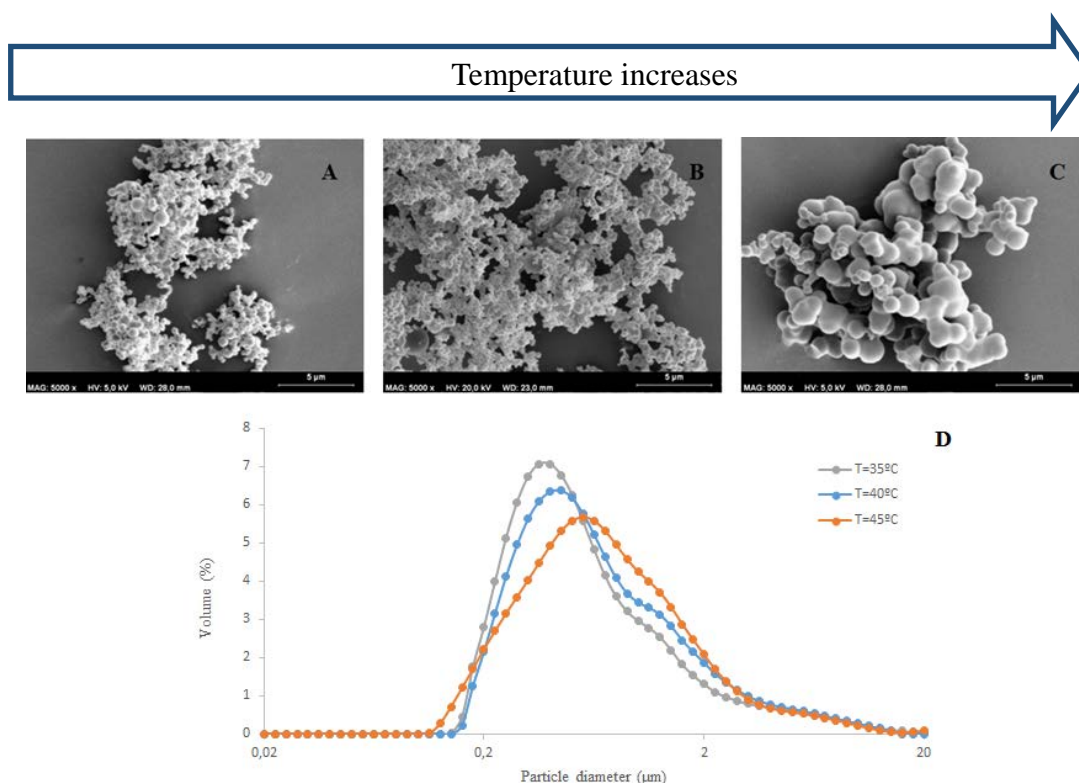


**Figure 7.** SEM images of magnesium acetate obtained at 90 bar, 30 mg/mL, 2 Kg/h CO<sub>2</sub> and 4 mL/min of solution A ) produced at 35 °C (run 7); B) produced at 40 °C (run 2), C) produced at 45 °C (run 6) D) PSD at different temperatures. All micrographs are reported with a magnification ratio of 5000x and a size bar of 5 µm

The influence of the proportion between methanol and  $\text{CO}_2$  was analyzed with experiments 2 and 8-11 of Table 1. The proportion between the two fluids was varied maintaining a constant  $\text{CO}_2$  flowrate of 2 kg/h and varying the flowrate of the solution between 1 and 5 mL/min. As observed in Figure 8, this parameter had a small influence on the particle size, limited to a minor enlargement of the tail of the particle size distribution with smaller  $\text{CO}_2$ /methanol proportions (or higher methanol flowrates), yielding mean particle sizes near 0.6  $\mu\text{m}$  in all experiments.

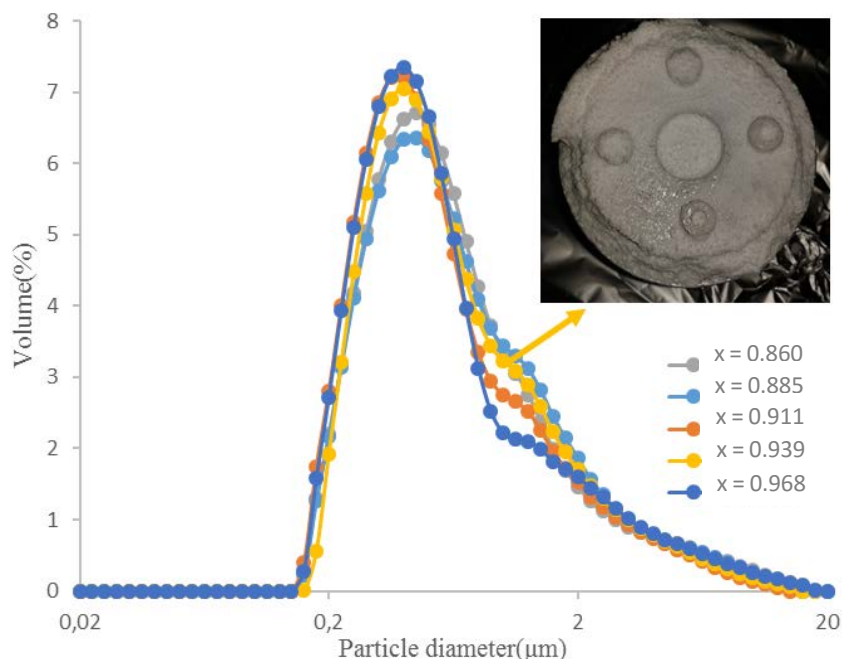


**Figure 8.** Influence of  $\text{CO}_2$  molar fraction on the PSD at 40 °C, 90 bar and 30 mg/mL. On the upper-left corner insert, a photograph of the precipitator filter after SAS processing run 10 is presented, showing the bulk appearance of the powder

The morphological variations in SAS-processed magnesium acetate are associated with variations in the crystalline structure of the material, as it is demonstrated by the X-ray diffractograms of unprocessed and processed using either SAS or mechanical milling magnesium acetate, presented in Figure 9. While the unprocessed and milled material were crystalline, as evidenced by several well-defined peaks in the diffractogram, the X-ray diffractogram of the SAS-processed compound was completely flat, indicating an amorphous structure. This result agrees with the spherical morphology of particles observed in SEM micrographs that generally indicates an amorphous structure of the material<sup>22</sup>. For clarity, Figure 9 only shows the diffractogram of particles obtained with experiment 6 of Table 1, but identical results were obtained in all experiments.

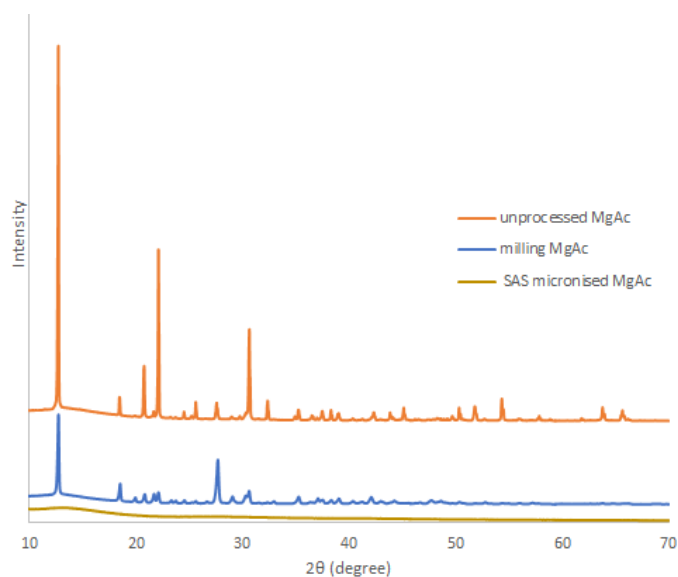


**Figure 9.** XRD of unprocessed , SAS-processed (run 6) and mechanical milling magnesium acetate.

Figure 10 presents the room temperature Fourier transform infrared (FTIR) spectra of unprocessed and micronized magnesium acetate. The spectra of the unprocessed compound agreed well with results reported in the literature<sup>24</sup>. Comparing the spectra of the unprocessed and SAS-processed material, the most notable difference was the drastic reduction of the broad peak near 3000 cm<sup>-1</sup> by SAS processing, which indicates the removal of water from the compound. At other wavenumbers, the same characteristic peaks were observed in the two spectra, with some modifications in the relative intensity of peaks that could be due to the variation of the crystalline structure of the material evidenced by XRD assays.

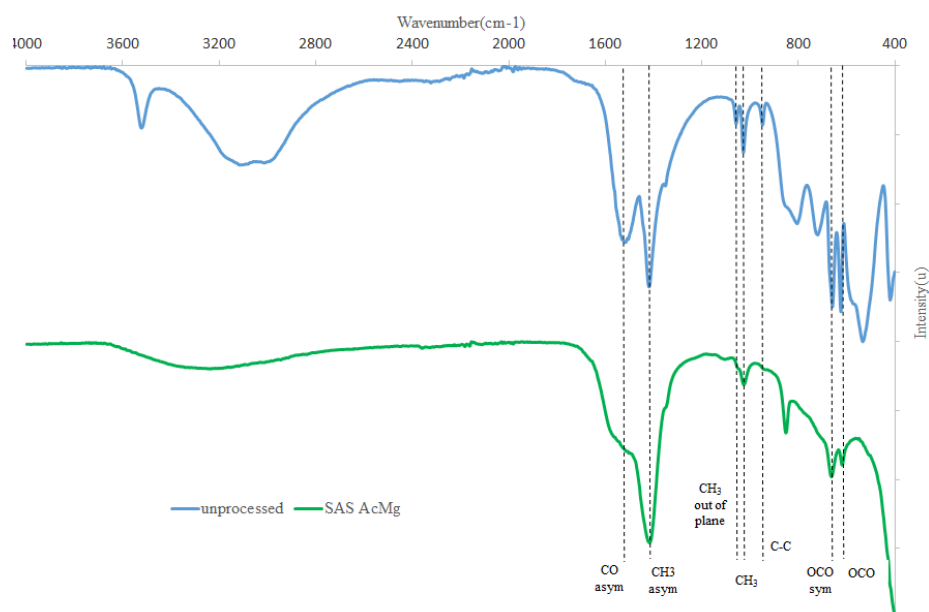


**Figure 10.** FTIR of unprocessed SAS-processed magnesium acetate (run 6)

### 3.2 Production of magnesium oxide

As previously described, SAS-micronized magnesium acetate samples were calcined at 400 °C in order to remove the organic acetate groups and obtain magnesium oxide. The obtained mean particle sizes are shown in Table 2, while Figure 11 presents micrographs of MgO samples.

Run	T (°C)	C (mg/mL)	xCO <sub>2</sub>	Mean diameter d <sub>0,5</sub> (μm)	%Weight loss (w/w)
0c	unprocessed			177±20	79.5
1c	40	35.0	0.885	134±28	68.0
2c	40	31.4	0.885	141±8	-
3c	40	20.1	0.885	70±5	65.0
4c	40	40.3	0.885	173±17	70.7
5c	40	50.3	0.885	117±16	66.3
6c	45	29.9	0.885	56±5	67.3
7c	35	30.0	0.885	132±18	67.8
8c	40	30.6	0.911	157±17	67.6
9c	40	30.1	0.860	139±18	68.7
10c	40	30.1	0.939	132±5	68.2
11c	40	30.0	0.968	151±3	71.8

**Table 2.** MgO results after calcination treatment at 400 °C

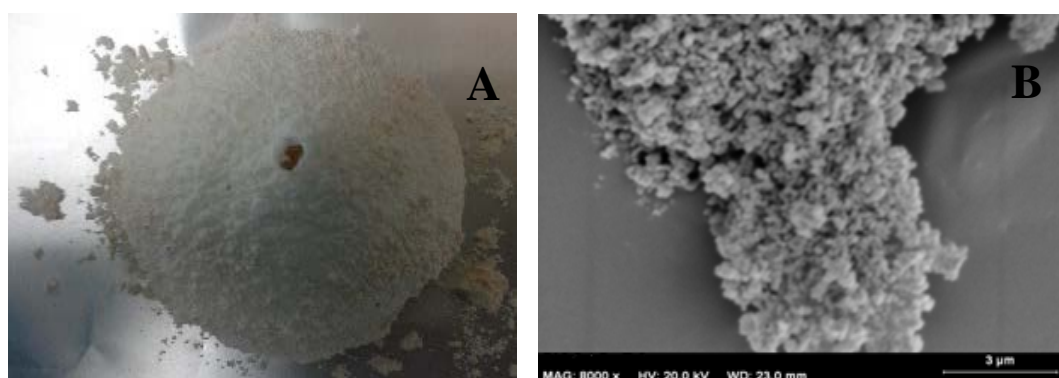


**Figure 11.** A) Photograph of sintered block of MgO obtained after calcination of unprocessed MgAc B) SEM micrograph after calcination of SAS processed MgAc (run 2c), with a magnification ratio of 8000 x and size bar of 3 μm

In Figure 11, it can be seen that upon calcination, unprocessed magnesium acetate formed a solid block that could not be analyzed by SEM. With SAS-processed samples, a powder was

obtained, that as shown in the SEM micrograph was constituted by spherical particles with a smaller size than the original particles of magnesium acetate (see Figures 6 and 7), but highly agglomerated and fused together. This visual impression was confirmed by laser diffraction size measurements, that yielded mean particle sizes ranging from 50 to 180  $\mu m$ . Comparing this measurement with the morphology of particle shown in Figure 10, it can be concluded that these measurements correspond to the size of agglomerates, and not of the individual spherical particles.

Analyzing the particle size distributions, presented in Figure 12, it can be seen that all distributions showed a long head, probably corresponding to small spherical particles that were detached from the agglomerates, and practically no tail. An analysis of the influence of the parameters which were studied in SAS process reveals, in general, the same trends observed in SAS experiments reported in section 3.1: the particle size of calcined, SAS-processed samples was lower than that of calcined unprocessed samples, and the size increased when the concentration of magnesium acetate in the initial solution was higher. Interestingly, a different result was obtained in the case of the operating temperature: higher temperatures yielded bigger MgAc particles, but after calcination the size of the resulting MgO particles was significantly lower. Probably, this result is associated with the variation in the morphology of magnesium acetate particles with process conditions described in section 3.1: slightly larger spherical particles with increased agglomeration when the initial concentration was increased, that form bigger agglomerates after calcination, compared to significantly larger spherical particles but without so much agglomeration when temperature was increased, thus leading to the formation of smaller agglomerates after calcination.

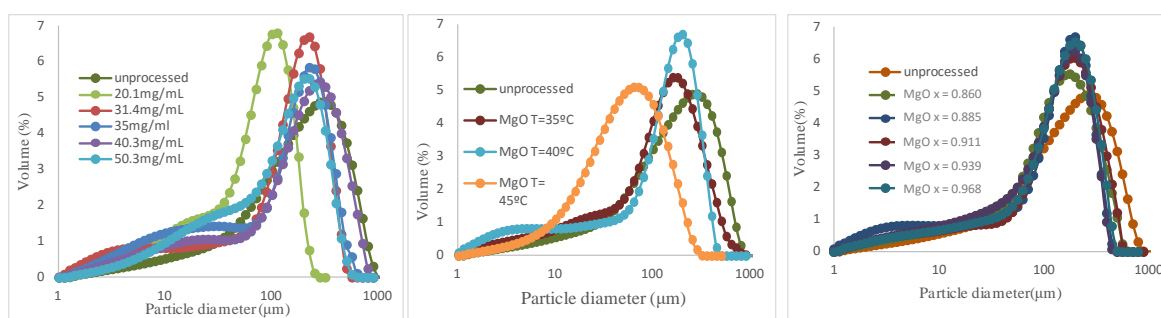


**Figure 12.** Effect of concentration, temperature and molar fraction of  $CO_2$  in SAS process on PSD of MgO obtained after thermal treatment at 400 °C

Regarding to the weight loss associated with the removal of the organic part of the molecule in the thermal treatment, for unprocessed magnesium acetate tetrahydrate the expected weight loss in the transformation to magnesium oxide is 81.2 wt%. As reported in Table 2, a weight

loss of 79.5 wt% was observed experimentally, in good agreement with the theoretical value corresponding to a nearly total oxidation of the compound. In contrast, in all SAS-micronized samples a weight decrease between 68 wt% and 72 wt% was observed. These values correspond to an expected weight loss of 71 wt% in the formation of oxide from dehydrated magnesium acetate, in agreement with the results of FT-IR assays presented in Figure 9, that indicated that hydration water was removed by SAS treatment, and therefore also correspond to a practically complete conversion into oxide.

Figure 13 shows the XRD of MgO samples that have been obtained from micronized and unprocessed precursor. In all the cases, crystalline powders with a cubic structure are obtained according to the International Centre Diffraction Data Power Diffraction File (ICCD-PDF2) standards. Three peaks are observed at  $2\theta = 36.8, 42.8$  and  $62.1^\circ$  which correspond to the (111), (200) and (220) faces respectively, indicating the presence of random crystallites.

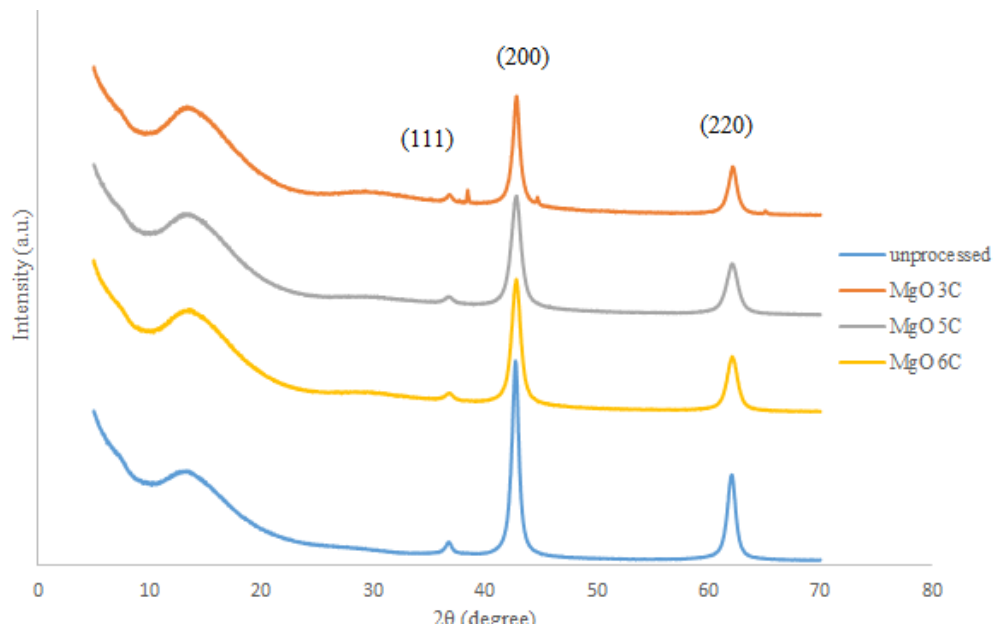


**Figure 13.** Diffractograms of MgO powders obtained at 400 °C from MgAc (unprocessed and micronized with SAS process)

Using the results reported in Figure 13, the average crystallite size of the samples ( $D$ ) was calculated using Scherrer's formula<sup>25</sup> and considering the mean of each diameter obtained for every peak:

$$D = \frac{K\lambda}{\beta \cos\theta} \quad (2)$$

where  $K$  is a Scherrer constant (0.9 for spherical particles),  $\lambda$  is the wavelength of the incident x-rays ( $1.5418 \text{ \AA}$ ),  $\beta$  is the full width at half maximum (FWHM) and  $\theta$  is the Bragg angle.

On the other hand, particle size and strain was estimated by Williamson-Hall plot<sup>26</sup>:

$$\beta \cos \theta = \frac{K\lambda}{D} + 4\epsilon \sin \theta \quad (3)$$

where K,  $\beta$ ,  $\lambda$ ,  $\theta$  have the same values than in Scherrer equation and  $\epsilon$  is the effective strain. By representing  $4\epsilon \sin \theta$  against  $\beta \cos \theta$ , the strain is obtained from the slope and the diameter of the grain (D) from the intercept value on y-axis. The results are summarized in Table 3. In this table, it can be observed a reduction in the crystallite size due to SAS processing of the precursor material. Regarding to the strain, it is tensile in all the cases (positive) and with a similar value due to the thermal treatment at the same temperature (400 °C) in all the experiments. Compared with literature values, that report grain sizes in the range 5-50 nm<sup>27,28,29</sup>, the values obtained in this work (10-13 nm) are slightly smaller.

	Cristallite size (nm)		Strain ( $\times 10^{-4}$ )
	D <sub>Debye-Scherrer's</sub>	D <sub>W-Hplot</sub>	
Unprocessed	12.6 $\pm$ 1.4	19.5	25
SAS3c	12.0 $\pm$ 1.0	17.1	22
SAS5c	8.9 $\pm$ 0.5	10.9	18
SAS6c	9.7 $\pm$ 0.9	13.7	27

**Table 3.** Estimated crystalline structure parameters of MgO

### 3.3 Production of magnesium hydride

As described in section 2.4, particles of magnesium hydride were obtained by reduction of micronized magnesium acetate with hydrogen. Figure 14 shows FT-IR spectra of magnesium acetate, magnesium hydride obtained by reduction of acetate, and magnesium after dehydrogenation of the hydride by thermolysis. The spectra of MgAc show peaks characteristic of C-O bonds present in the acetate group. After hydrogenation, these peaks are replaced by characteristic peaks of Mg-H bonds and, as expected, these peaks are not observed in the spectra of the dehydrogenated product<sup>30</sup>.

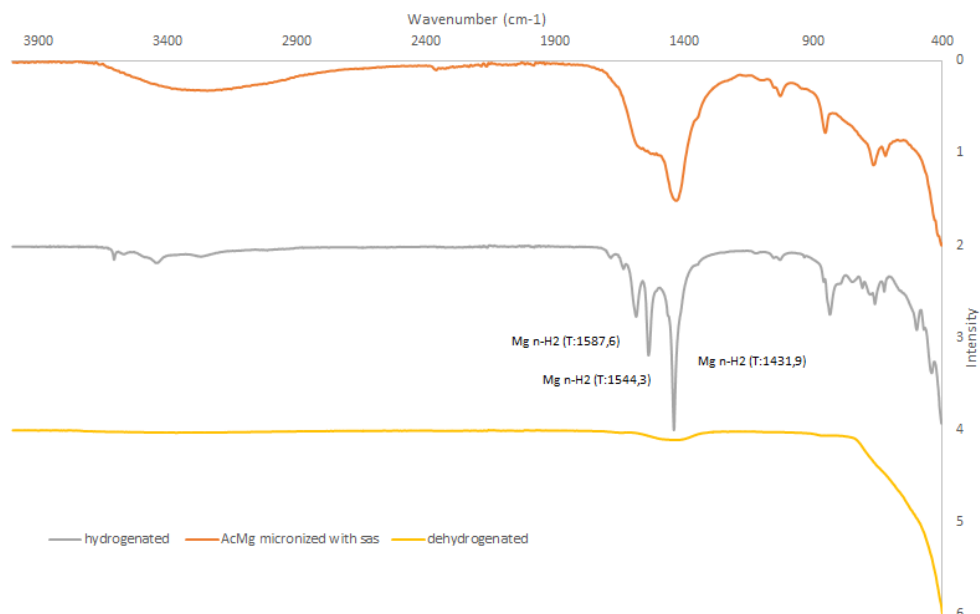


**Figure 14.** FT-IR spectra of  $MgH_2$  obtained after treating the precursor  $MgAc$  with hydrogen at different conditions

Figure 15 shows the kinetics hydrogen from unprocessed and SAS-processed samples. It can be seen that SAS processing improves the kinetics, considerably reducing the time needed to release 2 wt% of  $H_2$  from 10 h in unprocessed  $MgAc$  to 4 h (SAS run 6), 2 h (SAS run 5) or 1 h (SAS run 14). This improvement is due to the reduction of particle size and the corresponding reduction of hydrogen diffusion lengths. The differences in the kinetics observed from different SAS-processed samples can be related to the differences in the size and morphology of the particles of  $MgAc$  precursor. As presented in Figure 16, the product obtained in SAS experiments 5 and 6 show similar PSDs, with a slightly smaller mean particle size in the case of SAS experiment 5 that as shown in Figure 14 produces a moderately faster  $H_2$  release. In the case of experiment 14, a significantly smaller particle size was obtained, that as shown in Figure 15 results in a faster  $H_2$  release and a higher final  $H_2$  yield.

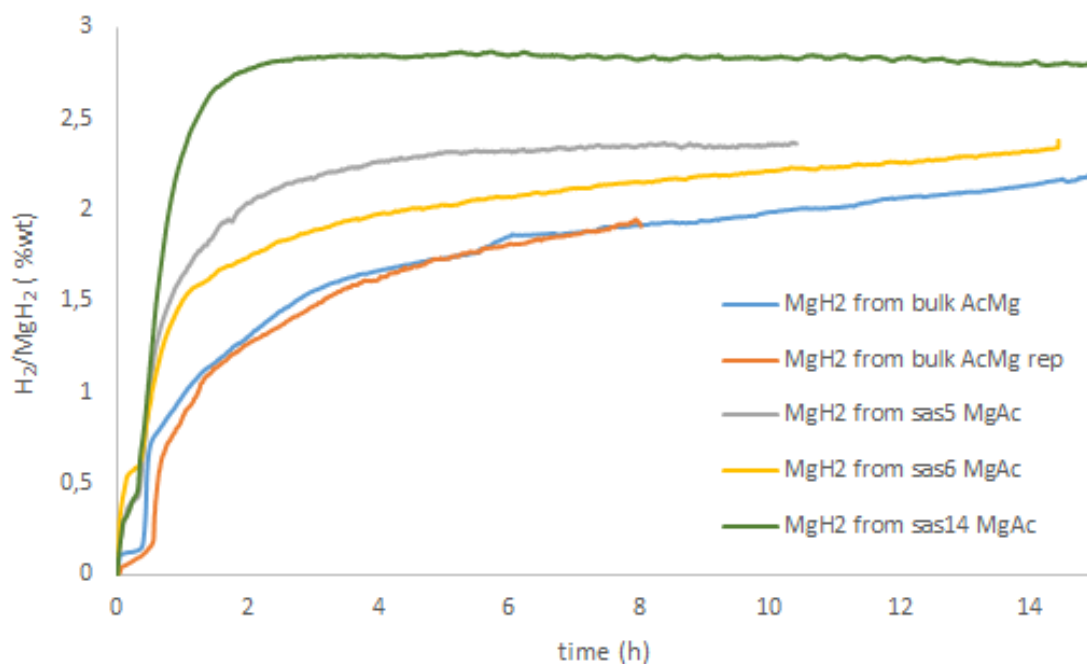


**Figure 15.** Hydrogen release kinetics by thermolysis of  $MgH_2$  at 350 °C

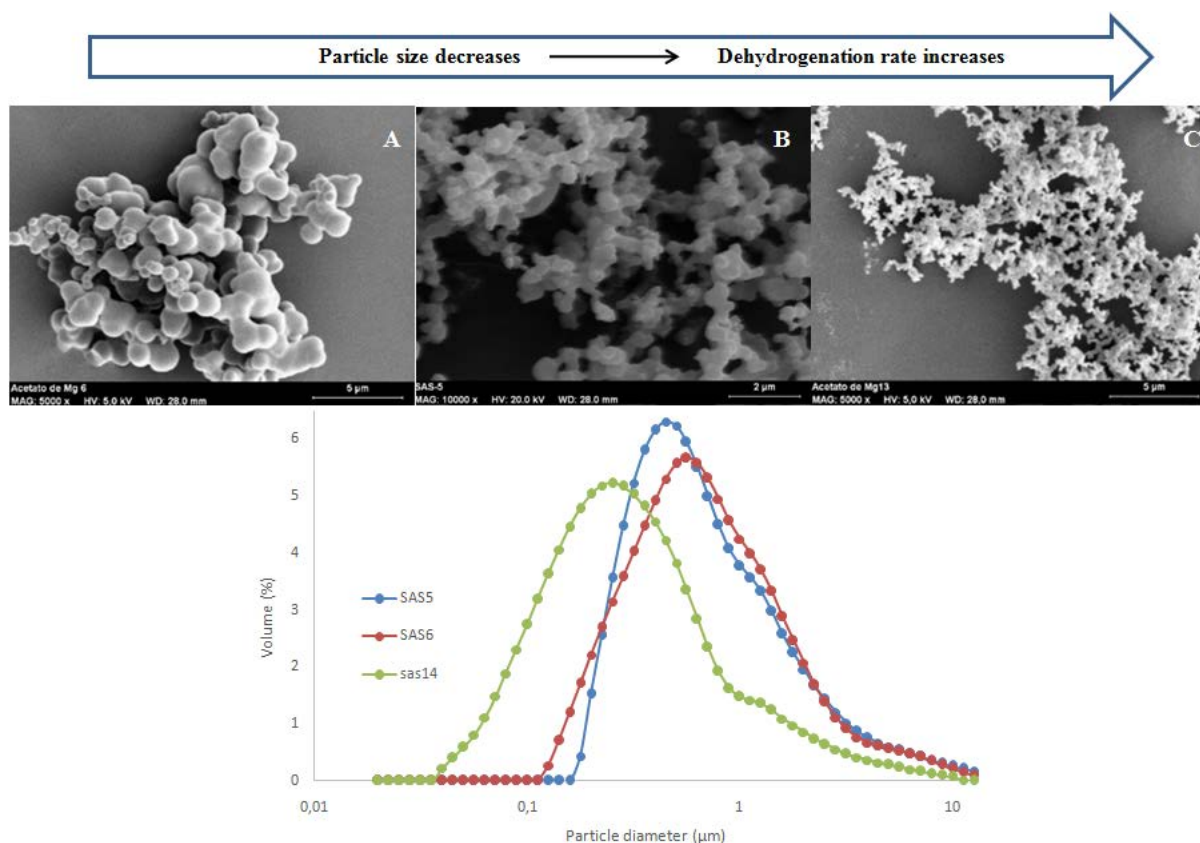


**Figure 16.** SEM and PSD of SAS-processed  $MgAc$  precursor A) sample 6 B) sample 5 and C) sample 14

It is remarkable that, compared to a theoretical hydrogen storage capacity of  $MgH_2$  of 7.6 %wt, hydrogen yields ranging from 2 wt% to 3 wt% were obtained in all experiments, corresponding

to about one third of the maximum theoretical capacity of the hydride. This result indicates that, in all cases, a significant fraction of the compound did not participate in the hydrogenation - dehydrogenation reactions, probably corresponding to material in the core of particles that remained inaccessible for the formation of hydride by reaction with gaseous hydrogen, or to magnesium lost through formation of magnesium oxide<sup>31</sup>.

#### 4. CONCLUSIONS

Magnesium acetate was successfully micronized by Supercritical Anti Solvent (SAS) technique. Sub-micrometric particle sizes (300 nm - 600 nm) were obtained, with bigger particle sizes when the operating temperature or the initial solution concentration was increased. In contrast with milled particles, that showed similar mean sizes but had very irregular morphologies and were crystalline, SAS - processed particles were amorphous and showed a regular spherical morphology, but with considerable agglomeration. SAS-micronized magnesium acetate could be converted into powderous magnesium oxide, preserving the spherical morphology of particles, or into magnesium hydride. The release rate of hydrogen by thermolysis of magnesium hydride was enhanced by the micronization, with a direct relationship between the particle size of the magnesium acetate precursor and the rate of release of hydrogen from the hydride. However, the obtained hydrogen yield indicated that a significant fraction of the particle remained inaccessible for the hydrogenation-dehydrogenation reactions.

## REFERENCES

- (1) Dresselhaus, M. S.; Thomas, I. L. *Nature* **2001**, *414*, 332-337.
- (2) [www1.eere.energy.gov/hydrogenandfuelcells/storage/pdfs/targets\\_onboard\\_hydro\\_storage.pdf](http://www1.eere.energy.gov/hydrogenandfuelcells/storage/pdfs/targets_onboard_hydro_storage.pdf)
- (3) Liu, C.; Li, F.; Ma, L. P.; Cheng, M. H. *Adv. Energy Mater.* **2010**, *22*, 28-62.
- (4) Delhomme, B.; De Rango, P.; Marty, P.; Bacia, M.; Zawilski, B.; Raufast, C.; Miraglia, S.; Fruchart, D. *Int. J. Hydrogen Energ.* **2011**, *37*, 9103-9111.
- (5) Chaise, A.; De Rango, P.; Marty, P.; Fruchart, D. *Int. J. Hydrogen Energ.* **2010**, *35*, 6311-6322.
- (6) Bérubé, V.; Radtke, G.; Dresselhaus, M.; Chen, G. *Int. J. Energ. Res.* **2007**, *31*, 637-663.
- (7) Niemann, U.; Srinivasan, S. S.; Phani, A. R.; Kumar, A.; Goswami, D. Y.; Stefanakos, E. K. *J. Nanomater.* **2008**, Article ID 950967, 1-9.
- (8) Nielsen, T. K.; Polanski, M.; Zasada, D.; Javadian, P.; Besenbacher, F.; Bystrzycki, J.; Skibsted, J.; Jensen, T. R. *ACS Nano* **2011**, *5*, 4056-4064.
- (9) Vajeeston, P.; Ravindran, P.; Vidya, R.; Fjellvag, H.; Kjekshus, A. *Cryst. Growth Des.* **2004**, *4*, 471-477.
- (10) Aramini, M.; Milanese, C.; Pontiroli, D.; Gaboardi, M.; Girella, A.; Bertoni, G.; Riccò, M. *Int. J. Hydrogen Energ.* **2014**, *39*, 2124-2131.
- (11) Vajo, J.; Mertens, F.; Ahn, C.; Bowman, R.; Fultz, B. *J. Phys. Chem.* **2004**, *108*, 13977-13983.
- (12) Zhu, Z.; Hosokai, S.; Matsumoto, I.; Akuyama, T. *Cryst. Growth Des.* **2010**, *10*, 5123-5128.
- (13) Martín, A.; Cocero, M. J. *Adv. Drug Delivery Rev.* **2008**, *60*, 339-350.
- (14) Martín, A.; Scholle, K.; Mattea, F.; Meterc, D.; Cocero, M. J. *Cryst. Growth Des.* **2009**, *9*, 2504-2511.
- (15) Rueda, M.; Sanz-Moral, L. M.; Nieto-Márquez, A.; Longone, P.; Mattea, F.; Martín, A. Production of silica aerogel microparticles loaded with ammonia borane by batch and semicontinuous supercritical drying techniques. *J. Supercrit. Fluids* **2014**, *92*, 299-310.
- (16) Dedrick, D. E.; Behrens, R.; Bradshaw, R. W. The reactivity of sodium alanates with O<sub>2</sub>, H<sub>2</sub>O and CO<sub>2</sub>. *Sandia Report SAND2007-4960*, **2007**, 1-55.
- (17) Nielsen, T. K.; Manickam, K.; Hirscher, M.; Besenbacher, F.; Jensen, T. R. *ACS Nano* **2009**, *3*, 3521-3528.

- (18) Severa, G.; Rönnebro, E.; Jensen, C. M. *Chem. Commun.* **2010**, *46*, 421-423.
- (19) Aguey-Zinsou, K. F.; Ares Fernandez, J. R.; Klassen, T.; Bormann, R. *Mater. Res. Bull.* **2006**, *41*, 1118-1126.
- (20) Tochigi, K.; Namae, T.; Suga, T.; Matsuda, H.; Kurihara, K.; dos Ramos, M.; McCabe, C. J. *Supercrit. Fluids* **2010**, *55*, 682-689.
- (21) Bazhan, Z.; Ghodsi, F.; Mazloom, B. *Mater. Sci.* **2013**, *36*, 899-905.
- (22) Martín, A.; Cocero, M. J. J. *Supercrit. Fluids* **2004**, *32*, 203-219.
- (23) Reverchon, E.; Adami, R.; Caputo, G.; De Marco, I. *J. Supercrit. Fluids* **2008**, *47*, 70-84.
- (24) Koleva, V.; Stoilova, D. *J. Mol. Struct.*, **2002**, *611*, 1-8.
- (25) Patterson, A. *Phys. Rev.* **1939**, *56*, 978-982.
- (26) Williamson, G.; Hall, W. *Acta Metall.* **1953**, *1*, 22-31.
- (27) Alvarado, E.; Torres-Martinez, L.; Fuentes, A.; Quintana, P. *Polyhedron* **2000**, *19*, 2345-2351.
- (28) Devaraja, P.; Alvalhani, D.; Prashantha, S.; Nagabhushana, H.; Sharma, S.; B. Nagabhushana, B.; Nagaswarupa, H. *Spectrochim. Acta A* **2014**, *118*, 847-851.
- (29) Moses, A.; Nehru, L.; Jayachandran, M.; Sanjeeviraja, C. *Cryst Res. Technol.* **2007**, *42*, 867-875.
- (30) Wang, X.; Andrews, L. *J. Phys. Chem. A* **2004**, *108*, 11511-11520.
- (31) Selvam, P.; Viswanathan, B.; Swamy, C. S.; Srinivasan, V. *Int. J. Hydrogen Energ.* **1986**, *11*, 169-192.

# **CHAPTER 2**

**Enhancement of hydrogen release kinetics  
from ethane 1,2 diamineborane (EDAB) by  
micronization using Supercritical  
Antisolvent (SAS) Precipitation**



## Enhancement of hydrogen release kinetics from ethane 1,2 diamineborane (EDAB) by micronization using Supercritical Antisolvent (SAS) Precipitation<sup>1</sup>

### Abstract

Ethane 1, 2 diamineborane (EDAB) was micronized from THF solutions using Supercritical Antisolvent (SAS) process. The influence of temperature, solute concentration and carbon dioxide fraction on the final properties of EDAB particles was studied. By SAS micronization, the original prismatic EDAB particles of about 400  $\mu\text{m}$  with a crystallite size of 100 nm were converted into microspheres of less than 2  $\mu\text{m}$  with a crystallite size of 50 nm. This reduction in the particle and grain sizes resulted in an improvement in thermal properties. The kinetics of release of hydrogen by thermolysis at 100 °C was also significantly enhanced due to the reduction in the diffusion length, reducing the time needed for the decomposition of the hydride by a factor of six. Moreover, a suppression of induction time was obtained by destabilization of the hydride after treatment. XRD and FTIR analyses showed that no chemical decomposition and no variation of the crystalline structure took place by SAS processing.

**Keywords:** Hydrogen storage; Ethane diamineborane; micronization; kinetics; supercritical carbon dioxide; supercritical anti solvent

<sup>1</sup> Chemical Engineering Journal 306 (2016), 164-173

## 1. INTRODUCTION

In recent years, important efforts have been made in order to find renewable energy sources that can satisfy the current necessities. This is promoted by the depletion of fossil fuels and the climate change due to the release of greenhouse gases [1]. However, an important limitation of the main renewable energy resources is the unpredictability of fluctuations in their output. In this context, hydrogen could be a solution to these problems using it as an energy vector, in an approach known as 'hydrogen economy' or 'hydrogen society' [2].

In the case of onboard applications, the simplest idea would be to use hydrogen as gas or a liquid. However, in the case of gas, high pressures tanks would be necessary in order to have the required high density of hydrogen and this would mean high volumes of tanks and, therefore, high costs of material. Using hydrogen at cryogenic conditions, a considerable energy input (estimated around 30% of the total energy stored in hydrogen) would be required in order to maintain the desired temperature [3]. For these reasons, solid state hydrogen storage appears as a compelling alternative.

Different solid hydrogen storage materials have been tested, such as metal hydrides, complex hydrides [4], metal organic frameworks (MOF) [5], adsorbents, polymer composites or clathrate hydrates [6], among others [7,8]. However, till now, no material satisfies all the latest targets set for onboard applications by the US Department of Energy (DoE) for 2017 for a practical automotive application (5.5 wt% hydrogen content, release temperature at 85 °C, 100% reversibility, good cyclability) [9].

Many recent research works have been focused in boron-nitrogen-hydrogen systems, especially in ammonia borane (AB). AB has been widely investigated due to its high content of hydrogen (19.6 wt%) which is released at moderate temperatures. Moreover, it is non-toxic and stable at room temperature. However, the most important limitations related to this compound are the regeneration and cyclability of the compound and the emission of some volatile byproducts as borazine, diborane or ammonia during the release of hydrogen which could be poisonous for the fuel cell [10].

Carbon derivatives of AB, such as ethane 1,2 diamineborane ( $\text{BH}_3\text{NH}_2\text{CH}_2$ )<sub>2</sub>, known as EDAB, are promising alternatives. EDAB has a high content in hydrogen (10 wt%), which is released below 200 °C in a two-step reaction. Moreover, it is also very stable under ambient conditions (particularly, against ambient oxygen and humidity), even more than AB, which facilitates the manipulation of this material. However, only a few works can be found related to this compound [11,12,13]. Among other results, it has been observed that the modification of AB

to obtain EDAB produces a chemical structure with a stronger B-H bond and a more thermal stable B-N bond due to the existence of C-N and C-C bonds, resulting in the production of less non-desirable volatile gases in the hydrogen outstream [11]. However, more investigation is necessary in order to destabilize the compound during thermal decomposition process at moderate temperatures, in order to improve the kinetics of release of hydrogen.

Nanoengineering could be a solution to reduce the crystallite size and improve the decomposition rate by increasing the diffusion rate and therefore, reduce the hydrogen release temperature [7]. Different methods can be used in order to reduce the size of the metal hydride such as laser ablation, vapor condensation, sputtering or ball milling [14]. One of the most used methods is ball milling [4,15]. With this method, hydrogen release kinetics are enhanced due to the reduction of the diffusion lengths without any cost of a catalyst or a reduction of storage capacity. Milling can also induce other material changes, such as an increase in the number of defects [16], create more disorder and strain into the material [17], and therefore improve surface properties.

The problem of this method is the inhomogeneity of the product after milling [18]. Because of this disadvantage, Supercritical Antisolvent Solution is proposed as a promising alternative method in order to micronize the hydride controlling the reduction of the particle size by changing the conditions and the supersaturation driving forces. In this way, the advantages of milling are present in this method, while obtaining a much more homogeneous product. This technique has been used to micronize a wide range of compounds such as polymers, pharmaceutical compounds [19] or catalysts. For its application, the only requirement is that the compound which is going to be micronized needs to be soluble in an organic solvent and stable in CO<sub>2</sub> atmosphere [20].

In this work, the micronization of EDAB from THF solutions using Supercritical Antisolvent (SAS) process is reported. The influence of the concentration of the solution, the temperature and the carbon dioxide molar fraction on the properties of the micronized product has been studied. Scanning electron microscopy, FT-IR spectroscopy, X-ray diffraction, DSC analyses and the measurement of hydrogen release kinetics by thermal decomposition at 100 °C have been done in order to characterize and compare the final products obtained at different conditions in contrast to the bulk EDAB.

## **2. EXPERIMENTAL METHODS**

### **2.1 Materials**

Ethane 1,2 diamineborane (EDAB, purity: 96 wt%) was supplied by Sigma-Aldrich. As shown in the SEM micrograph presented in Figure 1, the material was constituted by prismatic particles of around 400  $\mu\text{m}$ .

Dry tetrahydrofuran (with maximum water of 0.0075 wt%) was purchased from Panreac (Spain). Carbon dioxide (purity: 99.95 wt%) was supplied from Carbueros Metálicos S.A. (Spain).

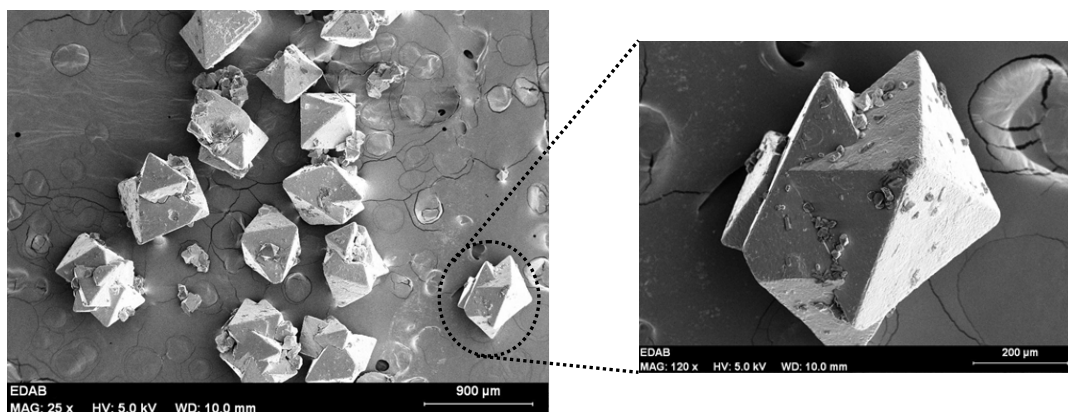


**Figure 1.** SEM image (magnification ratio: 25x/120x, size bar: 900  $\mu\text{m}$ /200  $\mu\text{m}$ ) of unprocessed EDAB

## 2.2 Micronization of EDAB by Supercritical Anti Solvent (SAS) process

Supercritical Antisolvent technique is the process used to micronize EDAB in this work. It takes place in the same semi continuous equipment reported in a previous work [18], and schematically represented in Figure 2.

A cylindrical vessel of 1.5 L was used as precipitator. First, preheated carbon dioxide was pumped at a flowrate of 2 kg/h with a diaphragm pump (Dosapro Milton Roy, Spain) until stable conditions of temperature and pressure were reached. The pressure was maintained in all the experiments at 100 bar in order to have a single phase in the system [21]. Pressure was controlled with a back pressure valve (model BP66, GO, USA).

Then, pure THF was flowed to the precipitator in order to obtain steady composition conditions of the fluid phase. After this, 0.5 g of EDAB dissolved in different volumes (0.02-0.15 L) of THF, depending on the concentration studied in each experiment, were pumped to the precipitator using a HPLC pump Jasco model PU-2080, maximum flow rate: 10 mL/min (flow rate control with an accuracy of 1%). Both solutions were pumped continuously through a coaxial nozzle which was located in the upper zone of the vessel in which the solution flowed through the inner tube, with an inner diameter of 100  $\mu\text{m}$ , and  $\text{CO}_2$  flowed through the coaxial annulus. At this point of the vessel, the mixture produces the super saturation of the dispersed phase and the particles are formed [22]. The particles thus formed were collected in a stainless

steel frit covered with a polymeric membrane filter (pore size of 0.1  $\mu\text{m}$ ) which was located at the bottom of the precipitator. Once the solution was pumped,  $\text{CO}_2$  was flowed for 1 h to assure the total elimination of the solvent and after this time, the system was depressurized till ambient conditions.

The influence of the concentration of EDAB in THF in the range 3-25 g/L, which is within the solubility limit of EDAB in THF (46-47 g/L at 25  $^\circ\text{C}$ ) [23], the temperature (35-45  $^\circ\text{C}$ ) and the molar fraction of  $\text{CO}_2$  in the  $\text{CO}_2$ -THF fluid mixture (0.96-0.98) were studied.

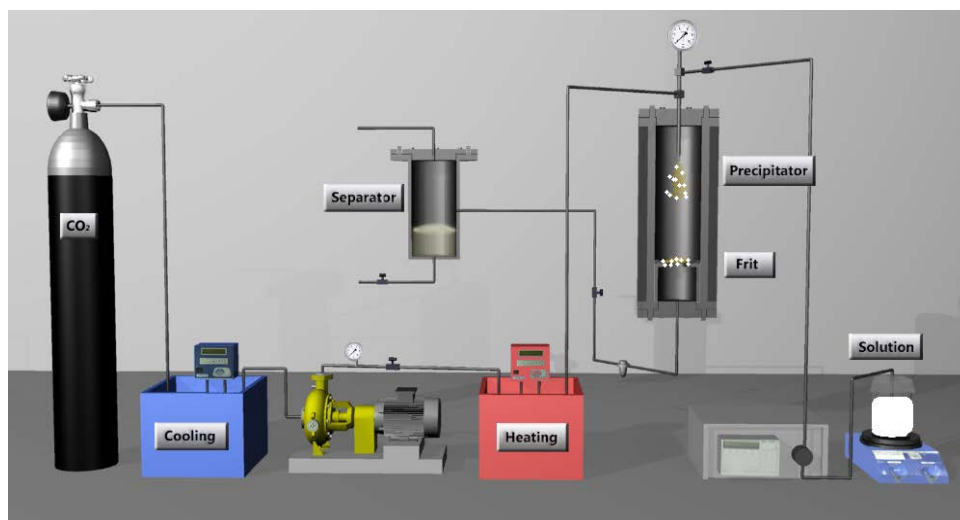


**Figure 2.** Schematic diagram of the Supercritical Anti Solvent apparatus

### 2.3 Product characterization

Particle morphology was observed by Scanning Electron Microscopy (SEM) using Jeol JSM 820 equipment. A gold sputter was used to cover the samples with a thin layer of gold to allow the electron reflection for particle evaluation. To determine particle size from SEM micrographs, around 100 individual particles were counted from SEM photos using Image J software. The mean particle size was calculated as number average diameter [24].

Crystallinity of the different samples obtained after micronization was examined using an X-ray powder diffractometer (model Bruker Discover D8). The measuring conditions were  $\text{CuK}\alpha$  radiation,  $\lambda=1.5418 \text{ \AA}$ ,  $2\theta$  angle ranging from  $5^\circ$  to  $70^\circ$  with a scan rate of 4 s/step and a step size of  $0.020^\circ$ . Also, Fourier Transform Infrared Spectroscopy (FT-IR) assays were performed using a BRUKER ALPHA spectrometer with a Platinum-ATR single diffraction sampling module.

Regarding the thermal characterization of products, differential scanning calorimetry (DSC) analyses were carried out in a Mettler Toledo model 822e with a ceramic sensor of high

sensitivity. Nitrogen gas flowed at 60 mL/min, with a heating rate of 5 °C/min from 0 to 250 °C (273.15 to 523.15 K) using less than 1 mg of sample in each analysis.

Hydrogen release kinetics were measured by a volumetric method employing a stainless steel cell of 4.7 mL. The cell was loaded with around 30 mg of EDAB, weighed using a balance with  $\pm 0.1$  mg of uncertainty. Air was then removed from inside the cell with a vacuum pump, down to an absolute pressure of less than 0.02 bar. After that, the sample was heated to 100 °C (373.15 K), introducing the cell in a chromatographic oven. The release rate of hydrogen from the sample was determined by measuring the increasing gas pressure inside the cell, which was recorded with a certified pressure transducer model DPI-104 (GE Druck from Germany) with an accuracy of 0.001 MPa, connected to a data acquisition computer that recorded the pressure measurement every 10 seconds. The amount of hydrogen released was calculated from pressure recordings assuming that the gas phase formed was entirely constituted by hydrogen according to [12], using the Hydrogen Reference Equation of State [25] implemented in the Reference Fluid Thermodynamic and Transport Properties Database (REFPROP) software developed by the National Institute of Standards and Technology (NIST) [26].

### 3. RESULTS AND DISCUSSION

Table 1 shows a summary of the conditions for the different SAS experiments performed, together with the particle size obtained by image analysis of SEM micrographs. As previously described, different experiments were carried out varying the concentration of EDAB in the solution (runs 1-7), the temperature (runs 7-9) and the molar fraction of CO<sub>2</sub> (runs 7, 10 and 11).

Run	T (°C)	c EDAB (g/L)	x CO <sub>2</sub> (mol frac)	Dp ( $\mu$ m)
0		as received		400
1	40	3.3	0.964	2.3
2	40	6.1	0.964	2.3
3	40	8.1	0.964	2.2
4	40	10.0	0.964	2.7
5	40	12.5	0.964	1.7
6	40	16.7	0.964	2.1
7	40	25.0	0.964	2.3
8	35	25.0	0.959	2.0
9	45	25.0	0.971	2.2
10	40	25.2	0.975	2.3
11	40	24.8	0.981	2.0

**Table 1.** Experimental conditions of different experiments carried out to micronize EDAB using Supercritical Antisolvent process (SAS)

### 3.1 Structural properties of micronized EDAB

Regarding the crystallinity, Figure 3 shows the diffractogram of unprocessed EDAB which agrees well with those previously reported [27]. As it can be observed in Figure 3, the diffractogram of micronized samples corresponds to that of unprocessed material, indicating that the crystalline structure of the material was preserved. While Figure 3 only presents the results corresponding to the micronized sample obtained in experimental run 9, similar spectra were obtained in all SAS experiments.

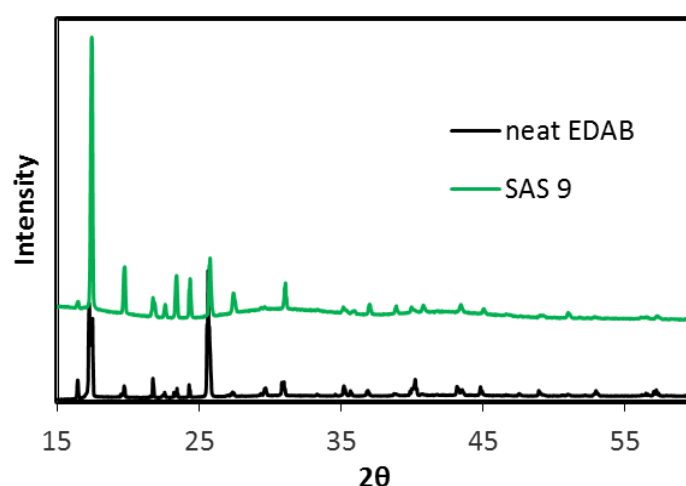


**Figure 3.** XRD spectra of unprocessed and SAS EDAB samples. Curves are vertically displaced for clarity.

The average crystallite size was calculated using the Scherrer equation [28] which is shown in equation 1.

$$D = \frac{K\lambda}{\beta \cos\theta} \quad \text{eq[1]}$$

Where K is a Scherrer constant (0.9 for spherical particles),  $\lambda$  is the wavelength of the incident x-rays (1.5418Å),  $\beta$  is the full width at half maximum (FWHM) and  $\theta$  is the Bragg angle. The final diameter is the mean of the diameter obtained for the peaks at  $2\theta = 16.4^\circ$ ,  $19.7^\circ$ ,  $23.4^\circ$ ,  $24.4^\circ$  and  $25.6^\circ$ . Table 2 shows the crystallite size obtained for unprocessed EDAB and micronized SAS in experiments 1, 7, 8 and 9.

Run	Crystallite size (nm)
unprocessed	93.1±10.7
SAS 1	59.6±4.1
SAS 7	52.6±3.1
SAS 8	57.4±6.0
SAS 9	52.6±3.0

**Table 2.** Crystallite size obtained by Scherer equation for unprocessed and SAS micronized EDAB samples

As table 2 shows, crystallite size was reduced by SAS micronization, but a big difference is not observed between the different experiments carried out using SAS technique.

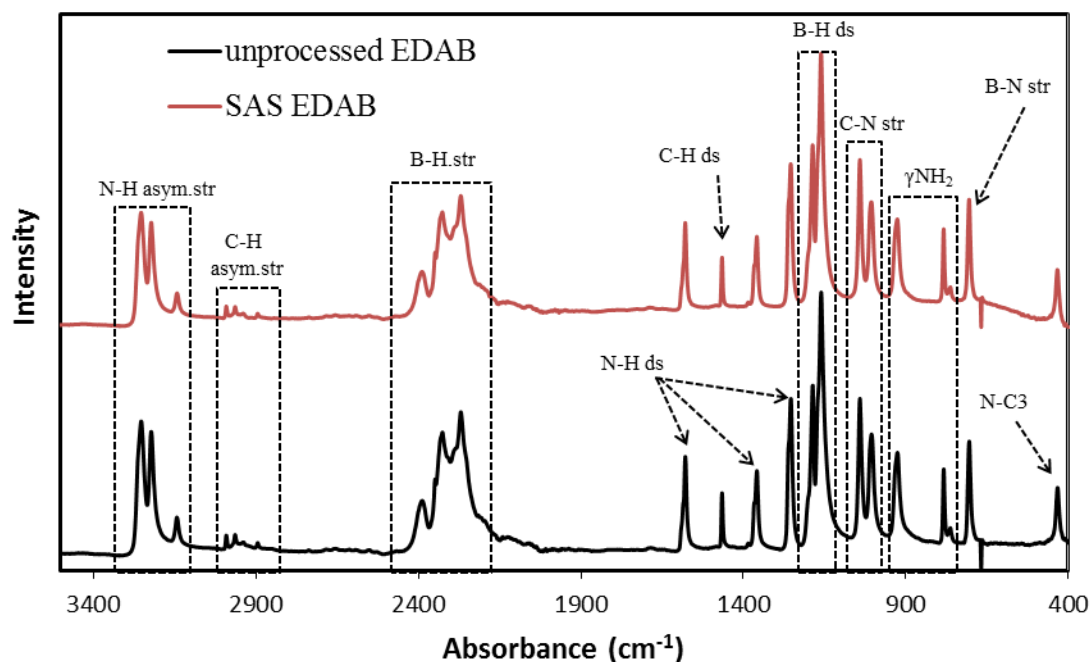


**Figure 4.** FTIR spectra of unprocessed and SAS-micronized EDAB samples. Curves are vertically displaced for clarity.

Regarding the results of FTIR analyses, the peaks identified correspond with those reported for EDAB in [11,29]. Figure 4 shows no variation in the FTIR spectra of EDAB after SAS process (for all the conditions tested). This result indicates that no chemical decomposition took place during recrystallization process at supercritical conditions. B-H stretching and N-H bands appeared at the same wavenumber value without any shift that could indicate a weakening in the bond. This is due to the strong C-N and C-C bond that makes this compound much more thermal stable compared to other compounds from the family of Ammine Boranes [11].

Regarding the results obtained from microscopy (figures 5, 6 and 7), a considerable reduction in the particle size was observed after SAS micronization (table 1). The mean particle size was reduced from 400  $\mu\text{m}$  (unprocessed EDAB) to around 2  $\mu\text{m}$ . The particle morphology also changed: the prismatic structure of unprocessed EDAB was converted into microspheres interconnected between them due to the droplet and particle coalescence phenomena during SAS process.

With respect to the influence of the conditions tested in the different SAS experiments, the mean particle size and particle size distribution (PSD) did not change significantly. First, particle size distribution is shifted to the right when the concentration increases till  $c=10$  g/L. At higher concentration than 10 g/L, the opposite behavior is observed. This means that till this

concentration, the coagulation and condensation mechanisms allow the growth of the particles inside the droplets and limit SAS process [30]. However, at higher concentration of the solution than 10 g/L, higher supersaturations were achieved, and therefore the rate of formation of new particles by nucleation increased exponentially obtaining particles with lower mean size [31].

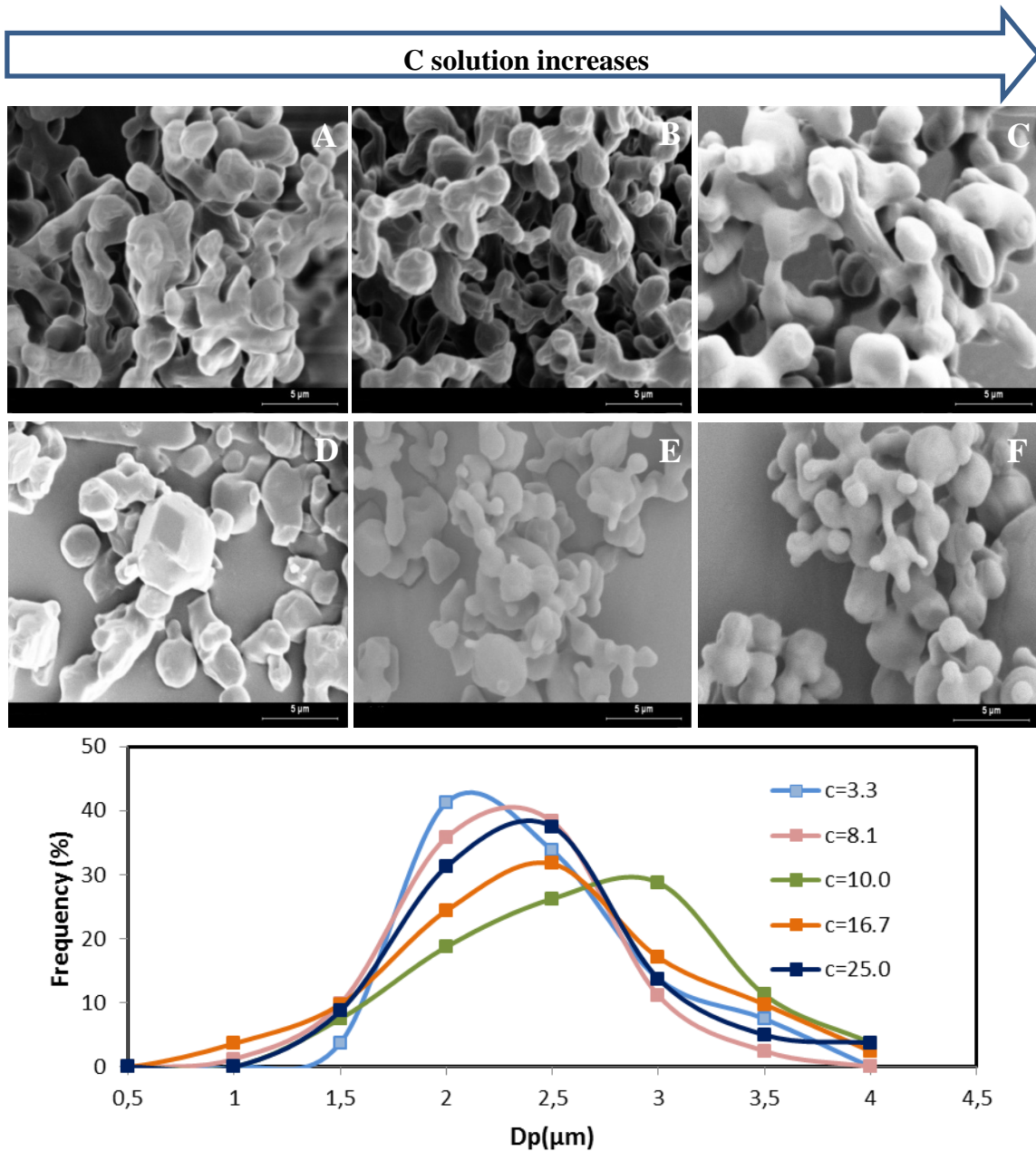


**Figure 5.** a) SEM for micronized EDAB samples at different concentration of the solution. A)  $c=3.3$  g/L; B)  $c=8.1$  g/L; C)  $c=10.0$  g/L; D)  $c=12.5$  g/L; E)  $c=16.7$  g/L; F)  $c=25.0$  g/L (magnification ratio: 5000 X; size bar: 5 μm). b) Particle size distribution of the samples obtained from SEM.

In the case of the temperature, figure 6 shows that when temperature in SAS process is increased, more agglomeration is observed but a similar mean particle size is obtained for the range of temperature studied 35-45 °C (308.15-318.15 K).

Similarly, only small differences were observed in the experiments carried out at different CO<sub>2</sub> molar fractions by varying the flow of CO<sub>2</sub> or the flow of the inlet solution, as it can be seen in figure 7.

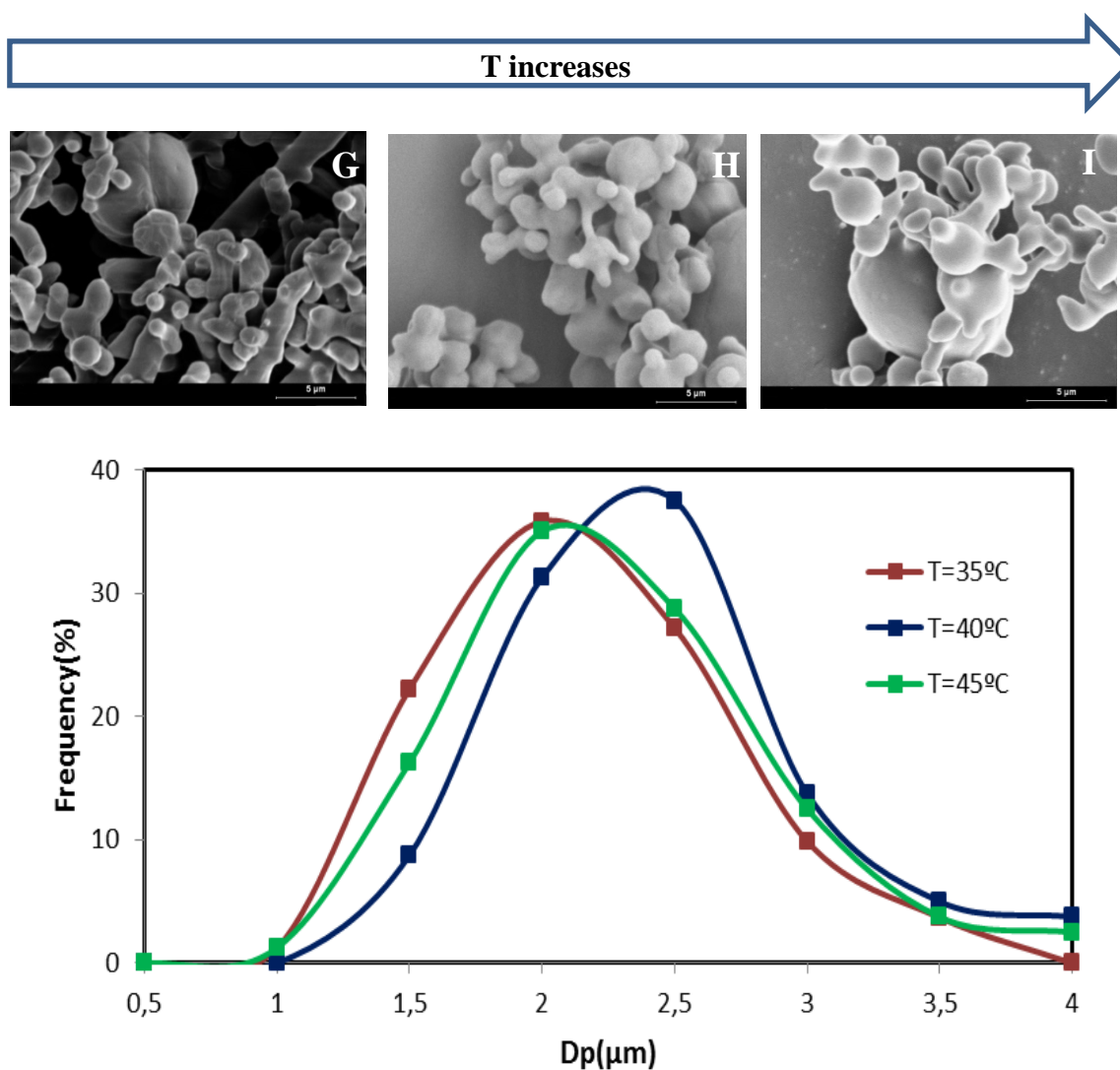


**Figure 6.** a) SEM for micronized EDAB samples at different temperature and  $c=25$  g/L. G)  $T=35$  °C (308.15 K); H)  $T= 40$  °C (313.15 K); I)  $T= 45$  °C (318.15 K) (Magnification ratio: 5000 X; size bar: 5 µm). b) Particle size distribution of the samples obtained from SEM.

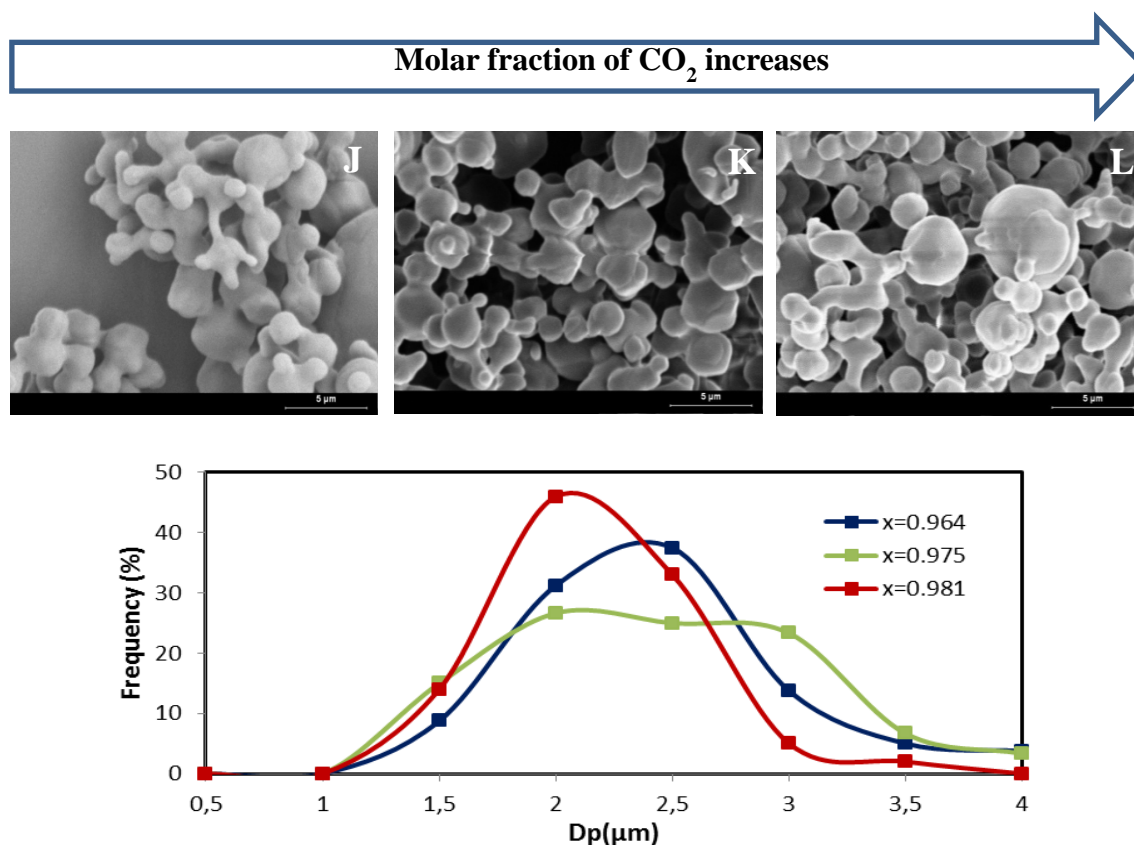


**Figure 7.** a) SEM for micronized EDAB samples at different molar fraction of CO<sub>2</sub> at 40 °C (313.15 K) and  $c=25$  g/L. J)  $x=0.964$ ; K)  $x=0.975$ ; L)  $x=0.981$  (Magnification ratio: 5000 X; size bar: 5 μm). b) Particle size distribution of the samples obtained from SEM.

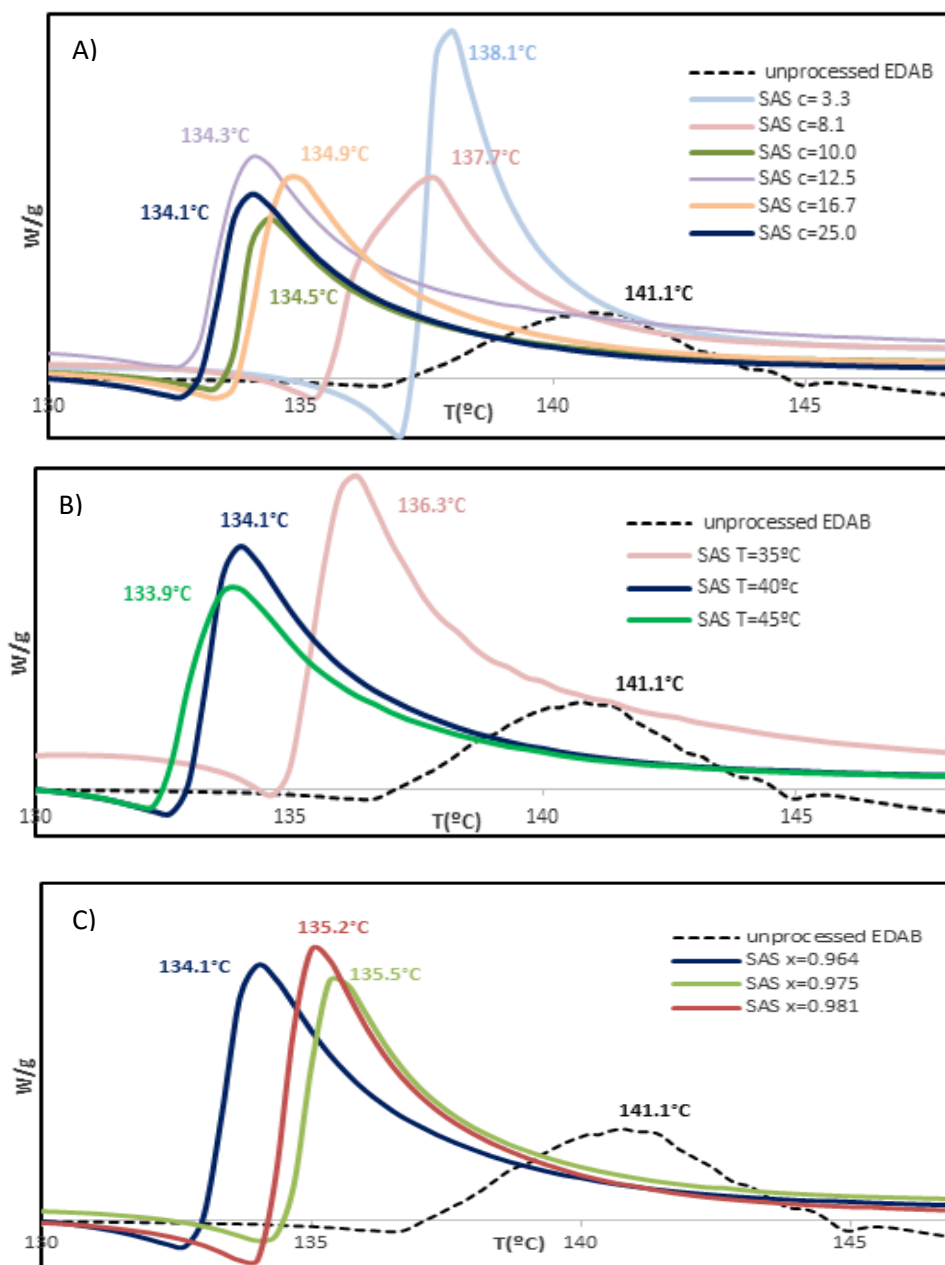
### 3.2 Thermal properties of micronized EDAB

Figure 8 shows the Differential Scanning Calorimetry (DSC) of the different samples treated in SAS process in contrast to unprocessed EDAB. As shown in this figure, the first exothermic peak related to the decomposition of EDAB has been shifted from 141 °C (414.15 K) in unprocessed EDAB to 134 °C (407.15 K) for the best SAS micronized sample (run 9). This improvement is due to the lower particle and grain size obtained in treated samples in contrast to unprocessed EDAB. Similar results have been reported in the case of milled MgH<sub>2</sub> [15], getting a reduction of the hydrogen desorption temperature which indicates faster hydrogen desorption kinetics and lower activation energy or the production of nanoparticles of AB through a solvent-free method [32] which showed superior dehydrogenation behaviour.

Regarding the influence of the concentration in the inlet solution (figure 8A), a higher shift to lower temperatures is observed when the concentration increases till  $c=10$  g/L. This could be due to the lower grain size and thinner bridges between the particles. At higher concentration (12.5-25.0 g/L), the same tendency is followed obtaining almost the same peak temperature.

In the case of the temperature of SAS process (figure 8B), the variation of the peak temperature in DSC assays follows the same tendency that the grain size calculated with Scherrer equation and the PSD obtained from SEM images. Lower exothermic temperature peak is observed in samples processed by SAS at higher temperatures.

Varying the molar fractions of carbon dioxide (figure 8C), a significant difference is not observed.



**Figure 8.** DSC curves of unprocessed EDAB and micronized SAS samples at different conditions. A) Influence of the concentration of the inlet solution B) Influence of the temperature of the SAS process C) Influence of the molar fraction of CO<sub>2</sub>.

Regarding the second step of hydrogen release, similar results were obtained for all the micronized samples with a peak temperature in the range 187 °C-190 °C (460-463 K). It is observed in figure 9 that samples obtained at different conditions in SAS process show the same tendency than in the first peak.

Comparing with previous results [12], both decomposition peak temperatures are higher than previously reported. This can be explained by the difference in gradient temperature in the analyses (5 °C/min instead of 1 °C/min) or due to the different stability of bulk EDAB due to the different source of the chemical compound.

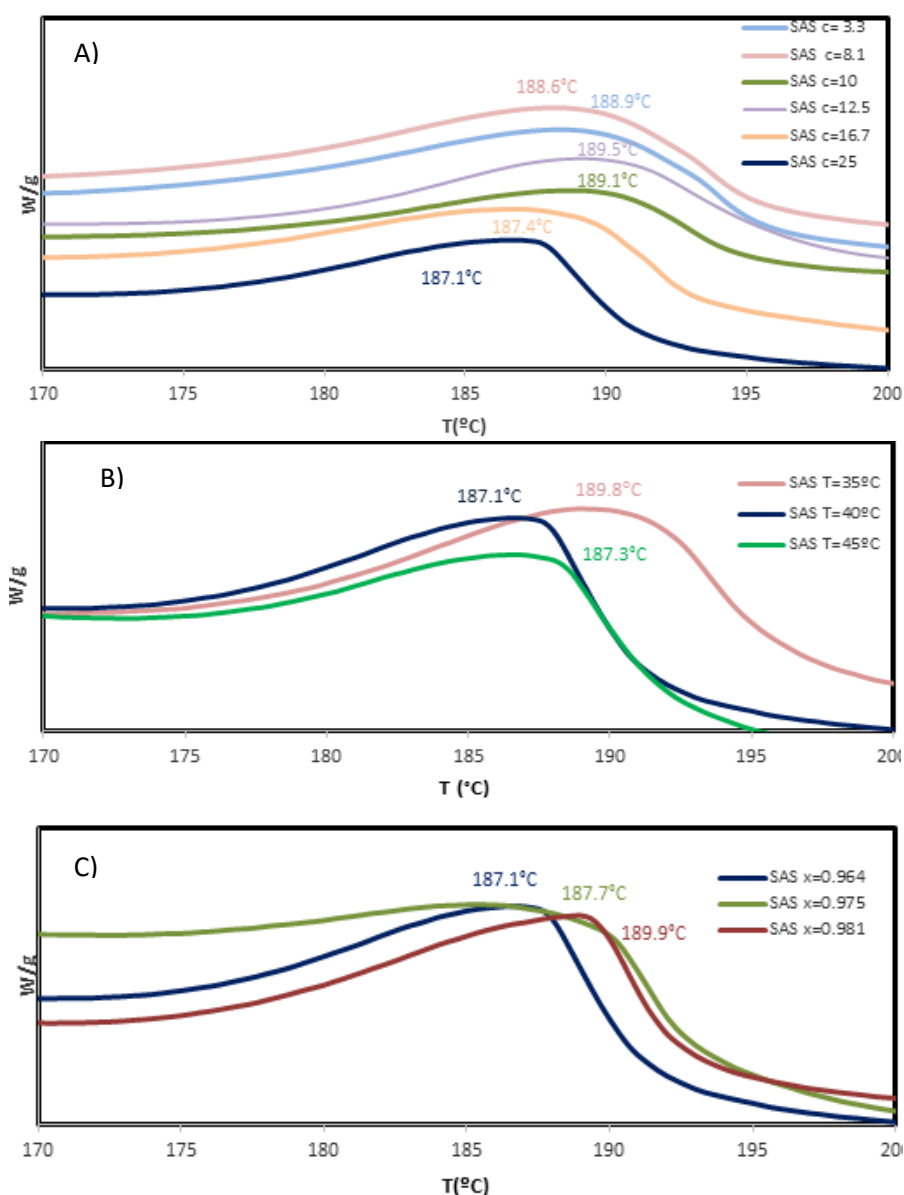


**Figure 9.** DSC curves of micronized SAS samples at different conditions in the range 170-200 °C (443.15-473.15 K). A) Influence of the concentration of the inlet solution B) Influence of the temperature of the SAS process C) Influence of the molar fraction of CO<sub>2</sub>.

The variations in particle morphology and decomposition temperature reported in the previous section result in important variations in the hydrogen release kinetics. Figure 10 shows the kinetic of hydrogen released by thermolysis at 100 °C (373.15 K) for unprocessed EDAB in contrast to micronized EDAB in SAS process.

As presented in this figure, the kinetic has been considerably improved after micronization due to the reduction of the particle and grain size. Moreover, it induces the increase of surface area and surface energy, reducing the diffusion lengths and therefore improving the decomposition rate [33]. Almost 1 day is taken to release 1 mol of H<sub>2</sub> in unprocessed EDAB, whereas less than 4 hours are taken for sample 9 after SAS process, which means a reduction by a factor of 6.

Comparing the different SAS samples obtained after treatment at different conditions, they follow the same tendency that was reported in the previous analyses, without any significant difference among them.

In the case of unprocessed EDAB, in this work different kinetic properties have been observed with respect to the results reported in previous works [12]. In our case, neat EDAB seems to be more stable than in previous works due to the slower kinetic that has been measured at the same temperature and the induction time of more than 1 hour. This fact was also seen in DSC analyses. This difference can be attributed to the different starting material. In our work, EDAB was supplied by Sigma-Aldrich whereas Neiner et al. prepared it according to Moore and Kelly [34].

On the other hand and following the mechanism proposed by Neiner et al. [12] and corroborated by Leardini et al. [11], this difference could be explained by the higher stability of unprocessed EDAB from this work to initiate the isomerization in order to form the borohydride. Neiner et al. [12] reported the appearance of this isomer at 98 °C (371.15 K) after 15 min by NMR whereas kinetic measurements from this work indicate that a longer induction time is required to form this intermediate compound.

In SAS samples, not only an improvement in the kinetic of H<sub>2</sub> release is observed, but also the elimination of induction time can be seen in micronized samples. This indicates that the reduction of particle size achieved by SAS process is accompanied by a destabilization of the molecule, leading to a faster dimerization and the consequent reduction of induction time.

Regarding the amount of H<sub>2</sub> released, an amount of 3.9 wt% H<sub>2</sub> is obtained with respect to unprocessed EDAB or 3.7 wt% regarding pure EDAB, taking into account that the purity is 96%, whose value is similar to those reported in the literature at the same temperature [12].

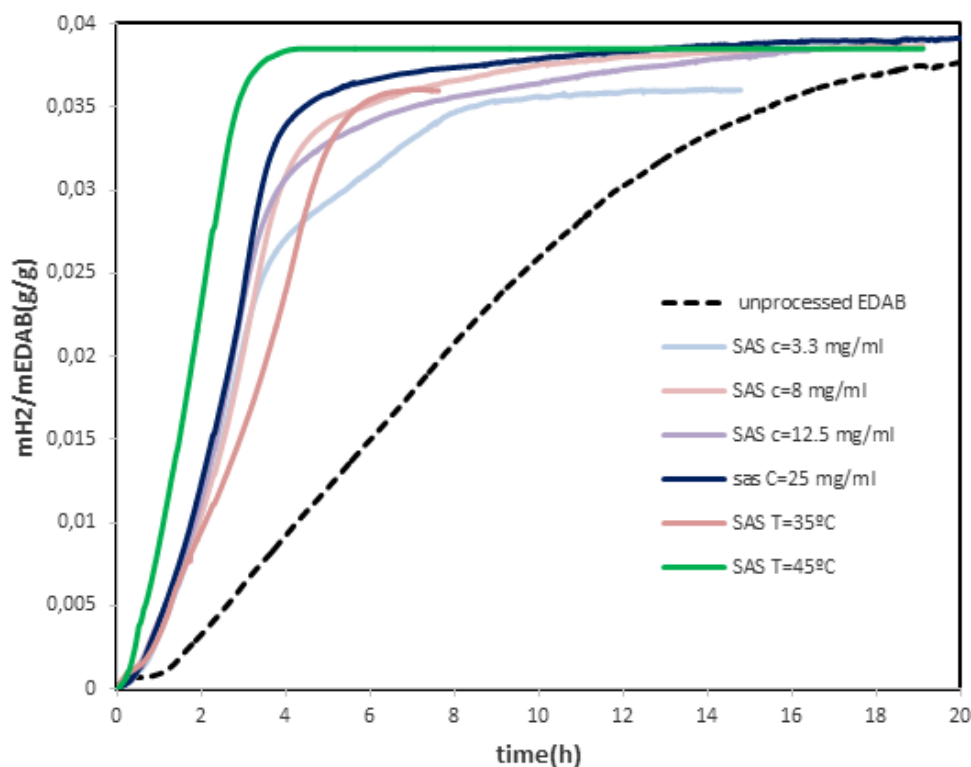


**Figure 10.** Isothermal kinetic of hydrogen released from unprocessed and SAS EDAB samples at 100 °C

In order to clarify the compounds that are formed after thermal decomposition at 100 °C (373.15 K) and the mechanism that is followed, FTIR analyses were performed and shown in figure 11. The same spectrum is obtained for unprocessed EDAB and SAS samples, but only one is shown for simplicity.

These spectra are similar to those reported by Leardini et al. [11]. Lattice mode at  $435\text{ cm}^{-1}$  disappears but a new one at around  $420\text{ cm}^{-1}$  is detected. On the other hand, B-N stretching peak at  $706\text{ cm}^{-1}$  is attenuated after thermal decomposition accompanied by the formation of a broader peak around  $805\text{ cm}^{-1}$  related to a new B-N stretching mode. Regarding B-H and N-H bands, they are broadened but they are still present after releasing almost 4 wt%  $\text{H}_2$ . This is due to the proposed polymerization mechanism, similar to those reported in AB [35]. In this case, chains of molecules of EDAB are formed with new B-N bonds resulting in a polyaminoborane with still more solid hydrogen stored which can be released at higher temperature. The bands corresponding to C-H groups remain after thermal decomposition due to the stability of these bonds at this temperature.

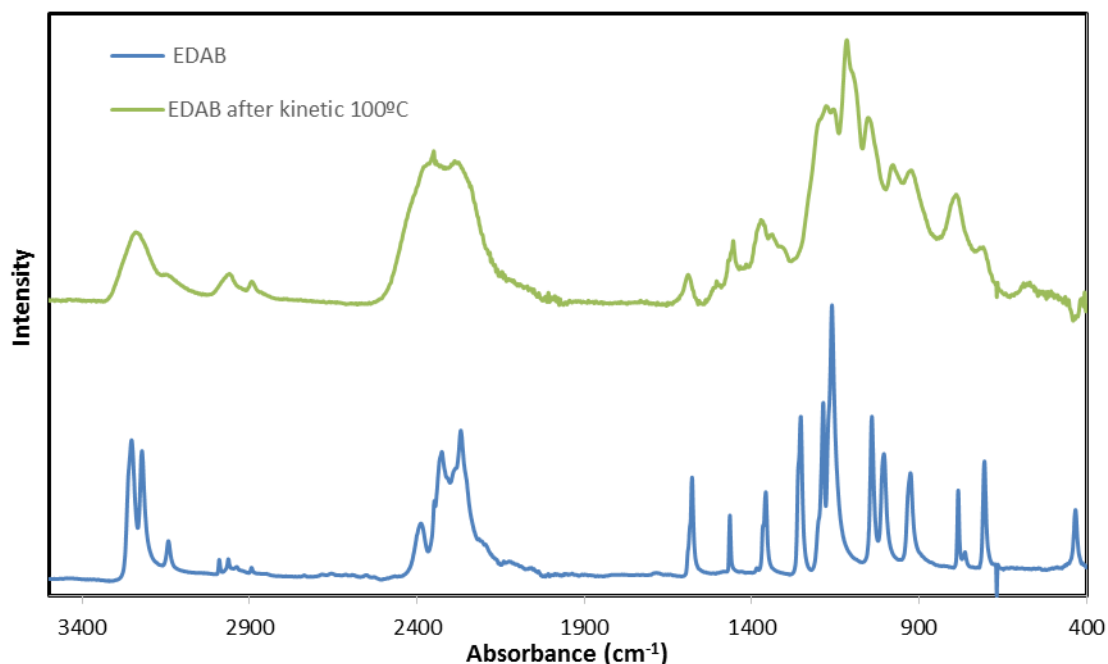


**Figure 11.** FTIR spectra of EDAB before and after thermal kinetic at 100 °C (373.15 K). Curves are vertically displaced for clarity

#### 4. CONCLUSIONS

1, 2 diamineborane (EDAB) was successfully micronized using Supercritical Antisolvent (SAS) Process. Therefore, SAS process could be suitable for the micronization of other hydrides compounds, especially boron-nitrogen-hydrogen compounds, in the case that the compound dissolved in an organic solvent is stable in CO<sub>2</sub> atmosphere. The influence of the concentration of THF solutions, the temperature of the process and the fraction of carbon dioxide in the fluid phase on the final structural and thermal properties of EDAB was studied. Similar results were obtained for all the studied conditions regarding particle size, calorimetry and kinetic results.

After micronization process of EDAB, the particle size of about 400 μm with a crystallite size of 100 nm were drastically reduced to 2 μm with a crystal size of 50 nm. Also, the shape suffered variations after SAS process: prismatic structure from unprocessed EDAB changed into microspheres showing agglomeration. XRD and FTIR analyses showed that no chemical decomposition and no variation of the crystalline structure was produced by SAS processing.

Thermal analyses showed a reduction in decomposition temperatures after SAS process. DSC showed a reduction of 7 °C in the decomposition peak temperature after micronization process, releasing hydrogen in a 2 step pathway whose peak temperatures were 134.1 °C (407.25 K) and 187.1 °C (460.25 K) respectively. In the case of the kinetics of release of hydrogen at 100 °C (373.15 K), the reduction of the particle and grain size resulted in a

considerable acceleration of kinetics, reducing by a factor of 6 the time required to release 3.9 wt% H<sub>2</sub>, comparing to unprocessed EDAB. Moreover, a suppression of induction time was observed due to the destabilization of the hydride after SAS treatment.

**REFERENCES**

- [1] M.Balat, Potential importance of hydrogen as a future solution to environmental and transportation problems, *Int. J. Hydrogen Energ.* 33 (2008) 4013-4029.
- [2] F.H.Sobrinho, C.R.Monroy, J.L.H.Pérez., Critical analysis on hydrogen as an alternative to fossil fuels and biofuels for vehicles in Europe, *Renew. Sust. Energ. Rev.*, 14 (2010) 772-780.
- [3] V.Strubel. StorHY. Available at [http://www.storhy.net/pdf/StorHy\\_FourthActivityReport\\_PES.pdf](http://www.storhy.net/pdf/StorHy_FourthActivityReport_PES.pdf). (Accessed on October 15th, 2015)
- [4] B.Sakintuna, F.Lamari-Darkrim, M.Hirschet, Metal hydride materials for solid hydrogen storage: A review, *Int. J. Hydrogen Energ.* 32 (2007) 1121-1140.
- [5] M.P.Suh, H.J.Park, T.K.Prasad, D.Lim, Hydrogen storage in Metal Organic framework, *Chem. Rev.* 112 (2012) 782-835.
- [6] Y.H.Hu, E.Ruckenstein, Clathrate hydrogen hydrate- A promising material for hydrogen storage, *Angew. Chem. Int. Ed.* 45 (2006) 2011-2013
- [7] M.Niemann, S.S.Srinivasan, A.R.Phani, A.Kumar, D.Y.Goswami, E.K.Stefanakos, Nanomaterials for Hydrogen Storage Applications: A review, *J. Nanomater.* (2008) 1-9.
- [8] A.Züttel, Materials for hydrogen storage, *Mater. Today* 6 (2003) 24-33.
- [9] Office of Energy Efficiency and Renewable Energy. DoE targets. Available at [http://www1.eere.energy.gov/hydrogenandfuelcells/storage/pdfs/targets\\_onboard\\_hydro\\_storage.pdf](http://www1.eere.energy.gov/hydrogenandfuelcells/storage/pdfs/targets_onboard_hydro_storage.pdf). (accessed on October 14th, 2015.)
- [10] S.D.Rassat, C.L.Aardahl, T.Autrey, R.S.Smith, Thermal stability of ammonia borane: A case study for exothermic hydrogen materials, *Energ. Fuel.* 24 (2010) 2596-2606.
- [11] F.Leardini, M.J.Valero-Pedraza, E.Perez-Mayoral, R.Cantelli, M.A.Bañares, Thermolytic decomposition of ethane 1,2 -diamineborane investigated by thermoanalytical methods and in situ vibrational spectroscopy, *J. Phys. Chem. C.* 118 (2014) 17221-17230.
- [12] D.Neiner, A.Karkamkar, M.Bowden, Y.J.Choi, A.Luedtke, J.Holladay, A.Fisher, N.Szymezak, T.Autrey, Kinetic and thermodynamic investigation of hydrogen release from ethane 1,2-diamineborane, *Energ. Environ. Sci.* 4 (2011) 4187-4193.

- [13] S.Sahler, H.Konnerth, N.Knoblauch, M.H.G.Prechtl, Hydrogen Storage in Amine Boranes: Ionic Liquid supported thermal dehydrogenation of Ethylene Diamine Bisborane, *Int. J. Hydrogen Energ* 38 (2013) 3283-3290.
- [14] V.Bewrubé, G.Radtke, M.Dresselhaus, G.Chen, Size effects on the hydrogen storage properties of nanostructured metal hydrides: A review, *Int. J. Energ. Res.* 31 (2007) 637-663.
- [15] J.Huot, G.Liang, S.Boily, A.Van Neste, R.Schulz, Structural study and hydrogen sorption kinetics of ball-milled magnesium hydride, *J. Alloy. Compd.* 293-295 (1999) 495-500.
- [16] P.E. de Jongh, P. Adelhelm, Nanosizing and Nanoconfinement: New Strategies towards Meeting Hydrogen Storage Goals, *ChemSusChem* 3 (2010) 1332-1348.
- [17] L.Zaluski, A.J, Nanocrystalline metal hydrides, *J. Alloy. Compd.* 253-254 (1997) 70-79
- [18] M.Rueda, L.M.Sanz-Moral, A.Martín, Micronization of Magnesium Acetate by the Supercritical Antisolvent Process as a Precursor for the Production of Magnesium Oxide and Magnesium Hydride, *Cryst. Growth Des.* 14 (2014) 4768-4776.
- [19] A.Martín, K.Xcholle, F.Mattea, D.Meterc, M.J.Cocero, Production of Polymorphs of Ibuprofen Sodium by Supercritical Antisolvent (SAS) Precipitation, *Cryst. Growth Des.* 9 (2009) 2504-2511.
- [20] E.Reverchon, Supercritical antisolvent precipitation of micro and nano particles, *J. Supercrit. Fluids* 15 (1999) 1-21.
- [21] J.Li, M.Rodrigues, A.Paiva, H.A.Matos, E.Gomes, Vapor-liquid equilibria and volume expansion of the tetrahydrofuran/CO<sub>2</sub> system: Application to a SAS-atomization process, *J. Supercrit. Fluids* 41 (2007) 343-351.
- [22] F.Mattea, A.Martín, A.Matías-Gago, M.J.Cocero, Supercritical antisolvent precipitation from an emulsion: beta-Carotene nanoparticle formation, *J. Supercrit. Fluids* 51 (2009) 238-247.
- [23] H.C.Kelly, J.O.Edwards, Evidence for the Open Chain Structure of Ethane 1,2-Diamineborane, *Inorg. Chem.* 2 (1963) 226-227.
- [24] C.Amorim, M.A.Keane, Palladium supported on structured and nonstructured carbon: A consideration of Pd particle size and the nature of reactive hydrogen, *J. Colloid Interf. Sci.* 322 (2008) 196-208.

- [25] J.W.Leachman, R.T.Jacobsen, S.G.Penoncello, E.W.Lemmon, Fundamental Equations of State for Parahydrogen, Normal Hydrogen and Orthohydrogen, *J. Chem. Eng. Data*, 38 (2009) 721-748.
- [26] E.W.Lemmon, M.L.Huber, M.O.McLinden. NIST Standard Reference Database 23: Reference Fluid Thermodynamic and Transport Properties-REFPROP, Version 9.1. National Institute of Standards and Technology, Standard Reference Data Program. Gaithersburg : s.n., 2013.
- [27] H.Ting, W.H.Watson, C.Kelly, The molecular and crystal structure of Ethylenediamine-Bisborane, *Inorg. Chem.* 11 (1972) 374-376.
- [28] L.Alexander, H.P.Klug, Determination of crystallite size with the XRay Spectrometer, *J. Appl. Phys.* 21 (1950) 137-142.
- [29] J.Goubeau, H.Schneider, Borin-Anlagerungsverbindungen des Äthylenamins, *Chem. Ber.* 94 (1961) 816-821.
- [30] I. de Marco, E.Reverchon, Influence of pressure, temperature and concentration on the mechanisms of particle precipitation in supercritical antisolvent micronization, *J. Supercrit. Fluids* 58, (2011) 295-302.
- [31] A.Martín, M.J.Cocero, Numerical modeling of jet hydrodynamics, mass transfer and crystallization kinetics in the supercritical antisolvent (SAS) process, *J. Supercrit. Fluids* 32 (2001) 203-219.
- [32] Y.Song, N.Ma, X.Ma, F.Fang, X.Chen, Y.Guo, Synthesis of Ammonia Borane Nanoparticles and the Diammoniate of Diborane by direct combination of Diborane and Ammonia, *Chem. Eur. J.* 22 (2016) 6228-6233.
- [33] Bérubé V; Radked G; Dresselhaus M; Chen G, Size effects on the hydrogen storage properties of nanostructured metal hydrides: A review. *Int. J. Energ. Res.* 31 (2007) 637-663
- [34] R.C.W.Moore, S.S.Kelly. *Inorganic Syntheses*. s.l.: Mc-Graw Hill Book Company, (1970) 109-115.
- [35] S.Frueh, R.Kellett, C.Mallery et al, Pyrolytic decomposition of ammonia borane to boron nitride, *Inorg. Chem.* 50 (2011) 783-792.

# **CHAPTER 3**

**Production of silica aerogel microparticles  
loaded with ammonia borane by batch and  
semicontinuous supercritical drying  
techniques**



## **Production of silica aerogel microparticles loaded with ammonia borane by batch and semicontinuous supercritical drying techniques<sup>1</sup>**

### **Abstract**

Silica aerogel microparticles were prepared by supercritical drying and used as support for hydrogen-storing ammonia borane (AB). The formation of aerogel microparticles was done using two different processes: batch supercritical fluid extraction and a semicontinuous drying process. Silica aerogel microparticles with a surface area ranging from 400 to 800 m<sup>2</sup>/g, a volume of pores of 1 cm<sup>3</sup>/g, and a mean particle diameter ranging from 12 to 27 μm were produced using the two drying techniques. The particle size distribution (PSD) of the microparticles was influenced by shear rate, amount of catalyst, hydrophilic-hydrophobic solvent ratio and hydrophobic surface modification. In particular, irregular aerogel particles were obtained from hydrophilic gels, while regular, spherical particles with smooth surfaces were obtained from hydrophobic gels. AB was loaded into silica aerogel microparticles in concentrations ranging from 1% till 5% wt. Hydrogen release kinetics from the hydride-loaded aerogel was analyzed with a volumetric cell at 80 °C. By stabilization of AB into the silica aerogel microparticles, an improvement of the release rate of hydrogen from AB was observed.

**Keywords:** silica aerogel, microparticles, supercritical drying, particle size distribution, ammonia borane, hydride, hydrogen storage.

<sup>1</sup>Journal of Supercritical Fluids 92 (2014) 299-310

## 1. INTRODUCTION

Aerogels show some extraordinary properties such as high specific area (500-1200 m<sup>2</sup>/g), high porosity (80-99.8%), low density (0.003 g/cm<sup>3</sup>), high thermal insulation (0.005 W/mK), and low dielectric constant (1-2) and index of refraction (1.05) [1]. These outstanding properties make them useful materials for several applications such as thermal insulation [2], filters to removal toxic compounds [3], or as supports for inorganic nanoparticles [4].

Silica alcogels can be produced by a hydrolysis-condensation sol-gel reaction using tetramethylortosilicate (TMOS) as a precursor, producing siloxane bonds, plus water as a by-product, as presented in reactions 1 and 2. Condensation reactions continue forming a three-dimensional network through a polimerization reaction, producing a silica gel immersed in a alcoholic medium known as alcogel [5].



The drying of the alcogel is an essential step in order to preserve the microstructure of the material and key properties such as surface area or pore volume. Different techniques have been used to dry the alcogel, including atmospheric and freezing drying. Also, since supercritical carbon dioxide is completely miscible with many volatile organic solvents, supercritical drying with carbon dioxide has been employed by several authors because it prevents fractures caused by the capillary stresses in the vapor-liquid interface that are unavoidable with other processes [6].

Aerogels can be syntesized as monoliths or alternatively as microparticles. Aerogel microparticles are of great interest in applications in which the aerogel acts as carrier material of an active compound, because by the reduction of the aerogel particles size the intraparticle diffusion processes can be adjusted to the requirements of the product. Therefore, aerogel microparticles have been used in different applications, and particularly in biomedicine, for drug delivery or encapsulation of active compounds [7].

Aerogel microparticles can be obtained by milling of monoliths, but since milling can damage the pore structure of the aerogel, the development of methods for the direct production of aerogel microparticles is of interest. Alnaief and Smirnova [8] presented a new method to produce spherical aerogel microparticles with a controlled particle size distribution and a mean diameter ranging from 200 μm to 1.7 mm. This method was based on a sol-gel method. The gel phase was made of tetramethylorthosilicate as precursor, methanol as solvent, and aqueous

ammonia and HCl solutions as catalysts, diluted in ethanol in order to obtain the desired density. By mechanical stirring, this gel phase was broken into small droplets and dispersed within a continuous phase formed by canola oil saturated with ethanol. After gelation of the dispersed phase took place, gel spheres were left overnight for aging and later dried by supercritical extraction using supercritical carbon dioxide to remove the solvent and oil, thus producing dry aerogel particles. Also, Montes et al. [9], compared two processes for the production of silica microparticles: a conventional batch aerogel drying process using supercritical ethanol, and a novel process consisting in a simultaneous sol-gel reaction and drying, based on the continuous injection of precursors into supercritical carbon dioxide. In both processes, silica microparticles with spherical morphology and amorphous nature were obtained. However, by the continuous process bigger particles, more hydrophilic and with almost no porosity were obtained.

Due to their controlled size, thermal stability, and capacity to host and stabilize particles of an active compound in their pore volume, silica aerogel microparticles can be promising carrier materials for different active compounds, like hydrides used as solid state hydrogen storage materials. In particular, ammonia borane (AB) is a promising chemical hydride due to its potential to store a significant amount of hydrogen (up to 19.6 wt%), low molecular weight (30.7 g/mol) and stability and safety in handling [10, 11]. For these reasons, it has been considered as a candidate for storing hydrogen as needed for the implementation of the "hydrogen economy" [12]. However, ammonia borane also presents some shortcomings that must be overcome before this material can be applied for hydrogen storage applications. First, there are thermodynamic limitations because high temperatures are required in order to decompose the material and release all the stored hydrogen. The thermal decomposition of AB above 70 °C has been studied [13,14,15] using volumetric measurements, which showed that 1.1 mol of hydrogen per mol of AB were released at temperatures below 120 °C and another 1.1 mol was released at higher temperatures. This limitation can be improved modifying the chemical composition of the mixture adding compounds to de-stabilize the hydride, thus reducing the thermodynamic stability and the temperature required to decompose it [16]. On the other hand, ammonia borane has kinetic limitations due to a too slow release of hydrogen. It is believed that reducing the dimensionality of crystalline AB when it is confined in the mesopores of silica scaffolds results in changes in thermal properties and hydrogen-releasing kinetics [17] shortening diffusion distances. Other approaches for speeding-up kinetics and decreasing the onset temperature of the reaction include the use of ionic liquids as solvents for ammonia borane, [18] or using catalysts of Ru, Co, Ni or Pd in order

to accelerate the generation of hydrogen from the methanolysis of ammonia borane [19].

In this work, the synthesis of silica aerogel microparticles has been studied. Two different methodologies have been tested: a batch drying process and a semicontinuous spray process. The results of both techniques have been compared examining the particle size, particle size distribution (PSD), textural properties (surface area and pore volume) and particle morphology. Next, silica aerogel microparticles have been used as vehicles for the incorporation of ammonia borane to apply it as a solid state hydrogen storage material. Since some hydrides are unstable in CO<sub>2</sub> atmosphere [20], and some contradictory results are presented regarding to the behavior of ammonia borane in CO<sub>2</sub> environment [21], as a previous step the stability of pure solid ammonia borane and ammonia borane dissolved in methanol during exposure to carbon dioxide has been analyzed. Ammonia borane-loaded aerogel microparticles have been produced by precipitation of ammonia borane inside the pores of the alcogel using two different methods: precipitation before supercritical aerogel drying, and conventional homogenization by mechanical milling. Finally, kinetics of hydrogen release from the resulting material have been analyzed employing a volumetric cell at 80 °C.

## 2. EXPERIMENTAL METHODS

### 2.1 Materials

Tetramethylorthosilicate (TMOS, 98.0% purity), trimethylethoxylane (TMES, 98% purity), ammonium hydroxide (28.0-30.0% ammonia purity) and ammonia borane (AB, 97% purity) were supplied by Sigma-Aldrich. Methanol (99.8% purity), n-hexane (95% purity) and dichloromethane (98% purity) were purchased from Panreac. Carbon dioxide (99.95% purity) was purchased from Carbueros Metálicos S.A.

### 2.2 Methods

#### 2.2.1 Preparation of silica alcogels

Silica alcogel was produced by the standard sol-gel reaction used to synthesize aerogel monoliths, with a key modification of the process: hexane was added to the reaction mixture, acting as a hydrophobic phase that enables the dispersion of the alcogel into small droplets, which after drying lead to the production of aerogel microparticles, as described by Alnaief and Smirnova [8]. The process was carried out under strong mechanical agitation in order to allow a better dispersion of these droplets.

TMOS was used as a precursor and it was mixed with methanol, water and hexane with a molar ratio of 1 mol TMOS: 4.4 mol MeOH: 3.3 mol H<sub>2</sub>O: 2.3/4.5/6.8 mol hexane. Mechanical stirring at 500, 600 or 700 rpm was applied using a two bladed axial stirrer (Caframo). After 10 minutes, 250 µL of ammonium hydroxide diluted with water, with a ratio of 0.04, 0.08 or 0.12 mol NH<sub>4</sub>OH: 1 mol TMOS were added to the first solution as condensation catalyst. Then, the solution was stirred for two hours while the gelation of silica alcogel particles took place. After that, an ageing period of the alcogel immersed in methanol for one day was allowed in order to strengthen its structure. These steps were performed at ambient conditions. The hydrophobic alcogels were prepared in the same way using TMES as precursor with a ratio TMOS:TMES 1:2 or 1:5, without variations in the proportion of the rest of reagents.

### 2.2.2 Drying of alcogel microparticles by batch supercritical fluid extraction

The apparatus used to produce aerogel microparticles by batch supercritical drying is shown in Figure 1. It was designed and supplied by Eurotechnica (Hamburg, Germany). It comprises the following main components: a stainless steel CO<sub>2</sub> buffer vessel with a capacity of 100 mL, an extraction vessel of 85 mL with a magnetic stirrer, and two pumps: an air-driven pump used for loading CO<sub>2</sub> into the system, and a gear pump (Micropump 180 Series mod. GAH-T23) used to recirculate CO<sub>2</sub> through the system in order to improve the contact between the supercritical fluid and the organic solvent. Both vessels and the gear recirculation pump are placed inside a hot air oven in order to achieve the desired temperature and to keep it constant during all the process.

First, ~1 g of alcogel particles were placed in the extractor, covering it with 15 mL of methanol in order to avoid the collapse of the particles pore structure by evaporation of the solvent during their exposure to ambient conditions. Then, the set-up was heated to 40 °C and the system was pressurized with CO<sub>2</sub> pumped at a rate of 3-5 bar/min. When the desired operating conditions were reached (40 °C and 110 bar), the recirculation pump was activated. As during the batch extraction CO<sub>2</sub> becomes gradually saturated with methanol, after a predefined extraction time, CO<sub>2</sub> in the buffer vessel and circuit was renewed, isolating the extraction vessel from the rest of the circuit closing the valves in its inlet and outlet connections, and maintaining it under pressure in order to avoid the depressurization process in the extractor and damages in the particles structure that could be produced by repeated pressurization-depressurization processes. After preliminary experiments, it was determined that a total of 5 of such extraction cycles were needed in order to obtain dry aerogel particles, with extraction times of 30 min, 40 min, 50 min, 70 min and 90 min, with longer extraction times in the last

cycles in order to achieve the diffusion of the remaining organic solvent through the pores of the aerogel [22]. Finally, the unit was slowly depressurized at a rate of 3 bar/min in order to prevent the collapse of the pore structure of aerogels by mechanical stress. Aerogel particles were collected and stored under dry conditions.

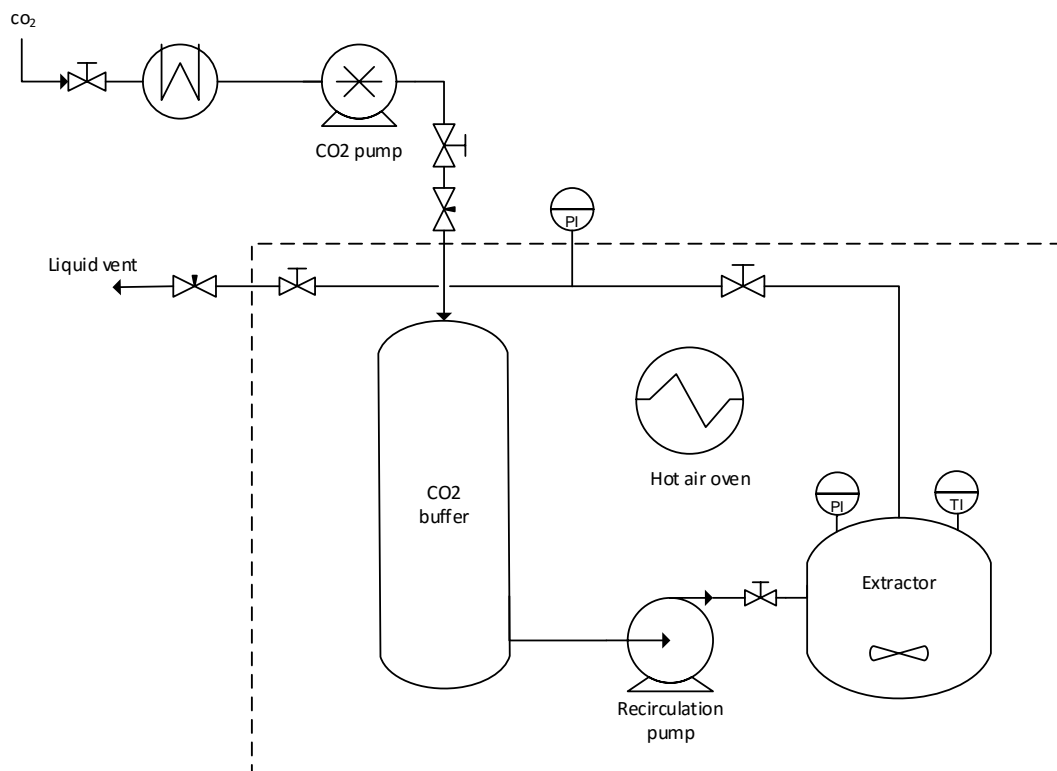


**Figure 1.** Batch supercritical drying apparatus flow diagram

### 2.2.3 Semi-continuous supercritical drying process

A schematic diagram of the plant used for semicontinuous drying is shown in Figure 2. This system comprises a jacketed vessel of 2.5 L of volume which is heated with a water bath and a concentric tube nozzle for the continuous injection of the CO<sub>2</sub> and the suspension of alcogel particles in methanol. At the outlet of the vessel, the precipitated particles are collected in a metallic frit. The pressure is controlled with a back pressure valve which is placed after a safety filter to assure that all the particles are collected in the outlet stream. Another vessel is used to separate the solvent (methanol and hexane) and CO<sub>2</sub> after pressure is released in the process.

First, supercritical fluid was introduced in the vessel using a Dosapro Milton Roy diaphragm pump until the desired pressure, temperature and flow (90 bar, 40 °C and 2 kg/h CO<sub>2</sub>) were reached in the system and maintained constant. Then, the suspension of alcogel particles was pumped into the precipitator with a Gilson 305 piston pump (maximum flow rate: 25 mL/min, flow rate control with an accuracy of 0.1 mL/min), at a flow rate of 4 mL/min. A total volume of

150 mL of suspension was pumped. Afterwards, CO<sub>2</sub> flow was maintained for 1 hour in order to assure the complete solvent elimination that could remain in the pores of the particles. After the decompression of the system, the particles were collected from the filter and stored under dry conditions.

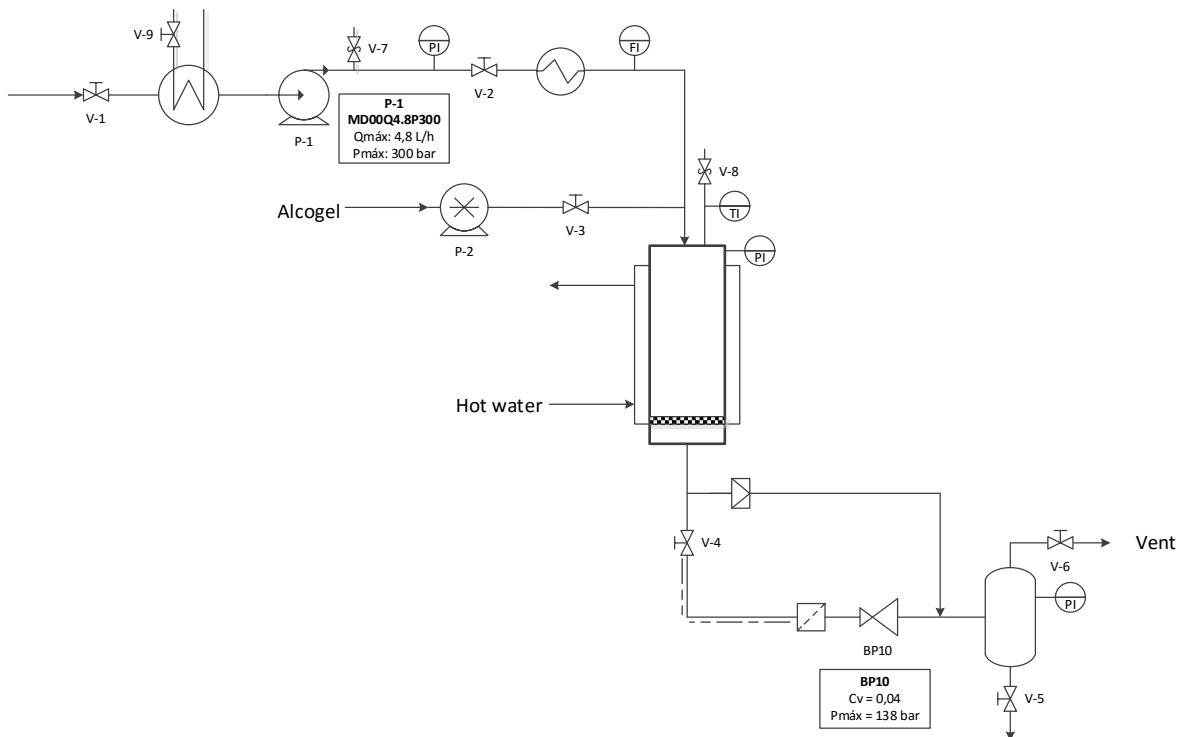


**Figure 2.** Semicontinuous supercritical drying apparatus flow diagram

#### 2.2.4 Loading of ammonia borane in silica microparticles

Two different methods of deposition of ammonia borane into the aerogel were tested: precipitation of ammonia borane inside the pores of the alcolgel before supercritical drying, and a conventional homogenization of ammonia borane and aerogel by mechanical milling.

In the experiments where ammonia borane was precipitated inside the alcolgel, 0.3 g of ammonia borane were dissolved in 4 mL of methanol employed as solvent in the sol-gel synthesis of the alcolgel. Ammonia borane was then precipitated inside the alcolgel by addition of dichloromethane, which acts as an antisolvent for ammonia borane. The alcolgel particles were then washed twice with dichloromethane in order to remove all methanol employed in the gel synthesis. The resulting dispersion was dried with supercritical CO<sub>2</sub> according to the batch method presented in section 2.2.2.

Conventional homogenization of ammonia borane and silica aerogel took place in a Retsch GmbH PM100 planetary ball mill. It consists of a vessel of 50 mL of zirconium oxide filled with 10 balls of 10 mm of the same material. Samples were milled at 600 rpm for a total time of 1

hour, with periods of 1 minute of milling separated by turn-off periods of 5 minutes in order to avoid the decomposition of ammonia borane by excessive heating during the milling process. For safety reasons, charging and discharging of the sample was done in an inert nitrogen atmosphere using a glove box.

#### 2.2.5 Evaluation of the stability of ammonia borane solid particles and ammonia borane dissolved in methanol in a supercritical CO<sub>2</sub> environment

In previous works [23] it was observed that the promoting effect of CO<sub>2</sub> on H<sub>2</sub> release from AB was dependent on the pressure of CO<sub>2</sub> at 80 °C. Because of that, different experiments were carried out to evaluate the influence of ammonia borane treated with CO<sub>2</sub> at high pressure. Ammonia borane was introduced into a high pressure visual cell, where CO<sub>2</sub> was loaded at different pressures and temperatures. The selected conditions that were tested were 40 and 50 °C of temperature and 100, 110 and 150 bar of pressure, close to the conditions used during the supercritical processing of ammonia borane loaded aerogels. Once the conditions of pressure and temperature were reached, they were maintained for different times, from 80 min to 3 h, in order to study also the influence of this parameter. Since a chemical absorption of CO<sub>2</sub> was determined on similar experiments at lower pressures by Raman spectroscopy [23], Raman spectra of the solid treated ammonia borane were acquired and compared with untreated ammonia borane samples after the reactor was opened to check possible variations in the chemical composition of the material.

Other works reported the decomposition of ammonia borane in methanol at 25 °C by methanolysis, by adding 2 mol% of different catalysts of Ru, Ni, Pd, Ni or Rh [19]. In order to test if methanolysis could occur in the conditions employed in the supercritical drying process, ammonia borane dissolved in methanol was treated in a high pressure visual cell with CO<sub>2</sub> at 80 bar and 35 °C checking if the decomposition of ammonia borane took place. FT-IR spectra of the solution before and after treatment were acquired to test also the differences in the chemical composition.

### 2.3 Analysis

The produced aerogel microparticles were characterized using different methods to evaluate the effect of the processing parameters. Particle size distribution was measured using a laser diffraction instrument, (Autosizer Lo-C, Malvern Instruments). This instrument is equipped with a diode laser of 4 mW (wavenumber of 670 nm). This analytical procedure was performed in triplicate for each sample.

Scanning electron microscopy pictures were obtained using a Jeol JSM 820 equipment. A gold sputter was used to cover the samples with a thin layer of gold to allow the electron reflection for particle evaluation.

Surface area and pore volume was analyzed using a Quantasorb Sorption System (Quantachrome Instruments, UK) with  $N_2$  at  $-196\text{ }^\circ\text{C}$  as sorbate. Prior to analysis, the samples were outgassed overnight at  $180\text{ }^\circ\text{C}$ . Total specific surface areas were determined by the multipoint BET method at  $P/P_0 \leq 0.3$ , and total specific pore volumes were evaluated from  $N_2$  uptake at  $P/P_0 = 0.99$ .

Silica aerogels loaded with ammonia borane were characterized by Fourier Transform Infrared Spectroscopy FT-IR (BRUKER, model ALPHA) in order to determine the amount of ammonia borane loaded and the possible variations in the chemical composition of the mixtures.

$CO_2$  - treated ammonia borane was analyzed with a portable Raman spectrometer BWTEK i-Raman (BWS415) equipped with a 40 mW diode laser.

The hydrogen release rate from samples was measured employing a volumetric cell of 5.4 mL of volume. For doing so, a certain amount of sample (typically in the range of 0.1 g) was weighed and loaded into the apparatus. Then vacuum was applied to the system and it was maintained at a temperature of  $80\text{ }^\circ\text{C}$  inside a Hewlett Packard 5890 chromatographic oven. The pressure evolution, which is proportional to the amount of released hydrogen, was recorded employing a GE Druck DPI-104 pressure transducer with an accuracy of 0.001 bar.

### 3. RESULTS AND DISCUSSION

#### 3.1 Discontinuous drying of aerogel microparticles

As described in section 2.2.2, batch drying experiments were carried out testing different combinations of process parameters, including: stirring rate, ratio between the amount of hydrophilic and hydrophobic organic solvents during the emulsion preparation, and amount of ammonium hydroxide catalyst. Table 1 presents a summary of the tested operation conditions together with the mean particle size obtained in each experiment. As shown in Figure 3, in general particles were not uniform in shape and some of them resembled broken pieces of aerogel, probably due to the action of the mechanical stirrer. These particles had BET areas in the range of  $600\text{ m}^2/\text{g}$  and pore volumes in the range of  $1\text{ cm}^3/\text{g}$ , similar to the textural properties of larger aerogel monoliths [24].

	Stirring rate (rpm)	Catalyst concentration (mM)	Hydrophobic- hydrophilic solvent ratio (mol/mol)	Average particle diameter ( $\mu\text{m}$ )
Sample 1	500	4.2	0.6	24.1 $\pm$ 0.3
Sample 1 - REP	500	4.2	0.6	24.5 $\pm$ 3.0
Sample 2	600	4.2	0.6	13.1 $\pm$ 0.8
Sample 2 - REP	600	4.2	0.6	16.4 $\pm$ 0.8
Sample 3	700	4.2	0.6	29.8 $\pm$ 4.7
Sample 3 - REP	700	4.2	0.6	23.7 $\pm$ 11.6
Sample 4	600	2.3	0.6	27.1 $\pm$ 0.9
Sample 5	600	5.8	0.6	19.6 $\pm$ 0.1
Sample 5 - REP	600	5.8	0.6	26.2 $\pm$ 10.4
Sample 6	600	4.2	0.3	22.1 $\pm$ 1.2
Sample 7	600	4.2	0.9	16.9 $\pm$ 0.3
Sample 7 - REP	600	4.2	0.9	11.5 $\pm$ 0.2

**Table 1.** Summary of experiments of hydrophilic aerogel microparticle synthesis by batch supercritical drying

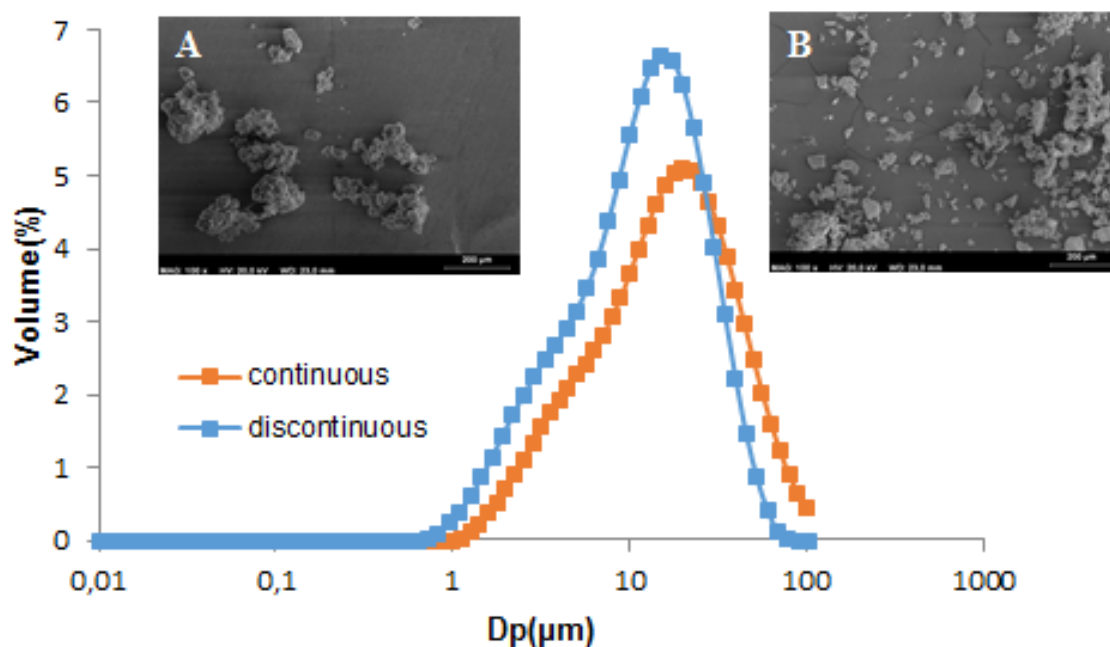


**Figure 3.** PSD and SEM micrographs of microparticles of hydrophilic silica aerogel obtained using discontinuous and semi-continuous drying processes (samples 2 and 11 of Table 1 respectively)

In order to ensure the reproducibility of results, several experiments were carried out in duplicate. Table 1 reports the mean particle sizes obtained in repeated experiments, while

Figure S1 of the Supplementary Material (at the end of the chapter) presents the corresponding particle size distributions. In general, the main differences between repetitions were observed in the tail of the particle size distributions, associated with small variations in the amount of particles with larger diameters that probably were produced as a result of agglomeration processes that are difficult to control. In some cases, as in experiment 5 of Table 1, these variations in the tail of the PSD cause significant variations in the mean particle size, although as shown in Figure S1 the PSD in the size range below 100  $\mu\text{m}$  was very similar in the repeated experiments. Therefore it can be concluded that the formation of large particles by agglomeration is the main parameter that influences the reproducibility of results.

Regarding the influence of process conditions on the dispersion of gel droplets and the subsequent formation of particles, it is known that increasing delivered energy by rising the mixer speed in general results in a reduction of particle size and an increase of the surface area [8]. In this study, three different mixer speeds (500, 600 and 700 rpm, samples 1-3 of Table 1) were used in order to corroborate this effect. As it can be seen in Figure S2, by increasing the rotational speed from 500 rpm to 600 rpm, a decrease in particle size was observed. However, a further increase of stirring rate to 700 rpm led to an increase in particle size due to the agglomeration of gel particles in the walls of the vessel. Furthermore, as presented in Figure S2, at 600 rpm the particle size distribution (PSD) was less broad than the one obtained at the other studied conditions, obtaining particles with an average diameter ( $d_{0.5}$ ) of 13  $\mu\text{m}$ . On the other hand, when the amount of  $\text{NH}_4\text{OH}$  used in the alcogel synthesis was varied, two opposite effects were produced: increasing the amount of catalyst produces particles with a lower diameter since nucleation rate is faster and more nuclei are formed. However, polycondensation rate also increases when more  $\text{NH}_4\text{OH}$  is added and the particles diameter increases as the amount of catalyst is increased [25]. Experimental results showed the effect of these competitive mechanisms, and as it is shown in Figure S3, an increase of the catalyst concentration from 2.3 mM to 4.2 mM led to a reduction of particle size, while a further increase to 5.8 mM led to an increase of particle size. In general, these results obtained with hydrophilic aerogel particles showed that there is a delicate balance between the reduction of size of individual particles, and the increment of agglomeration, as both processes are promoted when the stirring rate or the amount of catalyst are increased.

Hydrophobic solvent (hexane) was added in order to obtain a better dispersion of particles in the solution. Varying the amount of this solvent resulted in slightly different particle sizes due to variations in the dispersion conditions. As it is shown in Figure S4, the particle distribution with the lowest mean diameter was obtained with a hydrophilic/hydrophobic solvent molar

ratio of 0.6 (sample 2). Probably, an increase in the proportion of hydrophobic solvent allows for lower particle agglomeration and therefore a better dispersion. Nevertheless, PSD were very similar in all the experiments carried out with different solvent proportions.

In experiments carried out with hydrophobic aerogels, particles with a mean particle size between 17 and 22.5  $\mu\text{m}$  were produced, as shown in table 2. These sizes were in the same range as those obtained with hydrophilic aerogels. However, in experiments with hydrophobic aerogels, very regular spherical particles with smooth surfaces were obtained, as presented in Figure 4. This striking difference with respect to the irregular morphology of hydrophilic particles can be due to the mechanical properties of the particles, because the structure of hydrophobic aerogels is relatively flexible, a property that can contribute to prevent the erosion of gel particles during stirring. Additionally, the formation reaction of hydrophobic alcogels by cross-linking is slower than that of hydrophilic alcogels. This slow growth and ageing of gels can also contribute to the formation of particles with a more homogeneous morphology and smoother surface in the experiments with hydrophobic gels.

	<b>Stirring rate (rpm)</b>	<b>Catalyst concentration (mM)</b>	<b>Hydrophobic-hydrophilic solvent ratio (mol/mol)</b>	<b>Ratio TMOS/TMES</b>	<b>Average particle diameter (<math>\mu\text{m}</math>)</b>
Sample 8	600	4.2	0.6	1/5	17.4 $\pm$ 0.3
Sample 8-REP	600	4.2	0.6	1/5	19.0 $\pm$ 0.5
Sample 8-REP2	600	4.2	0.6	1/5	22.1 $\pm$ 0.4

**Table 2.** Summary of experiments of hydrophobic aerogel microparticle synthesis by batch supercritical drying

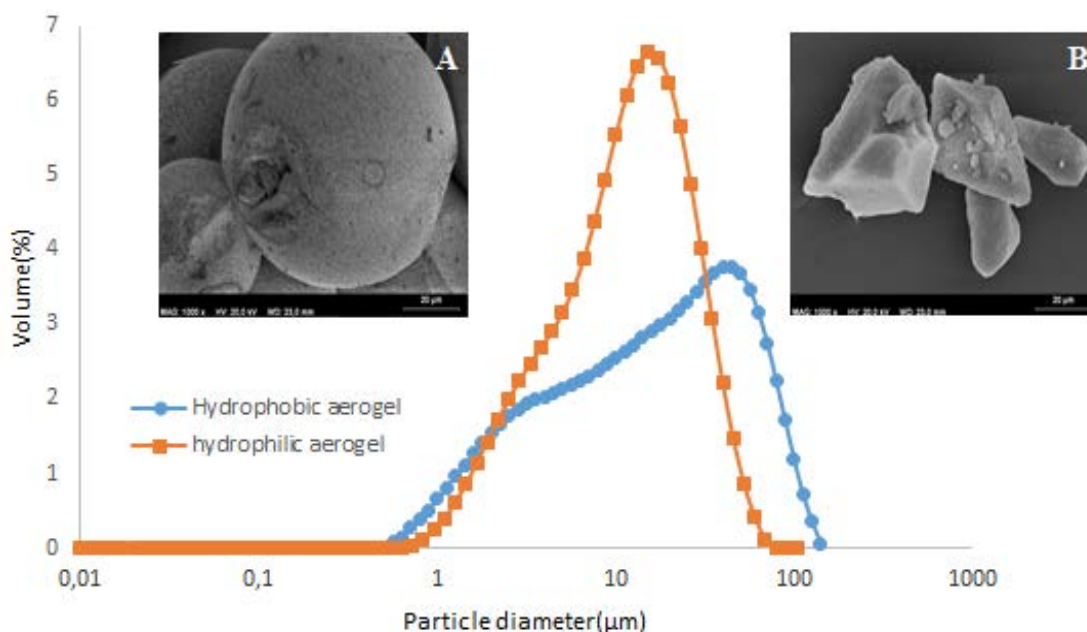


**Figure 4.** PSD and SEM of (A) hydrophobic silica aerogel microparticles with a ratio TMOS/TMES 1/5 and (B) hydrophilic silica aerogel

### 3.2. Semicontinuous drying of aerogel microparticles

As presented in Table 3, several experiments were performed in the semicontinuous plant, obtaining dried microparticles with a mean particle size between 17 and 19  $\mu\text{m}$ , and similar particle morphology and particle size distributions as in batch drying experiments, as shown in Figure 3. Furthermore, in all experiments porous particles were obtained with high surface area and relatively high pore volume, similar to those obtained in the batch drying experiments. Therefore, it can be concluded that particles obtained in this work by batch and semicontinuous drying methods presented equivalent morphological and textural properties. In comparison, a much lower surface area ( $53 \text{ m}^2 \text{ g}^{-1}$ ) practically without porosity ( $\sim 0 \text{ g cm}^{-3}$ ) was obtained by Montes et al. [9] when silica particles were produced by a simultaneous sol-gel reaction and drying in a supercritical  $\text{CO}_2$  environment.

	<b>C alcogel</b>	<b>A<sub>BET</sub></b>	<b>V<sub>Pore</sub></b>	<b>Average</b>
	<b>(g/L MeOH)</b>	<b>(m<sup>2</sup>/g)</b>	<b>(cm<sup>3</sup>/g)</b>	<b>particle diameter</b>
				<b>(μm)</b>
Sample 2 (Discontinuous)	-	582	1	16.4±0.8
Sample 9	3	671	0.77	17.6±0.6
Sample10	4	404	0.54	18.9±0.1
Sample11	6	790	0.81	17.6±0.8

**Table 3.** Textural properties of silica aerogels dried by semicontinuous and discontinuous technique

Comparing sample 9 and 11 of Table 3, it was observed that an increase in the concentration of alcogel in the methanol suspension pumped into the plant led to microparticles with higher surface area and volume of pores. With respect to particle sizes, negligible variations were observed when the concentration of alcogel in the initial suspension was varied. Thus, in the range of parameters considered in this work, the optimum conditions correspond to the highest possible concentration of alcogel in the suspension, being the limitation the maximum solid concentration allowed by the pump.

Regarding to the operation time, only 2 hours were needed to produce dry aerogel microparticles using the semicontinuous plant whereas 11.7 hours were required to produce an equivalent product by the batch process. This represents a considerable reduction in the required operation time which can be associated to a reduction of costs.

### 3.3 Incorporation of ammonia borane in silica microparticles

#### 3.3.1 Evaluation of ammonia borane stability in supercritical CO<sub>2</sub> environment

Zhang et al. [23] reported an enhanced release of hydrogen from ammonia borane treated with carbon dioxide at pressures in the range of 4-20 bar and temperatures of 85 °C. Raman analysis showed the formation of carbon-nitrogen and carbon-hydrogen bonds, which indicate a chemical absorption of CO<sub>2</sub> into ammonia borane, and thus the participation of carbon dioxide in the decomposition reactions of ammonia borane.

As presented in sections 3.1 and 3.2, during the aerogel drying experiments performed in this work, higher CO<sub>2</sub> pressures (90-110 bar) but lower temperatures (40 °C) than in the experiments of Zhang et al. [23] were used. In order to test whether the exposure of ammonia borane to carbon dioxide under these conditions causes any effect on the hydrogen release properties of the hydride, several experiments were performed putting ammonia borane into contact with supercritical carbon dioxide and analyzing the particles by Raman spectroscopy.

Similar results were obtained in Raman spectra for all the tested conditions. As it can be seen in Figure 5, bonds of N-H, B-H and B-N were unchanged when ammonia borane was treated with CO<sub>2</sub> at 50, 100 and 150 bar and a temperature of 40 °C, and the same result was also observed for a temperature of 50 °C. Moreover, no significant effect was observed on ammonia borane treated with CO<sub>2</sub> at high pressure for 45 to 240 min regarding to the characteristic peaks of the hydride as it can be seen in Figure 6, where the area of each representative peak in the Raman spectra has been represented after several processing times at 50 °C and 150 bar.

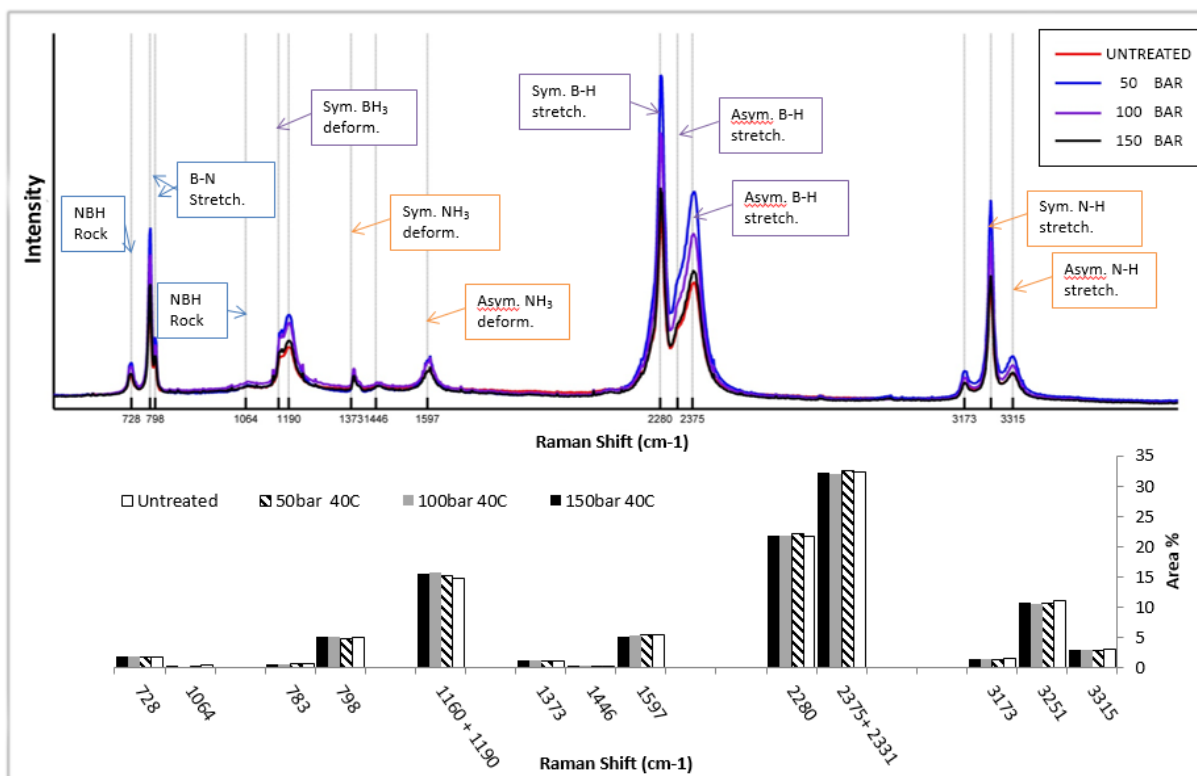


**Figure 5.** Raman spectra of  $\text{CO}_2$  treated ammonia borane at a temperature of  $40\text{ }^\circ\text{C}$  and pressures of 50, 100 and 150 bar

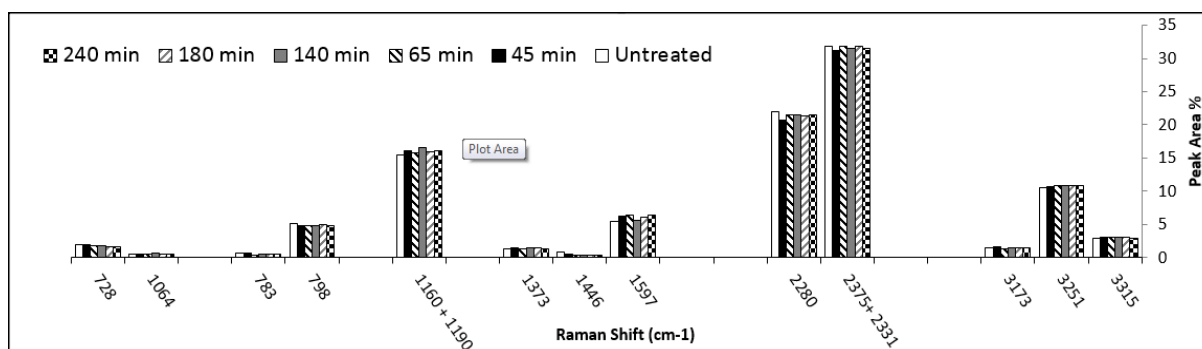


**Figure 6.** Raman spectra peak Area % of ammonia borane treated with  $\text{CO}_2$  at  $50\text{ }^\circ\text{C}$  and 150 bar at different treatment times from 0 min (untreated) to 240 min.

Special attention was taken in the wavenumber region where a chemical adsorption of  $\text{CO}_2$  can be observed according to Zhang et al [23]. Nevertheless none of the reported characteristic peaks of C-N, O=C=O and C-O bonds were observed in the  $\text{CO}_2$  treated ammonia borane samples. As a general result, no effect of  $\text{CO}_2$  over solid ammonia borane was observed at the temperature and pressure ranges used in aerogel drying experiments.

However, different results were observed when a solution of ammonia borane dissolved in methanol was treated with supercritical  $\text{CO}_2$ . Figure 7 presents the evolution of the solution along the process. First, after the solution reached 50 bar approximately at  $35\text{ }^\circ\text{C}$ , precipitation

of ammonia borane by  $\text{CO}_2$  antisolvent effect was observed at the bottom of the cell (photo B). After a few minutes, ammonia borane in the solution started to decompose releasing small bubbles of hydrogen that got bigger with time (photo C). This indicates that methanolysis was taking place and  $\text{CO}_2$  in supercritical conditions was performing a catalytic function in this reaction. After 1 hour, the system was depressurized and ammonia borane which had not been decomposed and was precipitated, was solubilized again in methanol (photo D).

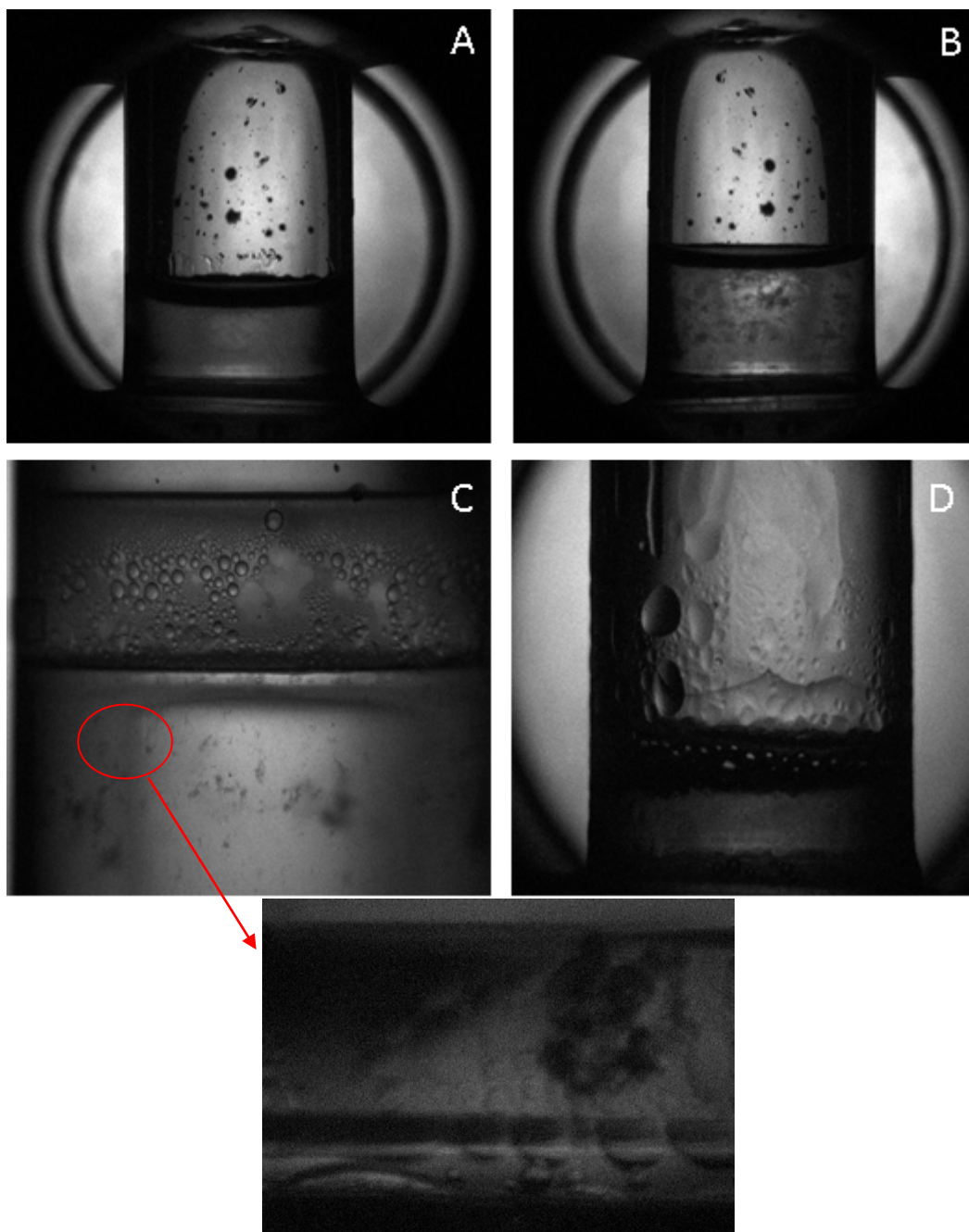


**Figure 7.** Pictures of the treatment of a solution of methanol with ammonia borane ( $c = 1.6 \times 10^{-3} \text{ mol}_{\text{AB}}/\text{mL}_{\text{MeOH}}$ ) with  $\text{CO}_2$  at 80 bar and 35 °C. A: Pressurized at 10 bar. B: Precipitation occurs at 50 bar. C: Hydrogen bubbles release. D: Dissolution of ammonia borane in methanol during the depressurization process

The decomposition of ammonia borane was confirmed by FT-IR analysis of the methanol solutions before and after the CO<sub>2</sub> treatment. As it is presented in Figure 8, the characteristic peaks corresponding to stretching of BH bonds of ammonia borane in the wavenumber range of 2500 cm<sup>-1</sup> - 2000 cm<sup>-1</sup> could be observed in both samples, indicating that a certain fraction of ammonia borane was not decomposed. However, a new peak near 1600 cm<sup>-1</sup> appeared after CO<sub>2</sub> treatment which could indicate the formation of C-N bonds, and peaks near this wavenumber showed a certain displacement which may be related to a new chemical structure in the molecule of AB.

As a summary, stability tests indicated that particles of solid ammonia borane do not suffer of decomposition mechanisms when exposed to supercritical carbon dioxide, but a gradual decomposition of ammonia borane dissolved in methanol occurs under supercritical CO<sub>2</sub> conditions. Therefore, ammonia borane must be precipitated before its exposure to supercritical carbon dioxide, as otherwise a significant decomposition of ammonia borane would take place during the long processing periods required for supercritical CO<sub>2</sub> drying of gels.



**Figure 8.** FTIR spectra of a) solution of ammonia borane in methanol b) solution of ammonia borane in methanol treated with CO<sub>2</sub> at 80 bar and 35 °C

### 3.3.2 Precipitation of ammonia borane inside alcogel particles followed by supercritical drying

Several experiments were carried out in order to encapsulate ammonia borane in hydrophilic and hydrophobic silica aerogel by adding dichloromethane, which produces an antisolvent

effect, followed by supercritical drying. Alcolgel particles were prepared at the same conditions than sample 2 of Table 1. Although several experiments were carried out employing ammonia borane concentrations in the initial methanol solution that should lead to concentrations in the dried particles of up to 10 wt%, only about 1 wt% of ammonia borane was precipitated in the final product as determined from hydrogen release measurements when hydrophilic alcolgel was used.

In order to understand these unwanted results, the samples were studied with FT-IR analysis according to literature data [26], which is shown in Figure 9. The spectra of hydrophilic silica aerogel loaded with ammonia borane reveals that bands corresponding to stretching vibrations of B-H and N-H have disappeared, and a broad peak is observed in this range of wavenumbers instead. Moreover, C-H stretching is observed at  $2800\text{ cm}^{-1}$  and C=O at  $1660\text{ cm}^{-1}$  due to the presence of  $\text{CO}_2$  during the process. This low encapsulation efficiency and the disappearance of some peaks could be because of the decomposition of the hydride during the drying process as a result of the reaction with active superficial groups of silica alcolgel [27], or by reaction with methanol that was not removed in the previous washing step.

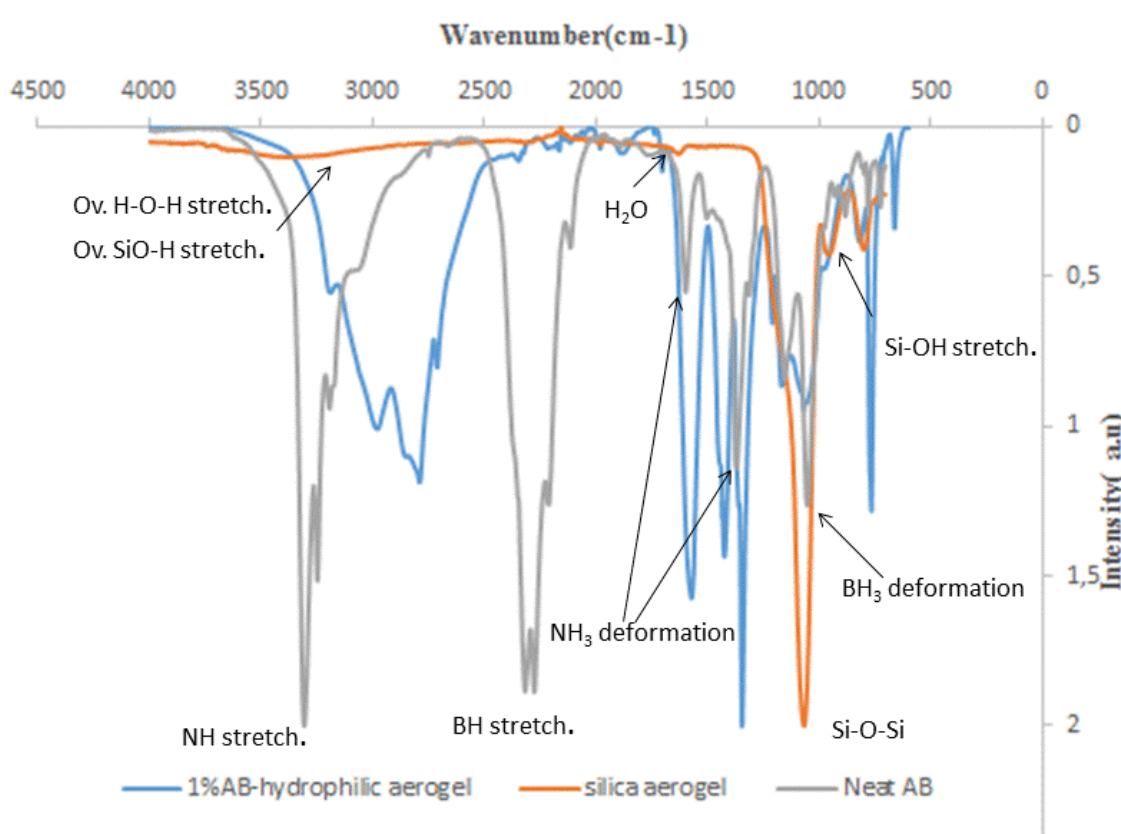


**Figure 9.** FTIR spectra of a) 1 wt% AB loaded in hydrophilic silica aerogel b) hydrophilic silica aerogel c) Pure ammonia borane

However, the concentration of ammonia borane loaded in hydrophobic aerogel increased to near 5 wt%, suggesting that the reaction of ammonia borane with silica aerogel surface groups or with water adsorbed in hydrophilic aerogels may be an important cause for ammonia borane decomposition. The chemical structure of ammonia borane in hydrophobic silica aerogel was also analyzed by FT-IR spectroscopy to confirm that the hydride was loaded in the aerogel. As it can be seen in Figure 10, a slight peak corresponding to N-H stretching is observed, although displaced to lower wavenumbers, and peaks corresponding to  $\text{NH}_3$  deformation were also observed. However, bonds related to B-H could not be detected with this technique when ammonia borane is loaded in the aerogel, possibly due to the relatively lower intensity of these peaks in the spectra of ammonia borane and the low concentration of ammonia borane in samples.

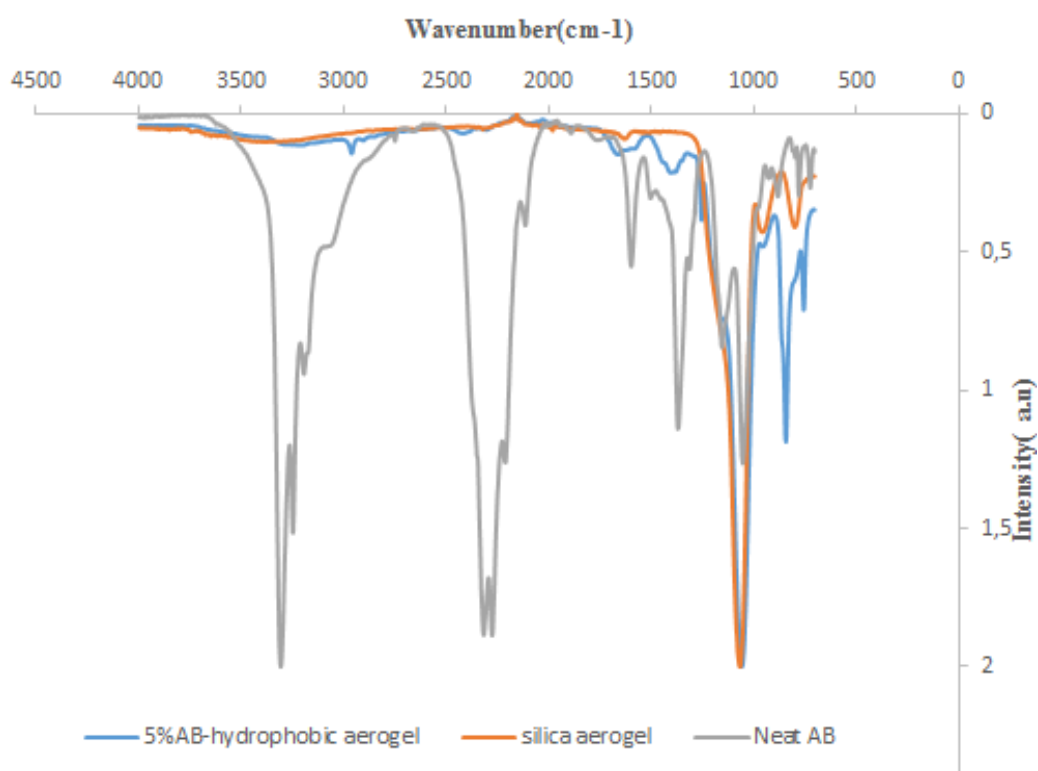


**Figure 10.** FTIR spectra of a) 5 wt% AB loaded in hydrophobic silica aerogel b) Pure ammonia borane

### 3.3.4 Evaluation of hydrogen release kinetics

The measurements results of hydrogen release kinetics are presented in Figure 11. As presented in this figure, by the incorporation of ammonia borane into aerogel particles the hydrogen release kinetics are substantially accelerated in comparison with the kinetics from pure ammonia borane. The fastest kinetics were observed in the products where ammonia borane was incorporated in hydrophobic aerogels. As it is seen in SEM pictures included in

Figure 11, AB was incorporated not only in the pores of the silica aerogel but also in the surface. Moreover, it is observed that the pore structure, which is preferably in a diagonal direction, are not completely blocked by the hydride nor collapsed after its precipitation.

As a reference, a simple physical mixture of ammonia borane and silica aerogel produced by mechanical milling presented a certain increase in the decomposition kinetics with respect to the pure hydride, but not as pronounced as the result obtained in the samples produced by supercritical drying. This improvement in the kinetics can be due to the reduction of particle size of the hydride and the stabilization of the hydride inside the pores of the aerogel, and the consequent reduction of diffusion distances.

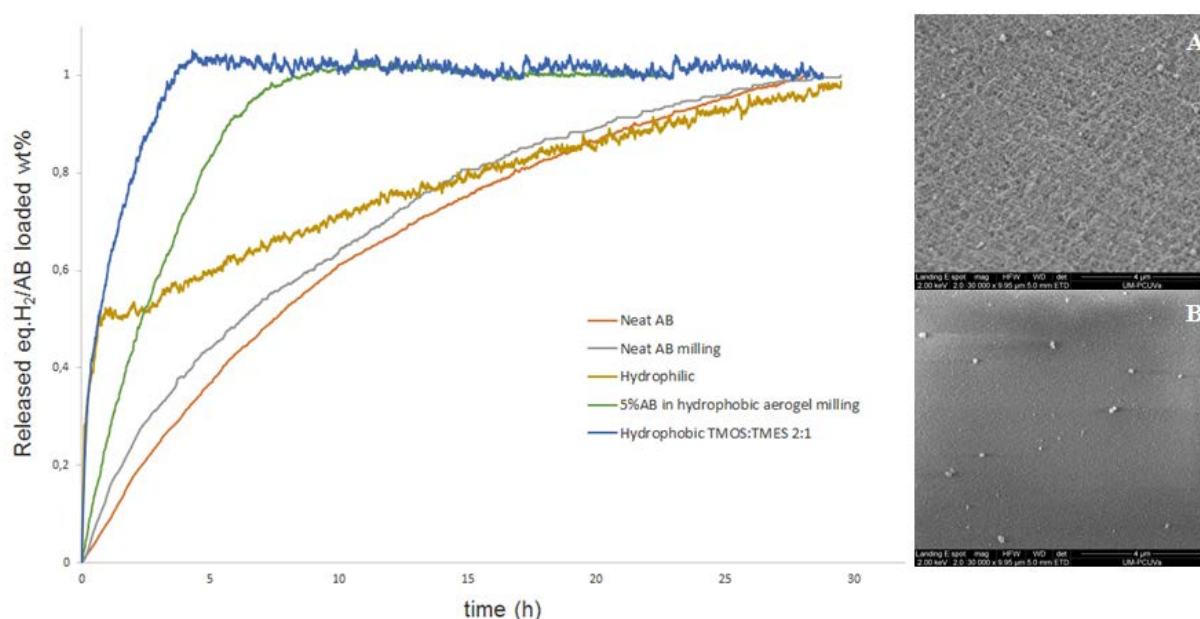


**Figure 11.** Hydrogen release kinetics from silica aerogel microparticles loaded with ammonia borane at 80 °C. Inserts show SEM micrographs of (A) the inner pore structure and (B) the surface of AB-loaded hydrophobic aerogel particles

#### 4. CONCLUSIONS

Silica aerogel microparticles were synthesized combining a sol-gel process with supercritical fluid drying techniques. In order to assess the feasibility of producing particles in a continuous regime and reducing processing times, two methods were applied: a batch and a semicontinuous drying process. The influence of different parameters (stirring rate, catalyst amount, hydrophilic-hydrophobic solvent ratio and hydrophobic functionalization) on the particle size distribution of the particles were investigated. Particles obtained by discontinuous and semicontinuous experiments presented similar morphological and textural properties, with mean diameters ranging from 13  $\mu\text{m}$  to 30  $\mu\text{m}$ , surface areas ranging from 400 to 800

$\text{m}^2/\text{g}$ , and pore volumes ranging from 0.5 to 1.0  $\text{cm}^3/\text{g}$ . Very significant morphological differences between the aerogel particles obtained from hydrophobic or hydrophilic gels were found: irregular shapes were observed in particles of hydrophilic aerogels, while regular, spherical particles with smooth surfaces were obtained with hydrophobic aerogels. Possible reasons for these differences are certain elasticity and a slow rate of formation of hydrophobic gels.

The aerogel microparticles were loaded with the hydrogen-storing hydride ammonia borane. Stability tests indicated that ammonia borane solutions undergone degradation by exposure to supercritical  $\text{CO}_2$  environment, while solid ammonia borane particles did not suffer degradation. Therefore, ammonia borane was precipitated inside the alcogels by a liquid antisolvent technique before supercritical  $\text{CO}_2$  drying. Using aerogels as a support to load ammonia borane resulted in enhanced hydrogen release kinetics compared to pure or milled ammonia borane due to the reduction of particle size and of diffusion distances.

Supplementary material

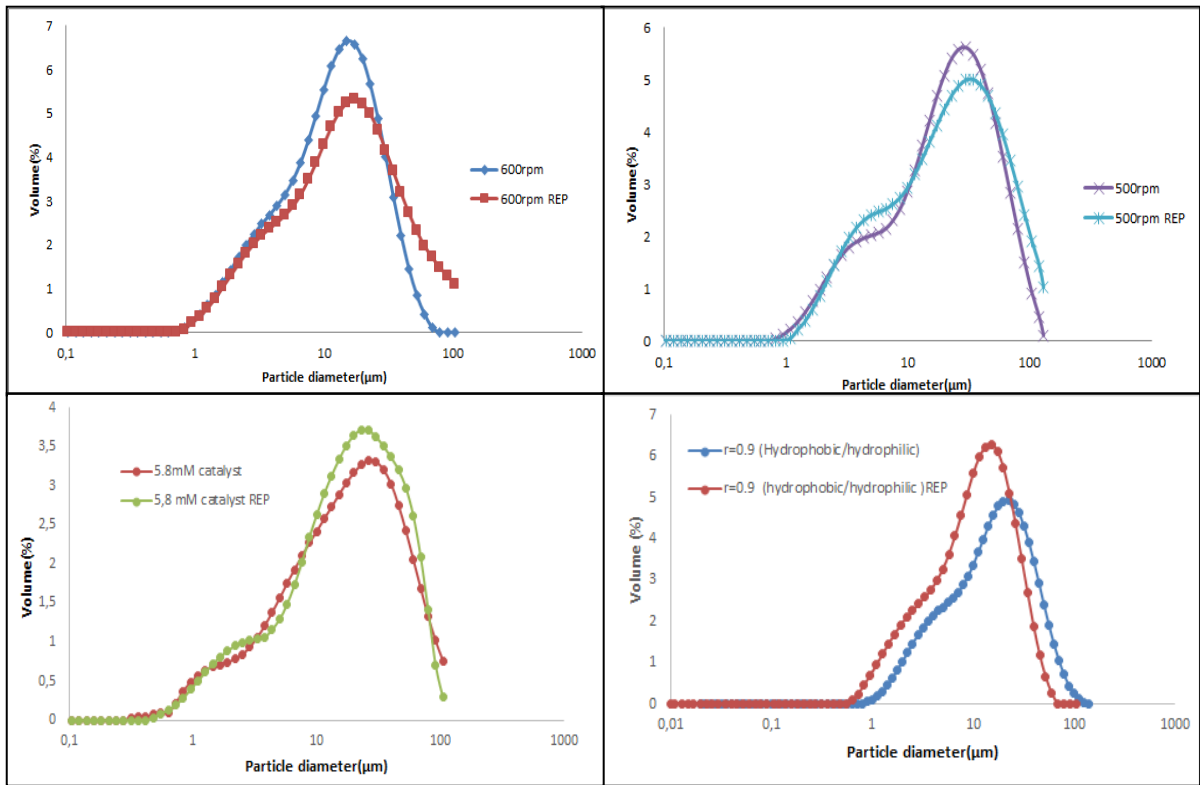


Figure S1. Comparison between particle size distributions obtained in batch drying experiments repetitions

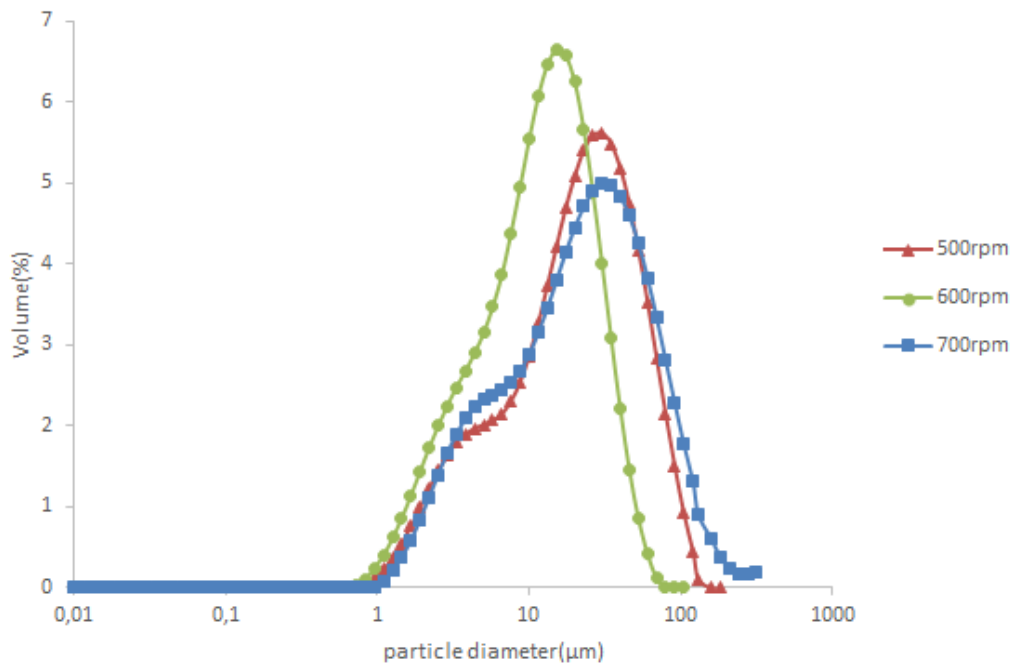
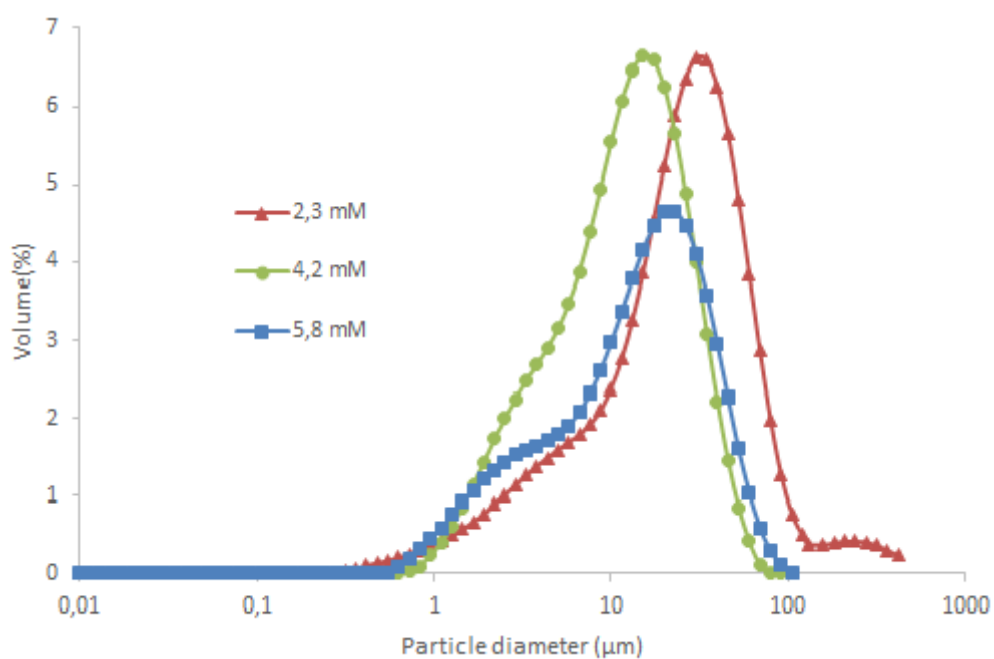
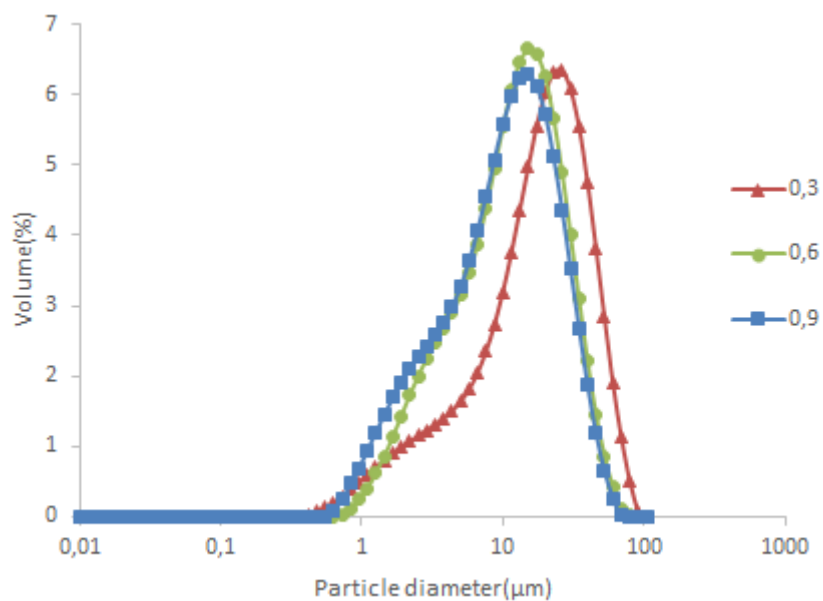


Figure S2. PSD of microparticles of silica aerogel prepared with different stirring rates



**Figure S3.** PSD of microparticles of silica aerogel prepared with different catalyst concentrations



**Figure S4.** PSD of microparticles of silica aerogel prepared with different hydrophilic-hydrophobic solvent ratios

**REFERENCES**

- [1] J.Fricke. Aerogels. Springer proceedings in Physics 6 (1986) 2-19.
- [2] Hrubesh, L.W. Aerogel applications. Journal of Non-Crystalline Solids 225 (1998) 335-342.
- [3] M.L.N.Perdigoto, R. N.-F. Application of hydrophobic silica based aerogels and xerogels for removal of toxic organic compounds form aqueous solutions. Journal of Colloid and Interface Science 380 (2012). 134-140.
- [4] J.Zhang, Z. B. Preparation of silica and  $\text{TiO}_2\text{-SiO}_2$  core-shell nanoparticles in water-in-oil microemulsion using compressed  $\text{CO}_2$  as reactant and antisolvent. Journal of Supercritical Fluids 36(2006) 194-201.
- [5] C.Folgar, D. C. Microstructural evolution in silica aerogel. Journal of Non-Crystalline Solids 353 (2007). 1483-1490.
- [6] A.Soleimani Dorcheh, M. Silica aerogel: synthesis, properties and characterization. Journal of Materials Processing Technology 199 (2008) 10-26.
- [7] I.Smirnova, S.Suttiruengwong, W.Arlt. Feasibility of hydrophilic and hydrophobic silica aerogels as drug delivery systems. Journal of Non-Crystalline Solids 350 (2004) 54-60.
- [8] M.Alnaief, I.Smirnova. In situ production of spherical aerogel microparticles. Journal of Supercritical Fluids 55 (2011). 1118-1123.
- [9] A.Montes, M.D.Gordillo, C.Pereya, N. de la Rosa-Fox, E.J.Martinez de la Ossa. Silica microparticles precipitation by two processes using supercritical fluids. Journal of Supercritical Fluids 75 (2013) 88-93
- [10] B.Peng, J. Ammonia borane as an efficient and lightweight hydrogen storage medium. Energy and Environmental Science 1 (2008) 479-483.
- [11] L.Song, S. C. Thermodynamics study of hydrogen storage materials. Journal of Chemical Thermodynamics 46 (2012) 86-93.
- [12] D.Pukazhselvan, V. S. High capacity hydrogen storage: Basic aspects, new developments and milestones. Nano Energy 1 (2012) 566-589.
- [13] G.Wolf, J.Baumann, F.baitalow, F.P.Hoffman. Calorimetric process monitoring of thermal decomposition of B-N-H compounds. Thermochemica Acta 343 (2000) 19-25
- [14] M.Bowden, T.Autrey, I.Brown, M.Ryan. The thermal decomposition of ammonia borane: A potential hydrogen storage material. Current Applied Physics 8 (2008) 498-500
- [15] M.R. Weismiller, S.Q.Wang, A.Chowdhury, S.T.Thynell, R.A.Yetter. Confined rapid thermolysis studies of ammonia borane. Thermochemica Acta 554 (2013) 110-117
- [16] J.Yang, S.Hirano. Improving the hydrogen reaction kinetics of complex hydrides. Advanced materials 21 (2009) 3023-3028.

- [17] S.Lai, H.Lin, T.L.Yu, L.Lee, B.Weng Hydrogen release from ammonia borane embedded in mesoporous silica scaffolds: SBA 15 and MCM-41. *International Journal of Hydrogen Energy* 37 (2012) 14393-14404.
- [18] S. Basu, Y. Zheng, J.P. Gore. An experimental study of neat and ionic liquid-aided ammonia borane thermolysis. *Journal of Power Sources* 196 (2011) 734-740.
- [19] P. V. Ramachandran, Pravin D. Gagare. Preparation of Ammonia Borane in high yield and purity, methanolysis, and regeneration. *Inorganic Chemistry* 46 (2007) 7810-7817.
- [20] D.E. Dedrick, R. behren, R.W.bradshaw. The reactivity of sodium alanates with O<sub>2</sub>, H<sub>2</sub>O and CO<sub>2</sub>. An investigation of complex hydride contamination in the context of automotive systems.Sand2007-4960.
- [21] R.Xiong, J.Zhang, Y.Zhao, D.L.Akins, J.W.Lee. Rapid release of 1.5 equivalents of hydrogen from CO<sub>2</sub>-treated ammonia borane. *International Journal of Hydrogen Energy* 37 (2012) 3344-3349.
- [22] C.A. García González, M.C.Camino-Rey, M.Alnaief, C.Zetzl, I.Smirnova. Supercritical drying of aerogels using CO<sub>2</sub>: Effect of extraction time on the end material textural properties. *Journal of Supercritical Fluids* 66 (2012) 297-306.
- [23] J.Zhang, Y.Zhao, D.L.Akins, J.W.Lee. CO<sub>2</sub>-Enhanced thermolytic H<sub>2</sub> release from ammonia borane. *The Journal of Physical Chemistry C* 115 (2011) 8386-8392.
- [24] L.M.Sanz-Moral, M.Rueda, A.Nieto, Z.Novak, Z.Knez, A.Martín. Gradual hydrophobic surface functionalization of dry silica aerogels by reaction with silane precursors dissolved in supercritical carbon dioxide. *Journal of Supercritical Fluids* 84 (2013) 74-79.
- [25] C.Oh, S. Y. Effects of the concentration of precursor and catalyst on the formation of monodisperse silica particles in sol-gel reaction. *Materials Research Bulletin* 46 (2011) 2064-2069.
- [26] R.Al-Oweini, H. El-Rassy. Synthesis and characterization by FTIR spectroscopy of silica aerogels prepared using several Si(OR)<sub>4</sub> and R''Si(OR')<sub>3</sub> precursors. *Journal of Molecular Structure* 919 (2009) 140-145.
- [27] A.C.Gangal, P.Kale, R.Edla, J.Manna, P.Sharma. Study of kinetic and thermal decomposition of ammonia borane in presence of silicon nanoparticles. *International Journal of Hydrogen Energy* 37 (2012) 6741-6748



# **CHAPTER 4**

**Improvement of the kinetics of hydrogen  
release from ammonia borane confined in  
silica aerogel**



## Improvement of the kinetics of hydrogen release from ammonia borane confined in silica aerogel

### Abstract

Ammonia borane is a promising hydrogen storage material due to its high gravimetric capacity (19.6 wt%), but it also presents limitations such as a slow hydrogen release with a long induction time, a difficult regeneration, or the formation of foams and gaseous by-products during thermolysis. Previous studies have shown that by nanoconfinement of ammonia borane within a porous support some of these limitations can be overcome due to the reduction and stabilization of ammonia borane particle size. However, this effect was only observed with moderate ammonia borane loadings, as with higher loadings the pores of the support became obstructed. In this work, silica aerogels produced by CO<sub>2</sub> drying, with pore volumes up to 2 cm<sup>3</sup>/g, have been used to confine ammonia borane. The influence of the amount of ammonia borane loaded on the aerogel support on the thermal and structural properties of the material has been analyzed. It has been found that more than 60 wt% of ammonia borane can be effectively stored in the pores of the aerogel support. The resulting material shows faster hydrogen release kinetics by thermolysis at 80 °C, due to a significant reduction in the mean size of ammonia borane after confinement and the participation of SiOH and SiOSi groups of silica aerogel in the decomposition mechanism.

**Keywords:** solid state hydrogen storage, ammonia borane, silica aerogel, nanoconfined, supercritical carbon dioxide.

## 1. INTRODUCTION

As fossil fuel reserves are increasingly limited and their use constitute a constant source of greenhouse gases and other environmental problems, the development of alternative energy sources is attracting a considerable attention [1, 2]. In contrast with fossil fuels, which can be easily stored and used when needed, the production of energy from most renewable sources is variable and it cannot be directly controlled. A possible solution for this limitation could be to use hydrogen ( $H_2$ ) as an energy vector, according to the approach commonly known as 'hydrogen economy' or 'hydrogen society' [3]. Hydrogen can be produced from water (by electrolysis, thermal decomposition, thermochemical processes, photolysis etc.) using renewable energy sources, and stored until needed. Furthermore, the efficiency of the combustion of hydrogen (by combustion in internal combustion engines, catalytic combustion or fuel cells) is high, and it is one of the most environmentally favorable fuels, as it produces nearly zero gaseous emissions.

At large scales, hydrogen can be transported through pipelines (gas  $H_2$ ) or tankers (liquid  $H_2$ ), and it is a good energy vector with an energy density of 33 kWh/kg, containing three times more energy than any hydrocarbon fuel on a weight basis [4]. However, the storage of hydrogen in small mobile units such as vehicles or small electronic equipment is more challenging.

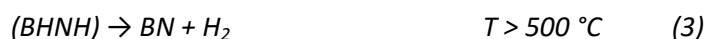
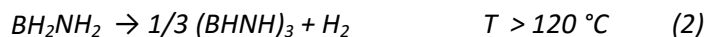
These challenges can be quantified analyzing the targets set by the US Department of Energy for 2020 for automotive hydrogen systems: a hydrogen storage gravimetric capacity of 5.5 wt% and a volumetric capacity of 0.040 kg/L, with a maximum cost of 333 \$/kg  $H_2$  stored [5]. Hydrogen storage by some of most obvious systems using compressed or condensed  $H_2$  cannot fulfill these requirements due to the physical properties of hydrogen. In the former case, high pressures (700 bar to reach a volumetric concentration of 0.042 kg  $H_2$ /L) or huge volumes are needed, and in the latter, high energy consumption is unavoidable in order to maintain the required cryogenic temperatures [6]. For these reasons, solid state hydrogen storage materials have been intensively studied, as hydrates [7], metal-organic frameworks [8] or metallic and chemical hydrides [9].

Ammonia borane (AB) is considered as a promising chemical hydride, due to its high hydrogen gravimetric capacity (19.6 wt%  $H_2$ ) and volumetric capacity (140 g/L), moderate decomposition temperature, non-toxicity [10] and stability at room temperature, even in the range 50-60 °C, which is important from the point of view of safety and engineering implications [11]. The thermal decomposition of neat AB releases one mole of hydrogen per mole of AB in each of

the following reactions (1), (2) and (3) [12]. In the first decomposition step, AB releases H<sub>2</sub> forming a complex polymeric aminoborane (PAB) below its melting point (114 °C):



Thereafter, PAB decomposes above 120 °C, forming polymeric iminoborane and small fractions of undesirable volatile byproducts:



Nevertheless, the use of this compound as hydrogen storage material also faces some important limitations. One of them is the kinetic limitation due to the long induction time needed to disrupt the dihydrogen bonding and initiate the release of hydrogen. Furthermore, AB is difficult to regenerate: after thermolysis, it is not possible to restore the initial AB by direct hydrogenation, and complex chemical regeneration routes comprising several steps are needed. Additionally, it forms foams during thermolysis that also complicate the regeneration due to the disruption of the physical structure of the material. Moreover, during the decomposition process, the emission of some volatile byproducts as borazine, diborane or ammonia can be released which could be poisonous for downstream processes and, particularly, hydrogen fuel cells.

Several strategies have been tested to overcome these barriers, including the addition of catalysts as silicon (Si), nickel (Ni), ruthenium (Ru), palladium (Pd) or zinc (Zn) [13-16], confinement of ammonia borane into porous solid supports [17-21], dissolution of AB in ionic liquids [22,23] or using polymers composites [24]. Regarding confinement of AB, different supports have been tested: silica scaffolds as SBA-15 or MCM-48 [18], metal organic frameworks (MOF) [16, 25] or carbon based materials [17] among others. The amount of AB that has been successfully loaded in the support depends on their structural properties ( $S_{\text{BET}}$  and  $V_{\text{pores}}$ ), getting a maximum amount of 50 wt% using silica scaffolds [17]. In all the cases that have been reported, hydrogen kinetic and thermodynamic properties have been improved respect to neat hydride due to the reduction in mean size. In our previous work [26], microparticles of silica aerogel were used as support, getting a maximum concentration of 5 wt% AB loaded in hydrophobic silica aerogel. Liquid antisolvent technique was used to precipitate the hydride prior supercritical carbon dioxide drying, resulting in enhanced hydrogen release kinetic compared to pure AB.

In this work, we report the confinement of AB using silica aerogel as porous host. The aerogel has been produced by liquid or supercritical CO<sub>2</sub> drying, a technique that enables to produce a

silica material with a high pore volume, and a correspondingly high potential capacity for storage of ammonia borane inside its pores. Several samples with different concentrations of AB up to 60 wt% have been prepared in order to analyze the influence of the loading of AB on the thermal and structural properties of the material. Scanning electron microscopy,  $N_2$  adsorption isotherms, FT-IR spectroscopy and X-ray diffraction have been used in order to characterize the final product prior to the measurement of hydrogen release kinetics by decomposition at 80 °C.

## 2. EXPERIMENTAL METHODS

### 2.1 Materials

Tetramethylorthosilicate (TMOS, 98.0% purity), ammonium hydroxide ( $NH_4OH$ , 28.0-30.0% ammonia purity) and ammonia borane (AB, 97% purity) were supplied by Sigma-Aldrich. Figure 1 shows a micrograph of neat AB as received. As shown in this figure, AB was constituted by agglomerated particles with sizes in the range of 100  $\mu m$  and with a porous structure. Methanol (MeOH; 99.8% purity), n-hexane (95% purity) and dry tetrahydrofuran (THF; with maximum water of 0.0075 wt%) were purchased from Panreac. Carbon dioxide ( $CO_2$ , 99.95% purity) was supplied by Carbueros Metálicos S.A.

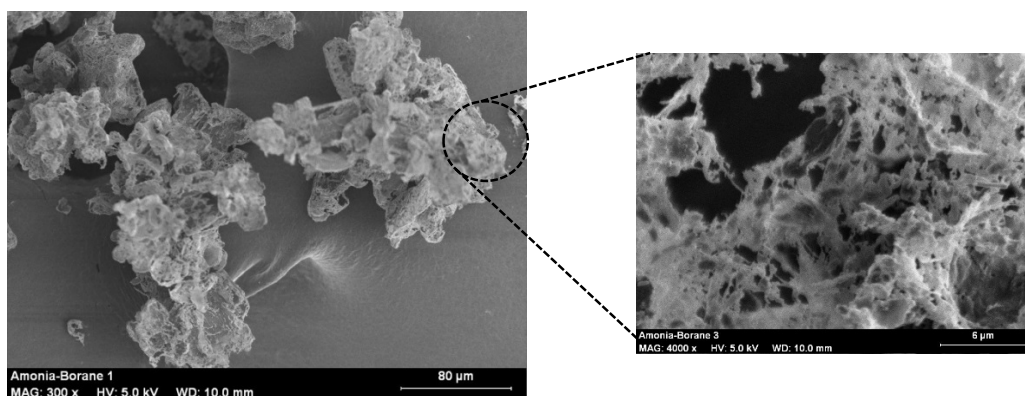


**Figure 1.** SEM micrograph of neat ammonia borane as received

### 2.2 Preparation of AB loaded in silica aerogel microparticles

As presented in Figure 2, the procedure for the preparation of AB-loaded silica aerogel microparticles consists of three key steps: preparation of silica gel microparticles, addition of ammonia borane by a wet impregnation method, and drying of the AB-loaded gel particles

with pressurized carbon dioxide in order to produce the final, dry AB-loaded aerogel microparticles.

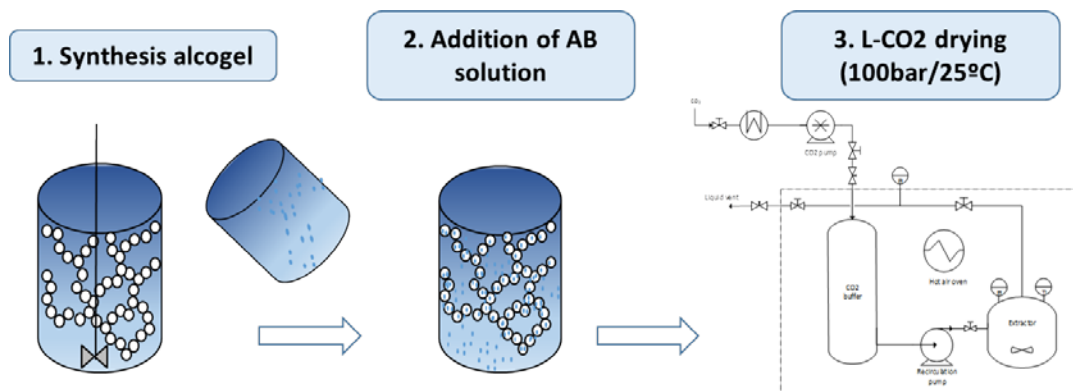


**Figure 2.** Steps for preparation of silica aerogel microparticles loaded with ammonia borane

In the first step of this procedure, hydrophilic silica alcogel was prepared using the well-known method of hydrolysis condensation sol-gel reaction, using TMOS as precursor and methanol as solvent. While with this procedure it is common to prepare large gel monoliths, in this work the gel was synthesized as microparticles, in order to reduce the possible heat and mass transfer resistances that could be caused by larger aerogel monoliths. To do this, and according to the procedure described in a previous work [26], the sol-gel reaction media was dispersed in hexane under mechanical stirring, in order to obtain small droplets of TMOS in methanol dispersed within the hexane continuous phase. After 10 minutes of mechanical stirring of this mixture with a two bladed axial stirrer set at 600 rpm, an aqueous solution of  $\text{NH}_4\text{OH}$  was added as condensation catalyst, which induced the gelation of TMOS. The molar ratio used was the following: 1 mol TMOS: 4.4 mol MeOH: 3.3 mol  $\text{H}_2\text{O}$ : 4.5 mol hexane: 0.08 mol  $\text{NH}_4\text{OH}$ . As methanol or water produced during the condensation reaction can induce the decomposition of ammonia borane during the subsequent drying processes [26], after 2 hours of gelation the alcogel microparticles were retrieved and immersed in THF. Gel particles were then kept during 7 days immersed in THF in a closed vessel, to let the gel age and strengthen its structure. During this ageing period, the THF solvent was renewed at least twice in order to remove the last traces of methanol and water.

After the ageing process, microparticles of alcogel are ready for wet impregnation, adding a solution of ammonia borane dissolved in THF. This method has the advantage that impregnation can be performed under milder temperature conditions compared to melt infiltration, and only one impregnation step is necessary in contrast to incipient impregnation methods [27]. Again, THF was used instead of methanol as solvent in order to avoid

methanolysis and therefore the decomposition process of the hydride not only during wet impregnation (due to SiOH groups) but also during drying process [26].

Different samples with different concentrations of ammonia borane were prepared, adding different amounts of hydride (0-0.4 g AB dissolved in 5mL of THF) to 2 g of microparticles of alcogel (gel before drying, therefore with the pores filled with the organic solvent) in order to study his influence on the properties of the final solid product. With this, concentrations of AB in the final product ranging from 10 to 60 wt% AB were obtained, where the concentration of AB is defined as presented in equation (4):

$$\%AB = \frac{g_{AB}}{g_{AB} + g_{aerogel}} \quad (4)$$

The third and last step is the removal of the organic solvent in order to obtain the final, dry AB/SiO<sub>2</sub> particles. The drying method employed is a key aspect that determines the textural properties of the porous support. If the solvent is removed by evaporation or lyophilization, the capillary stresses associated to the formation of vapor-liquid interfaces inside the pores of the support cause fractures and a partial collapse of the pore structure of the material. In the case of SiO<sub>2</sub> matrixes, the materials obtained by these drying methods usually show pore volumes below 0.5–1.0 cm<sup>3</sup>/g. Some examples are the well-known SBA-15 or MCM-41 mesoporous silica matrixes. In contrast, if pressurized or supercritical carbon dioxide is used to extract the solvent, the collapse of the pore structure is minimized, because under these conditions carbon dioxide can be completely miscible with the organic solvent, and therefore the extraction proceeds without formation of gas-liquid interfaces and without capillary stresses. Due to this enhanced preservation of the pore structure, with this method it is possible to reach pore volumes in the range 2–4 cm<sup>3</sup>/g [28]. Additionally, during this drying process CO<sub>2</sub> can act as antisolvent for solutes dissolved in the organic solvent, as it is completely miscible with the organic solvent, but it cannot dissolve high-molecular weight solutes dissolved in the organic solvent. This precipitation method is commonly referred in the literature as “Gas Anti Solvent” (GAS) or “Supercritical Anti Solvent” (SAS) precipitation [29,30]. In the case of this work, as ammonia borane is insoluble in CO<sub>2</sub> [26], when the THF-immersed alcogels are mixed with CO<sub>2</sub>, AB dissolved in the THF that fills the pores of the alcogels quickly precipitates according to a GAS precipitation mechanism, thus favoring the formation of small particles within the pores of the gels.

In a previous work, it was observed that due the interaction of AB with the SiO<sub>2</sub> matrix, the temperature needed to initiate the decomposition of AB is drastically decreased [26]. Thus, in order to avoid the thermolysis of AB, the drying process was carried out at a near-ambient

temperature of 25 °C and at a pressure of 100 bar, thus employing pressurized, liquid CO<sub>2</sub>. As in the previous work [26], a batch drying apparatus, depicted in Figure 2, was used. Using this apparatus, the alcogels immersed in THF were loaded into the extraction vessel and the system was pressurized with CO<sub>2</sub> using an air-driven piston pump. The system was slowly pressurized at a rate of 0.5 bar/min in order to avoid breakages in the alcogel/aerogel and mechanical stresses that could damage the structural properties of the final product. Once the desired pressure and temperature were reached, the recirculation pump that connects the extraction vessel with the CO<sub>2</sub> reservoir was connected, thus bubbling CO<sub>2</sub> through the THF-immersed alcogels and enhancing the extraction of the solvent. As CO<sub>2</sub> gradually becomes saturated with the solvent during the extraction process, CO<sub>2</sub> in the system was renewed after a predefined extraction time. In this work, four drying cycles were needed (each cycle lasting 60 min, 60 min, 120 min and finally 40 min) to assure the total elimination of organic solvent from the final solid sample. During the CO<sub>2</sub> renewal step after every cycle, the extraction vessel was isolated closing its inlet-outlet valves and kept at the pressure conditions of the drying process to avoid the damages in the structure of the aerogels that could be caused by repeated pressurization-depressurization processes. The rest of the circuit was depressurized till ambient pressure and refilled with the air-driven pump until the extraction pressure of 100 bar. After the last cycle, the entire system was slowly depressurized at a rate of 0.5 bar/min, and samples were retrieved from the extractor and stored until further analysis.

Finally, neat ammonia borane was also recrystallized by GAS process using pressurized CO<sub>2</sub> as antisolvent. These experiments allow evaluating if the recrystallization has a separate, specific influence on the hydrogen release properties of the material. As during aerogel drying AB precipitates inside the pores of the aerogel by a similar mechanism as in these GAS experiments, a similar influence of the recrystallization may be expected that would be combined with the influence of the nanoconfinement within the pores of the aerogel. In these GAS experiments, the same apparatus and experimental procedure previously described for aerogel drying experiments was used, loading the extraction cell with a solution of AB in THF (concentration: 24 mg AB/mL THF).

### 2.3 Characterization of AB loaded in silica aerogel

#### 2.3.1 Properties of AB/SiO<sub>2</sub>

Structural properties were analyzed by Fourier Transform Infrared Spectroscopy (FTIR Bruker, model Alpha with a Platinum-ATR single diffraction sampling module). These analyses were

performed before and after dehydrogenation for every concentration of AB loaded in silica aerogel.

The N<sub>2</sub> adsorption-desorption isotherms data were acquired using a Micrometrics Analyzer (ASAP 2020) with N<sub>2</sub> at -196 °C as sorbate. Prior to the analyses, the samples loaded with AB were outgassed under vacuum at room temperature for 2 hours and the silica aerogel without any impregnation compound was degassed under vacuum at 150 °C for several hours (3-5 h) until the mass of the sample was constant. Total specific surface areas were determined by the multipoint BET method at  $P/P_0 = 0.3$ , and total specific pore volumes were evaluated from N<sub>2</sub> uptake at  $P/P_0 = 0.99$ . Pore sizes were calculated using BJH equations.

Scanning electron microscopy (SEM) was performed using a Jeol JSM 820 equipment. Energy Dispersive Microanalysis (EDX) was done with microanalysis Bruker Quantax 2000 at 20 KV obtaining 10000 signals/second. No metallic coating pretreatment was necessary prior to analyses.

X-ray diffraction (XRD) analyses (model Bruker Discover D8) were done at CuK $\alpha$  radiation,  $\lambda = 1.5418 \text{ \AA}$ ,  $2\theta$  angle ranging from 5° to 7° with a scan rate of 4 s/step and a step size of 0.020°. These analyses were also performed before and after thermal dehydrogenation.

### 2.3.2 Thermal decomposition properties

Thermal gravimetric analyses (TGA) were undertaken in a Mettler Toledo TGA system from 30 to 300 °C at 5 °C/min heating rate under a nitrogen flow rate of 60 mL/min. Differential scanning calorimetry (DSC) assays were carried out in a Mettler Toledo model 822e with a ceramic sensor of high sensitivity. Nitrogen gas flow was also used at 60 mL/min, with the same heating rate (5 °C/min) from 0 to 250 °C using 5-8 mg of sample.

Kinetic measurements of hydrogen release by thermolysis were carried out using a stainless steel cell of 4.7 mL equipped with a certified pressure transducer model DPI104 provided by GE Druck (Germany), which had an uncertainty of  $\pm 0.01$  bar and was connected to a data acquisition computer. The cell was loaded with about 100 mg of sample, determining the precise sample weight with an analytical balance with an uncertainty of  $\pm 0.0001$  g. Then, the cell was subjected to vacuum, down to an absolute pressure below 0.04 bar. The sample was maintained under vacuum at ambient temperature for at least some minutes, in order to remove small amounts of entrapped gases or moisture that could influence the measurement. Afterwards, the sample was heated to 80 °C introducing the cell inside a chromatographic oven. The pressure evolution in the cell was recorded every 10 seconds using the pressure

transducer acquisition software. The amount of hydrogen released was calculated from pressure recordings using the Hydrogen Reference Equation of State [31] implemented in the Reference Fluid Thermodynamic and Transport Properties Database (REFPROP) software developed by the National Institute of Standards and Technology (NIST) [32].

### 3. RESULTS AND DISCUSSION

#### 3.1 Incorporation of ammonia borane in silica aerogel

##### 3.1.1 FT-IR studies of neat AB and AB/SiO<sub>2</sub> before thermal decomposition

Figure 3 shows the FT-IR spectra of neat and recrystallized AB [33-35], and of samples with AB-loaded silica aerogel with different concentrations of AB. In the spectra of neat AB, absorption peaks from 3000 to 3500 cm<sup>-1</sup> can be associated to N-H stretching whereas B-H stretching appears in the range 2000-2500cm<sup>-1</sup>. Other characteristic peaks in the IR of neat AB appear at 1602 cm<sup>-1</sup> (N-H deformation), 1372 cm<sup>-1</sup>(which may be attributed to double B-N bonds [33] or N-H bonds [34]), 1155 cm<sup>-1</sup> (B-H scissor), 1051 cm<sup>-1</sup> (N-B-H rock), and N-B bond in the range 720-800 cm<sup>-1</sup>. As shown in Figure 3, the FT-IR spectrum of recrystallized AB is nearly identical as that of neat AB, indicating that AB has not undergone degradation during the recrystallization.

As presented in Figure 3, the spectrum of silica aerogel shows characteristic peaks at 798 cm<sup>-1</sup> (Si-O-Si bond), 950 cm<sup>-1</sup> (Si-OH) and 436 cm<sup>-1</sup> (O-Si-O) [36]. Samples with silica aerogel loaded with AB yield a combination of the characteristic spectra of AB and silica. AB peaks corresponding to B-H bonds near 2000-2500 cm<sup>-1</sup> and N-H bonds near 1600 cm<sup>-1</sup> are particularly prominent. It can be also observed that, as expected, these peaks show higher intensities in samples with higher proportion of AB. These results indicate that AB is present in samples and has also not undergone degradation during drying of silica aerogel with CO<sub>2</sub>.

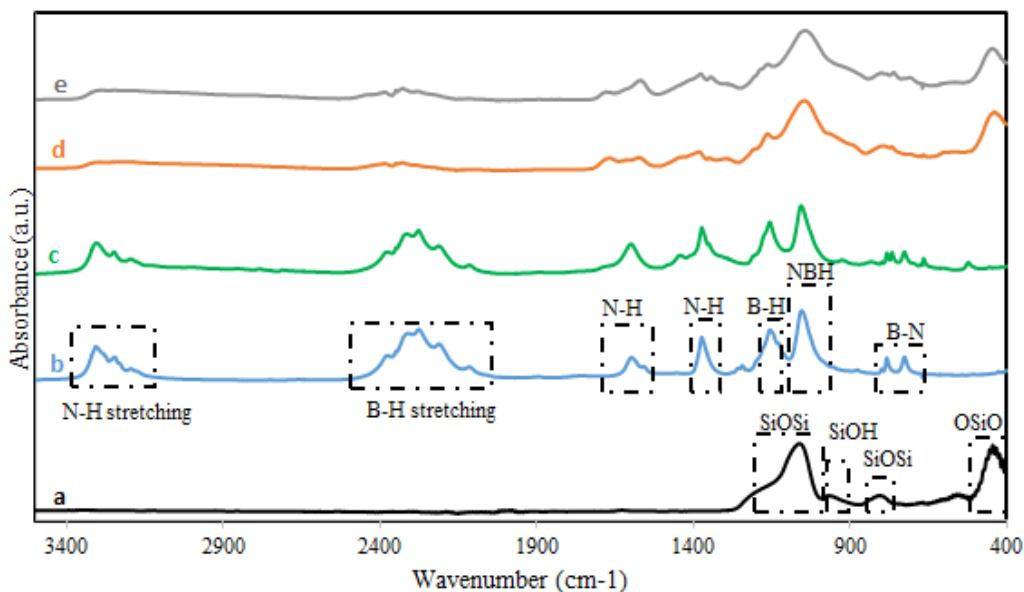


**Figure 3.** FTIR spectra of a) silica aerogel b) neat AB c) recrystallized AB d) 30 %AB/SiO<sub>2</sub> e) 60% AB/SiO<sub>2</sub>. Curves are vertically displaced for clarity.

### 3.1.2 Textural properties of AB-loaded silica aerogels

Figure 4 shows the nitrogen adsorption and desorption isotherms of different samples, and Table 1 shows the textural properties obtained from these isotherms. All these isotherms correspond to class IV according to the classification of International Union of Pure and Applied Chemistry (IUPAC), which is typical of mesoporous materials. They show hysteresis due to the capillary condensation, which is observed at higher relative pressure in samples with a higher amount of AB.

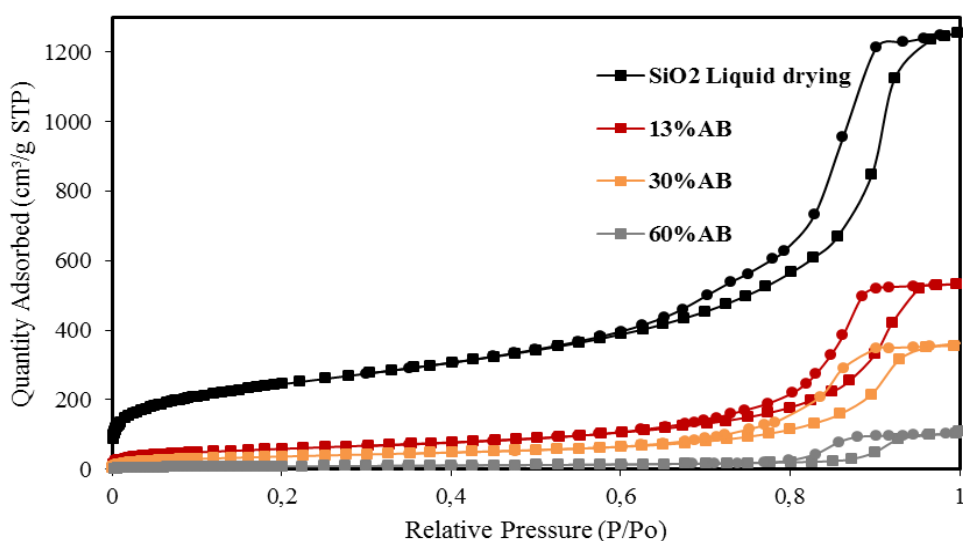


**Figure 4.** Nitrogen adsorption-desorption isotherms and BJH pore size distribution of silica aerogel and AB loaded in silica with different concentration (● adsorption (○) desorption)

Sample	BET surface area ( $\text{m}^2 \text{g}^{-1}$ )	Pore volume ( $\text{cm}^3 \text{g}^{-1}$ )	Pore diameter (nm)
<b>SiO<sub>2</sub> sc drying</b>	723.1±2.0	1.35	7.6
<b>SiO<sub>2</sub> Liquid drying</b>	887.3±1.4	1.94	8.7
<b>13AB/SiO<sub>2</sub></b>	216.6±0.3	0.82	11.1
<b>30AB/SiO<sub>2</sub></b>	137.3±0.3	0.56	10.9
<b>60AB/SiO<sub>2</sub></b>	30.4±0.1	0.17	13.7

**Table 1.** BET surface areas and BJH pore volumes and pore diameters of silica aerogel dried with liquid or supercritical CO<sub>2</sub> at and AB-loaded silica aerogel

The support obtained in this work shows the typical textural properties of silica aerogels reported in many previous works [37, 38]. Comparing to other mesoporous materials, the surface area of the silica aerogel obtained in this work is similar to that of the Santa Barbara Amorphous (SBA) or MCM silica materials used in previous studies of nanoconfinement of AB, but the pore volume is almost twice as high [18, 39], which is a favorable property since this higher pore volume can host a higher concentration of AB.

Moreover, both BET and BJH analyses (see Table 1) demonstrate that the surface area and the volume of free pores decrease linearly as concentration of AB increases, variations that correspond well with the amount of AB incorporated into the material [17]. Regarding the BJH distributions of pore volume, the bimodal distribution of the empty support is converted to a unimodal distribution for the sample with highest concentration of AB, as the pores with lower size are filled first with AB, leaving partially empty the biggest ones. In the case of the sample with the highest concentration of AB (60 wt%), only 8% of the pore volume remains free, indicating that this concentration of AB is close to the maximum host capacity of the aerogel. These results suggest that AB was successfully confined inside the pores of the aerogel.

In comparison, in previous works the maximum amount of ammonia borane loaded in SBA or MCM silica supports by a conventional solvent infiltration method was 50 wt% [18, 40], but it was observed that when the concentration of AB was higher than 33 wt%, it started to aggregate outside the pores of the silica support as the internal pore volume of the material became saturated [25]. In the case of metal organic frameworks (MOF), from 20 wt% AB [16] till 50 wt% AB [41] has been encapsulated depending on the impregnation method or the MOF used. Also, carbon cryogels have been used as supports employing a wet impregnation

method, but achieving a maximum concentration of only 24 wt% AB [17] due to the comparatively lower surface area ( $300 \text{ m}^2/\text{g}$ ) and volume of pores ( $0.70 \text{ g}/\text{cm}^3$ ) of this support.

### 3.2 Structural characterization of AB-loaded silica aerogels

#### 3.2.1 Morphology of neat AB, recrystallized AB and AB loaded in silica aerogel

Figure 5-A shows a SEM micrograph of AB recrystallized from THF solutions using pressurized  $\text{CO}_2$  as antisolvent. As observed in this figure, the compound is recrystallized as highly agglomerated flat particles. Due to this morphology, it is difficult to obtain precise particle size measurements, but the size estimated by image analysis of SEM micrographs is in the range of  $0.5 \text{ }\mu\text{m}$  of thickness and  $5 \text{ }\mu\text{m}$  of length, values that are considerably smaller than the dimensions of neat AB particles as presented in Figure 1. Furthermore, the recrystallized particles do not show the porous, intertwined structure observed in neat AB (Figure 1).

Figure 5-B shows a micrograph of silica aerogel loaded with a 30 wt% of AB. It can be observed that the host silica material is constituted by prismatic particles of  $10\text{--}20 \text{ }\mu\text{m}$ , in agreement with the results obtained in a previous work [26]. Furthermore, in SEM micrographs of AB- $\text{SiO}_2$  samples (Figure 5-B), particles with the flat morphology and the dimensions observed in the recrystallized AB (Figure 5-A) are not observed, suggesting that AB did not precipitate as segregated particles outside the aerogel. This impression is confirmed by the results of mapping assays of silica and nitrogen presented in Figure 5. Silica mapping confirms that all the particles that can be observed in the SEM micrograph presented in Figure 5-B indeed correspond to silica aerogel, while nitrogen mapping show that ammonia borane is dispersed within all these particles and is not present as segregated crystals. Therefore it can be concluded that AB is homogeneously embedded in the pores of the aerogel. Similar results were obtained in the mapping of samples with higher concentration of AB, up to the maximum concentration of 60 wt% tested in this work.

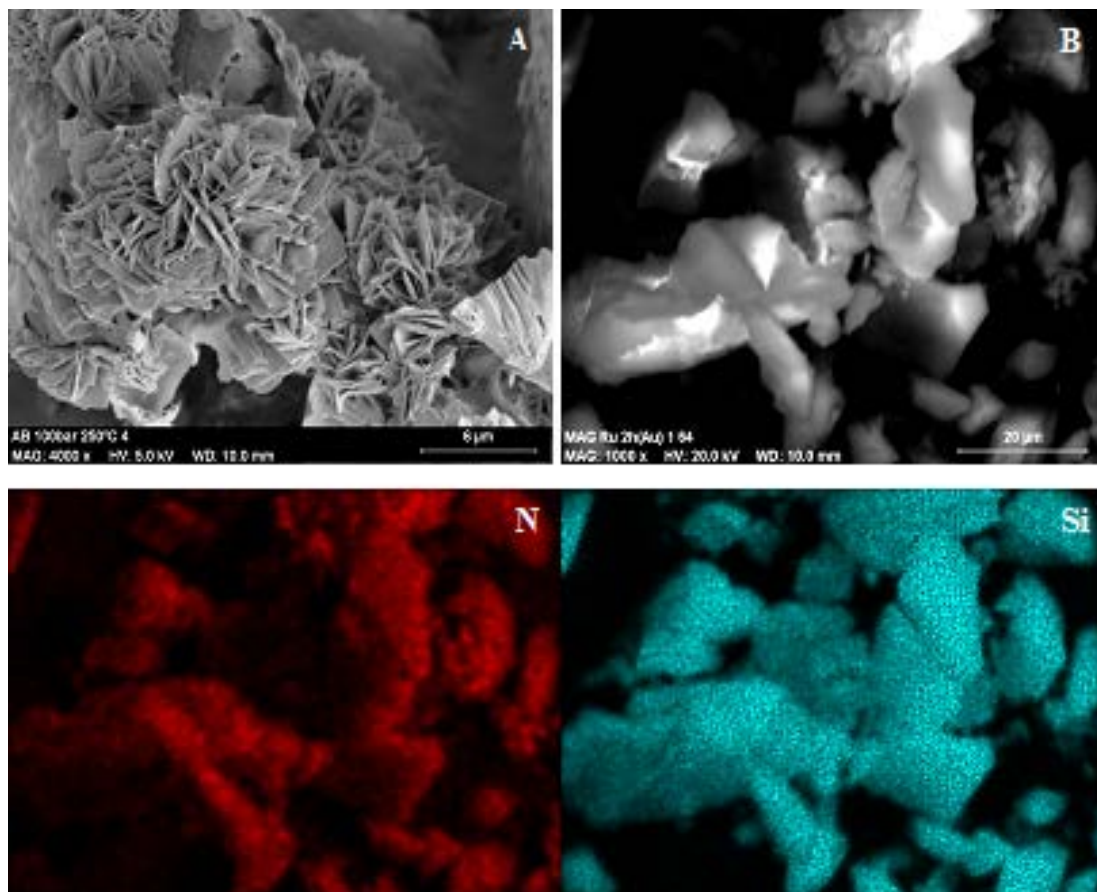


**Figure 5.** SEM images of A) Recrystallized AB after recrystallization in THF using liquid CO<sub>2</sub> as drying method B) 30 wt% AB loaded in silica aerogel and mapping of sample B (blue is referred to silica and red to Nitrogen)

### 3.2.2 XRD patterns

Figure 6 shows the XRD pattern of neat ammonia borane, which matches well with JCPDS reference 01-074-0894 suggesting the typical polycrystalline structure with tetragonal lattice symmetry, in agreement with literature information about the structure of AB at ambient temperature [42]. The crystallite size estimated using the Scherrer's equation formula is 40 nm, and the dominant sharp peak of the pattern is located at  $2\theta = 23.75^\circ$ , corresponding to (110) planes. After recrystallization by GAS process, slight modifications in the XRD pattern can be observed at  $2\theta = 17$  and  $30^\circ$ . A similar modification can be observed in silica-loaded AB samples, although with less defined peaks due to the strong signal produced by the silica support. This modification in the pattern can suggest the formation of diammoniate of diborane (DADB), an isomer of AB. This compound shows some differences regarding the hydrogen release mechanism compared to its isomer AB: the temperature for decomposition of DADB is about 10 °C lower than that of AB, and DADB undergoes solid-phase decomposition without melting or induction period even at moderate temperature, while AB suffers from a

long induction period prior to H<sub>2</sub> release [43]. Therefore, the formation of this compound may justify some of the observed thermal properties, as it will be discussed in the following sections.

Nevertheless, in GAS recrystallized samples, the dominant pattern is equivalent to that of neat AB, also corresponding to tetragonal crystal structure is observed, although diffraction peaks are not so well defined, and the estimated crystallite size increases to 75 – 150 nm. In the case of AB loaded in silica aerogel, the peaks are merged, therefore suggesting a reduction of crystallinity or an increased inhomogeneity in the properties of the crystals due to the incorporation in the pores [44]. Additionally, as shown in Figure 5b it can be seen that the XRD pattern of amorphous silica, characterized by a broad peak around 24°, is overlaid to the dominant peaks related to AB. Therefore results show that AB retains its crystalline structure after nanoconfinement within the pores of the aerogel, with estimated crystallite sizes in the range 100–200 nm, similar to those obtained by recrystallization of AB by GAS process.

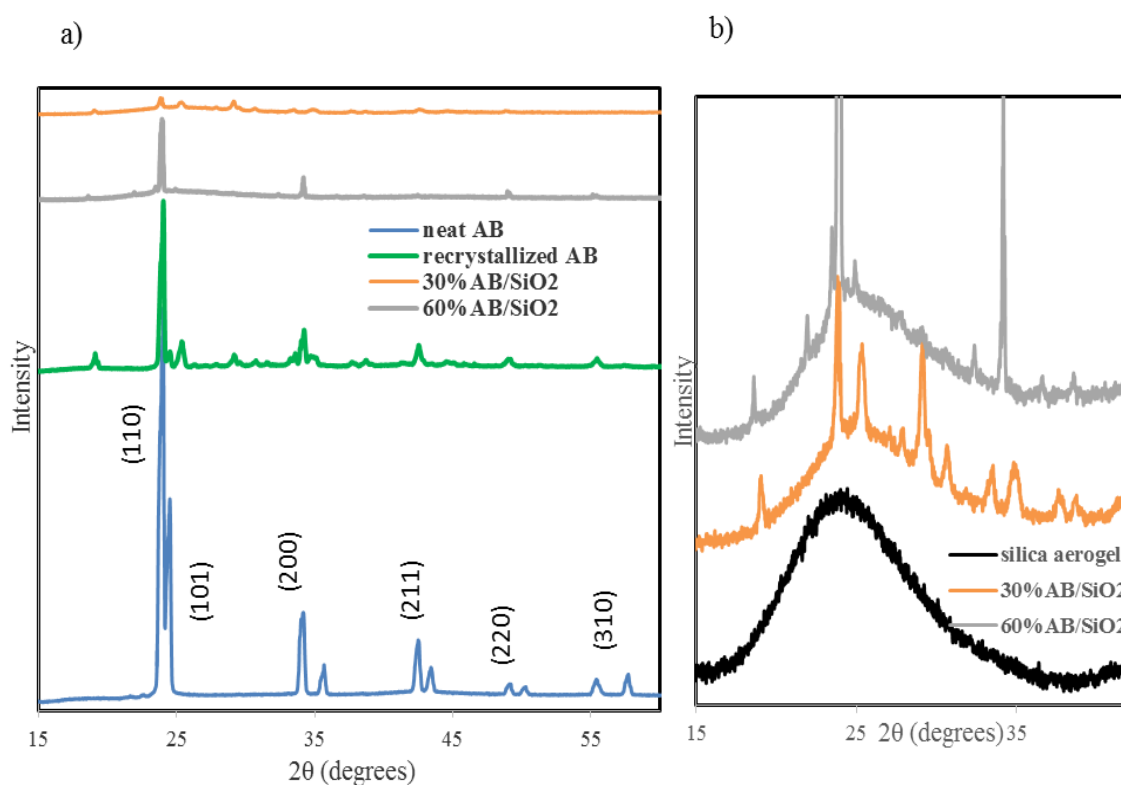


**Figure 6.** a) XRD of neat ammonia borane, recrystallized ammonia borane and AB loaded in silica aerogel with different concentrations b) Amplification of XRD signal showing the characteristic pattern of silica aerogel. Curves are vertically displaced for clarity

### 3.3 Thermal characterization of AB-loaded silica aerogels

Figure 7 shows the differential scanning calorimetry (DSC) traces of neat and recrystallized AB compared to samples in which the hydride is loaded in silica aerogel. In the case of the curve of neat AB, a sharp endothermic peak is observed whose onset temperature ( $T_{on}=108.5\text{ }^{\circ}\text{C}$ ) and peak temperature ( $T_p=110.8\text{ }^{\circ}\text{C}$ ) is dramatically reduced when AB is loaded in silica aerogel (see Table 2). This first peak is associated to the melting point [14] or the dissociation of the intermolecular hydrogen bonding [18]. The reduction or elimination in this first peak suggests that the degree of hydrogen bond in the samples in which AB is embedded in silica aerogel is decreased, favoring the reduction of the induction time. A similar result has been observed when AB was embedded in other silica supports [18]. Regarding recrystallized AB, DSC results also show reduction in the onset and peak endothermic temperatures, maintaining the shape of the curve of neat AB. In this case, variations in characteristic temperatures of the DSC traces can be associated to the reduction in the mean particle size achieved by recrystallization of AB. As described by Varin et al [45], a reduction of particle size into the submicrometric or nanometric scale is generally associated to a reduction of the onset and peak temperatures of hydrogen evolution thermal events, due to the destabilization of the material induced by the increased particle surface. Additionally, the reduction of onset temperatures and induction time can be associated to the formation of DADB by recrystallization suggested by XRD assays. Similar results have been obtained in other works where AB is confined in different supports. In the case of SBA and MCM silica supports, reductions in the onset and peak temperatures to  $48\text{ }^{\circ}\text{C}$  and  $100\text{ }^{\circ}\text{C}$  have been reported [18], but as previously described lower temperatures have been obtained in this work. This fact can be due to the higher volume of pores of aerogel support that avoids the agglomeration of AB in meso-channels. Therefore higher contact between the particle and the surface of the silica aerogel takes place, enhancing the influence of silica surface groups on the decomposition mechanism. In experiments with MOFs [42] or carbon cryogels [17, 20] as supports, similar modifications in the thermal response of the material have been reported. However, Srinivas et al. [16] observed a reduction of  $30\text{ }^{\circ}\text{C}$  in the onset and peak temperatures of decomposition using MOFs, whereas in our case a displacement of almost  $70\text{ }^{\circ}\text{C}$  is obtained.

Moreover, DSC results indicate a reduction of the exothermic enthalpy associated with hydrogen release as the proportion silica/AB is increased. The measured enthalpy of reaction for  $\text{H}_2$  release from neat AB is  $-24.9\text{ kJ/mol AB}$ , which is in good agreement with results reported in literature. However, when the proportion silica/AB is increased, the corresponding enthalpy of reaction changes to  $-10.9\text{ kJ/mol AB}$  for the sample with 60 wt% of AB, and  $-5.5\text{ kJ/mol AB}$  for the sample with 30 wt% of AB. A reduction of the enthalpy of reaction for  $\text{H}_2$

release from AB was also observed by Gutowska et al. [40] in their studies of incorporation of AB in mesoporous SBA-15 silica scaffold. However, these authors report a more drastic variation of the enthalpy to  $-1.0$  kJ/mol AB. These authors indicate that the reason for the reduced exothermicity is the suppression of the formation of boron compounds as byproducts of the PAB that is the main decomposition product of AB according to reaction 1, which had the favorable consequence of reducing the production of gaseous byproducts.

Sample	$T_{on1}$ (°C)	$T_{p1}$ (°C)	$T_{on2}$ (°C)	$T_{p2}$ (°C)	Total wt loss per wt AB
Neat AB	108.5	110.8	113.9	114.1	40.2
Recrystallized AB	70.5	77.9	102.4	113.4	-
60% AB/SiO <sub>2</sub>	37.6	62.3	84.8	108.9	33.0
30% AB/SiO <sub>2</sub>	39.5	68.7	83.1	99.0	-

**Table 2.** Temperature data and weight losses of neat and recrystallized AB vs loaded in silica aerogel with different concentration obtained from DSC and TGA analyses respectively

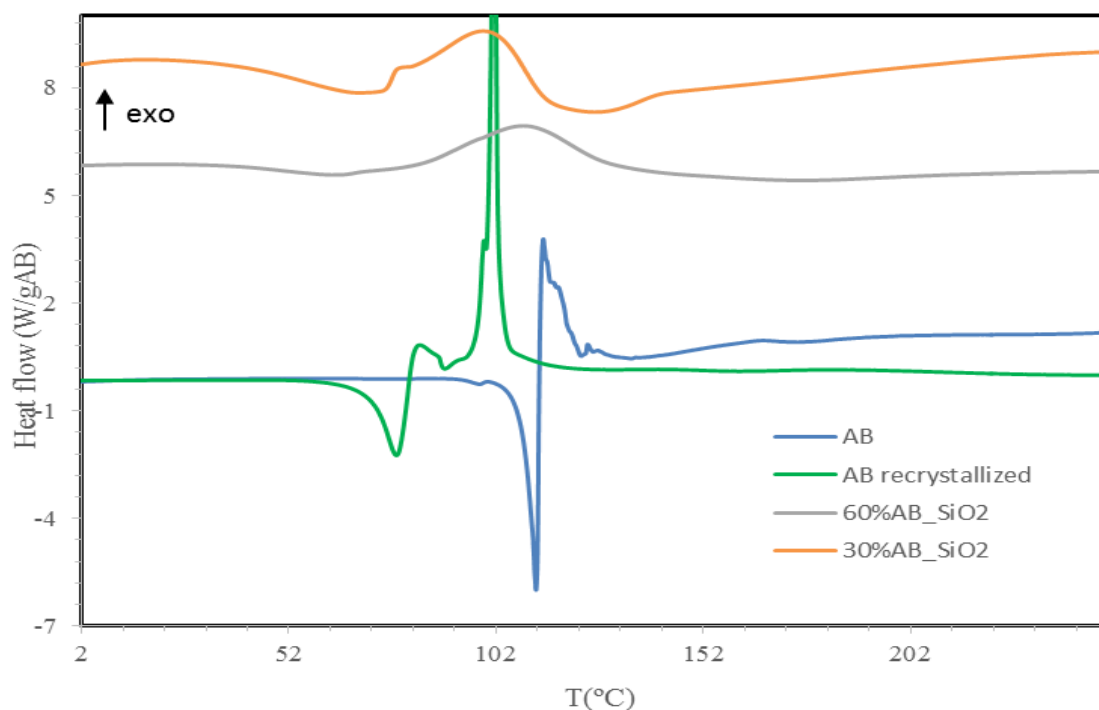


**Figure 7.** DSC curves of AB and AB loaded in silica aerogel with different concentration. The curves are normalized according to the weight of AB, and vertically displaced for clarity

This hypothesis agrees well with the results obtained in this work by TGA assays. Figure 8 shows the results of TGA analysis performed on neat AB and AB-loaded silica aerogel. In the case of neat AB, two important weight loss steps, which correspond to the decomposition of the hydride, are observed: the first one till 129 °C corresponds to a weight loss of 12.7 wt% and the second one, which finishes at 213 °C, corresponds to a weight loss of 27.5 wt%. In comparison, and in agreement with the results of DSC assays, TGA analysis shows that the AB confined in silica aerogel initiates its decomposition at lower temperatures. It is also noticeable that in this case, weight loss is not confined to sharp steps at defined temperatures, but it proceeds continuously over the temperature range studied. In particular, at temperatures above 200 °C, where as previously discussed neat AB does not experience any additional weight losses, a continuous weight loss is still observed in the case of AB confined in aerogel. This result indicates that the third step of the thermal decomposition mechanism, indicated in reaction (3), also begins at lower temperatures in the case of confined AB compared to neat AB. Moreover, as shown in Table 2, in both cases the total weight loss per unit mass of AB in the sample is significantly larger than the maximum amount of hydrogen that can be stored in the compound. Similar results have been reported in [18], suggesting that when AB is heated to high temperatures above 200 °C, other gases apart from hydrogen are produced, as borazine, diborane, ammonia, etc. However, analyzing the results reported in Table 2, it is noticeable that the total amount of volatile compounds produced by heating up to 300 °C is reduced when AB is confined in silica aerogel. This result, together with the variations in DSC assays of confined AB presented before, suggest that interactions between AB and the silica support are taking place that influence the decomposition mechanism of AB. Such interactions were suggested to happen between AB and hydroxyl groups from the silica surface of the host by Lai et al. [18]. These groups can interact with the BH<sub>3</sub> group, loosening the covalent bond between BH<sub>3</sub> and NH<sub>3</sub> groups of AB, thus destabilizing and promoting the decomposition of the compound. Furthermore, by this interaction BH<sub>3</sub> is kept bound to the scaffold reducing the production of borazine and precluding the formation of polyimino-borane.

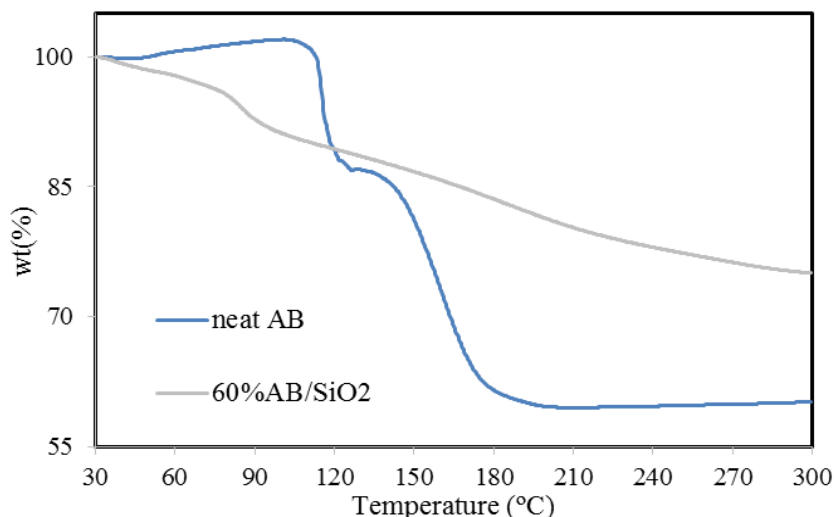


**Figure 8.** TGA curves of AB and AB loaded in silica aerogel

In Figure 9, FTIR of neat AB and AB loaded in silica aerogel is shown before and after dehydrogenation at 80 °C. It is observed that most of the peaks at frequencies related to N-H and B-H bonds are broadened, shifted and decreased of intensity which indicates the disruption of the bonds due to the release of hydrogen [13] in both samples. The same behavior is observed for all the concentrations of AB loaded in silica aerogel, although it is more pronounced at higher concentrations of AB. B-N band in the range 700-900  $\text{cm}^{-1}$ , which is observed in all the samples, is weakened but is still detected after dehydrogenation; this fact clarifies that B-N is not disrupted and ammonia formation is avoided during the decomposition [14]. On the other hand, in the sample in which AB is loaded, the bonds related to silica are present without any change after thermal treatment due to its stability at these conditions.

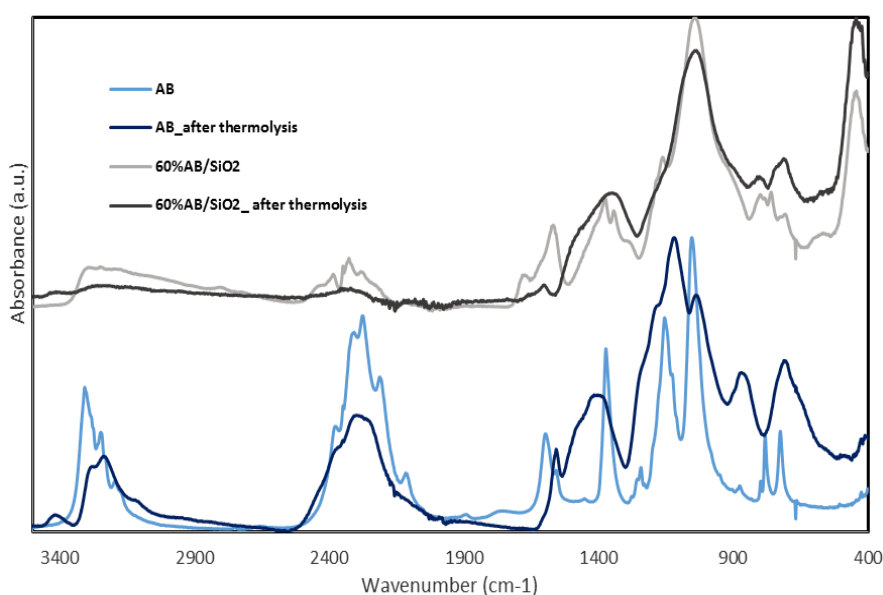


**Figure 9.** FTIR spectra of neat AB and AB loaded in silica aerogel before and after thermolysis dehydrogenation at 80 °C. Curves are vertically displaced for clarity

Regarding the crystallinity of the samples after thermal dehydrogenation, Figure 10 shows XRD analyses of byproduct after isothermal dehydrogenation at 80 °C. According to ICDD 00-019-0418,  $2\theta = 20.1^\circ$ ,  $23.6^\circ$  and  $41.1^\circ$  are assigned to amorphous PAB ( $\text{NH}_2\text{BH}_2$ )<sub>5</sub> [46]. In the case of AB/SiO<sub>2</sub> samples, amorphous silica peak is present apart from amorphous PAB byproduct.

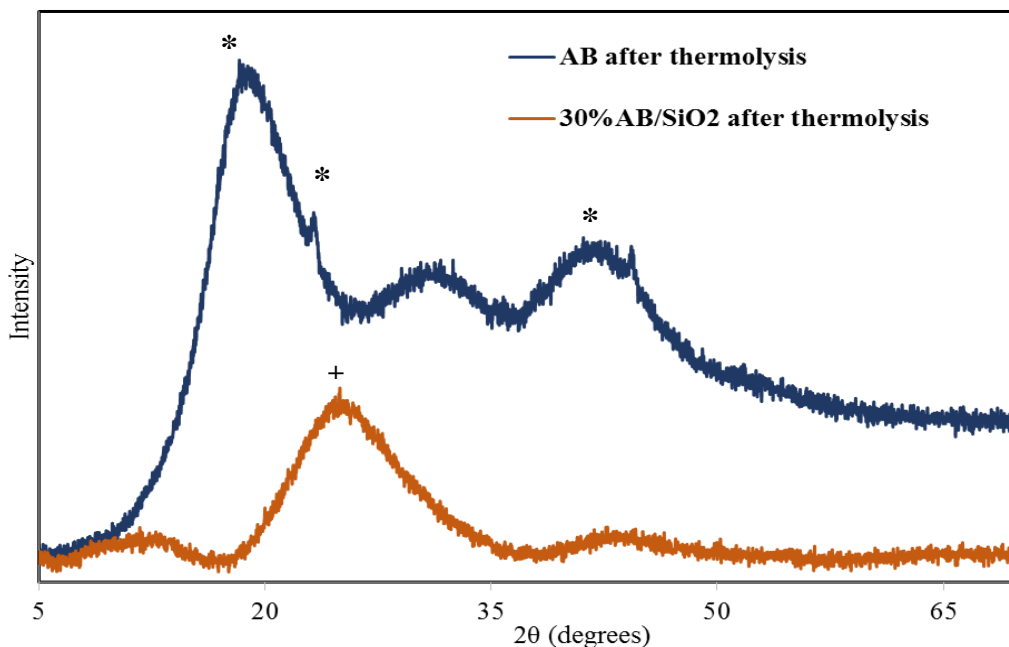


**Figure 10.** XRD of neat AB and AB loaded in silica aerogel after thermolysis dehydrogenation at 80 °C. \* indicates the peaks related to polyaminoborane (PAB) and + refers to amorphous silica peak

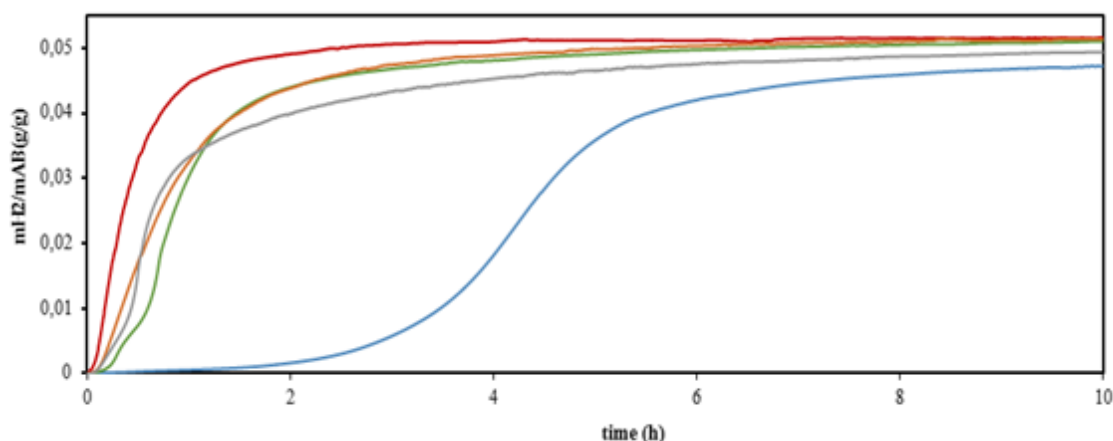
### 3.4 Kinetics of hydrogen release by thermolysis at 80 °C

Figure 11 shows the kinetics of hydrogen release by thermolysis at 80 °C of neat AB compared with AB confinement in silica aerogel. Results in this figure are normalized reporting the amount of hydrogen released by unit mass of AB in the sample. Due to the design of the cell used to measure kinetics, it was not possible to analyze samples of the gas evolved during thermolysis. However, it is assumed that at this temperature, the gas which is released is H<sub>2</sub> [12, 19, 41, 47] and no other volatile gases are present in the gas stream in neat AB nor confined in silica aerogel. Regarding the shape of the curve in neat AB, it follows a sigmoidal kinetic, typical of nucleation and growth pathway, with a long induction time of more than 2 h, as reported in previous works [48]. After confinement in silica, the induction time is reduced significantly. This means that the silica could act as a catalyst (SiOH groups) [40] creating defect sites in the support that initiate the decomposition at lower temperature. On the other hand, at lower concentration of AB in the solution (prior to the drying), the hydride could precipitate in the pores of the silica with lower mean size as was also suggested with XRD analyses and corroborated in BET results. This suggests that smaller particles have more contact with the

surface of the silica and an easier way to form different bonds between the two free pair of electrons of O in the Lewis base of Si-O-Si or Si-OH bond from the silica with BH<sub>3</sub> or NH<sub>3</sub> from AB. As result, the intermolecular hydrogen bond is reduced, following the mechanism proposed by Lai et al. [18].

In the case of neat AB, 2 hours are needed to start releasing H<sub>2</sub>, and more than 4 hours to get half of its content in H<sub>2</sub> at this temperature (0.025 gH<sub>2</sub>/gAB) whereas only it takes 22 minutes in the case of 13 wt% AB loaded in silica aerogel. This fact shows the improvement of silica aerogel as support for this chemical hydride system.

Regarding to recrystallized sample, it can be observed that the release profile maintains the sigmoidal shape characteristic of neat AB, with a slower hydrogen release than samples loaded in silica aerogel during the first 30 min of thermolysis. However, compared with neat AB, with the particle size reduction achieved by GAS recrystallization the induction time is drastically reduced and the release of hydrogen is accelerated, to the point that after one hour an equivalent amount of hydrogen is released from GAS-recrystallized AB as from AB loaded silica aerogel with a 30 wt% of AB.



**Figure 11.** Isothermal kinetic of hydrogen releases from AB and AB loaded in silica aerogel with different concentrations at 80 °C. The curves are normalized according to the amount of AB in the sample

As a complement to Figure 11, Table 3 presents the total hydrogen release per unit mass of solid product (AB + silica aerogel support). Results in this table clearly indicate the weight penalty caused by the use of silica aerogel as porous host, as this material does not contribute to the hydrogen storage capacity, thus reducing the total gravimetric capacity of the material [27]. However, it can be seen that this disadvantage is counterbalanced by a faster hydrogen release during the first 1-2 h of thermolysis.

	15 min	30 min	45 min	1 h	2 h	final
Sample	mgH <sub>2</sub> /gtotal					
neat AB	0	0	0	0	2	52
AB recrystallized	1,66	7,45	20,19	30,45	43,98	52
13%AB/SiO <sub>2</sub>	2,26	4,28	5,28	5,80	6,38	6,76
30%AB/SiO <sub>2</sub>	1,69	4,43	7,30	9,07	12,31	14,56
60%AB/SiO <sub>2</sub>	2,48	9,42	17,79	20,65	27,27	32,24

**Table 3.** Amount of H<sub>2</sub> released at different times by isothermal thermolysis at 80 °C in neat and recrystallized vs. AB loaded in silica aerogel with different concentration

Moreover, there is a significant visual change in the morphology of neat AB in contrast to AB encapsulated in silica aerogel. Figure 12 shows the different result of AB after thermal decomposition at 80 °C. In the case of neat AB, foaming process takes place at the same time that H<sub>2</sub> is released from the hydride. Thus, even if the material was micronized before thermolysis, this morphology and its associated advantages are completely lost during the thermolysis and therefore in possible future hydrogen cycles, if the material is regenerated [49]. However, when AB is encapsulated in silica aerogel, this process is avoided obtaining particles with the same physical appearance. To confirm this observation, Figure 13 presents SEM/EDX micrographs of the 60%AB/SiO<sub>2</sub> sample after thermolysis. As shown in this figure, the original morphology of the material is preserved after the thermolysis. Furthermore, as indicated by the results of nitrogen mapping, the decomposition products of AB remain homogeneously dispersed within the SiO<sub>2</sub> aerogel matrix. Therefore it can be concluded that by incorporation of AB inside the aerogel the morphological variations of the material due to foaming are avoided.

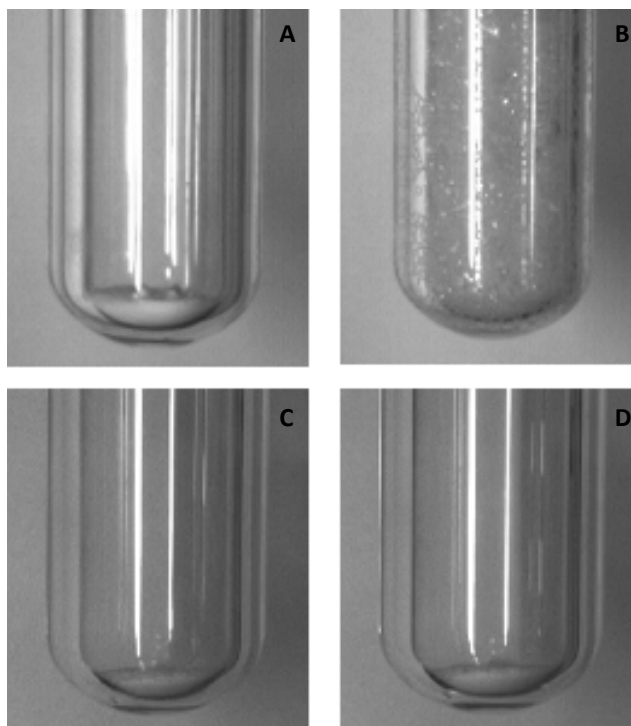


**Figure 12.** Photographs of neat AB and 60 wt% AB/SiO<sub>2</sub> before and after the isothermal H<sub>2</sub> release by thermolysis at 80 °C a) neat AB before thermolysis, b) neat AB after thermolysis, c) AB/SiO<sub>2</sub> before thermolysis, d) AB-SiO<sub>2</sub> after thermolysis.

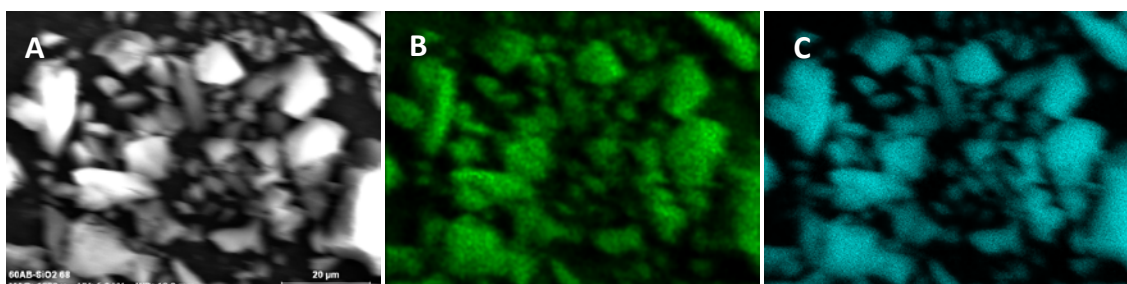


**Figure 13.** SEM image of 60 wt% AB/SiO<sub>2</sub> sample after thermolysis (A), with results of N (B) and Si (C) mapping.

#### 4. CONCLUSIONS

Ammonia Borane has been recrystallized and nanoconfined inside the pores of silica aerogel by a novel process, based on a simultaneous aerogel drying and ammonia borane gas antisolvent precipitation using compressed carbon dioxide. Due to the favorable textural properties of the aerogel materials obtained with this method, it has been possible to load aerogels with up to 60 wt% of ammonia borane, without blocking of pores and with a homogeneous dispersion of ammonia borane within the aerogel. By analysis of the thermolysis process, it has been observed that by nanoconfinement the temperature required to initiate the thermolysis process is reduced and the release kinetics are accelerated as they do not

show induction time. Furthermore, by nanoconfinement of AB, the morphological properties of the material are stabilized and foaming is eliminated, which could be favorable properties for a subsequent material regeneration process. The feasibility of implementation of the multi-step chemical process required to re-hydrogenate AB when this compound is embedded in the silica matrix remains to be tested.

**REFERENCES**

- [1] M. Balat, *Int. J. Hydrogen Energ.* 33 (2008) 4013-4029
- [2] M. Hook, X. Tang, *Energ. Policy* 52 (2013) 797-809
- [3] S. A. Sherif, F. Barbir, T. N. Veziroglu, *Electricity J.* 18 (2005) 62-76
- [4] J. Graetz, *Chem. Soc. Rev.* 38 (2009) 73-82
- [5] DOE: US Department of Energy. Web site: <http://www.doe.gov>.
- [6] L. O. Williams, D. E. Spond, *Appl. Energ.* 6 (1980) 99-112.
- [7] H. P. Veluswamy, R. Kumar, P. Linga, *Appl. Energ.* 122 (2014) 112-132.
- [8] M. Paik Suh, H. J. Park, T. K. Prasad, D. Lim, *Chem. Rev.* 112 (2012) 782-835
- [9] B. Sakintuna, F. Lamari-Darkrim, M. Hirscher, *Int. J. Hydrogen Energ.* 32 (2007) 1121-1140
- [10] B. Peng, J. Chen, *Energ. Environ. Sci.* 1 (2008) 479-483
- [11] S. D. Rassat, C. L. Aardahl, T. Autrey, R. S. Smith, *Energ. Fuel.* 24 (2010) 2596-2606
- [12] G. Wolf, J. Baumann, F. Baitalow, F. P. Hoffmann, *Thermochim. Acta* 343 (2000) 19-25
- [13] D. Kumar, H. A. Mangalvedekar, S. K. Mahajan, *Mater. Renew. Sustain. Energy* 3 (2014) 23
- [14] A. C. Gangal, P. Kale, R. Edla, J. Manna, P. Sharma, *Int. J. Hydrogen Energ.* 37 (2012) 6741-6748
- [15] B. Roy, J. Manna, P. Sharma, *J. Alloy Compd.* 645 (2015) S234-S238.
- [16] G. Srinivas, J. Ford, W. Zhou, T. Yildirim, *Int. J. Hydrogen Energ.* 37 (2012) 3633-3638
- [17] A. Feaver, S. Sepehri, P. Shamberger, A. Stowe, T. Autrey, G. Cao, *J. Phys. Chem. B* 111, (2007) 7469-7472
- [18] S-W Lai, H-L. Lin, T.L.Yu, L-P. Lee, B-J. Weng, *Int. J. Hydrogen Energ.* 37 (2012) 14393-14404
- [19] T. Autrey, A. Gutowska, L. Li, J. Linehan, M. Gutowski, *Preprints of Papers- American Chemical Society, Division of Fuel Chemistry* 49 (2004) 150-151
- [20] S. Sepehri, B. B. Garcia, G. Cao, *J. Mater. Chem.* 18 (2008) 4034-
- [21] S. Sepehri, A. Feaver, W. J. Shaw, C. J. Howard, Q. Zhang, T. Autrey, G. Cao, *J. Phys. Chem. B* 111 (2007) 14285-14289
- [22] R. K. Ahluwalia, J. K. Peng, T. Q. Hua, *Int. J. Hydrogen Energ.* 36 (2011) 15689-15697

- [23] M. J. Valero-Pedraza, A. Martín-Cortés, A. Navarrete, M. D. Bermejo, Á. Martín. Kinetics of hydrogen release from dissolutions of ammonia borane in different ionic liquids. *Energy* 91 (2015) 742-750.
- [24] S.F.Li, Z.W.Tang, Y.B.Tan, X.B.Yu, *J. Phys. Chem. C* 116 (2012) 1544-1549
- [25] L-Q Wang, A.Karkamkar, T.Autrey, G.J.Exarhos, *J. Phys. Chem. C* 113 (2009) 6485-6490
- [26] M.Rueda, L.M.Sanz-Moral, A. Nieto-Márquez, P.Longone, F.Mattea, A.Martín, *J. Supercrit. Fluids* 92 (2014) 299-310
- [27] T. Nielsen, F.Besenbacher, T.R.Jensen, *Nanoscale* 3, (2011) 2086-2098
- [28] A.S. Dorcheh, M. H. Abbasi., *J. Mater. Process. Tech.* 199 (2008) 10-26
- [29] E. Reverchon, R.Adami, G.Caputo, I. de Marco, *J. Supercrit. Fluids* 47 (2008) 70-84
- [30] M.Rueda, L.M Sanz-Moral, A.Martín, *Cryst. Growth Des.* 14 (2014) 4768-4776
- [31] J. W. Leachman, R. T. Jacobsen, S. G. Penoncello, E. W. Lemmon, *J. Phys. Chem. Ref. Data* 38 (2009) 721-748.
- [32] E. W. Lemmon, M. L. Huber, M. O. McLinden. NIST Standard Reference Database 23: Reference Fluid Thermodynamic and Transport Properties-REFPROP, Version 9.1, National Institute of Standards and Technology, Standard Reference Data Program, Gaithersburg, 2013.
- [33] M.R.Weismiller, S.Q.Wang, A.Chowdhury, S.T.Thynell, R.A.Yetter, *Thermochim. Acta* 551 (2013) 110-117
- [34] F.Leardini, M.J.Valero-Pedraza, E.Perez\_Mayoral, R.Centelli, M.A.Bañares, *J. Phys. Chem.C* 118 (2014) 17221-17230
- [35] J.Smith, K.S.Seshadri, D.White, *J. Mol. Spectrosc.* 45, (1973) 327-337
- [36] R.Al-Oweini, H. El-Rassy, *J. Mol. Struct.* 919 (2009) 140-145
- [37] M.Alnaief, I.Smirnova, *J. Supercrit. Fluids* 55 (2011) 1118-1123
- [38] S.Smitha, P.Shaiesh, P.R.Aravind, S.R.Kumar, *Micropor. Mesopor. Mat.* 91 (2006) 286-292
- [39] W-J Son, J-S Choi, W-S Ahn, *Micropor. Mesopor. Mat* 113 (2008) 31-40
- [40] A.Gutowska, L.Li, Y.Shin, C.M.Wang, X.S.Li, J.C.Linehan, R.S.Smith, B.D.Kay, B.Schmid, W.Shaw, M.Gutowski, T.Autrey, *Angewa. Chem. Int. Ed.* 44 (2005) 3578-3582
- [41] Z.Li, G.Zhu, G.Lu, S.Qiu, X.Yao, *J. Am. Chem. Soc.* 132 (2010) 1490-1491

- [42] A.Paolone, O.Palumbo, P.Rispoli, R.Cantelli, T.Autrey, *J. Phys. Chem. C* 113 (2009) 5872-5878
- [43] Z. Fang, J. Luo, X. Kang, H. Xia, S. Wang, W. Wen., X. Zhou, P. Wang, *Phys. Chem. Chem. Phys.* 13 (2011) 7508-7513.
- [44] H.Kim, A.Karkamkar, T.Autrey, P.Chupas, T.Proffen, *J. Am. Chem. Soc.* 131 (2009) 13749-13755
- [45] R. A. Varin, T. Czujko, Z. S. Wronski. *Nanomaterials for Solid State Hydrogen Storage*, Springer, New York, 2009.
- [46] U.B.Demirci, S.Bernard, R:Chiriac, F.Toche, P.Miele, *J. Power Sources* 196 (2011) 279-286
- [47] F.Baitalow, J.Baumann, G.Wolf, K.Jaenicke-Robler, G.Leitner, *Thermochim. Acta* 391 (2002) 159-168
- [48] A.C.Stowe, W.J.Shaw, J.C.Linehan, B.Schmid, T.Autrey, *Phys. Chem. Chem. Phys.* 9 (2007) 1831-1836
- [49] A.D.Sutton, A.K.Burrel, D.A.Dixon, E.B.Garner, J.C.Gordon, T.Nakagawa, K.C.Ott, J.P.Robinson, M.Vasiliu, *Science* 331 (2011) 1426-1429

# **CHAPTER 5**

**Reversible hydrogen sorption in the  
composite made of Magnesium  
Borohydride and silica aerogel**



## Reversible Hydrogen Sorption in the Composite made of Magnesium Borohydride and Silica Aerogel<sup>1</sup>

### Abstract

Magnesium borohydride  $\text{Mg}(\text{BH}_4)_2$  is a promising hydrogen storage material as it releases high hydrogen amount at mild desorption temperatures, but it is still limited by slow dehydrogenation kinetics and harsh conditions are required for rehydrogenation. In this work, composites made of commercial  $\text{Mg}(\text{BH}_4)_2$  and synthesized silica aerogel microparticles were prepared by thermal treatment under 120 bar of hydrogen and 200 °C. As a result, the sorption properties of the hydride are improved: calorimetric measurements show that the decomposition temperature is reduced by 60 °C, and the typical 3-steps decomposition mechanism of  $\text{Mg}(\text{BH}_4)_2$  changes to a single-step mechanism in range of 220-400 °C. The kinetics of the first dehydrogenation at 300 °C was two times faster in  $\text{Mg}(\text{BH}_4)_2\text{-SiO}_2$  composites than in the case of bulk  $\gamma\text{-Mg}(\text{BH}_4)_2$ . Additionally, the rehydrogenation of this material at comparatively moderate conditions of 390 °C and 110 bar of  $\text{H}_2$  is presented for the first time, achieving cyclability with a reversible release of hydrogen up to 6 wt%  $\text{H}_2$ . Different amounts of hydrogen were exchanged depending on the working temperature (300 °C or 400 °C) and the presence or absence of silica aerogel. This result indicates that silica aerogel influence the performance of  $\text{Mg}(\text{BH}_4)_2$ , acting as an additive, which can result in different hydrogenation-dehydrogenation routes in which different amounts and types of intermediates are formed, influencing the kinetics and reversibility.

**Keywords:** *hydrogen storage, magnesium borohydride, additive, kinetics, reversibility*

<sup>1</sup> International Journal of Hydrogen 41 (2016) 15245-15253

## 1. INTRODUCTION

Hydrogen society, which is related to the use of hydrogen as an energy vector, could be a solution to current environmental and economic problems associated to the use of fossil fuels [1][2]. Due to the low density of hydrogen gas, an important challenge for onboard applications is the search of an effective technology to reversibly store hydrogen in a compact system [3].

Among currently studied solid state hydrogen storage materials, complex metal hydrides, such as  $\text{LiBH}_4$  [4] or  $\text{NaAlH}_4$  [5], are very attractive due to their high hydrogen storage capacity, but they are limited by their kinetics and thermodynamics. In this work, magnesium borohydride  $\text{Mg}(\text{BH}_4)_2$  is also considered as effective storage material due to its high gravimetric (14.8 wt%  $\text{H}_2$ ) and volumetric capacity (0.112 kg/L) [6], which exceeds the ultimate targets from Department of Energy (DoE) for 2020. Because of these outstanding properties, it could be also of interest in batteries applications, since Mg metal holds better volumetric capacity and is more abundant than Li. Battery-related applications of this complex hydride has been recently reviewed in [7].

Moreover,  $\text{Mg}(\text{BH}_4)_2$  starts the decomposition at 270 °C, and although this decomposition temperature still is too high, it is lower than the decomposition temperature of similar alternative compounds. However, due to the formation of stable intermediates [6], rehydrogenation still remains as the main challenge for the use of  $\text{Mg}(\text{BH}_4)_2$  or its composites.

High conditions of pressure and temperature are necessary in order to obtain a complete conversion grade to  $\text{Mg}(\text{BH}_4)_2$  from decomposed products. Reversibility of 11 wt% of hydrogen [8] was experimentally shown starting from  $\text{MgB}_2$  to  $\text{Mg}(\text{BH}_4)_2$  at 950 bar  $\text{H}_2$  and 400 °C during 108 hours. In another work of Newhouse et al. [9],  $\text{MgB}_2$  obtained after thermal decomposition at 600 °C was partially rehydrogenated, getting 9.7 wt%  $\text{H}_2$  by treatment at similar conditions of pressure and temperature (900 bar  $\text{H}_2$  and 390 °C) for 3 days. Li et al. [10][11] reported 6.1 wt %  $\text{H}_2$  absorbed after rehydrogenation at 400 bar  $\text{H}_2$  and 270 °C for 48 h through the formation of the stable  $\text{MgB}_{12}\text{H}_{12}$  intermediate. However, when mild pressure and temperature conditions (134 bar  $\text{H}_2$  and ~300 °C) were used during rehydrogenation, only 2.7-3.1 wt%  $\text{H}_2$  [6] or 3.5 wt%  $\text{H}_2$  [12] was achieved which most probably corresponded to the formation of  $\text{MgH}_2$ . Also in [13] a triborane  $\text{Mg}(\text{B}_3\text{H}_8)_2$  in addition to  $\text{MgH}_2$  was experimentally found after dehydrogenation of  $\text{Mg}(\text{BH}_4)_2$  at 200 °C for 5 weeks and around 2.5 wt%  $\text{H}_2$  was rehydrogenated at 250 °C and 120 bar for 48 hours. In a recent work [14], the rehydrogenation was performed at similar conditions of 280 °C and 120 bar  $\text{H}_2$  for 14 hours, reabsorbing only

2.5 wt% H<sub>2</sub> suggesting the formation of two Mg-B-H phases during desorption, only one of which being reversible and could explain the limited absorption. The other intermediate compound could be too stable and prevent the complete rehydrogenation.

Different strategies have been tested in order to improve not only the reversibility but also the kinetics and to decrease temperature of the desorption reactions [15]. The addition of different additives or catalysts such as NbF<sub>5</sub>, TiO<sub>2</sub>, CoCl<sub>2</sub>, CoF<sub>2</sub> or TiCl<sub>3</sub> among others [14-15][18][19], the confinement in porous materials (mainly in carbon materials) [20–22], their combinations [23] or the formation of composites [24] are some of the proposals that have been studied.

Fitchner et al. [21], successfully confined around 44 wt% of the hydride in activated carbon (BET area of 860 m<sup>2</sup>/g and pore volume of 0.61 g/cm<sup>3</sup>) using wet impregnation as method and diethyl ether as solvent. As a result, a composite with lower decomposition temperature and lower activation energy was obtained. Wahab et al. [23] infiltrated 45 wt% of Mg(BH<sub>4</sub>)<sub>2</sub> in ordered mesoporous carbon CMK-3 scaffold (BET area of 1499 m<sup>2</sup>/g and a volume of pores of 1.63 cm<sup>3</sup>/g) with addition of 5 wt% of Ni. In this case, a lowering of 200 °C in the decomposition temperature was obtained and kinetics of hydrogen release were 10 times faster compared to the bulk Mg(BH<sub>4</sub>)<sub>2</sub> due to the synergic effect of nanoconfinement and of the addition of the Ni catalyst.

Since decomposition tends to occur before melting point, melt infiltration is not a suitable approach for nanoconfinement in this case [20][25]. The only possibility is to confine MgH<sub>2</sub> in a support via melt infiltration and then treat the composite with B<sub>2</sub>H<sub>6</sub> in order to obtain Mg(BH<sub>4</sub>)<sub>2</sub> infiltrated in the matrix [22].

In the case that composites are formed [24], 3.6 wt% H<sub>2</sub> was reabsorbed in 1 h at 90 bar of hydrogen, after 12 h of decomposition process at 180 °C for 20 cycles due to the formation of polyborane intermediates which could transform to [BH<sub>4</sub>]<sup>-</sup>, and make the whole system reversible under mild conditions.

In this work, we report the experimental trial to confine Mg(BH<sub>4</sub>)<sub>2</sub> in microparticles of silica aerogel by heat treatment in hydrogen atmosphere. Microparticles of silica aerogel, which were used for the first time with this complex hydride, have been produced by supercritical CO<sub>2</sub> drying, a technique that enables to produce a material with outstanding surface properties. The employed drying method is a key aspect that determines the textural properties of this porous host. If the solvent is removed by evaporation or lyophilization, the capillary stresses associated to the formation of vapor-liquid interfaces inside the pores of the

support are responsible of partial collapses of the pore structure of the material. In case of SiO<sub>2</sub> matrixes, the materials obtained by these drying methods usually show pore volumes below 0.5 – 1.0 cm<sup>3</sup>/g, such as SBA-15 or MCM-41 mesoporous silica. In contrast, if pressurized or supercritical carbon dioxide is used to extract the solvent, the collapse of the pore structure is avoided or minimized, because under these conditions carbon dioxide is completely miscible with the organic solvent, and therefore the extraction proceeds without formation of gas-liquid interfaces[26] and without capillary stresses, thus resulting in pore volumes up to 4 cm<sup>3</sup>/g [27].

The prepared Mg(BH<sub>4</sub>)<sub>2</sub>-SiO<sub>2</sub> composites were characterized by SEM, XRPD and coupled calorimetric-manometric technics. Their kinetic curves were obtained during several hydrogen desorption-absorption cycles and compared to those of the bulk γ-Mg(BH<sub>4</sub>)<sub>2</sub>.

## 2. EXPERIMENTAL METHODS

### 2.1 Reactants

The commercial γ-Mg(BH<sub>4</sub>)<sub>2</sub> powder (Sigma Aldrich, 95%), thereafter referred to as MBH, was constituted by prismatic particles of around 100 μm (see SEM images reported in Section 3).

Tetramethylorthosilicate (TMOS, 98.0% purity) and ammonium hydroxide (NH<sub>4</sub>OH, 28.0-30.0% ammonia) were supplied by Sigma-Aldrich. Methanol (MeOH; 99.8%) and n-hexane (95%) were purchased from Panreac. Gaseous Carbon dioxide (CO<sub>2</sub>, 99.95%) was supplied by Carbueros Metálicos S.A. These reactants are necessary to obtain microparticles of silica aerogel.

Microparticles of silica aerogel were synthesized using a batch supercritical equipment as drying method as reported in a previous work [28]. They were prepared by sol-gel reaction, using TMOS as precursor and methanol as solvent. While with this procedure it is common to prepare large gel monoliths, in this work the gel was synthesized as microparticles, in order to reduce the possible heat and mass transfer resistances that could be caused by larger aerogel monoliths. To do this, the sol-gel reaction media were dispersed in hexane under mechanical stirring, in order to obtain small droplets of TMOS in methanol dispersed within the hexane continuous phase. After 10 minutes of mechanical stirring of this mixture, an aqueous solution of NH<sub>4</sub>OH was added as condensation catalyst, which induced the gelation of TMOS. The molar ratio used was the following: 1 mol TMOS: 4.4 mol MeOH: 3.3 mol H<sub>2</sub>O: 4.5 mol hexane: 0.08 mol NH<sub>4</sub>OH. Gel particles were then kept in a closed vessel immersed in methanol for an aging period of at least 4 days. During this time, the methanol was renewed 2-3 times in order to

remove the water content of the solution. After this time, microparticles of alcogel immersed in methanol were dried using supercritical CO<sub>2</sub> at 110 bar and 40 °C, employing supercritical drying apparatus described in a previous work [28]. For this, the system was slowly pressurized and depressurized at a rate of 3 bar/min in order to avoid the cracking of the alcogel/aerogel and mechanical stresses that could damage the structural properties of the final product. Saturated CO<sub>2</sub> in the system was renewed four times in order to obtain completely dried particles. Dried silica aerogel microparticles had a porous structure with surface area of 723 m<sup>2</sup>/g and a pore volume of 1.35 cm<sup>3</sup>/g (mean pore size =7.5 nm) [29]. Obtained SiO<sub>2</sub> aerogel particles were collected and stored in a closed vial at room temperature until used for MBH–SiO<sub>2</sub> composite preparation.

### 2.2 The MBH-SiO<sub>2</sub> preparation and characterization

All handling and preparation of the samples took place in a MBRAUN Unilab glove box which continuously purified argon atmosphere where oxygen and moisture values were kept below 1 ppm.

Commercial  $\gamma$ -MBH and silica aerogel particles were treated via a pressure-temperature method. First, SiO<sub>2</sub> aerogel was heated at 5 °C/min in a alumina boat placed in a tubular oven at 110 °C in the Ar glove-box for 2 hours in order to remove moisture adsorbed by the aerogel from the air. Subsequently, MBH and silica aerogel particles were mixed in a mortar with a mass ratio of 1:1. Around 200 mg of the mixture were introduced in a high pressure stainless steel sample holder under Ar atmosphere in the glove box and then transferred to the Sievert type apparatus (PCT-Pro 2000, Setaram and Hy-Energy), whose experimental set-up is schematically shown in Figure 1. The sample was treated at 120 bar H<sub>2</sub> and 200 °C for 3 hour in order to obtain a composite in which after phase transformation [6] the irreversible  $\beta$ -phase of MBH, can be coated by SiO<sub>2</sub>.

Kinetic measurements and the study of reversibility were done in the same Sievert type apparatus. The prepared MBH–SiO<sub>2</sub> composite was dehydrogenated and rehydrogenated for 3 cycles in the same high pressure cell. Hydrogen desorption was tested both at 300 and 400 °C both in static vacuum while rehydrogenation was done at 390 °C under 110 bar H<sub>2</sub>. The same conditions were used for bulk  $\gamma$ -MBH in order to compare its reversibility and cyclability with those of the prepared composites.

The gases evolved from the sample during dehydrogenation were analyzed in a residual gas analyzer (RGA Pro, Setaram & Hy-Energy) connected to the manometric instrument.

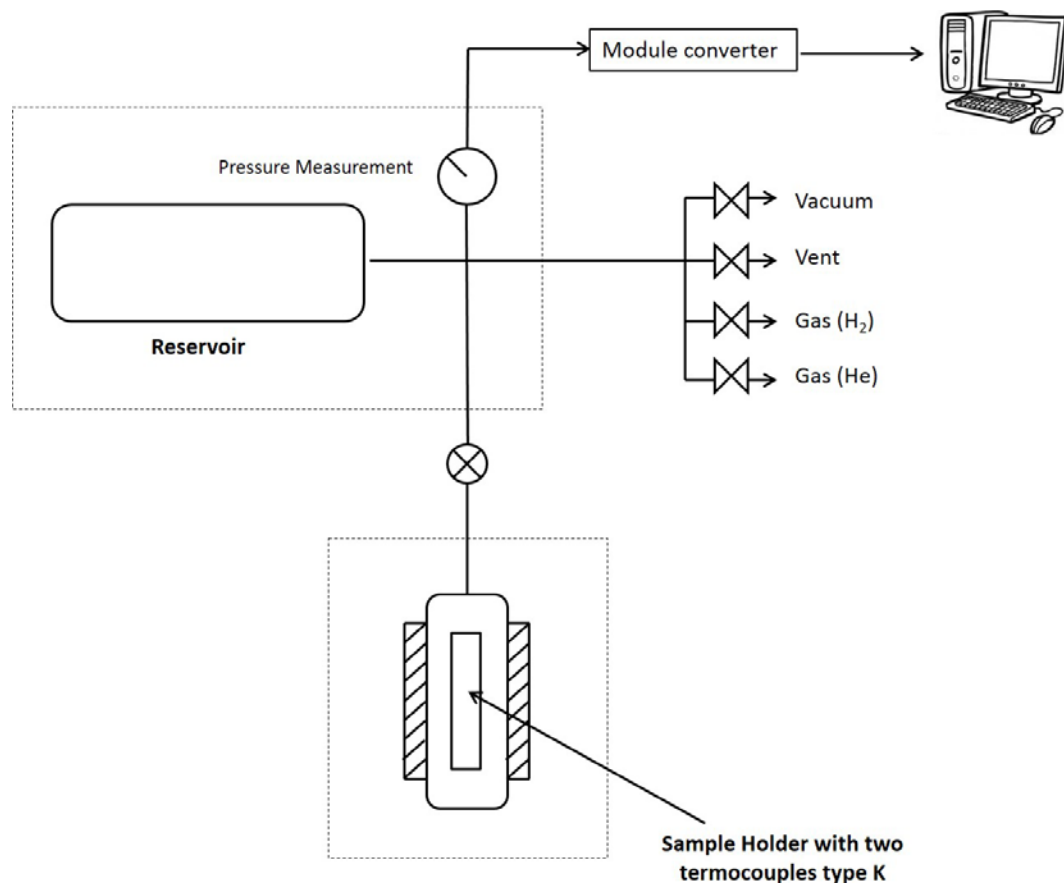


**Figure 1.** Schematic diagram of Sievert-type apparatus used during preparation of composite MBH-SiO<sub>2</sub> and kinetics measurement during several cycles

Coupled manometric-calorimetric measurements were done by connecting the Sievert apparatus to a high pressure differential scanning calorimeter (DSC, Sensys Setaram) in order to study the influence of silica aerogel in the composite system. The calorimeter cell was loaded with around 19 mg of the sample and heated up to 460 °C at a rate of 5 °C/min in static vacuum. Argon was used as carrier gas at 10 mL/min. Calisto was used as software for data acquisition and processing.

Crystallinity of the different samples was examined using an ex-situ X-ray powder diffractometer (model D5005 Bruker). The measuring conditions were CuK $\alpha$  radiation,  $\lambda=1.54060$  Å,  $2\theta$  angle ranging from 5 ° to 90 ° with a scan rate of 10 s/step and a step size of 0.020°. A Bruker-dome was used in order to avoid the contact with air and perform measurements under Argon (gas in the glove-box) and room temperature.

Particle morphology was observed by Scanning Electron Microscopy (SEM) using EVO-MA10-HR (Zeiss, Germany) with energy-dispersive microprobe analyzer INCA Energy 350X Max from Oxford instruments. A special home-made sample holder was used in order to avoid the

contact of the powders with atmospheric oxygen and humidity: in particular, the samples were fixed on Al stubs by C-tapes in the glove box and closed in the sample holder. Rough vacuum was created in it by a vacuum pump before its extraction from the glove box. Only after reaching high vacuum in the SEM, the sample holder was open and thanks to the 3D movements of the SEM stage and the samples could be analyzed.

### 3. RESULTS AND DISCUSSION

#### 3.1 XRD and SEM analyses

XRD profiles showed that crystalline  $\gamma$ -MBH and amorphous  $\text{SiO}_2$  (Figure 2c) were converted into an amorphous mixture after infiltration treatment (Figure 2b). A XRPD pattern with the characteristic features of an amorphous sample was obtained after several cycles. This fact suggests that in the prepared composites MBH was amorphous or infiltrated into the pores of  $\text{SiO}_2$  aerogel.

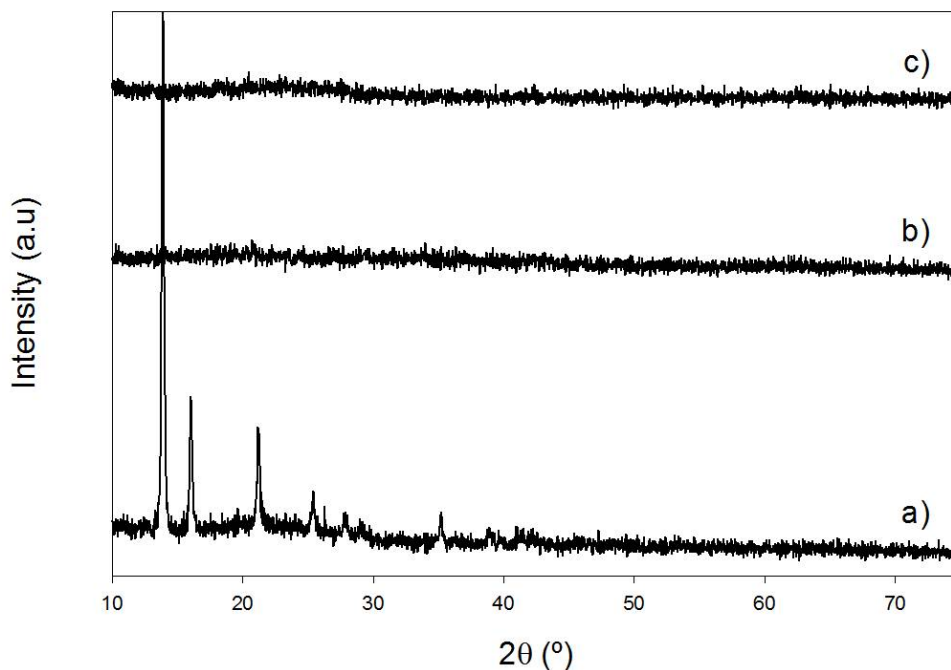


**Figure 2.** XRD profiles for hand-made mixture of MBH and  $\text{SiO}_2$  aerogel (a), the prepared MBH- $\text{SiO}_2$  composites (b) and pure  $\text{SiO}_2$  aerogel (c)

For the hand-made mixture of MBH and  $\text{SiO}_2$  aerogel Rietveld refinement was performed similar to the method proposed in [30]. Obtained results suggest that crystalline powder has particle size around 138 nm and a cell parameter of cubic structure was estimated equal to 1.5 nm.

In Figure 3, the SEM image of the prepared MBH-SiO<sub>2</sub> composite is shown. SEM-EDX analysis suggested that MBH and silica were mixed uniformly and their homogeneity and contact of both components was higher compared to that of their hand-made mixture. At these conditions of pressure and temperature, it was difficult to conclude whether MBH was infiltrated into the pores of the silica aerogel. More pressure would be necessary in order to achieve this, or alternatively another infiltration method such as wet impregnation should be used. A similar morphology of the composite was observed after the 3<sup>rd</sup> desorption, as it is observed in Figure 3b, which means that silica coating avoided the aggregation of MBH during the performance of cycles. In comparison, the powder of bulk MBH was sintered into a single aggregate after three dehydrogenation-hydrogenation cycles (Figure 4). In Figure 4b some single grains of the compacted pellet obtained after cycling were observed. The experimental results suggest that used SiO<sub>2</sub> aerogel worked as nanoscaffold avoiding aggregation of MBH during hydrogen cycling.

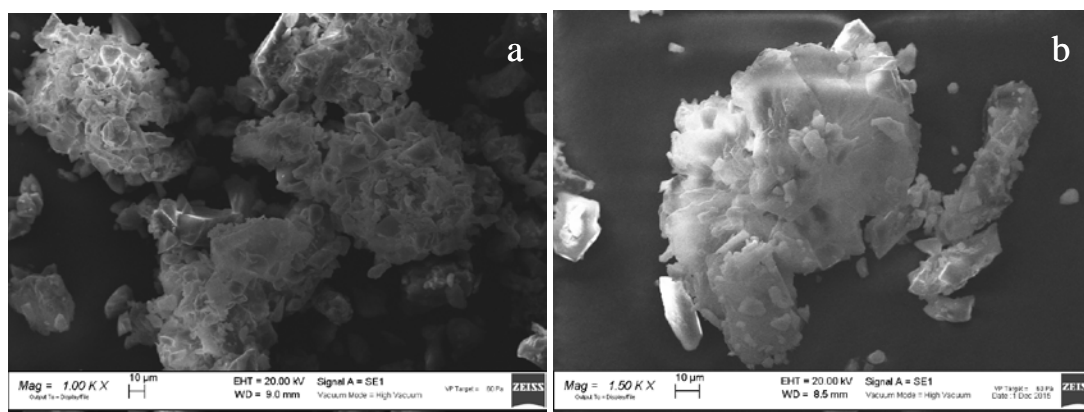


**Figure 3.** SEM image of the MBH-SiO<sub>2</sub> composite a) as prepared and b) after cycling (magnification ratio: 1.0 KX and 1.5 KX respectively, size bar: 10 µm)

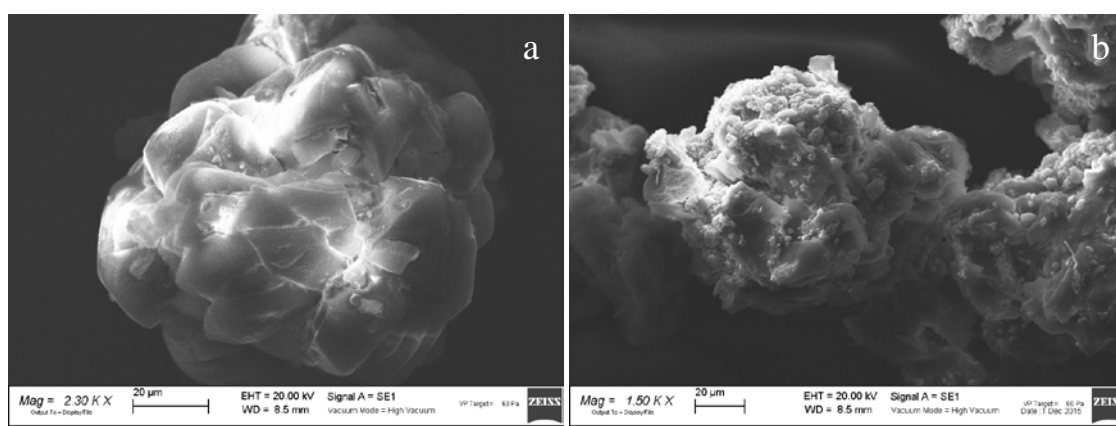


**Figure 4.** SEM image of the bulk MBH a) as received and b) after cycling (magnification ratio: 2.30 KX and 1.5 KX respectively, size bar: 20 µm)

### 3.2 Coupled calorimetric-manometric measurements.

DSC results obtained with bulk  $\gamma$ -MBH are shown in Figure 5 (separately in Figure S1). Obtained results are in good agreement with those previously reported in [6][12][31]. Small temperature differences between the results obtained in this work and those from the references can be due to different working conditions of pressure and heating rate during the measurement [31]. According to Soloveichik et al. [6], Li et al. [10], the first two endothermic peaks (162 and 194 °C) are related to the phase transformation of MBH. Then, in the range of 300-450 °C, MBH was decomposed in 3 different steps (D1-D3). During the first two steps ( $T=307$  °C and  $T=361$  °C, respectively), MBH was decomposed into  $MgH_2$  (crystallized during E1) and amorphous boron. After this two-step reaction,  $MgH_2$  was decomposed into Mg in the third step ( $T= 384$  °C) [32][12]. Since MBH-SiO<sub>2</sub> composites preparation was done at 200 °C, the used MBH should be converted to its  $\beta$  modification.

Coupled DSC-manometric measurements were carried out for both bulk  $\gamma$ -MBH and the prepared MBH-SiO<sub>2</sub> composite (Figure 5). Onset of decomposition for the composite was shifted to lower temperature (approximately 60 °C) compared to bulk MBH. A similar result was obtained in a previous work [33], in which TiO<sub>2</sub> was used as additive. In this case, the dehydrogenation temperature was lowered of 50 °C. Therefore, in this work silica could also act as additive improving the breakage of B-H bond from MBH which is the limitation of the decomposition process [22], similarly to the data reported in [29].

Moreover, Figure 5 showed that silica changes the mechanism of the decomposition reaction. Three decomposition steps for bulk MBH were converted into only one broad endothermic peak and a shoulder at higher temperature in case of the prepared MBH-SiO<sub>2</sub> composite that is a typical behavior of confined hydrides [21]. This fact could be related to the intimate contact between silica and MBH. A similar result was observed in the case of MBH-0.5LiH composite [24], where only one broad peak centered at 210 °C, involving complicated interactions which may lead to the formation of metastable phases. Also in [34] hydrogen was evolved only during one step after the formation of MBH-ethylendiamine composite.

Since the mass of MBH in the prepared composite was 50 wt%, the final hydrogen release was ~6.6 wt% H<sub>2</sub> that is two times lower than for the bulk MBH (almost 12.0 wt% H<sub>2</sub>). The small difference in the final amount that is released till 450 °C could be due to a small instrumental error during the preparation of the MBH-SiO<sub>2</sub> sample or surface oxidation of MBH before the measurement. Otherwise it could be due to an effect of the SiO<sub>2</sub> matrix. This would mean that silica not only lowered the decomposition temperature but also its presence makes MBH to

release more hydrogen. As it is known, MBH has a theoretical content of hydrogen of 14.8 wt%  $H_2$ , so higher conditions of temperature ( $>500\text{ }^\circ\text{C}$ ) are necessary for complete hydrogen desorption.

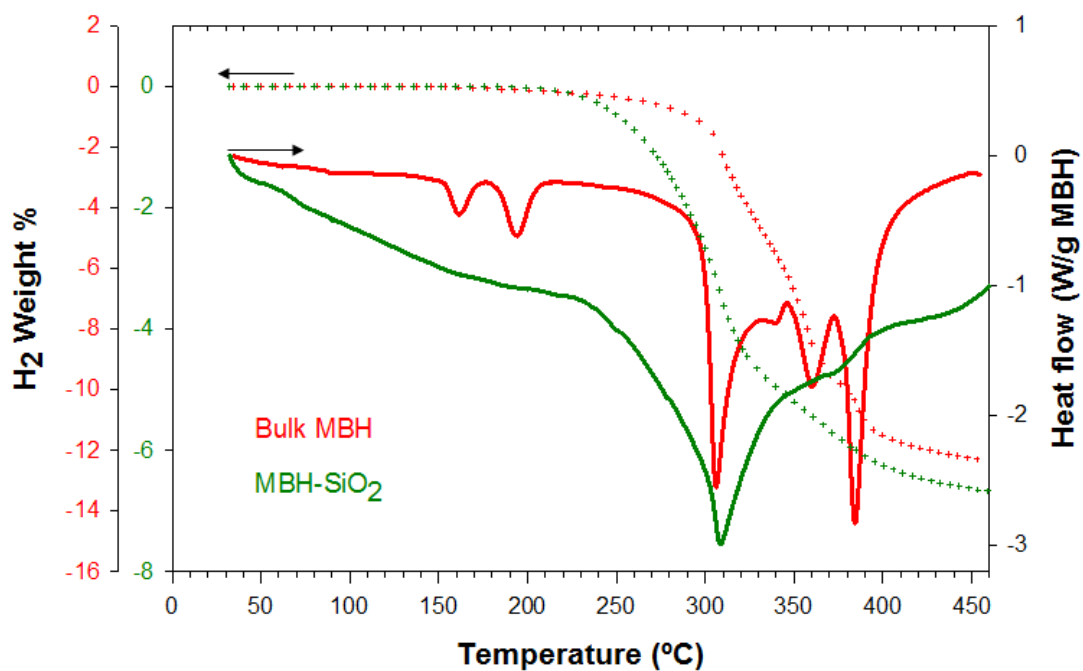


**Figure 5.** Coupled DSC-manometric measurement of bulk MBH and the prepared MBH-SiO<sub>2</sub> composite.

Solid lines correspond to DSC analyses (right y-axis) and dotted lines correspond to manometric measurements (left y-axis)

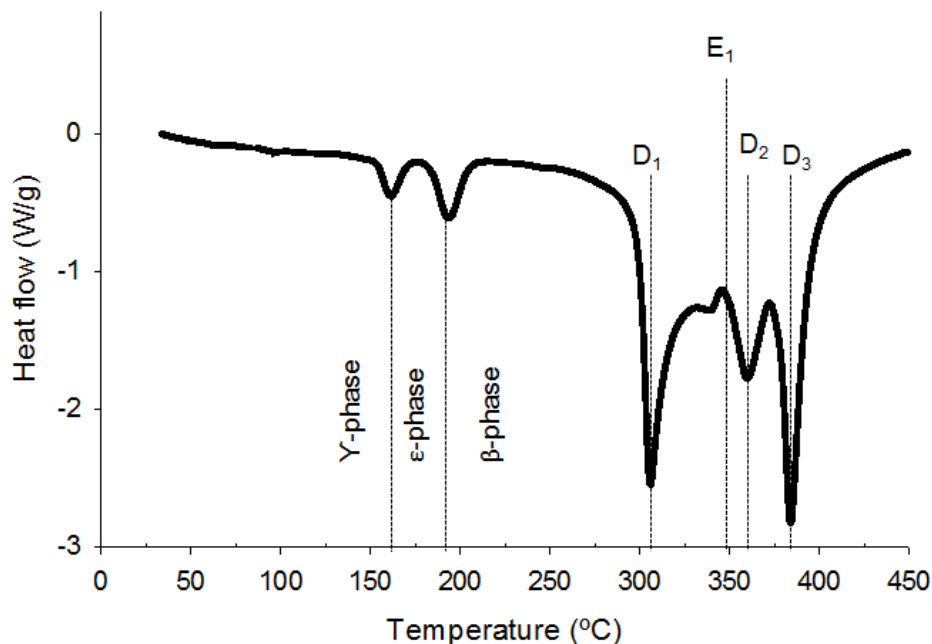


**Figure S1.** DSC measurement of bulk MBH

### 3.3 Hydrogen desorption at 300 °C and 400 °C

Figure 6 shows the kinetics curves of hydrogen desorption for the first desorption cycle at 300 °C and 400 °C for bulk  $\gamma$ -MBH and the prepared MBH-SiO<sub>2</sub> composite.

Hydrogen release kinetics at 300 °C was improved in the sample in which silica was present. Different results were obtained respect to the work of Al-Kukhun et al. [16]. In this work, no changes in hydrogen release kinetics from MBH at 300 °C were observed after addition of SiO<sub>2</sub>. This fact confirmed our SEM observation that a better contact between MBH and SiO<sub>2</sub> was found in the prepared composite, which was not obtained with the simple mixing employed by Al-Kukhun et al. [16], therefore the used aerogel might be considered as nanoscaffold for MBH. Alternatively, it could be also due to some different properties of the silica used in this work and in the work of Al-Kukhun et al. [16], such as acidity, which could be responsible of the weakening of B-H bond and the kinetic improvement during dehydrogenation [17].

Regarding the kinetics at the lowest temperature, it took less than 4 h to complete desorption from MBH-SiO<sub>2</sub> composite (~5 wt% H<sub>2</sub>), while around 8 h were necessary to release the same normalized amount of hydrogen (~10 wt% H<sub>2</sub>) from bulk MBH. This means that dehydrogenation time was reduced by a factor of 2. Similar results were observed in [9] using TiF<sub>3</sub> and ScCl<sub>3</sub> as additives ball milled with MBH.

At 400 °C, the release kinetics was similar in both samples. In the case of the composite, the kinetic was shifted to the left because borohydride was decomposed in a shorter time, as observed in the calorimetric measurements discussed in the previous section. Moreover, a different pathway was followed during the dehydrogenation as it was also found in DSC measurements. Three different steps were distinguished in bulk MBH whereas only one was seen in the prepared MBH-SiO<sub>2</sub> composite.

The different mass of hydrogen that was released taking into account that MBH-SiO<sub>2</sub> sample was prepared in a ratio 1:1 can be explained by the same reasons reported in couple DSC-manometric measurements: a different degree of oxidation, or small errors during the preparation of samples.

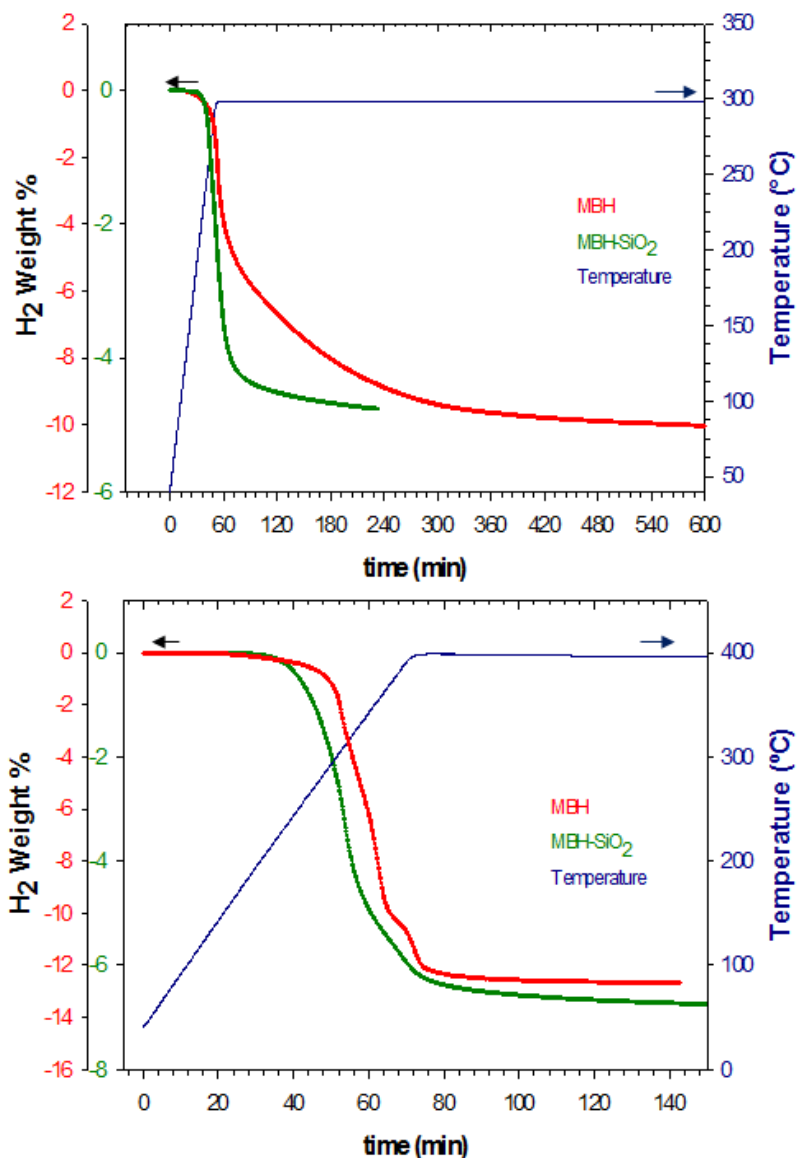


**Figure 6.** Kinetics curves of hydrogen desorption for bulk MBH and the prepared MBH–SiO<sub>2</sub> composite at 300 and 400 °C. Temperature profile is referred to the right y-axis.

### 3.4 Reversible hydrogen sorption

Figure 7 and 8 show the dehydrogenations at 300 °C and 400 °C, respectively for several cycles for bulk MBH and the prepared MBH–SiO<sub>2</sub> composite, performing the rehydrogenation at the same conditions of pressure and temperature (110 bar H<sub>2</sub> and 390 °C).

In the case that desorption was performed at 300 °C (Figure 7), both samples were successfully rehydrogenated at lower conditions than those reported in previous works. Around 3 wt% H<sub>2</sub> was released from bulk MBH after rehydrogenation. A similar amount was reported in [6], which could be related to the rehydrogenation of MgH<sub>2</sub>, after rehydrogenation of completely

decomposed MBH to  $MgB_2$ . However, in this work products after desorption at 300 °C (incomplete desorption) were partially rehydrogenated.

In the prepared composite, a lower amount of  $H_2$  was released (2.6 wt%  $H_2$  normalized for the amount of MBH in the sample). This could be due to the formation of more intermediates than in bulk MBH, which were formed during desorption and were more difficult to rehydrogenate, as it was also observed in [9]. Another possibility could be the formation of  $B(OH)_x$  compounds due to the presence of surface hydroxyl groups on silica aerogel particles which might be the reason of the surface deactivation. Thus, the formation of this irreversible compound would explain the lower amount of  $H_2$  released in the second cycle in MBH- $SiO_2$  composite.

Since RGA for the both samples confirmed mainly hydrogen gas release (diborane was suppressed), existence of stable solid polyboranes products might be the preliminary problem of reversible hydrogen sorption in MBH. More analyses could be necessary in order to clarify the different dehydrogenation-rehydrogenation mechanism that was followed in each sample.

Regarding the kinetics, it was observed that the second desorption was slower than the first one for both samples. A sluggish kinetic for both samples suggests the existence of a kinetic barrier that suppresses the fast development of the reaction. The addition of a catalyst could be a solution in order to enhance it.

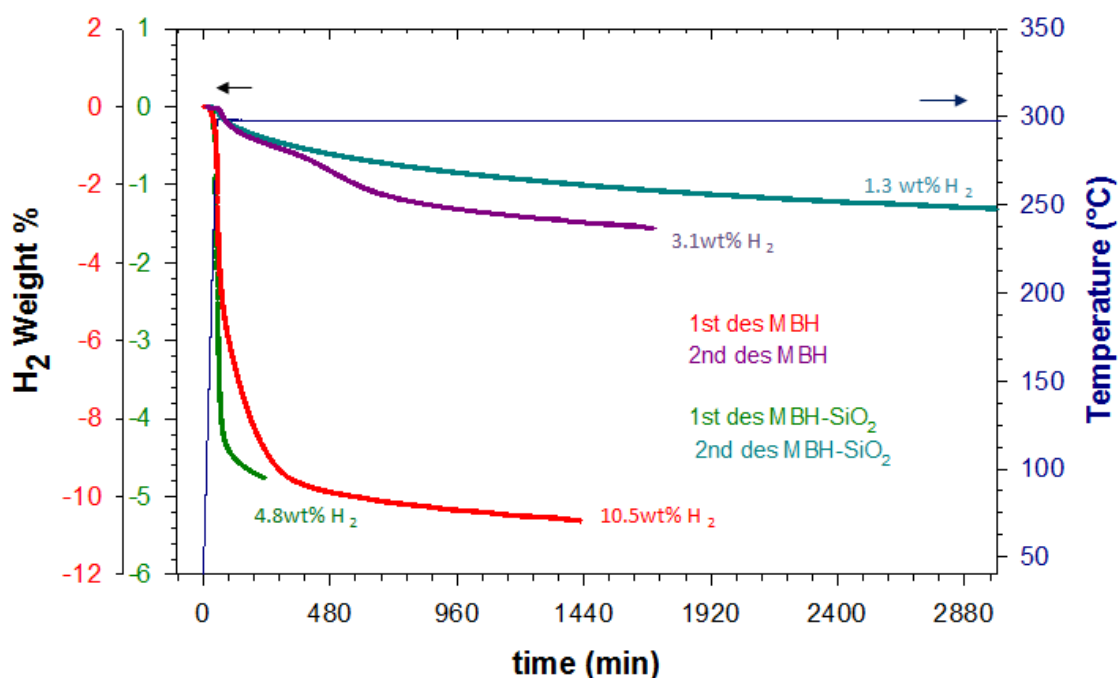


**Figure 7.** First and second hydrogen desorption for bulk MBH and the prepared MBH- $SiO_2$  composite at 300 °C. Temperature profile is referred to the right y-axis.

A different result was obtained in the case that the samples were rehydrogenated after dehydrogenation at 400 °C (Figure 8). After the 1-st desorption both samples showed 42 % of reversibility resulted in 5.4 wt% H<sub>2</sub> for bulk MBH and 2.9 wt% H<sub>2</sub> for the prepared MBH–SiO<sub>2</sub> composite.

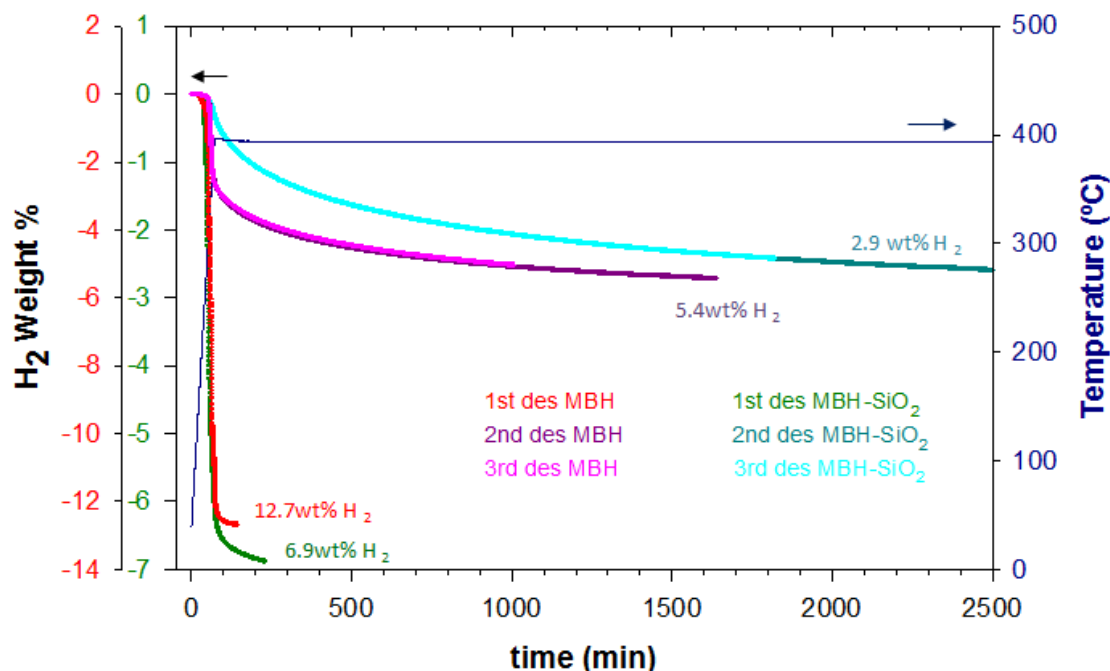


**Figure 8.** First, second and third hydrogen desorption for bulk MBH and the prepared MBH–SiO<sub>2</sub> composite at 400 °C. Temperature profile is referred to the right y-axis. (Second and third desorption curves could not be distinguished).

This is the first time that more than 3 wt% H<sub>2</sub> has been rehydrogenated at moderate conditions, not only in bulk MBH but also preserving the reversibility in MBH–SiO<sub>2</sub> composite. A similar amount was rehydrogenated by Li et al [10] and [11], but applying hydrogen pressure of 400 bar, whereas in this work the working pressure was reduced to 110 bar. Desorption curves during the 2-nd and 3-rd cycles were almost identical for both samples that suggest a good cyclability. It is visible that complete hydrogen release for both samples was very similar with the only difference of slower kinetics for the composite suggesting activated or deactivated (which is in our case) surface of MBH.

After three dehydrogenation-hydrogenation cycles at 400 °C, bulk MBH powder was sintered and converted into a single compacted pellet with the shape of the used reactor volume, in contrast to the fine powder morphology that was preserved in the case of the prepared MBH–SiO<sub>2</sub> composite. As it was seen in SEM analyses, SiO<sub>2</sub> helped to avoid MBH aggregation which could be very disadvantageous for the cyclability of the borohydride.

Most probably partial reversible hydrogen sorption at 400 °C might be explained by irreversible products formed during dehydrogenation of both bulk MBH and the prepared MBH-SiO<sub>2</sub> composite.

In order to analyze phase composition for the commercial bulk MBH before and after cycling, XRD measurements were performed for MBH as received and after second dehydrogenation at 400 °C (Figure 9). As it was expected, after dehydrogenation diffraction profile revealed the presence of Mg (74.9%) and some MgO (25.1%) that could be formed due to the presence of some oxygen during the applied measurement or the presence of nanocrystalline MgO already in the commercial MBH. In [14], MgO was also discussed which could form a shell around the reversible Mg<sub>x</sub>B<sub>y</sub>H<sub>z</sub> phases preventing the full rehydrogenation and therefore might be responsible for the reduced reversibility. In the case that some intermediates were present, they would be amorphous as in the case of pure boron. In the prepared MBH-SiO<sub>2</sub> composite, XRD analyses did not reveal any crystalline phase in the spectra after thermal treatment. Some additional methods to analyze amorphous species during dehydrogenation-rehydrogenation would be helpful to clarify the difference in the reaction mechanism between bulk MBH and the prepared MBH-SiO<sub>2</sub> composite.

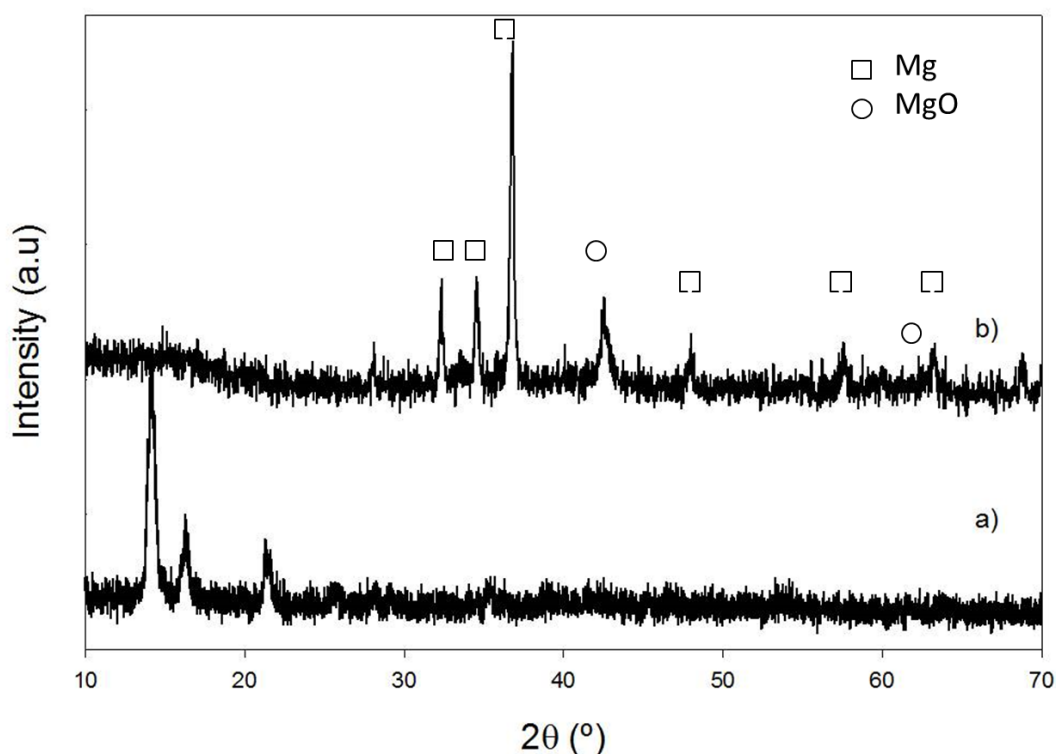


**Figure 9.** XRD profiles for bulk MBH a) as received and b) after 2-nd dehydrogenation at 400 °C

#### 4. CONCLUSIONS

Microparticles of silica aerogel were proposed as host to infiltrate MBH using a thermal treatment in hydrogen at 200 °C and 120 bar H<sub>2</sub> for 3 h. According to the pores volume of microparticles of SiO<sub>2</sub> aerogel calculations, it would be possible to infiltrate up to 50 wt% of MBH.

However, as this method was not satisfactory to confine MBH in the pores of the support, less amount of silica could be used in a future work. As a result, a composite in which silica behaves as additive and a storage material with a higher H<sub>2</sub> content could be obtained. Wet impregnation is also proposed as future technique to infiltrate MBH in the pores of silica selecting the correct solvent in order to avoid the decomposition of the hydride.

The temperature of the decomposition of bulk MBH was decreased almost 60 °C and the mechanism of the decomposition was changed in the prepared composite. Calorimetric measurements showed that the three steps of decomposition of bulk MBH were converted into only one in range of 240-400 °C for MBH-SiO<sub>2</sub> composites. This result indicates an intimal contact between MBH and silica, which acts as an additive changing the decomposition route, was successfully acquired with this method. Additionally, their kinetics of the first dehydrogenation at 300 °C was two times faster compared to that of the bulk MBH.

Moreover, for the first time MBH has been demonstrated to be partially reversible at moderate conditions of pressure and temperature (110 bar H<sub>2</sub> and 390 °C). Almost 6 wt% H<sub>2</sub> was rehydrogenated when hydrogen desorption was performed at 400 °C.

#### 5. ACKNOWLEDGEMENTS

Authors thank the University of Valladolid fellowship research program FPI-UVa, for the financial support for the stay at the Pavia University.

**REFERENCES**

- [1] Sharma S, Krishna S. Hydrogen the future transportation fuel : From production to applications. *Renew Sustain Energy Rev* 2015;43:1151–8. doi:10.1016/j.rser.2014.11.093.
- [2] Sobrino FH, Monroy CRR, Pérez JLHLH, Perez JLH. Critical analysis on hydrogen as an alternative to fossil fuels and biofuels for vehicles in Europe. *Renew Sustain Energy Rev* 2010;14:772–80. doi:10.1016/j.rser.2009.10.021.
- [3] Balat M. Potential importance of hydrogen as a future solution to environmental and transportation problems. *Int J Hydrogen Energy* 2008;33:4013–29. doi:10.1016/j.ijhydene.2008.05.047.
- [4] Züttel A, Wenger P, Rentsch S, Sudan P, Mauron P, Emmenegger C.  $\text{LiBH}_4$  a new hydrogen storage material. *J Power Sources* 2003;118:1–7. doi:10.1016/S0378-7753(03)00054-5.
- [5] Bogdanovic, B, Brand, R, Marjanovic, A, Schwickardi, N, Tolle J. Metal-doped sodium aluminium hydrides as potential new hydrogen storage materials. *J Alloys Compd* 2000;302:36–58.
- [6] Soloveichik GL, Gao Y, Rijssenbeek J, Andrus M, Kniajanski S, Bowman RC, et al. Magnesium borohydride as a hydrogen storage material : Properties and dehydrogenation pathway of unsolvated  $\text{Mg}(\text{BH}_4)_2$ . *Int J Hydrogen Energy* 2009;34:916–28. doi:10.1016/j.ijhydene.2008.11.016.
- [7] Zavorotynska O, El-Kharbachi A, Deledda S, Hauback BC. Recent progress in magnesium borohydride  $\text{Mg}(\text{BH}_4)_2$ : Fundamentals and applications for energy storage. *Int J Hydrogen Energy* 2015. doi:10.1016/j.ijhydene.2016.02.015.
- [8] Severa G, Rönnebro E, Jensen CM. Direct hydrogenation of magnesium boride to magnesium borohydride: demonstration of >11 weight percent reversible hydrogen storage. *Chem Commun (Camb)* 2010;46:421–3. doi:10.1039/b921205a.
- [9] Newhouse RJ, Stavila V, Hwang SJ, Klebanoff LE, Zhang JZ. Reversibility and improved hydrogen release of magnesium borohydride. *J Phys Chem C* 2010;114:5224–32. doi:10.1021/jp9116744.
- [10] H.W.Li, K.Kikuchi, Y.Nakmori, N.Ohba. M.Miwa, S.Towata SO. Dehydriding and rehydriding processes of well-crystallized  $\text{Mg}(\text{BH}_4)_2$  accompanying with formation of intermediate compounds. *Acta Mater* 2008;56:1342–7. doi:10.1016/j.actamat.2007.11.023.

- [11] H.W.Li, Miwa K, Ohba N, Fujita T, Sato T, Yan Y, et al. Formation of an intermediate compound with a  $B_{12}H_{12}$  cluster: experimental and theoretical studies on magnesium borohydride  $Mg(BH_4)_2$ . *Nanotechnology* 2009;20:204013. doi:10.1088/0957-4484/20/20/204013.
- [12] Chłopek K, Frommen C, Léon A, Zabara O, Fichtner M. Synthesis and properties of magnesium tetrahydroborate,  $Mg(BH_4)_2$ . *J Mater Chem* 2007;17:3496. doi:10.1039/b702723k.
- [13] Chong M, Karkamkar A, Autrey T, Orimo S, Jalisatgi S, Jensen CM. Reversible dehydrogenation of magnesium borohydride to magnesium triborane in the solid state under moderate conditions. *Chem Commun (Camb)* 2011;47:1330–2. doi:10.1039/c0cc03461d.
- [14] Zavorotynska O, Deledda S, Hauback BC. Kinetics studies of the reversible partial decomposition reaction in  $Mg(BH_4)_2$ . *Int J Hydrogen Energy* 2016;41:9885–92. doi:10.1016/j.ijhydene.2016.02.153.
- [15] Li H, Yan Y, Orimo S, Züttel A, Jensen CM. Recent Progress in Metal Borohydrides for Hydrogen Storage. *Energies* 2011;4:185–214. doi:10.3390/en4010185.
- [16] Al-Kukhun A, Hwang HT, Varma A.  $NbF_5$  additive improves hydrogen release from magnesium borohydride. *Int J Hydrogen Energy* 2012;37:17671–7. doi:10.1016/j.ijhydene.2012.09.097.
- [17] Paduani C, Jena P. Role of Ti-based catalysts in the dehydrogenation mechanism of magnesium borohydride: A cluster approach. *Int J Hydrogen Energy* 2013;38:2357–62. doi:10.1016/j.ijhydene.2012.11.060.
- [18] Zavorotynska O, Saldan I, Hino S, Humphries TD, Deledda S, Hauback BC. Hydrogen cycling in  $\gamma$ - $Mg(BH_4)_2$  with cobalt-based additives. *J Mater Chem A* 2015;3:6592–602. doi:10.1039/C5TA00511F.
- [19] Saldan I, Frommen C, Llamas-Jansa I, Kalantzopoulos GN, Hino S, Arstad B, et al. Hydrogen storage properties of  $\gamma$ - $Mg(BH_4)_2$  modified by  $MoO_3$  and  $TiO_2$ . *Int J Hydrogen Energy* 2015;40:12286–93. doi:10.1016/j.ijhydene.2015.07.082.
- [20] Au YS, Yan Y, de Jong KP, Remhof A, de Jongh PE. Pore Confined Synthesis of Magnesium Boron Hydride Nanoparticles. *J Phys Chem C* 2014;118:20832–9. doi:10.1021/jp507568p.
- [21] Fichtner M, Zhao-Karger Z, Hu J, Roth A, Weidler P. The kinetic properties of  $Mg(BH_4)_2$  infiltrated in activated carbon. *Nanotechnology* 2009;20:204029. doi:10.1088/0957-

4484/20/20/204029.

[22] Yan Y, Au YS, Rentsch D, Remhof A, de Jongh PE, Züttel A. Reversible hydrogen storage in  $\text{Mg}(\text{BH}_4)_2$ /carbon nanocomposites. *J Mater Chem A* 2013;1:11177. doi:10.1039/c3ta12222k.

[23] Wahab MA, Jia Y (Alec), Yang D, Zhao H, Yao X. Enhanced hydrogen desorption from  $\text{Mg}(\text{BH}_4)_2$  by combining nanoconfinement and a Ni catalyst. *J Mater Chem A* 2013;1:3471. doi:10.1039/c2ta00899h.

[24] Yang J, Fu H, Song P, Zheng J, Li X. Reversible dehydrogenation of  $\text{Mg}(\text{BH}_4)_2$ -LiH composite under moderate conditions. *Int J Hydrogen Energy* 2012;37:6776–83. doi:10.1016/j.ijhydene.2012.01.109.

[25] Paskevicius M, Pitt MP, Webb CJ, Sheppard D a., Filsø U, Gray EM, et al. In-Situ X-ray Diffraction Study of  $\gamma$ - $\text{Mg}(\text{BH}_4)_2$  Decomposition. *J Phys Chem C* 2012;116:15231–40. doi:10.1021/jp302898k.

[26] Sanz-Moral LM, Rueda M, Mato R, Martín Á. View cell investigation of silica aerogels during supercritical drying: Analysis of size variation and mass transfer mechanisms. *J Supercrit Fluids* 2014;92:24–30. doi:10.1016/j.supflu.2014.05.004.

[27] Soleimani Dorcheh A, Abbasi MH. Silica aerogel; synthesis, properties and characterization. *J Mater Process Technol* 2008;199:10–26. doi:10.1016/j.jmatprotec.2007.10.060.

[28] Rueda M, Sanz-Moral LM, Nieto-Márquez A, Longone P, Mattea F, Martín Á. Production of silica aerogel microparticles loaded with ammonia borane by batch and semicontinuous supercritical drying techniques. *J Supercrit Fluids* 2014;92:299–310. doi:10.1016/j.supflu.2014.06.012.

[29] Rueda, Miriam, Sanz-Moral, LM, Segovia JJ, Martín A. Improvement of the kinetics of hydrogen release from ammonia borane confined in silica aerogel n.d.

[30] Zavorotynska O, Deledda S, Vitillo J, Saldan I, Guzik M, Baricco M, et al. Combined X-ray and Raman Studies on the Effect of Cobalt Additives on the Decomposition of Magnesium Borohydride. *Energies* 2015;8:9173–90. doi:10.3390/en8099173.

[31] Hanada N, Chłopek K, Frommen C, Lohstroh W, Fichtner M. Thermal decomposition of  $\text{Mg}(\text{BH}_4)_2$  under He flow and  $\text{H}_2$  pressure. *J Mater Chem* 2008;18:2611. doi:10.1039/b801049h.

[32] Matsunaga T, Buchter F, Mauron P, Bielman M, Nakamori Y, Orimo S, et al. Hydrogen storage properties of  $\text{Mg}(\text{BH}_4)_2$ . *J Alloys Compd* 2008;459:583–8.

doi:10.1016/j.jallcom.2007.05.054.

[33] Li H-W, Kikuchi K, Nakamori Y, Miwa K, Towata S, Orimo S. Effects of ball milling and additives on dehydriding behaviors of well-crystallized  $\text{Mg}(\text{BH}_4)_2$ . *Scr Mater* 2007;57:679–82.

doi:10.1016/j.scriptamat.2007.06.052.

[34] Chen J, Chua YS, Wu H, Xiong Z, He T, Zhou W, et al. Synthesis, structures and dehydrogenation of magnesium borohydride-ethylenediamine composites. *Int J Hydrogen Energy* 2015;40:412–9. doi:10.1016/j.ijhydene.2014.11.020.

**CONCLUSIONS**

**&**

**FUTURE WORK**



This work is a contribution for the development of novel solid hydrogen storage materials based on hydrides with enhanced properties. Two different strategies have been tested in order to overcome the limitations of bulk hydrides. The main conclusions are summarized below:

### 1. Micronization of hydrides using supercritical CO<sub>2</sub> process

- Two different hydrides have been tested: MgAc, a precursor of MgH<sub>2</sub>, and EDAB have been successfully micronized using Supercritical Antisolvent Solution. In both studies, it was concluded that the concentration of the inlet solution, tested in the range 10-40 mg/mL for MgAc and 3.3-25 mg/mL for EDAB, was the main factor that influenced the particle size obtaining larger particles with enlarger particle size distribution at higher concentration of the solution, whose effect was more pronounced in the micronization of MgAc.
- After micronization of MgAc, a precursor of MgH<sub>2</sub>, crystalline particles of around 200 μm and irregular shape were transformed into amorphous micronized particles with a mean size in the range 300-600 nm with regular spherical morphology. Kinetics of MgH<sub>2</sub> were drastically enhanced, reducing the time to release 2 wt% H<sub>2</sub> from 10 h in bulk hydride to 1 h for the smallest micronized sample. This was associated to the reduction of particle size and therefore a reduction in hydrogen diffusion length. However, only 1/3 of the precursor could be converted into MgH<sub>2</sub> and released hydrogen, due to the inaccessibility to hydrogenate the core of the particle, or due to the oxidation of Mg.
- EDAB was also micronized using SAS process. In this case, prismatic EDAB particles of 400 μm with a crystallite size of 100 nm were reduced to 2 μm with a crystal size of 50 nm changing the shape to microspheres interconnected between them. This reduction in particle size resulted in a reduction of 7 °C in the decomposition peak temperature and acceleration of the kinetics after micronization process. In the case of the kinetics of release of hydrogen at 100 °C, the reduction of the particle and grain size resulted in a huge improvement, reducing by a factor of 6 the time required to release 3.9 wt% H<sub>2</sub>. Moreover, a suppression of induction time was observed due to a destabilization of the hydride after treatment.

It can be concluded that SAS process is a promising technique to micronize hydrides and therefore improve the kinetics of release of hydrogen due to the reduction of particle size and therefore the reduction of diffusion distances. With this technique, it was possible to control the particle size of the micronized sample by changing the conditions of the process and the particles were easily collected after micronization process in contrast to conventional technique, mechanical milling.

However, the reduction of particle size is lost after cycling. Thus, it was necessary to find an alternative that avoids the growth of the hydride during the performance of several cycles.

## **2. Nanoconfinement of hydrides in a scaffold**

- The production of silica aerogel was optimized in order to be used as scaffold for nanoconfinement of AB and  $\text{Mg}(\text{BH}_4)_2$ . It is the first time that this material has been used as host for this application. A support with outstanding properties has been obtained, comprising particles with a mean size in the range 13-30  $\mu\text{m}$  with surface area in the range 600- 900  $\text{m}^2/\text{g}$  and 0.5-2  $\text{cm}^3/\text{g}$  of volume of pores were obtained using sol-gel method followed by pressurized or supercritical  $\text{CO}_2$  drying.
- Irregular particles were obtained with hydrophilic silica aerogel whereas microspheres with smooth surface were formed in the case of hydrophobic silica aerogel. This difference could be attributed to elasticity and slower rate of formation for the latter particles.
- Hydrophilic microparticles of silica aerogel were used as support to confine till 60 wt% of AB using a novel process based on a simultaneous aerogel drying and ammonia borane gas antisolvent precipitation using compressed carbon dioxide. It is the first time that such high concentration of a hydride has been confined in a matrix. By nanoconfinement, a homogenous dispersion of AB in the aerogel was obtained with enhanced properties of decomposition of the hydride. Acceleration of the kinetics reducing drastically the induction time was obtained due to the reduction of particle size and the presence of Si-OH groups which could weaken B-H bonds and create defects in the support and therefore start the decomposition at lower temperature and favor the release of hydrogen. More than 12 h took to release 5 wt%  $\text{H}_2$  in bulk AB whereas less than 2 hours were necessary in AB confined in silica aerogel. Moreover, foaming process was avoided which could be very beneficial for the regeneration process.

- A composite of microparticles of silica aerogel and  $\text{Mg}(\text{BH}_4)_2$  was successfully obtained after thermal process in hydrogen atmosphere. The temperature of the decomposition of bulk MBH was decreased almost 60 °C and the mechanism of the decomposition was changed in the prepared composite. Calorimetric measurements showed that the three steps of decomposition of bulk MBH were converted into only one in the range of 240-400 °C for MBH-SiO<sub>2</sub> composites. In this case, silica acted as an additive changing the decomposition route. Additionally, their kinetics of the first dehydrogenation at 300 °C was two times faster compared to that of the bulk MBH. For the first time MBH infiltrated in silica was partially reversible at moderate conditions of pressure and temperature and almost 6 wt% H<sub>2</sub> was rehydrogenated after hydrogen desorption performed at 400 °C in vacuum.

#### **FUTURE WORK**

One of the aspects that is still necessary to study in order to have a hydrogen storage material that fulfill most of the requirements for DoE is the regeneration of these hydrides confined in silica aerogel, especially for the case of AB due to the high concentration of hydride confined in the pores of the support. In this way, we could check the preservation of enhanced properties during cycling.

Moreover, considering the promising properties of AB confined in microparticles of silica aerogel using the innovative process of pressurized CO<sub>2</sub> drying simultaneous to antisolvent process, a similar methodology could be tested with other hydrides. As EDAB and  $\text{Mg}(\text{BH}_4)_2$  could also be promising hydrides and they have been checked in this thesis, they could be further enhanced after nanoconfining in microparticles of silica aerogel using the same method.

This work is going to be done thanks to a financial support of Iberdrola in the frame 'Ayudas a la Investigación en Energía y Medio Ambiente 2016'.



# **RESUMEN**

**Estrategias innovadoras para mejorar  
propiedades de materiales de  
almacenamiento de hidrógeno en estado  
sólido basado en hidruros**



## 1. INTRODUCCIÓN

Se necesita fomentar el uso de energías renovables debido al progresivo agotamiento de los combustibles fósiles, así como el cambio climático y aceleramiento del calentamiento global asociado a los gases de efecto invernadero. De este modo se facilitarían el cumplimiento de los objetivos marcados en la XXI Conferencia sobre Cambio Climático (COP21), celebrado en París el pasado diciembre en el que se marcó como objetivo para los próximos años mantener el calentamiento global por debajo de los 2 °.

Sin embargo, establecer un sistema energético basado en energías renovables como recurso principal no es una tarea sencilla, entre otras razones por la naturaleza fluctuante de muchas de estas fuentes de energía (como la energía solar o eólica entre otras), que hace que tengan picos y valles de producción que pueden no corresponderse con la variación del consumo. Además, estas fuentes de energía en general no pueden utilizarse de forma directa en aplicaciones móviles (vehículos, pequeños equipos electrónicos, etc).

Una posible solución para estos problemas consiste en utilizar hidrógeno como vector o portador de energía, lo que se conoce como 'economía o sociedad del hidrógeno', tal como se muestra en la figura 1 [1][2]. El hidrógeno es un combustible muy atractivo por su alto contenido energético y contribuye al desarrollo de un modelo sostenible ya que se quema de forma muy limpia generando vapor de agua como subproducto. Respecto al medio de producción, entre otras opciones el hidrógeno se puede producir por electrólisis de agua utilizando energías renovables. Este hidrógeno puede almacenarse para utilizarlo en periodos en que no exista suficiente producción directa desde fuentes renovables para satisfacer el consumo, o puede transportarse y utilizarse en vehículos y otras fuentes móviles.

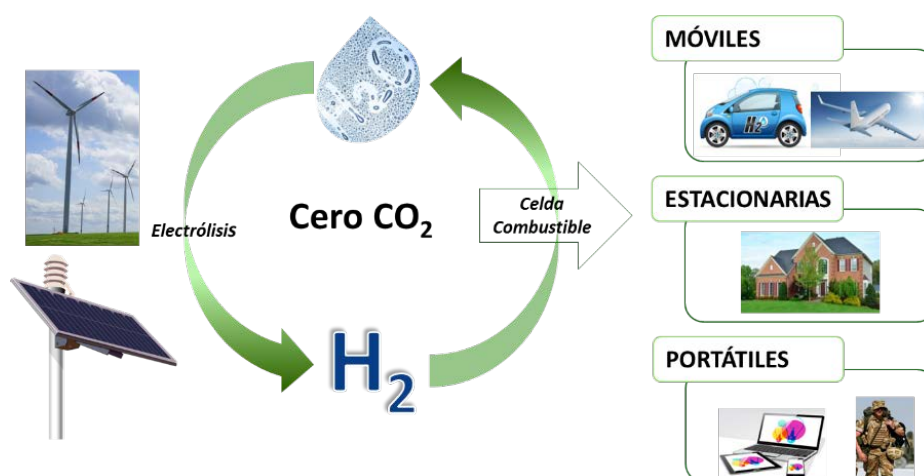


**Figura 1.** La "Sociedad del Hidrógeno"

Para convertir este nuevo paradigma en una realidad, hay que resolver diversas cuestiones técnicas, entre las que se incluye la producción eficiente del hidrógeno [3], la conversión del hidrógeno en electricidad (por ejemplo, mediante células de combustible), y el almacenamiento del hidrógeno [4].

Almacenar hidrógeno como combustible en vehículos u otras aplicaciones móviles es una tarea compleja, debido a las propiedades físicas del mismo ya que el tamaño y el peso del sistema de almacenamiento para este tipo de aplicaciones debe ser lo más reducido posible.

Las soluciones más obvias, como el almacenamiento como gas comprimido o licuado, presentan problemas debido a las propiedades físicas del hidrógeno, que es un gas muy poco denso por lo que requiere grandes tanques a altas presiones (en el caso de almacenarlo como gas comprimido), y además condensa a temperaturas muy bajas, lo que obliga a gastar mucha energía para mantenerlo en condiciones criogénicas. Por este motivo, en la actualidad se está desarrollando mucha investigación sobre diferentes métodos de almacenamiento de hidrógeno en estado sólido. El Departamento de Energía de EEUU (DoE) ha establecido como meta para el 2020 el desarrollo de un sistema de almacenamiento que consiga una concentración de hidrógeno de al menos 40 g/L en volumen y 5.5 wt% en peso. Es por eso que uno de los retos que queda por resolver es el desarrollo de un material de almacenamiento de hidrógeno que reúna los requisitos de elevada densidad gravimétrica y volumétrica de hidrógeno, adecuada cinética, reversibilidad, bajo coste y baja toxicidad.

Unos de los sistemas de almacenamiento en fase sólida más prometedores son los hidruros, que son compuestos químicos que liberan hidrógeno mediante una reacción química, generalmente reversible. Sin embargo, estos compuestos también presentan importantes limitaciones, principalmente, cinéticas y termodinámicas:

- Son compuestos muy estables en atmósfera inerte. Se necesitan altas temperaturas de descomposición (200-500 °C) y altas presiones de hidrógeno para regenerarlos (en algunos casos, presiones superiores a 100 bares H<sub>2</sub>).
- Cinéticas de liberación y absorción de hidrógeno lentas.

Uno de los métodos más explorados para mejorar las propiedades de los hidruros es la nanoingeniería o reducción del tamaño del mismo, para así aumentar las cinéticas de liberación de hidrógeno.

El método más utilizado para reducir el tamaño del hidruro es la molienda mecánica, permitiendo acortar las distancias de difusión del hidrógeno debido a la reducción de tamaño

de partícula y los defectos creados tanto en el interior como en el exterior de la superficie de dicho material. Sin embargo, esta técnica no puede utilizarse para aplicaciones finales debido a las desventajas que presenta y que se enumeran a continuación:

1. No permite alcanzar un buen control sobre las propiedades de las partículas producidas.
2. Recuperar el producto del molino no es fácil, dado que los hidruros en general son materiales blandos, y tras la molienda quedan reducidos a un aglomerado adherido a las paredes y bolas del molino.
3. La manipulación del producto puede ser peligroso, ya que es un polvo fino de un material altamente inflamable en contacto con el aire o con humedad.

Es por ello que en esta tesis se han desarrollado diferentes técnicas para mejorar las limitaciones de los hidruros y contribuir al desarrollo de un material de almacenamiento de hidrógeno en estado sólido con propiedades cinéticas y termodinámicas mejoradas.

## 2. OBJETIVOS

Los hidruros puros son compuestos muy prometedores para el almacenamiento de hidrógeno en estado sólido, pero presentan ciertas limitaciones termodinámicas y cinéticas. El **principal objetivo** de esta tesis es contribuir a la economía de hidrógeno mediante el desarrollo de materiales innovadores de almacenamiento de hidrógeno basados en hidruros con propiedades de liberación mejoradas en cuanto a cinéticas de liberación de hidrógeno, temperatura de descomposición y subproductos gaseosos.

Se han propuesto diferentes estrategias para superar estas limitaciones. En esta tesis se han considerados dos: (1) micronización del hidruro para reducir el tamaño de partícula y mejorar las cinéticas, y (2) confinamiento en un soporte para preservar las propiedades del material durante varios ciclos. Los objetivos específicos para llevar a cabo dichas estrategias son los siguientes:

1. Optimización de un proceso con CO<sub>2</sub> supercrítico como antisolvente para micronizar hidruros estudiando la influencia de diferentes variables de proceso (concentración de disolución, temperatura del proceso, fracción de CO<sub>2</sub>) en el tamaño de partícula final del hidruro micronizado y su influencia en las propiedades de liberación de hidrógeno. Se han comparado los resultados con los obtenidos mediante la técnica convencional de molienda mecánica.
2. Producción de aerogel con propiedades estructurales mejoradas, en términos de área superficial y poros (volumen y tamaño) utilizado como soporte en el confinamiento de hidruros, mediante proceso en batch y semicontinuo. Estudio de la influencia de las condiciones de producción de aerogel (velocidad de agitación, cantidad de catalizador, modificación superficial y relación de disolvente hidrofílico-hidrofóbico) en las propiedades finales de dicho soporte.
3. Desarrollo de diferentes procesos para confinar un hidruro (complejo) en micropartícula de aerogel de sílice como soporte.
4. Estudio de la influencia de la modificación de la superficie del soporte (aerogel de sílice hidrofílico e hidrofóbico) y proceso de impregnación en las propiedades finales de liberación de hidrógeno en el material sintetizado. Elucidar las propiedades que debería recoger el soporte y proceso de confinamiento ideal.

Se han probado varios hidruros que se han seleccionado por sus propiedades prometedoras como materiales de almacenamiento de hidrógeno: Borano de Amonio (AB, 19.6wt%), 1-2 Etano Diaminoborano (EDAB, 10 wt%), Hidruro de Magnesio ( $MgH_2$ , 7.8 wt%) y Borohidruro de Magnesio ( $Mg(BH_4)_2$ , 14.8 wt%). En la primera parte de la tesis (capítulos 1 y 2), se ha estudiado el efecto de micronización por SAS utilizando Acetato de Magnesio como precursor de  $MgH_2$  (capítulo 1), y EDAB (capítulo 2). En la segunda parte de la tesis, se ha propuesto confinamiento del hidruro como alternativa prometidora. AB ha sido confinado en micropartículas de aerogel mediante impregnación húmeda utilizando MeOH como disolvente y DCM como antisolvente seguido de secado supercrítico (capítulo 3). Previo a ello, se ha estudiado el comportamiento de AB y AB disuelto en MeOH a diferentes presiones de  $CO_2$ , para evaluar la degradación del hidruro en esas condiciones. Basado en estos resultados, se ha desarrollado un proceso novedoso para incrementar la concentración de hidruro (AB) confinado en el soporte, basado en secado con  $CO_2$  presurizado (capítulo 4). Por último,  $Mg(BH_4)_2$  fue confinado por proceso térmico en atmósfera de hidrógeno, estudiando la ciclabilidad del material de almacenamiento de hidrógeno y compararlo con el hidruro complejo puro (capítulo 5).

### 3. RESULTADOS Y DISCUSIÓN

Se ha hecho una **revisión del estado del arte** donde se recogen las diferentes técnicas que han sido investigadas para mejorar las limitaciones termodinámicas y cinéticas de los hidruros, con una búsqueda más exhaustiva en el nanoconfinamiento de hidruros en un soporte. Se podría concluir que hasta hoy en día, no existe ningún material que cumpla todas las especificaciones del Departamento de Energía (DoE).

A continuación, en los capítulos 1 y 2 de esta tesis se estudia una técnica mejorada de micronización de hidruros utilizando CO<sub>2</sub> en condiciones supercríticas. Como con esta técnica no se consigue la preservación de las propiedades durante los sucesivos ciclos, en los capítulos 3, 4 y 5 se ha estudiado el nanoconfinamiento de hidruros en partículas de aerogel de sílice utilizadas como soporte para aislar el hidruro en los poros del soporte, evitando que se aglomeren y sintericen durante su uso, y además reduciendo la posible emisión de partículas finas de hidruro inflamable.

#### CAPÍTULO 1

##### **MICRONIZACIÓN DE ACETATO DE MAGNESIO MEDIANTE PRECIPITACIÓN CON CO<sub>2</sub> SUPERCRÍTICO POR EFECTO ANTISOLVENTE (SAS) COMO PRECURSOR PARA LA PRODUCCIÓN DE HIDRURO DE MAGNESIO Y ÓXIDO DE MAGNESIO**

El objetivo de este capítulo es micronizar acetato de magnesio (MgAc), utilizado como precursor de hidruro de magnesio y de óxido de magnesio. Este hidruro ha sido muy investigado debido a su alta capacidad de almacenamiento de hidrógeno (7.8 wt%) y su bajo coste. Sin embargo, presenta limitaciones termodinámicas al necesitar temperaturas superiores a 300 °C para descomponerse así como cinéticas, debido a liberaciones lentas. Por eso ha sido propuesto la micronización de un precursor (MgAc) mediante la técnica SAS como técnica mejorada a la convencional, molienda mecánica. La ventaja de trabajar con el precursor en vez del propio hidruro, es que aquel es más estable en condiciones ambientales mientras que el hidruro de magnesio se oxida con mucha facilidad.

La técnica se basa en poner en contacto una solución orgánica en la que se encuentra disuelto el precursor del hidruro o el propio hidruro con CO<sub>2</sub> en condiciones supercríticas. Durante el proceso de mezcla, CO<sub>2</sub> se disuelve rápidamente en la solución (debido a las propiedades que presenta el CO<sub>2</sub> en este estado), produciendo la precipitación del compuesto que se quiere

micronizar por efecto antisolvente. Esta técnica se ha optimizado y utilizado en nuestro grupo de investigación para diversas aplicaciones.

Se utiliza acetato de magnesio con un tamaño de partícula medio de 200  $\mu\text{m}$ , el cual es micronizado y reducido al tamaño submicrométrico en el rango 300-700 nm tanto en el caso de molienda como mediante la técnica SAS.

Mediante la técnica convencional se obtienen partículas cristalinas con una distribución de tamaño de partículas bimodal, de forma irregular (figura 2) y bastante aglomeradas. Sin embargo, con la técnica mejorada SAS se obtienen partículas amorfas y esféricas más homogéneas con distribución de partícula unimodal ligeramente aglomeradas. Esto es debido a que esta técnica permite obtener partículas nanométricas con un mayor control sobre el tamaño final y la distribución del mismo en comparación con la molienda mecánica así como una mejora en la recogida de las mismas.

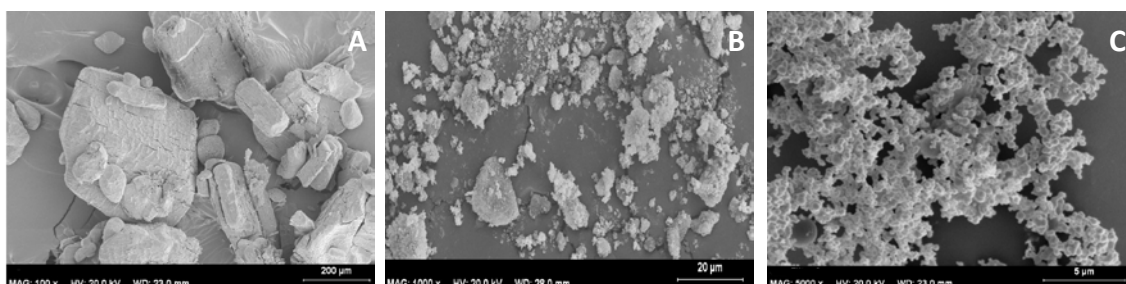


**Figura 2.** SEM de Acetato de Magnesio A) Sin procesar B) micronizado con molienda mecánica y C) micronizado mediante SAS

Se ha estudiado la influencia de la concentración de precursor en la disolución inicial (10-50 mg/mL), la temperatura (35-45  $^{\circ}\text{C}$ ) y la fracción de  $\text{CO}_2$  (0.885-0.968) del proceso de micronización SAS en el tamaño final del precursor. El factor que mayor influencia ha tenido es la concentración del precursor en la disolución inicial, obteniendo mayores tamaños de partículas con distribuciones de partículas más anchas y mayores aglomeraciones en las experiencias con mayores concentraciones de precursor. Después de ser reducido en atmósfera de hidrógeno o calcinado, el acetato se convierte en hidruro ( $\text{MgH}_2$ ) y óxido ( $\text{MgO}$ ), respectivamente.

En el caso del óxido de magnesio obtenido a partir del precursor micronizado con SAS, se ha preservado la morfología esférica de los cristales de tamaño 10-50 nm. Sin embargo,  $\text{MgO}$  obtenido directamente del precursor sin procesar era un bloque hueco con forma piramidal de varios cm de longitud.

Por otro lado,  $MgH_2$  obtenido a partir del precursor micronizado presenta cinéticas más rápidas (figura 3) debido a la reducción del tamaño y de las distancias de difusión, siguiendo la tendencia de mejores cinéticas aquellas partículas con menor tamaño del precursor. Sin embargo, sólo un tercio de la capacidad total de este hidruro ha sido liberado debido a la parcial oxidación del compuesto y/o inaccesibilidad del mismo en la reducción de la parte interna del compuesto precursor.

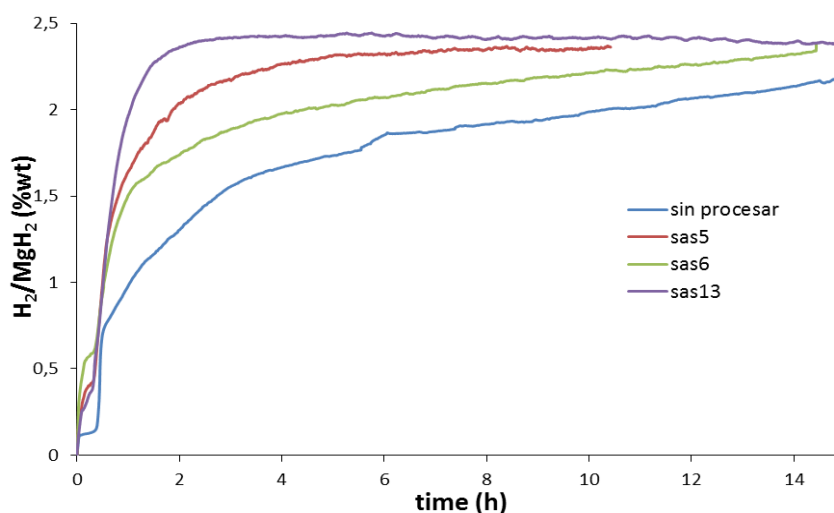


**Figura 3.** Comparativa cinéticas para  $MgH_2$  producido a partir del precursor sin procesar ( $200 \mu m$ ), después de ser micronizado en SAS obteniendo tamaños de partícula medio de  $660 \text{ nm}$  (SAS5),  $690 \text{ nm}$  (SAS6) y  $290 \text{ nm}$  (SAS13)

## CAPÍTULO 2

### **MEJORA DE LAS CINÉTICAS DE LIBERACIÓN DE HIDRÓGENO DESDE 1,2 ETANO DIAMINOBORANO (EDAB) MEDIANTE MICRONIZACIÓN CON PRECIPITACIÓN CON $CO_2$ SUPERCRÍTICO POR EFECTO ANTISOLVENTE (SAS)**

El objetivo de este capítulo es la micronización directa del hidruro 1, 2 etano diaminoborano, con un contenido en peso del 10 wt%  $H_2$  el cual es liberado a temperaturas inferiores a  $200 \text{ }^\circ C$  en una reacción de dos pasos.

Al igual que en el capítulo 1, se ha estudiado la influencia de la concentración de hidruro en la disolución inicial de THF (3.3-25.2 g/L), la temperatura del proceso en el rango  $35-45 \text{ }^\circ C$  y la fracción de  $CO_2$  (0.959-0.981). En este caso, se han obtenido tamaños de partícula similares en todas las muestras micronizadas en el rango  $1.7-2.7 \mu m$  y por tanto, los análisis calorimétricos y las cinéticas de liberación obtenidas han sido muy parecidas en todos los casos.

Como se observa en la figura 4, después de la micronización con SAS, se ha conseguido reducir el tamaño de partícula 200 veces, partiendo de un tamaño inicial de 400  $\mu\text{m}$  se ha reducido a 2  $\mu\text{m}$  con un tamaño de cristal medio de 50 nm, acortando así las distancias de difusión del hidrógeno. Este hecho ha favorecido las cinéticas de liberación de hidrógeno, reduciendo en 6 veces el tiempo necesario para liberar 3.9 wt%  $\text{H}_2$  a 100  $^\circ\text{C}$ . Además, el tiempo de inducción necesario en EDAB sin procesar para comenzar a liberar  $\text{H}_2$  es eliminado, debido a la desestabilización del mismo durante el proceso de micronización con SAS.

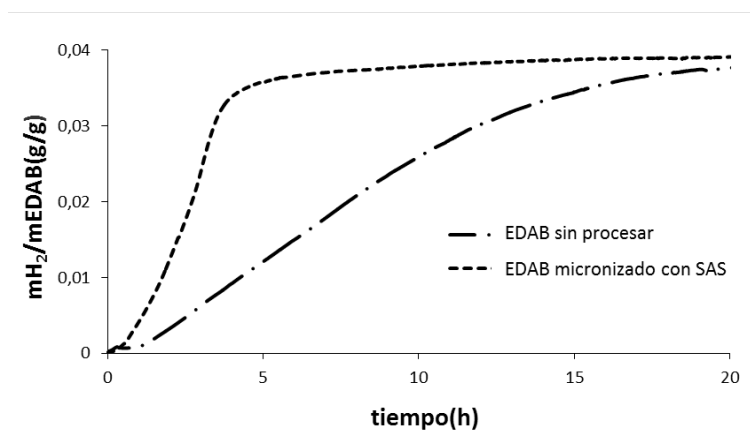
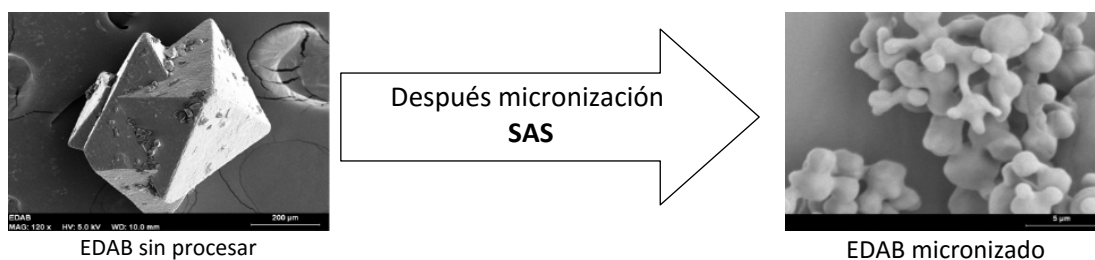


**Figura 4.** a) SEM y b) Cinéticas de liberación de hidrógeno a 100  $^\circ\text{C}$  de EDAB antes y después de micronización por SAS

Respecto a la forma que presentan las partículas, ésta también ha sufrido variaciones después de ser procesadas; la estructura prismática de EDAB puro se transformó en microesferas interconectadas entre ellas.

En cuanto a los análisis térmicos realizados (calorimetría diferencial de barrido, DSC) a las diferentes muestras micronizadas con SAS muestran una reducción de 7  $^\circ\text{C}$  y 3  $^\circ\text{C}$  en la temperatura de las dos etapas de descomposición de este hidruro, reduciendo los valores de los picos de temperaturas 141.1  $^\circ\text{C}$  y 190.9  $^\circ\text{C}$  observadas para EDAB sin procesar a 134.1  $^\circ\text{C}$  y 187.1  $^\circ\text{C}$  en la muestra de EDAB después de ser micronizada con SAS. Esto es debido a la reducción del tamaño de partícula y del grano, y por tanto reducción en la distancia de difusión.

El problema que presenta la micronización de hidruros es que esta técnica no evita ni asegura que las propiedades se preserven durante varios ciclos, produciéndose aglomeraciones de las partículas durante el proceso de calentamiento de las mismas que es necesario para liberar su contenido de hidrógeno por termólisis. Es por ello, que se ha propuesto el uso de un soporte para preservar las propiedades con el tiempo en los próximos capítulos.

### **CAPÍTULO 3**

#### **PRODUCCIÓN DE PARTÍCULAS DE AEROGEL DE SÍLICE CARGADAS CON BORANO DE AMONIO MEDIANTE SECADO SUPERCRÍTICO EN BATCH Y SEMICONTINUO**

En este capítulo, se ha utilizado borano de amonio (AB) como hidruro prometedor debido al alto contenido gravimétrico de hidrógeno (19,6 wt%), bajo peso molecular (30,7 g/mol), temperaturas moderadas de descomposición y estabilidad en condiciones atmosféricas. Sin embargo, presenta limitaciones cinéticas debido a largos tiempos de inducción para romper el enlace de dihidrógeno y liberaciones de hidrógeno lentas. Además, aparte de hidrógeno, este gas suele ir acompañado de otros gases volátiles como borazina o diborano que podrían dañar la celda de combustible. Por este motivo se estudia el nanoconfinamiento de AB en un soporte para mejorar las limitaciones que presenta.

Se han utilizado partículas de aerogel de sílice como soporte para estabilizar y encapsular el hidruro. El método de producción se basa en el método sol-gel seguido de secado en condiciones supercríticas. Para ello se utiliza tetrametilortosilicato (TMOS) como precursor y metanol como disolvente seguido por una reacción hidrólisis-condensación (reacciones 1 y 2) utilizando hidróxido amónico como catalizador.



Una vez que se ha sintetizado el alcogel, es necesario el envejecimiento del mismo en un medio alcohólico, en este caso, el mismo que durante la síntesis, metanol durante al menos 5 días. Durante este periodo, la dureza y rigidez del gel se ven modificadas debido a las reacciones de condensación y reordenación de los siloxanos dentro de la red del propio gel. La disolución y reprecipitación de sílice así como la unión de oligómeros que no hayan reaccionado o que se añadan, participan durante este periodo.

A continuación, es necesario el secado del gel, una de las etapas más críticas del proceso de producción de dichos materiales y que va a tener gran influencia en las propiedades

superficiales finales del mismo. Durante el proceso de secado, se procede a la extracción del disolvente (metanol en nuestro caso) de la estructura del alcogel.

Se ha secado utilizando CO<sub>2</sub> en condiciones supercríticas en batch y semicontinuo. El secado con fluidos supercríticos es una técnica que permite evitar los problemas inherentes a otras técnicas, preservando así las propiedades del material. Esto es debido a que al encontrarse en un estado supercrítico, no se forma interfase gas-líquido, y por lo tanto se eviten las tensiones mecánicas asociadas con esta interfase (por ejemplo, por fuerzas de capilaridad). De este modo se obtiene un soporte con propiedades superficiales superiores a los obtenidos con otros métodos de secado más tradicionales.

Durante el proceso de producción de partículas de alcogel se ha estudiado la influencia de la velocidad de agitación durante el proceso de producción de las partículas de alcogel en el rango 500-700 rpm, la cantidad de catalizador en el proceso sol-gel en el rango 2.3-5.8 mM, la cantidad de hexano utilizado como disolvente hidrofóbico dispersante para evitar que se aglomeren (relación disolvente hidrofóbico/hidrofílico entre 0.3 y 0.9) y la modificación de la hidrofobicidad superficial en el tamaño de partícula final de aerogel. Como resultado, se han formado partículas irregulares en el caso de aerogeles hidrofílicos, mientras que se han obtenido partículas regulares y esféricas en el caso de aerogeles hidrofóbicos. La distribución de tamaño de partícula ha sido similar en todos los experimentos realizados con un tamaño de partícula medio entre 12 y 30  $\mu\text{m}$ . La diferencia de esfericidad entre partículas hidrofílicas e hidrófobas puede ser debido a la mayor flexibilidad de las últimas que impide la erosión durante la agitación en el proceso sol-gel y las menores reacciones de reticulación durante el envejecimiento de las mismas.

En el caso del secado semicontinuo, con reducción del tiempo de operación respecto al proceso discontinuo, se formaron partículas con tamaño medio similares, en el rango 17-19  $\mu\text{m}$ . Se ha estudiado la influencia de la concentración del alcogel alimentado en la planta de secado en el rango 3-6 g/L en las propiedades superficiales del aerogel; obteniendo mayores áreas superficiales (400-800  $\text{m}^2/\text{g}$ ), y volúmenes de poro (0.5-0.8  $\text{cm}^3/\text{g}$ ) en los experimentos en los que se ha operado con mayores concentraciones de alcogel.

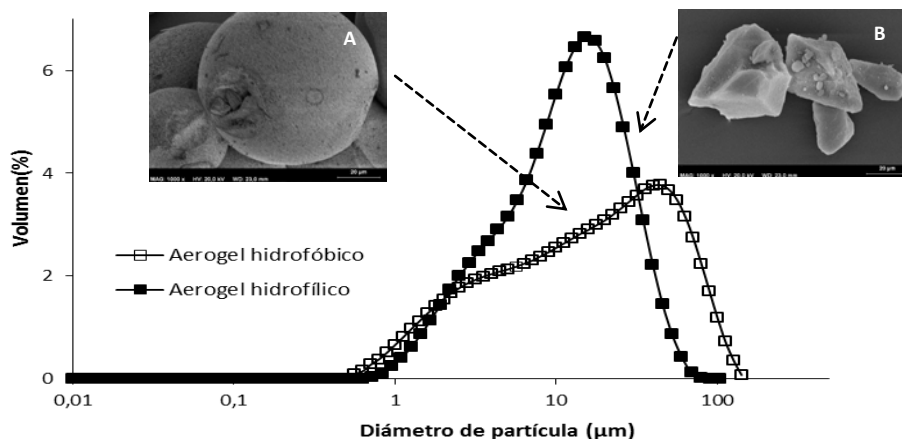


**Figura 5.** Distribución de tamaño de partícula y SEM de partículas hidrofóbicas (A) e hidrofílicas (B) de aerogel de sílice

Para confinar amonio de borano en las partículas de aerogel de sílice se ha utilizado el método de impregnación húmeda seguido de precipitación por adicción de diclorometano (DCM) por efecto antisolvente y secado en discontinuo con  $\text{CO}_2$  en condiciones supercríticas. Se ha conseguido encapsular entre 1-5 wt% AB dependiendo de la funcionalización superficial del soporte, siendo 1 wt% para partículas hidrofílicas (con grupos  $-\text{OH}$  en la superficie del aerogel) mientras que hasta 5 wt% en partículas hidrófobas, en las que se han intercambiado alguno de los grupos  $-\text{OH}$  por  $-\text{CH}_3$  en la superficie del aerogel. Esta baja eficiencia de carga podría ser explicada por la posibilidad de pérdida de AB durante el lavado con DCM y/o la descomposición del hidruro durante el secado supercrítico en presencia de la sílice.

Para analizar esta segunda opción de descomposición del hidruro durante la etapa de secado supercrítico, se ha comprobado que AB es estable con  $\text{CO}_2$  en condiciones sub y supercríticas, en el rango 5-15 MPa a 40-50  $^{\circ}\text{C}$ , estudiando los enlaces del hidruro después de estar en contacto desde 45 min y hasta 240 min. Sin embargo, en el caso de una solución de AB en metanol en contacto con  $\text{CO}_2$  incluso a 35  $^{\circ}\text{C}$  y presión de 5 MPa se descompone liberando hidrógeno debido a metanólisis acelerada por efecto  $\text{CO}_2$ .

Pese al problema de la baja carga, la figura 6 muestra la mejora significativa de las cinéticas de liberación, obteniendo mejores resultados en las muestras confinadas en aerogel de sílice, incluso más rápidas que después de ser micronizadas mediante molienda mecánica. Sin embargo, debido a la baja concentración de hidruro depositado en el aerogel, el contenido total de  $\text{H}_2$  en el material se encuentra aún por debajo de lo estipulado por el DoE.

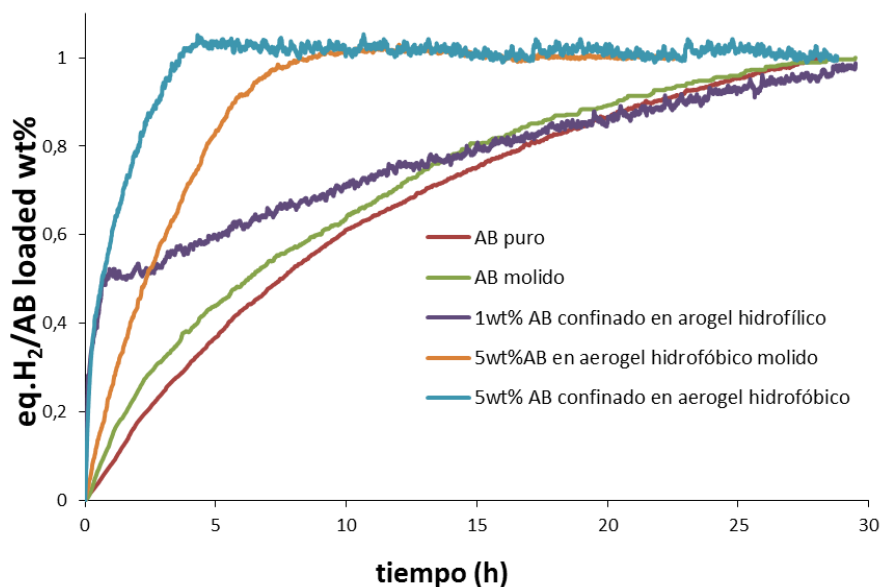


**Figura 6.** Cinéticas de liberación de hidrógeno a 80 °C. Comparativa de AB puro, AB después de ser molido y AB confinado en aerogel de sílice hidrofílico e hidrofóbico.

#### CAPÍTULO 4

##### **MEJORA DE LAS CINÉTICAS DE LIBERACIÓN DE HIDRÓGENO DE AMONIO DE BORANO CONFINADO EN AEROGEL DE SÍLICE**

El objetivo de este capítulo es incrementar la concentración de amonio de borano confinado conseguido en el anterior capítulo utilizando el mismo soporte, partículas de aerogel de sílice hidrofílicas. Para ello, se ha utilizado un proceso innovador que permite obtener partículas de aerogel de sílice con propiedades superficiales mejoradas, área superficial de 887 m<sup>2</sup>/g y hasta 2 cm<sup>3</sup>/g de volumen de poros. A la vista de los resultados obtenidos en el capítulo anterior, se plantea la hipótesis de que mediante la reducción de la temperatura se conseguirá limitar la descomposición del hidruro durante el proceso de secado.

Los resultados han permitido probar esta hipótesis, puesto que con esta modificación en las condiciones de secado se han conseguido concentraciones hasta 60 wt% AB, siendo la primera vez que se consigue superar concentraciones de 50 wt% de un hidruro estabilizado en un soporte. Para ello se ha seguido el método de impregnación húmeda seguido de secado con CO<sub>2</sub> en condiciones subcríticas para evitar la descomposición de AB y el arrastre del hidruro durante los lavados. Durante el secado, se produce la extracción de disolvente simultánea a la precipitación de AB por efecto antisolvente en los poros del aerogel de sílice.

Se ha estudiado la influencia de la concentración de AB confinado en las propiedades térmicas y estructurales del producto final sintetizado.

Como resultado, se ha obtenido un material homogéneo con propiedades cinéticas y termodinámicas mejoradas respecto AB puro. Por un lado, los análisis térmicos corroboran las mejoras del nanoconfinamiento al descomponerse a temperaturas inferiores al hidruro puro.

La entalpia de descomposición fue reducida después del nanoconfinamiento, de  $-24,9$  KJ/mol AB del hidruro puro a  $-5,5$  KJ/mol para la muestra con 30 wt% AB confinada en aerogel de sílice, obteniendo mayor reducción a mayores concentraciones de sílice. Además, la figura 7 muestra las cinéticas de liberación de hidrógeno a  $80$  °C, que son más rápidas con tiempos de inducción muy reducidos en las muestras donde AB está confinado respecto AB puro. Estas cinéticas son más rápidas en las muestras con mayor cantidad de sílice debido a que éste actúa como desestabilizador o catalizador, o lo que es lo mismo para concentraciones de AB bajas debido a que el efecto de superficie es mayor y además el hidruro precipita con menor tamaño en las muestras con menores concentraciones de AB.

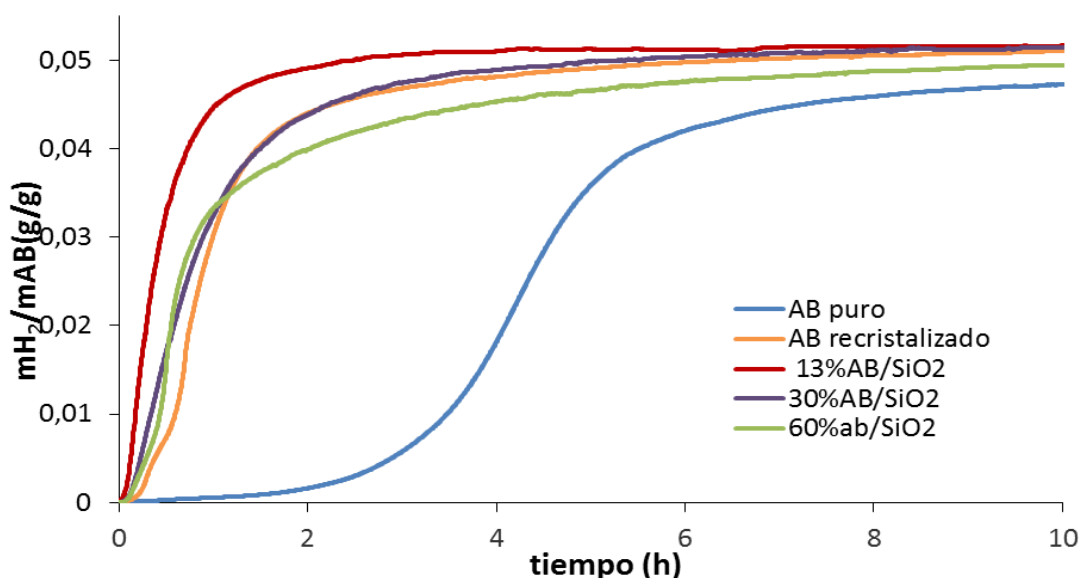


**Figura 7.** Cinéticas de liberación de hidrógeno isotérmicas a  $80$  °C en AB puro y AB confinado en aerogel de sílice hidrofílico con diferentes concentraciones. (Las curvas están normalizadas con la cantidad de AB en la muestra)

Por otro lado, se ha reducido la cantidad de gases volátiles que se liberan junto al hidrógeno y podrían dañar la celda de combustible debido a la reducción del tamaño del hidruro y la presencia de los grupos SiOH y SiOSi propios del aerogel de sílice.

Además, debido al nanoconfinamiento de AB, las propiedades morfológicas del material se han preservado después de la liberación isotérmica de hidrógeno, evitando el proceso 'foaming' típico de AB puro (figura 8). Así se facilita la recogida del poliaminoborano subproducto de la reacción y posiblemente favorecería el proceso de regeneración. Sin embargo, el estudio detallado de la regeneración es una de las tareas futuras a desarrollar para poder corroborar dicha mejora.

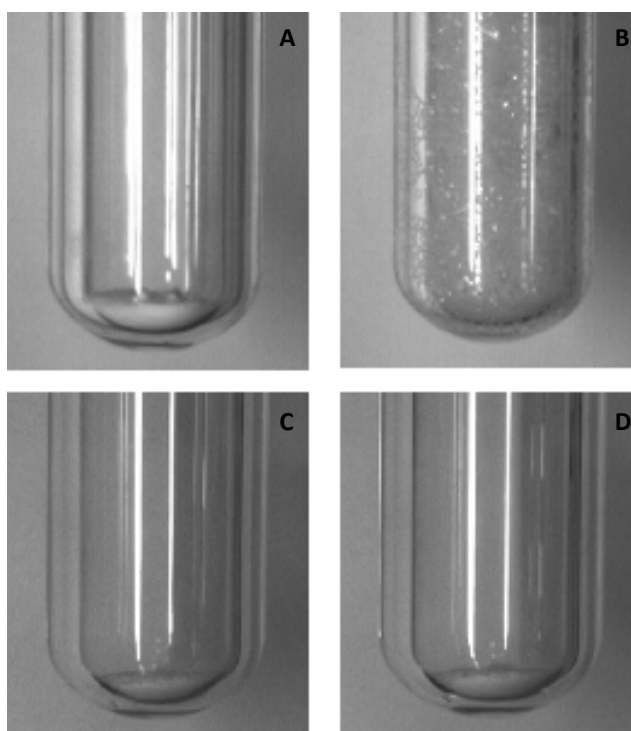


**Figura 8.** Fotografías de AB puro y 60 wt% AB confinado en aerogel de sílice antes y después de liberación de  $H_2$  a  $80\text{ }^\circ\text{C}$  a) AB puro antes liberación, b) AB puro después liberación, c) AB/SiO<sub>2</sub> antes liberación, d) AB-SiO<sub>2</sub> después liberación.

Todas estas mejoras podrían deberse por un lado a la formación de diamoniato de diborano (DEADB), isómero de AB identificado por difracción de rayos X y cuyas propiedades de descomposición térmicas son mejores respecto al AB puro. Por otro lado, a este hecho se le añade el efecto de interacción de AB con los grupos hidroxilos de la sílice, desestabilizando al hidruro y mejorando el proceso de descomposición y liberación de hidrógeno.

## **CAPÍTULO 5**

### **SORCIÓN DE HIDRÓGENO REVERSIBLE EN EL COMPOSITE FORMADO POR BOROHI DRURO DE MAGNESIO Y AEROGEL DE SÍLICE**

El trabajo de este capítulo ha sido realizado en los laboratorios de Hidrógeno de Pavía (Italia) durante dos estancias de 3 meses de duración cada una. El objetivo es estudiar las propiedades termodinámicas, cinéticas y la reversibilidad en el composite formado por  $\text{Mg}(\text{BH}_4)_2$  y partículas de aerogel de sílice hidrofílicas. Este hidruro con alta capacidad gravimétrica y volumétrica (14,8 wt%  $\text{H}_2$ , 0,112 Kg/L), presenta limitaciones cinéticas y termodinámicas, además de las altas condiciones de presión y temperatura en atmósfera de hidrógeno que son necesarias para ser regenerado debido a la formación de compuestos intermediarios estables.

Estos composites se han sintetizado por tratamiento térmico en atmósfera de hidrógeno a 120 bar y 200 °C. Como resultado, las propiedades de sorción del composite fueron mejoradas respecto al hidruro complejo puro. Por un lado, como muestra la figura 9, se ha reducido en 60 °C la temperatura de descomposición del borohidruro debido a la presencia de la sílice como desestabilizador. Además, las cinéticas de liberación de hidrógeno en el primer ciclo a 300 °C fueron 2 veces más rápidas en los composites que en  $\text{Mg}(\text{BH}_4)_2$  puro.

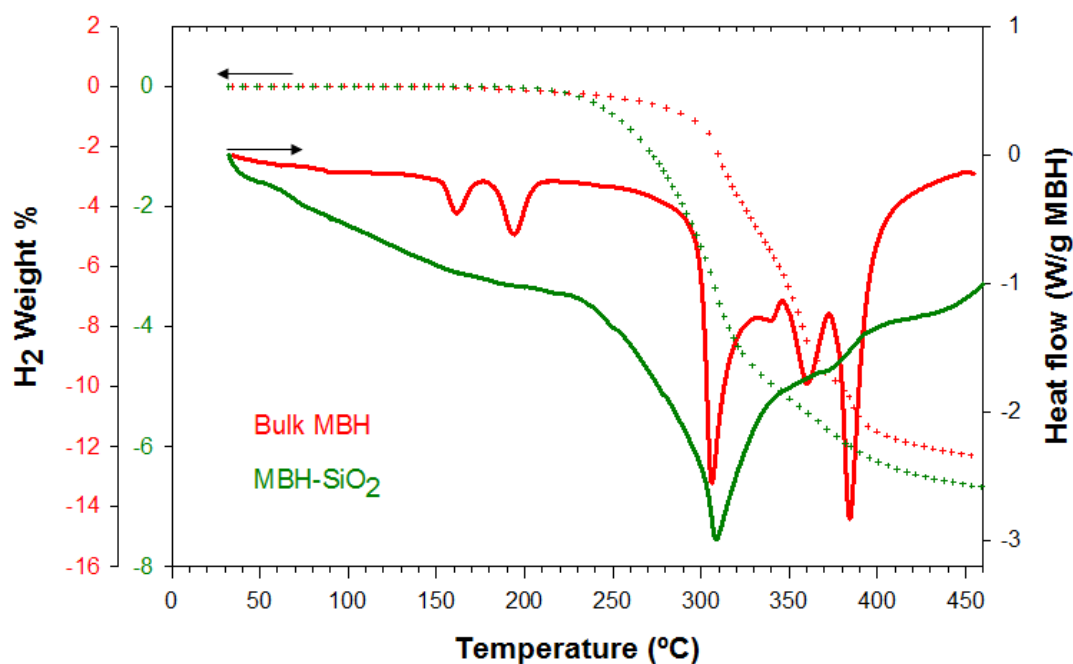


**Figura 9.** Medida simultánea de calorimetría de barrido (DSC) y manométrica de  $\text{Mg}(\text{BH}_4)_2$  puro y del composite  $\text{Mg}(\text{BH}_4)_2$  con aerogel de sílice. Las líneas sólidas se corresponden con los análisis DSC (eje 'y' derecha) y línea punteada corresponde a medida manométrica (eje 'y' izquierda)

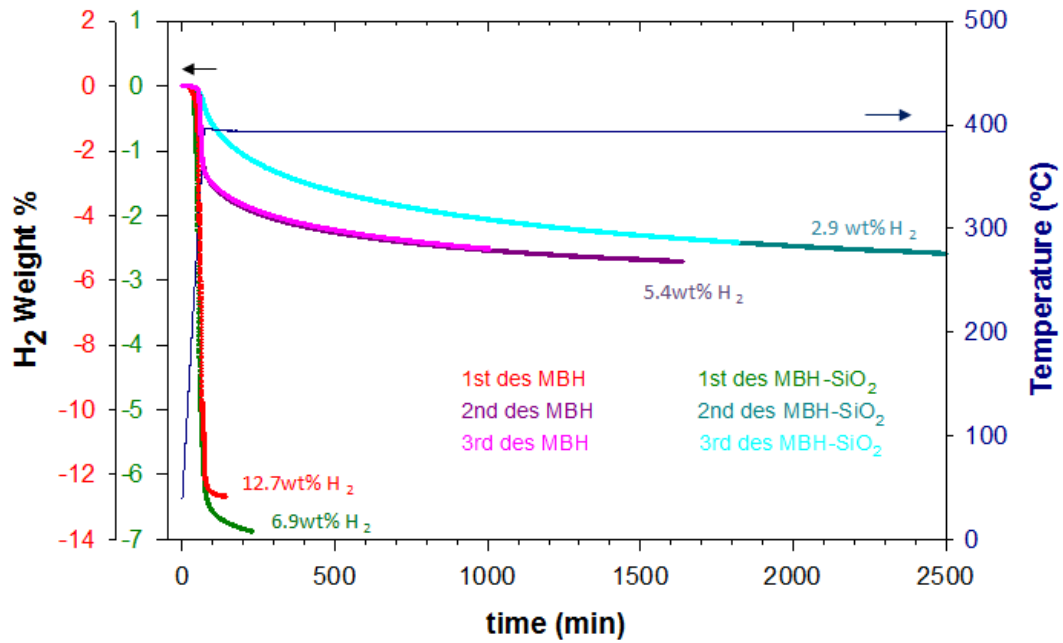


**Figura 10.** Cinéticas liberación hidrógeno durante 3 ciclos a 400 °C para  $Mg(BH_4)_2$  puro y composite formado por  $Mg(BH_4)_2$  y aerogel de sílice ( $SiO_2$ )

Respecto a la reversibilidad, ha sido la primera vez que se ha conseguido hasta 6 wt%  $H_2$  reversible en condiciones moderadas de 390 °C y 110 bar de hidrógeno, como se puede comprobar en la figura 10.

Estos resultados indican que el aerogel de sílice interactúa químicamente con el hidruro como aditivo, el cual podría afectar en la ruta de descomposición del mismo, formando diferentes cantidades de compuestos intermedios, mejorando las cinéticas y ciclabilidad de dicho material de almacenamiento de hidrógeno.

#### 4. CONCLUSIONES

Este trabajo contribuye al desarrollo de nuevos materiales de almacenamiento de hidrógeno sólido basado en hidruros con propiedades mejoradas. Se han evaluado dos alternativas diferentes para superar las limitaciones de los hidruros puros. Las conclusiones más importantes se resumen a continuación:

##### 1. Micronización de hidruros mediante proceso con CO<sub>2</sub> supercrítico

- Se han utilizado dos hidruros diferentes: MgAc, precursor de MgH<sub>2</sub>, y EDAB han sido micronizados con éxito mediante precipitación con CO<sub>2</sub> supercrítico por efecto antisolvente (SAS). En ambos estudios, se concluye que la concentración de la solución de entrada, que ha sido evaluada en el rango 10-40 mg/mL para MgAc y 3.3-25 mg/mL para EDAB, fue el parámetro más importante que influenció en el tamaño de partícula obteniendo partículas más grandes con distribución de la misma más anchas a mayores concentraciones de solución, cuyo efecto fue más pronunciado en la micronización de MgAc.
- Después de la micronización de MgAc, precursor de MgH<sub>2</sub>, partículas cristalinas de 200 μm con forma irregular fueron transformadas en partículas amorfas micronizadas con un tamaño medio de 300-600 nm con forma esférica regular. Las cinéticas de MgH<sub>2</sub> fueron drásticamente mejoradas, reduciendo el tiempo para liberar 2 wt% H<sub>2</sub> de 10 h en el hidruro puro a 1 h para el caso de las partículas micronizadas de menor tamaño. Este efecto fue asociado a la reducción del tamaño de partícula y por tanto de las distancias de difusión de hidrógeno. Sin embargo, sólo 1/3 del precursor se convirtió en MgH<sub>2</sub> y liberó hidrógeno, debido a la inaccesibilidad para hidrogenar la parte central de la partícula, o a la oxidación del metal, Mg.
- EDAB ha sido también micronizado mediante proceso SAS. En este caso, partículas prismáticas de EDAB de 400 μm con tamaño de cristal de 100 nm fueron reducidas a 2 μm con tamaño de cristal de 50 nm cambiando la forma a microesferas interconectadas entre ellas. Esta reducción en el tamaño de partícula se vio reflejado en reducción de 7 °C en la temperatura de descomposición y aceleración de las cinéticas después del proceso de micronización. En el caso de las cinéticas de liberación de hidrógeno a 100 °C, la reducción del tamaño de partícula y del grano hizo que el tiempo para liberar 3.9

wt% H<sub>2</sub> fuera reducido por un factor 6. Además, el tiempo de inducción fue suprimido debido a la desestabilización del hidruro después del tratamiento.

Se concluyó que el proceso SAS es una técnica prometedora para micronizar hidruros y mejorar las cinéticas de liberación de hidrógeno debido a la reducción del tamaño de partícula y por tanto de las distancias de difusión. Con esta técnica, fue posible controlar el tamaño de partícula de las muestras micronizadas modificando las condiciones del proceso y las partículas fueron recogidas con facilidad a diferencia de la técnica convencional, molienda mecánica.

Sin embargo, la reducción del tamaño de partícula se pierde después de varios ciclos. Por eso, fue necesario encontrar una alternativa que evitara el crecimiento del hidruro durante el ciclaje del mismo.

## **2. Nanoconfinamiento de hidruros en un soporte**

- La producción de micropartículas de aerogel de sílice ha sido optimizada para ser utilizada como soporte mediante nanoconfinamiento de AB y Mg(BH<sub>4</sub>)<sub>2</sub>. Es la primera vez que se utiliza este material como soporte para esta aplicación. Se ha obtenido un soporte con propiedades extraordinarias, con tamaño medio en el rango 13-30 μm con área superficial de 600-900 m<sup>2</sup>/g y 0.5-2 cm<sup>3</sup>/g de volumen de poros mediante el método sol-gel seguido de secado con CO<sub>2</sub> presurizado o en condiciones supercríticas.
- Partículas irregulares se formaron en el caso de aerogel de sílice hidrofílico mientras que microesferas con superficie lisa en el caso de aerogel de sílice hidrofóbico. Esta diferencia se atribuyó a la elasticidad y velocidad más lenta de formación de las últimas partículas.
- Micropartículas de aerogel de sílice se han propuesto como soporte para confinar hasta 60 wt% AB utilizando un proceso novedoso basado en secado de aerogel simultáneo a la precipitación de AB utilizando CO<sub>2</sub> comprimido. Es la primera vez que se han conseguido concentraciones tan altas de un hidruro confinado en una matriz. Mediante confinamiento, se ha obtenido una dispersión homogénea de AB en el aerogel con propiedades de descomposición del hidruro mejoradas. Las cinéticas han sido aceleradas con reducción drástica del tiempo de inducción debido a la reducción del tamaño de partícula y la presencia de los grupos Si-OH que podrían debilitar los enlaces B-H y crear defectos en el soporte y por lo tanto comenzar la descomposición a menores temperaturas favoreciendo la liberación de hidrógeno. Más de 12 h fueron necesarias

para liberar 5 wt% H<sub>2</sub> en AB puro mientras que menos de 2 h en el caso de AB confinado en aerogel de sílice. Además, el proceso 'foaming' se evitó, lo cual podría ser beneficioso para el proceso de regeneración.

- Ha sido obtenido un composite de micropartículas de aerogel de sílice y Mg(BH<sub>4</sub>)<sub>2</sub> después de un proceso térmico en atmósfera de hidrógeno. La temperatura de descomposición del MBH puro se redujo 60 °C y el mecanismo de descomposición se modificó en el composite. Las medidas calorimétricas mostraron que los tres pasos de descomposición de MBH puro se convirtieron en uno sólo en el rango 240-400 °C para los composites de MBH-SiO<sub>2</sub>. En este caso, la sílice actuó como aditivo cambiando la ruta de descomposición. Además, las cinéticas de la primera deshidrogenación a 300 °C fue dos veces más rápida comparadas con MBH puro. Es la primera vez que MBH infiltrado en sílice fue parcialmente reversible en condiciones de presión y temperatura moderadas y casi 6 wt% H<sub>2</sub> fue rehidrogenado después de realizar la desorción a 400 °C en vacío.

## **ACKNOWLEDGMENTS**

En primer lugar, quiero agradecer a mi director de tesis, Ángel Martín, por confiar en mí para llevar a cabo este proyecto así como por toda la ayuda recibida a lo largo de todos estos años; sus ideas, creatividad y rapidez a la hora de encontrar una alternativa han hecho que esta tesis continuara hacia adelante y me han hecho crecer como investigadora.

I would like to acknowledge Prof. Chiara Milanese and Prof. Amedeo Marini for giving me the opportunity to carry out a research in their group in Hydrogen Lab at Pavia (Italy) and for the guidance and advice during my stay. I also would like to thank Alessandro Girella for helping me in the lab with the analyses and the rest of members of the group for all the good advices and the pleasant work environment.

Me gustaría agradecer al programa de becas FPI-UVa (Formación del Personal Investigador de la Universidad de Valladolid) por la financiación recibida a lo largo de estos 4 años y a la Fundación Iberdrola por la ayuda recibida para poder dar continuidad a este tesis durante al menos un año (09-2016 a 09-2017).

A los compañeros del Departamento, los que están y los que ya se fueron, a todos aquellos que de alguna manera han contribuido en esta tesis con consejos, ideas y compartiendo momentos durante todo este camino.

Tengo que agradecer de forma especial a O.B.R., quien me ha dado fuerza para continuar con la tesis en aquellos momentos más difíciles, a tus consejos sabios, por enseñarme a confiar más en mí y todos esos momentos que han hecho que recuerde siempre estos años de manera muy especial. Todos esos logros que he ido consiguiendo al finalizar esta tesis no habrían sido posibles sin ti.

Por supuesto a mi familia y amigos/as, en especial a mis padres, mi hermana y a mi cuñado Roberto, porque como bien dices en tu libro, *'A veces no hacen falta los ojos para ver lo realmente importante'*. Por todo vuestro apoyo, por estar siempre ahí, vuestros consejos y la confianza que siempre tenéis en mí.

Simplemente, **GRACIAS.**



## ABOUT THE AUTHOR

---



**Miriam Rueda Noriega** (Valladolid, 1987) started the studies of Chemical Engineering at University of Valladolid in 2005. In the academic course 2010-2011 she spent 9 months at the Technical University of Denmark (DTU) for the development of the final project 'Oil water emulsions in advanced waterflooding' in the frame of the Erasmus Program, being the first contact with research.

At the return from Denmark, she graduated (September 2011) and joined to the High Pressure Processes Group of the Department of Chemical Engineering (University of Valladolid) for a M.S. in Thermodynamic Engineering of Fluids, and continued with the PhD in Chemical Engineering and Environmental Technology, framed in the National project ENE2011-24547 'Light Hydrogen Storage materials for mobile applications', starting in September 2012. During the Ph.D. Thesis the author completed its research work with two international doctoral internships at Pavia Hydrogen Lab, at the Chemistry Department of Pavia University (Italy) during 2014 and 2015.

## **LIST OF PUBLICATIONS**

---

- [1] **Rueda M.**, Sanz-Moral L.M, Segovia J.J, Martín A. 'Enhancement of hydrogen release kinetics from ethane 1,2 diamineborane (EDAB) by micronization using Supercritical Antisolvent Precipitation (SAS)'. *Chemical Engineering Journal* 306 (2016) 164-173
- [2] **Rueda M.**, Sanz-Moral L.M., Girella A., Cofrancesco. P., Milanese. C., Martín A. 'Reversible hydrogen sorption in the composite made of magnesium borohydride and silica aerogel'. *International Journal of Hydrogen Energy* 41 (2016) 15245-15253
- [3] Sanz-Moral L.M., Romero A., Holz F., **Rueda M.**, Navarrete A., Martín A. 'Tuned Pd/SiO<sub>2</sub> aerogel catalyst prepared by different synthesis techniques'. *Journal of the Taiwan Institute of Chemical Engineers* 65 (2016) 515-521
- [4] Mustapa A.N, Martín A, Sanz-Moral L.M, **Rueda M**, Cocero M.J. 'Impregnation of medicinal plant phytochemical compounds into silica and alginate aerogels'. *Journal of Supercritical Fluids* 116 (2016) 251-263
- [5] **Rueda M.**, Sanz-Moral L.M., Martín.A. 'Micronization of Magnesium Acetate by the Supercritical Antisolvent Process as a precursor for the production of magnesium oxide and magnesium hydride'. *Crystal Grow Design* 14 (2014) 4768-4776
- [6] **Rueda M.**, Sanz-Moral L.M., Nieto-Marquez A., Longone P., Mattea F., Martín A. 'Production of silica aerogel microparticles loaded with ammonia borane by batch and semicontinuous supercritical drying techniques'. *The Journal of Supercritical Fluids* 92 (2014) 299-310
- [7] Sanz-Moral L.M., **Rueda M.**, Mato R., Martín A. 'View cell investigation of silica aerogels during supercritical drying: Analysis of size variation and mass transfer mechanisms'. *The Journal of Supercritical Fluids* 92 (2014) 24-30
- [8] Sanz-Moral L.M., **Rueda M.**, Nieto A., Novak Z., Zeljknoz K., Martín A. 'Gradual hydrophobic surface functionalization of dry silica aerogels by reaction with silane precursors dissolved in supercritical carbon dioxide'. *The Journal of Supercritical Fluids* 84 (2013) 74-79

---

### Submitted

- [1] **Rueda M.**, Sanz-Moral, Segovia J.J, Martín A. 'Improvement of the kinetics of hydrogen release from ammonia borane confined in silica aerogel'. Microporous and Mesoporous Materials.

---

## **PATENTS**

**Rueda M.**, Sanz-Moral L.M, Navarrete A., Martín A. 'Material y procedimiento para el almacenamiento y regulación de la liberación de hidrógeno en estado sólido'. P201500170.

---

## **CONTRIBUTIONS TO CONFERENCES**

### ORAL COMMUNICATIONS

- **Rueda M.**, Sanz-Moral L.M., Saldan I., Girella A., Milanese C., Martín A. *Improvement properties in the composite magnesium borohydride infiltrated in silica aerogel*. 15th International Symposium on Metal-Hydrogen Systems, Interlaken (Switzerland). August 7-12, 2016.
- Sanz-Moral L.M., **Rueda M.**, Navarrete A., Sturm G., Link G., Stefanidis G., Martín A. *Microwave for H<sub>2</sub> release from ethane 1,2 diamineborane infiltrated in C/SiO<sub>2</sub> aerogel*. 15th International Symposium on Metal-Hydrogen Systems, Interlaken (Switzerland). August 7-12, 2016.
- Sanz-Moral L.M., Navarrete A., Sturm G., Link G., Stefanidis G., **Rueda M.**, Martín A. *Hydrogen from solids by microwave influence*. 3<sup>rd</sup> Global Congress on Microwave Energy Applications, Cartagena (Spain) July 25-29, 2016.
- Sanz-Moral L.M., **Rueda M.**, Navarrete A., Romero A., Nieto-Márquez A., Martín A. *Síntesis y funcionalización de aerogeles para su uso en catálisis y almacenamiento de hidrógeno*. II Encuentro de Jóvenes investigadores de la Secat, Ciudad Real (Spain) June 27-29, 2016.
- Sanz-Moral L.M., Holz F., **Rueda M.**, Romero A., Navarrete A., Martín A. *Silica aerogels; alternative matrix for catalytic palladium nanoparticles*. 5th Portuguese Young Chemists Meeting and 1st European Young Chemists Meeting, Guimaraes (Portugal). April 26-29, 2016.

- **Rueda M.** *Técnicas innovadoras para mejorar almacenamiento de hidrógeno en estado sólido basado en hidruros.* II Ciclo de Conferencias Investigadoras de la UVa en la Aventura de la Ciencia y la Tecnología, Escuela Ingenierías Industriales, Universidad Valladolid (España). March 4, 2016.
- **Milanese C.**, Girella A., Valsecchi G., Cabrini C., Pallavicini P., Galinetto P., Saldan I., **Rueda M.**, Martín A., Pontiroli D., Gaboardi M., Magnani G., Riccò M., Marini A. *Reversible hydrogen sorption for the infiltrated Magnesium Borohydride.* 10th Symposium Hydrogen Energy, , Sendai (Japan). February 21-26, 2016.
- **Rueda M.**, Sanz-Moral L.M., Martín A. *Enhanced hydrogen storage material by stabilization of ammonia borane in microparticles of silica aerogel.* E-MRS 2015 Fall Meeting, , University of Warsaw (Poland). September 15-18, 2015.
- **Saldan I.**, Milanese C., Girella A., **Rueda M.**, Martín A., Kovalyshyn Y., Reshetnyak O., Marzanoli V., Cabrini E., Pallavicini P., Marini A. *Reversible hydrogen sorption for the infiltrated Magnesium Borohydride.* Functional Materials and Nanotechnologies, Vilnius (Lituania). October 5-8, 2015,.
- **Sanz L.M.**, **Rueda M.**, Martín A., Cocero M.J. *View cell investigation of silica aerogels during supercritical drying: Analysis of size variation and mass transfer mechanisms.* International Seminar on Aerogels. Properties-Manufacture-Applications., Hamburg University (Germany). October 6-7, 2014.
- **Rueda M.**, Mattea F, Martín A., Cocero M.J. *Hydrogen storage in hydride-loaded silica aerogel microparticles.* 6th International Symposium on High Pressure processes Technology, Belgrade (Serbia). September 8-11, 2013,
- **Rueda M.**, Fraile M., Martín A., Cocero M.J. *Formulación de ibuprofeno mediante extracción de emulsiones.* 4th International Seminar on Engineering Thermodynamic of Fluids, Tarragona (España). July 23-24, 2012.

### **POSTER COMMUNICATIONS**

- **Martín A.**, Sanz-Moral L.M., **Rueda M.**, Valero-Pedraza M.J., Navarrete A. *Improvement of the kinetics from solid hydrides by nanoconfinement employing supercritical technologies.* 15th European Meeting on Supercritical Fluids, Essen (Germany). May 8-11, 2016

- Martín A., Navarretete A., **Rueda M.**, Sanz-Moral L.M., Romero A. *Improvement of the kinetics of hydrogen release from hydrides confined in silica aerogel*. IV Iberoamerican Conference Supercritical Fluids, Viña del Mar (Chile). March 28- April 4, 2016.
- Milanese C., Girella A., Saldan I., **Rueda M.**, Martín A., Marini A. *Reversible hydrogen sorption for the infiltrated Magnesium Borohydride*. 1<sup>st</sup> European Conference on Physical and Theoretical Chemistry and XLII Annual Meeting of the Physical Chemistry Division of SCI, Catania (Italia). September 14-18, 2015.
- **Rueda M.**, Sanz-Moral L.M., Martín A, Cocero M.J. *Hydrogen storage by stabilizing magnesium hydride in microparticles of silica aerogel*. International Seminar on Aerogels. Properties-Manufacture-Applications, Hamburg University (Germany). October 6-7, 2014.
- **Rueda M.**, Sanz-Moral L.M., Martín A. *Micronized MgH<sub>2</sub> and MgO by Supercritical Antisolvent process*. 14th International Symposium on Metal-Hydrogen Systems, Manchester (UK). July 20-25, 2014.
- Sanz-Moral L.M., **Rueda M.**, Martín A. *MgH<sub>2</sub>/Pd nanoparticles embedded in silica aerogel monoliths*. 14th International Symposium on Metal-Hydrogen Systems, Manchester (UK). July 20-25, 2014.
- **Rueda M.**, Sanz-Moral L.M., Martín A., Cocero M.J. *Micronization of magnesium acetate by Supercritical Antisolvent process as precursor for the production of magnesium oxide and magnesium hydride*. 14th European meeting on Supercritical Fluids, Marseille (France). May 18-21, 2014.
- **Rueda M.**, Fraile M., Martín A., Cocero M.J. *Development of nanocarriers for drug delivery by supercritical fluid extraction of emulsion*. 5<sup>èmes</sup> Entretiens du Centre Carrier, Lyon (France). November 19-21, 2012.

---

## AWARDS

- Research Grant in Energy and the Environment. **Iberdrola** Scholarship in the VII Program with the project 'Almacenamiento de hidrógeno en hidruros soportados en aerogels de sílice' to be developed from September 2016-september 2017 as main investigator in High Process Group at University of Valladolid.
- *1st position* in the Program **Yuzz** Valladolid 'Young with ideas' with the Project Light Energy. June 2016.

- **Prometeo Grant** with the project 'Diseño de materiales para la liberación rápida de hidrógeno desde hidruros en soportes porosos mediante aplicación de microondas' to protect innovative projects. Fundación General of Valladolid. October 2013.